THE DEVELOPMENT OF CONTROLLED-CHEMOTHERAPY DRUG DELIVERY SYSTEM

Yan Sim Lee

A thesis submitted for the degree of Doctor of Philosophy

University of Bath
Department of Chemical Engineering

June 2009

ABSTRACT

The aim of this thesis was to develop biodegradable devices loaded with chemotherapy drug. The system is targeted for advanced ovarian cancer treatment through the intraperitoneal (IP) route of administration. Polylactide-co-glycolide (PLGA) was selected as the model biodegradable polymer to produce drug-loaded microsphere, hollow and solid fibres. Copolymer PLGA with three different lactic:glycolic acids ratios; 50:50, 65:35 and 75:25 were used in order to compare their drug loading capacities and in *vitro* drug release profiles. Cisplatin, a cytotoxic drug with proven activity against ovarian cancer was selected as the model chemotherapy drug. Intraperitoneal administration is often associated with abdominal pain therefore a local anaesthetic; lidocaine, was selected for the purpose of pain relief.

Solvent evaporation with a single emulsion method (oil/water) was used to produce the drug-loaded PLGA microspheres. This method was selected due to the feasibility and robustness of the procedure and material involved. A number of double emulsion procedures were carried out but results show low robustness and no distinct advantage in the final products. Hollow and solid fibres were spun using a dry/wet-spinning method based on the phase inversion technique. The phase inversion process produces hollow fibre with unique finger-like microcavities and skin layer that offers high mass transfer resistance, which are useful features to prolong the drug release. Solid fibre was found to have similar characteristic but without a lumen.

The degradation profiles of PLGA microspheres, hollow and solid fibres before and after incubation in phosphate buffer saline solution were studied by means of SEM imaging and weight loss analysis. SEM images evidently show that these PLGA devices underwent bulk degradation based on their morphological changes during degradation. Autocatalytic degradation also occurred in hollow and solid fibres due to the accumulation of degraded acidic byproducts. A lag phase in mass loss of approximately two weeks was observed in 50:50 PLGA samples while it was few days longer in the cases of 65:35 and 75:25 PLGA.

Devices made of 50:50 PLGA exhibited the fastest degradation rate due to its highest glycolide acid content which is more prone to hydrolytic degradation. In contrast, devices made of 75:25 PLGA exhibited the highest degradation resistance, thought to be due to cause by a steric hindrance offered by the extra chiral methyl group in the lactide unit. This feature improves its chemical stability against hydrolytic attack.

The distribution of entrapped agent in 75:25 PLGA microspheres assessed by confocal laser scanning microscopy showed a heterogeneous distribution of the entrapped agent. Pulse field gradient-NMR was used to study pore evolution in the PLGA microspheres and results show that they underwent pore swelling and shrinking. During swelling, the system shifts from glassy state to rubbery state. Medium diffusion is faster in the latter state and therefore, swelling in PLGA microsphere was anticipated to increase drug diffusion. 50:50 PLGA microsphere was found to be most prone to swelling due to its higher amorphous region.

NMR-cryoporometry experiments permitted the studies of freezing of imbibed water in microsphere pores. It is suggested that the pores in the PLGA microspheres have "ink-bottle" geometry and the freezing of water confined in these pore occurs via solid ingress though the neck. Results show that 75:25 PLGA microsphere was inherited with biomodal necks system. It is thought that these necks also undergo similar swelling and shrinking mechanisms.

Cisplatin (CPt)-loaded PLGA solid fibres and microspheres were successfully produced with maximum drug loadings of approximately 15% and 10% respectively. CPt-loaded microsphere exhibited faster *in vitro* drug release compared to CPt-loaded solid fibre mainly due to its higher surface area:volume ratio which increased drug diffusion rate. Solid fibre exhibited slower drug release due to its smaller surface area and its unique fibre wall structure. *In vitro* CPt release results show promising potentials in mimicking an IP or IV doses of chemotherapy regimens.

Lidocaine (LID)-loaded PLGA microspheres and hollow fibre were successfully produced with maximum drug loadings of approximately 15% and 5% respectively. The lumen of the hollow fibre offers additional drug loading. In the case of drug solution-filled lumen, the drug release was faster due to the enhanced diffusion by the drug solution across the fibre wall. LID loaded-microsphere was also loaded into the fibre lumen. The combination of this duo reduced the drug release rate. This is because of the "retardant" effects of the fibre skin layers.

A number of basic empirical models were used to study the *in vitro* drug release profiles. Results show that these models are inadequate to characterise the overall drug release profiles possibly due to the degrading nature of these devices. However, a Higuchi-diffusional release model provides good fit to drug release during the first day for both LID- and CPt-loaded PLGA devices. A biexponential model with two fractions of drug present in the releasing-depot was derived and show reasonable fits to the *in vitro* CPt and LID release profiles.

ACKNOWLEDGEMENT

I would like to thank Semali Perera for her supervision at the Department and University of Bath for awarding the studentship. I was extremely fortunate to be co-supervised by Ed Gilby from RUH and Sean P. Rigby at the Department. I thank them for their guidance and criticisms in my work. Ed had been very patience and generous in teaching me his expertise and experience in medicine. I also wish to express my gratitude to his effort and RUH for the financial support for this project. Sean had been very encouraging in my NMR work as well as inspiring during my thesis write up and for future research perspective.

I feel like I almost owe to everyone for their second-to-none companionship and encouragement to make this period of time more pleasant, especially for Chin-Chih Tai and Holly Shearer who have led me in fibre spinning work. Christopher Campbell, who has been a true and dearest friend, riding alongside me through all the ups and downs. I could not have asked for a better friend.

Special thanks also go to John Lowe from the Dept. of Chemistry for his care and assistance in NMR analysis, Ursula Potter and Ann Reily for their support in SEM imaging, Adrian Roger for his help in CLSM analysis. I would also like to thank Merv, Fernando, Richard, Suzanne, John, Bob and Mac, the fabulous staffs from the Department for their "T.L.C".

Thank you, 'fluffy' Ian, Emily, Mari, 'tall' Ian, Delphine, Samantha, P□narcim, Janice, George, Andrew, Jason and Limin, for the friendships and aspirations all these years.

Last but not least, I wish to express my appreciation to my family members, especially Siang Yu and Yan Ning for their forbearance, without which I would have gotten no where.

TABLE OF CONTENTS

LIST OF TABLES

LIST OF FIGURES

LIST OF ABBREVIATION

50:50	PLGA comprising 50% lactic acid 50% glycolic acid
65:35	PLGA comprising 65% lactic acid 35% glycolic acid
75:25	PLGA comprising 75% lactic acid 25% glycolic acid
AAS	Atomic adsorption spectroscopy
A	Membrane surface area
AIC	Akaike's Information Criterion
ANOVA	Analysis of variance
cm	Centimeter
CPt	Cisplatin
C	Concentration
CLSM	Confocal laser scanning microscopy
D	Diffusion coefficient
Da	Dalton
DCM	Dichloromethane
DL	Drug Loading
ε_p / L_p	Effective surface porosity
DOSY	Diffusion ordered spectroscopy
EE	Encapsulation Efficiency
FDA	Food and Drug Association
FIGO	International Federation of Gynaecology and Obstetrics
g	Gram
g	Pulse field gradient strength
GMP	Good manufacturing practice
HCl	Hydrochloric acid
HF	Hollow fibre
I	Measured NMR intensity
J	Gas permeation flux
k	Gibbs-Thomson melting point constant
k_H	Higuchi rate constant
k_F	First order kinetic release rate constant
k_Z	Zero order kinetic release rate constant
k_o	Estimate first phase rate constant (mono-exponential rate equation)
k_2	Estimate first phase rate constant (bi-exponential rate equation)
k_3	Estimate second phase rate constant (bi-exponential rate equation)
kg	kilogram

ID	Inner diameter
IP	Intraperitoneal
IV	Intravenous
LID	Lidocaine
M_{Loss}	Mass loss
M_o	Initial mass of sample
M_n	Mass of sample after degradation
MS	Microsphere
M	Molar
M_W	Molecular weight
MHz	Mega Hertz
m	Meter
min	Minute
mg	Milli gram
ml	Milli litre
N	Gas molar flow rate
N_2	Nitrogen
NMP	1-methyl-2-pyrrolidane
NMR	Nuclear magnetic resonance
HNO_3	Nitric acid
OC	Ovarian cancer
OD	Outer diameter
o/w	oil-in-water
PBS	Phosphate buffered saline
PFG	Pulse field gradient
PGA	Polyglycolide
p	Fraction of free water
P_{in}	Pressure inside hollow fibre
P_o	Pressure outside hollow fibre / atmospheric pressure
PLA	Polylactide
PLGA	Poly(lactide-co-glycolide)
PVA	Poly-vinyl-alcohol
Q	Amount of drug
Q_t	Amount of drug released in time t
Q_o	Amount of drug remain in depot
$Q_o(\infty)$	Amount of drug in depot which will be released after a long time

$Q_2(\infty)$	Amount of drug in Pool A (of a depot) which will be released after a long time
$Q_3(\infty)$	Amount of drug in Pool B (of a depot) which will be released after a long time
R	Universal gas constant
R^2	Linear regression
$\overline{r^2}$	Molecular mean square displacement
rpm	Revolutions per minute
SEM	Scanning electron microscopy
SF	Solid fibre
Std. dev.	Standard deviation
t	Time
T	Temperature
T_g	Glass transition temperature
TNM	Tumour size, lymph nodes and metastasis
WHO	World Health Organizaion
wk	Week
w/o/w	Water-in-oil-in-water
w/v	Weight over volume
w/w	Weight over weight
μ_{N2}	Viscosity of gas nitrogen
γ	Gyromagnetic ratio
δ	Time of applied PFG
Δ	Diffusion time
τ	Correction time for the phasing and dephasing between bipolar gradients
κ	Tortuosity
ε	Voidage
μ	Micro ($x10^{-6}$)

CHAPTER 1: INTRODUCTION

1.1 Background Information

This thesis partly supports a project funded by the Department of Health, UK under the program of New and Emerging Application of Technology (NEAT, FSC020), and is in collaboration with the Royal United Hospital (RUH), Bath. In parallel to the aim of the NEAT project, the purpose of this thesis was to develop cisplatin-loaded microspheres for the treatment of advanced ovarian cancer. Details of objectives are defined in Section 1.2.

Approximately 6,600 women are diagnosed with ovarian cancer in the UK annually. It is the fourth commonest cancer in woman after breast, bowel and lung cancer. Statistics show that 5 out of every 100 women diagnosed with cancers suffer from ovarian cancer and the UK has one of the highest incidence of ovarian cancer in northern Europe (Cancer Research UK, 2008; WHO, International Agency for Research on Cancer, 2001). In the United States, ovarian cancer causes more deaths than other cancer of the female reproductive system. It is the seventh most common and the fifth leading cause of cancer death in women after lung and bronchus, breast, colorectal, and pancreatic cancers. In 2002, more than 19,000 women in the US were diagnosed with the disease and death rate was > 73% (US Dept. of Health & Human Services, National Cancer Institute, 2005).

The survival prospects greatly depend on prompt diagnosis, the effectiveness of cytoreductive surgery, the development of responsive chemotherapy regimens and novel drugs. In the 1960s, the 5-year survival rate for ovarian cancer was 30%, whereas recent statistics indicate an increase to 44% (Jemal *et al*., 2005). The increase in survival rate in the last 30 years is a result of improved management in chemotherapy treatment for the disease. Since 1990's, cytoreductive surgery and systemic combination chemotherapy with platinum and taxane compounds have become the standard treatment for this disease (McGuire and Markman, 2003). The route of administration of chemotherapy is usually intravenous (IV) in which the drug is delivered to the tumour site through the blood circulation.

Advanced ovarian cancer has an unusual pattern of spread and is usually confined to the abdominal cavity. This offers an opportunity to expose the tumour to cytotoxic agents by administration directly into the peritoneal cavity (Willemse and Vries, 2003). While intraperitoneal (IP) chemotherapy is unlikely to be beneficial in bulky disease because drug penetration into larger tumour nodules is limited, ovarian cancer often produces small seedlings or cellular dissemination invisible at surgery. Ovarian cancer is therefore an

attractive malignancy for IP chemotherapy (Dedrick *et al*., 1978; Kirmani *et al*., 1994 and, Willemse and Vries, 2003). The addition of IP chemotherapy to the management of ovarian cancer has demonstrated to be beneficial over IV chemotherapy (Hofstra *et al*., 2000 and Markman, 2004). In fact, in the early 1950s, the very first introduction of cytotoxic drugs into clinical practice was examined in IP delivery (Markman, 1986).

Studies from Markman *et al*. (1992) and Alberts *et al*. (1996) reported an improvement in overall survival rate after IP administered cisplatin compared to IV administered cisplatin. The direct IP administration not only provides a longer systemic drug exposure locally, but also lowers the cytotoxic effects of nephro- and neurotoxicities suffered from IV treatment. Occasionally, the site of injection can cause problems such as inflammation or patient discomfort. On the other hand, IP chemotherapy administration is associated with complications with the catheter instillation. Further evaluations on these subjects will be discussed in Chapter Two.

The on-going improvement of IP chemotherapy treatment for ovarian cancer and its shortcomings have provided the aspiration for this thesis. The ultimate aim of this thesis is thus to develop an improved system with the potential to address the problems encountered in the IP chemotherapy treatment. Today, new methods of drug administrations are available; the desired drug can be delivered directly to the target site by using rate-controlling and/or biodegradable devices containing the medication. Commonly reported in the literature, these controlled drug delivery systems can reduce the complications in conventional administration and provide a sustained release of the therapeutic agent in a predictable profile. This will improve localised effects and reduce systemic toxicities. Controlled drug delivery system will be further studied in Chapter Three.

In conjunction to the aim of this thesis, devices made of biodegradable polymer encapsulating medications have been developed and studied. First, a control delivery system in the form of microsphere was explored due to its capability for: (1) providing a controlled release of the therapeutic agent, (2) localising the therapeutic agents thus lowering their systemic toxicities, (3) these submicron spherical devices could improve *in situ* distribution and thus help to increase the exposure of tumour to drug, (4) the use of biodegradable system can also reduce clinic visits thereby improves patients compliance. Furthermore, the microspheres could also serve as protective coatings against *in vivo* enzyme biodegradation. Second, hollow and solid fibres were also developed with similar objectives. The characteristics of these drug-loaded microspheres and hollow/solid fibres were studied and compared.

1.2 Aims and Objectives

The aim of this thesis is to develop a controlled drug delivery system suitable for intraperitoneal (IP) treatment of advanced ovarian cancer. The proposed systems will take the forms of microsphere, hollow and solid fibres made of poly(lactide-co-glycolide) (PLGA). PLGA was selected because of its well-established biocompatibility and versatility. Cisplatin and lidocaine were selected as the encapsulation targets. Cisplatin is a common cytotoxic drug used to treat ovarian cancer. Patient receiving IP treatment often experience abdominal pain and local anaesthetic is used to suppress the pain. Thus, lidocaine was also used in this work. The development objectives are two-fold:

i. *To develop a microsphere system encapsulating the selected drugs*.
   Solvent evaporation technique with a single emulsion, water-in-oil (o/w) method was used to produce PLGA microspheres loaded with cisplatin and lidocaine.
ii. *To develop hollow and solid fibres systems encapsulating the selected drugs*.
   Phase inversion technique with a wet-spinning method was used to spin PLGA hollow and solid fibres loaded with lidocaine and cisplatin respectively.

The following objectives are aimed to gain better understandings of the developed systems:

iii. *Characterisation of microspheres, hollow and solid fibres*
   The developed PLGA devices were examined using scanning electron microscopy (SEM) for their morphologies. Confocal laser scanning microscopy (CLSM) was used to study the distribution of entrapped agent within a microsphere. Laser diffraction analysis was used to determine the size distribution of microsphere. Gas permeation analysis was conducted on hollow fibre to study its porosity.
iv. *Monitoring of PLGA Degradation*
   The morphology of the three PLGA devices before and during degradation was monitored using SEM and mass loss analysis.
v. *Pore Evaluation using Pulse Field Gradient (PFG) and Cryoporometry NMR*
   The pore information of microspheres was explored by measuring the diffusion of confined water using PFG NMR. NMR cryoporometry was used to study the pore structural information by following the freezing of confined water.
vi. *In Vitro Drug Release Profiles*
   In vitro drug release of cisplatin and lidocaine were measured based on their concentrations in buffer using atomic absorption spectroscopy for cisplatin, and uv-spectroscopy for lidocaine.

1.3 Thesis Outline

Chapter Two provides an introduction to ovarian cancer and emphasis is placed on conventional chemotherapy treatment (i.e. IV vs. IP administrations). The pharmacology profile of the model drug, cisplatin is also discussed. Chapter Three discusses the suitability of a biodegradable-controlled release system and its potential for improving IP chemotherapy. Both the model forms developed in the thesis, namely the microsphere and hollow fibre are also discussed in this chapter.

Chapter Four details the methodology used to conduct investigations presented thereafter. Chapter Five presents the development of a microsphere system using the solvent evaporation technique, followed by the development of hollow and solid fibres using the phase inversion technique. This chapter concludes the final and optimum production conditions for the subsequent experiments.

Chapter Six presents the morphological characterisations of the developed PLGA devices before and after degradation by means of SEM imaging, mass loss and pH profiles. This chapter closely studies the degradation behaviour of the developed systems and findings were correlated to *in vitro* drug release. Chapter Seven further studies the pore structural evolution of PLGA microspheres using PFG and cryoporometry NMR. The swelling mechanism in polymeric microsphere was proposed.

Chapter Eight investigates the cisplatin loadings in both PLGA microspheres and solid fibres. *In vitro* drug release profiles were studied in relation to PLGA degradation. Chapter Eight investigates the effects of both PLGA and lidocaine concentrations on drug loading. Following the production of lidocaine-loaded PLGA devices, the *in vitro* drug release profiles from these devices were studied.

Chapter Ten provides a summary of the thesis objectives and followed by an overall conclusion. This chapter ends with suggestions for further work.

CHAPTER 2: INTRODUCTION TO OVARIAN CANCER

Following the statistics information on the incidence of ovarian cancer presented in Section 1.0, this chapter studies the diagnosis and the treatment principles for the disease. Emphasis is placed on the conventional treatments for the disease; by intravenous and the less common intraperitoneal route chemotherapy. This chapter will also address the shortcomings of conventional treatments and, the rationale of developing a controlled release system for intraperitoneal administration. Cisplatin, a cytotoxic drug with proven activity in ovarian cancer is studied in order to understand its mode of action.

2.1 Overview of Ovarian Cancer

Cancer is a collection of diseases with a common feature of uncontrolled cell growth, which develops to produce a tumour. This unregulated growth can be:

i. benign – will not spread (i.e. only grows locally);
ii. malignant – will or can spread by direct invasion via metastasis. Metastasis is a complex process when cancer cells leaving the primary site, penetrating into either lymphatic or blood vessels or both and circulating through them to grow in normal tissues elsewhere in the body.

It is the disruption of normal tissues and organs that makes a cancer fatal. When cancer cells spread to form a secondary or metastatic tumour, it carries similar characteristic from its original tumour (McKinnell, 1998). Ovarian cancer (OC) occurs when malignant epithelial cells develop in the ovary. The primary site of this disease is within the abdominal cavity of the patient (Cannistra, 2004 and Thigpen, 2004). Spread of this disease is often by local extension, by intra-abdominal dissemination to other sites within the peritoneal cavity, or less commonly by lymphatic spread to pelvic and para-aortic nodes in the retroperitoneum (Bristow *et al*., 2003 and Fung *et al*., 2007).

The symptoms experienced by ovarian cancer patient can include back or leg pain, shortness of breath, loss of appetite and general abdominal discomfort such as swelling, pain, bloating, indigestion or cramps (Eltabbakh *et al*., 1999 and Donovan *et al*., 2005). One of the reasons contributing to OC having the highest death rate among gynaecologic malignancies is the non-specific nature of recognisable early symptoms, which also relates to the inadequacy of most OC screening tests. Thus, patients are often diagnosed at an advanced stage when the

cancer has spread beyond the ovary; i.e. beyond Stage II according to the International Federation of Gynecology and Obstetrics (FIGO) system (Landrum *et al*., 2008). Table 2.1 describes the different stages of OC according to the FIGO system.

Table 2.1: Different stages used to diagnose ovarian carcinoma (Eltabbakh *et al*., 1999).

Staging		Condition of Disease
Stage	I	Tumour is found in one or both of the ovaries and has not spread
	I A	Tumour limited one ovary
	I B	Tumour limited to both ovaries
	I C	Both ovaries and with capsule rupture or ascites
Stage	II	Tumour is found in one or both ovaries and has spread into other areas of the pelvis within the peritoneal cavity
	II A	Tumour extension to the uterus and/or tubes
	II B	Tumour extension to other pelvic tissues/organ
	II C	Tumour other pelvic tissues or with ascites
Stage	III	Cancer is found in one or both ovaries and has spread to other parts of the abdomen within the peritoneal cavity.
	III A	Microscopic peritoneal metastasis beyond the pelvis
	III B	Macroscopic peritoneal metastasis beyond the pelvis
	III C	Peritoneal metastasis beyond pelvis more than 2 cm in greatest dimension and/or regional lymph nodes metastasis
Stage	IV	Distant metastasis beyond the peritoneal cavity

2.2 Conventional Ovarian Cancer Treatment

In a case of suspected ovarian cancer (OC), conventional diagnosis these days always involves a computed tomography scan (Gilby, 2008). After that, common primary processes are such as primary surgery for diagnosis and staging, laparotomy is carried out to order to identify the stage of the disease. Consequently, surgical removal of the cancerous materials is performed (Fung *et al*., 2007). These processes are illustrated in Figure 2.1. Staging (Table 2.1) is a process to describe the progression of ovarian cancer based on the tumour size, spread to the lymph nodes and metastasis to distant sites, or known as the TNM system.

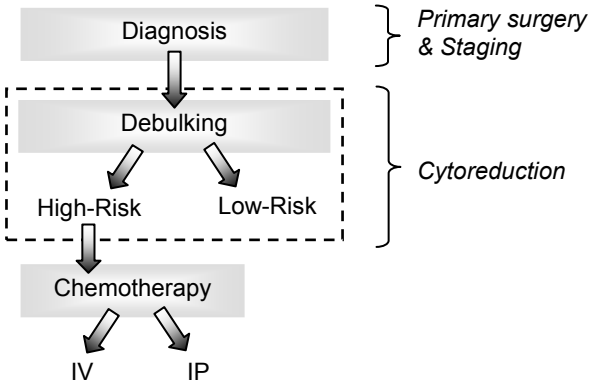

Figure 2.1: A conventional process of ovarian cancer treatment.

After staging is established, a strategy for treatment (cytoreduction) can be formulated. The main treatment options are surgery, chemotherapy and radiotherapy. Different treatments are required for cancers of different stages. Surgery is usually sufficient only for early stage ovarian cancer where the tumour is localised at Stage I to IB. Surgical therapy for women with advanced stage disease would include total abdominal hysterectomy (removal of uterus), and bilateral salpingo-oophorectomy (removal of ovary with Fallopian tube) and omentectomy (removal of the omentum); aiming to achieve the best cytoreductive effect. Unfortunately, surgery alone fails to cure majority of the patients (Gilby, 2008).

The majority of the patients will experience recurrence of the disease and the site of recurrence is still confined within the abdominal cavity (Landrum *et al*., 2008). Improvements in survival have been achieved through aggressive cytoreductive surgery followed by combination of chemotherapy (Ozols *et al*., 2003). In the late 1980's and early 1990's, standard combined regimens used for ovarian cancer chemotherapy were such as cisplatin with cyclophosphamide or doxorubicin. In the 1990's, the chemotherapy regimen after debulking is generally a combination of platinum and taxane drugs (McGuire *et al*., 1996). Examples of chemotherapy regimen are given in Table 2.2. The conventional administration routes for chemotherapy are discussed in the following section.

2.2.1 Chemotherapy Treatment: Intravenous and Intraperitoneal Administrations

The course of chemotherapy treatment is commonly given through intravenous (IV) administration by inserting a needle (through which medication is transported) into a vein, usually in the arm. The drug is then delivered to the disease site through blood circulation. The major setback of this administration is the systemic blood circulation which increases the risk of toxicities. Other problems with injection are such as patients discomfort and

inflammation at the injection site. Since chemotherapy is usually given after debulking to either kill residual tumour or later, recurrent tumours, various regimens are used for diseases of different stages. IV chemotherapy is often given in a combination of more than one chemotherapy drugs.

Owing to the localisation of the disease, regional delivery of chemotherapy directly into the peritoneal cavity is permitted and is termed intraperitoneal (IP) administration. This is done by surgical implantation of a catheter (Figure 2.2). The catheter is a hollow flexible tube used to deliver fluid into the abdominal cavity. IP administration requires the drugs to be dissolved in saline or dextrose solution (for adequate fluid distribution), prewarmed to body temperature (to avoid peritoneal irritation) before the drug solution is infused into the body via the catheter. Following IP administration, patients are also encouraged to frequently change their position to help drug distribution (Kirmani *et al*., 1994).

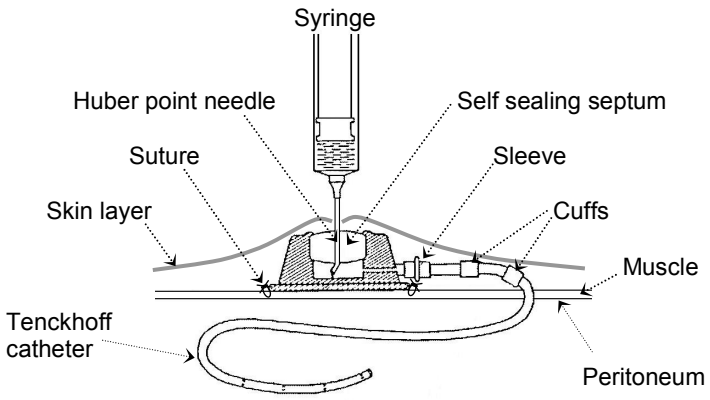

Figure 2.2: An ensemble of impaired peritoneal access system using a Port-A-Cath type catheter kit manufactured by Pharmacia Deltec Inc., US (adapted from McClay and Howell, 1990).

In cases where a patient is unable to tolerate the planned IV administration due to problems such as ineffective infusion or low tumour response rate, then the IP therapy offers an alternative. Conversely, if the patient is unable to receive IP administration due problems such as catheter-related complication, then conventional IV therapy will be assumed. Common IV and IP regimens and duration of course used to treat patients with advanced stages OC and residual tumour after debulking are given in Table 2.2. These studies are carried out in order to compare the effectiveness of IV and IP administrations.

The drug dosages are based on the body surface area of the patient. For example, IV cisplatin is given at 100 mg/m^2 per cycle once every 3 weeks. At a dose of 100 mg/m^2, for a patient of height 170 cm, weighing 70 kg with a surface area of 1.7 m^2 (Dearnaley *et al*., 2002 and

Gilby, 2008), the dose for the patient will be 170 mg. The duration of IV infusion in each cycle ranged from 1-2 hours. Factors such as the health condition of the patient, the response rate of the tumour and, the time allowance for the body's normal tissue to recover, will all influence the regimen and course of chemotherapy.

Table 2.2: Different regimens used to treat patients with advanced ovarian cancer.

Authors	Stages	Control Regimen (C)	Experimental Regimen (E)	Duration of course
Kirmani *et al*., 1994	IIC-IV	IV cisplatin, 100 mg/m^2 IV cyclophosphamide, 600 mg/m^2	IP cisplatin, 200 mg/m^2 IP etoposide, 350 mg/m^2	C: cycle/3 wk × 6 E: cycle/4 wk × 6
Alberts *et al*., 1996	III, ≤ 2 cm residual	IV cisplatin, 100 mg/m^2 IV cyclophosphamide, 600 mg/m^2	IP cisplatin, 200 mg/m^2 IV cyclophosphamide, 600 mg/m^2	C: cycle/3 wk × 6 E: cycle/3 wk × 6
Markman *et al*., 2001	III, ≤ 1 cm residual	IV cisplatin, 75 mg/m^2 IV paclitaxel, 135 mg/m^2	IP cisplatin, 100 mg/m^2 IV paclitaxel, 135 mg/m^2	C: cycle/3 wk × 6 E: cycle/3 wk × 6
Yen *et al*., 2001	III, ≤ 1 cm residual	IV cisplatin, 50 mg/m^2 IV cyclophosphamide, 50 mg/m^2 IV Epidoxorubicin/ Doxorubicin, 50 mg/m^2	IP cisplatin, 100 mg/m^2 IV cyclophosphamide, 50 mg/m^2 IV Epidoxorubicin/ Doxorubicin, 50 mg/m^2	C: cycle/3 wk × 6 E: cycle/3 wk × 6
Armstrong *et al*., 2006	III, ≤ 1 cm residual	IV cisplatin, 75 mg/m^2 IV paclitaxel, 135 mg/m^2	IP cisplatin, 100 mg/m^2 IP paclitaxel, 60 mg/m^2 IV paclitaxel, 135 mg/m^2	C: cycle/3 wk × 6 E: cycle/3 wk × 6

IV cisplatin = cisplatin given intravenously; IP cisplatin = cisplatin given intraperitoneally; wk = week.

The classic rationale of IP administration was first published by Dedrick *et al*. (1978). This philosophy has since encouraged studies exploring both the safety and pharmacokinetic advantage of IP administration. Figure 2.3 shows the early findings from Dedrick *et al*. (1978).

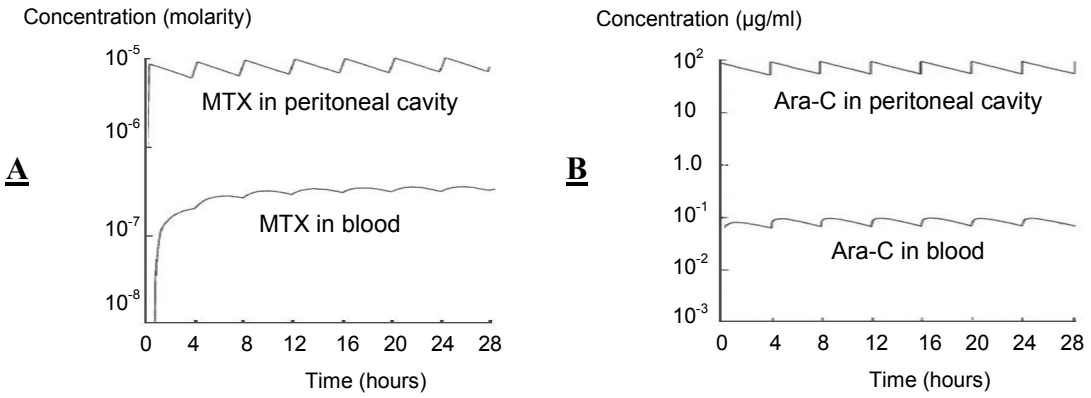

Figure 2.3: Model simulations of concentrations of (A) Methotrexate, MTX and (B) Cytosine arabinose, Ara-C in peritoneal cavity and plasma (adapted from Dedrick *et al*., 1978).

Figure 2.3 (A) and (B) are the model simulations of plasma and peritoneal fluid concentrations of methotrexate (MTX) and cytosine arabinose (Ara-C) respectively, based on known physiologic and anatomic characteristics of the peritoneal cavity. Continuous infusion produces the "saw-tooth" profiles due to drug absorptions by the peritoneum, liver, kidney, skin and muscle. MTX is an antimetabolite used in cancer treatment such as leukemia. Ara-C is an agent used in intraperitoneal disease such as hematological malignancies. Figure 2.3 shows that both concentrations of MTX and Ara-C in peritoneal cavity are a few orders higher than those in blood plasma. Their results showed that the peritoneal route has a lower clearance of chemotherapeutic agents than the plasma.

Since the principle site of OC is confined to the peritoneal cavity, IP administration could be expected to result in a significant drug concentration difference between the peritoneal cavity and blood plasma. This confinement provides pharmacologic advantages whereby the tumour (1) can be exposed to a more sustained and higher concentration of chemotherapeutic agents while; (2) the drugs remains active in the IP cavity longer compared to those of IV administration (Kirmani *et al*., 1994 and, Willemse and de Vries, 2003). A study by Markman (1996) collected evidence that IP cisplatin was able to increase the exposure of peritoneal cavity to the drug by a factor of 10- to 20-fold compared with IV cisplatin. This IP route was also able to overcome some degree of drug resistance and partial sensitivity towards cytotoxic agent associated with tumours, which could not be achieved with an IV cisplatin. Owing to the drug slowly leaving the peritoneal cavity to enter the bloodstream, there is lower systemic toxicity than with IV drug administration. Meanwhile, normal tissues such as the bone marrow are relatively spared (Armstrong *et al*., 2006).

From the clinical studies tabulated in Table 2.2, the number of patients included in the clinical trials by Alberts *et al*. (1996) was 546 patients. They reported a median overall survival of 49 months for advanced stage patients treated with IP cisplatin compared to 41 months for those treated with IV cyclophosphamide. This translated to a higher survival rate for the patients group receiving IP chemotherapy compared to the IV patients group.

In a study involving a total of 118 patients carried out by Yen *et al*. (2001), the patients group receiving IP chemotherapy had a median overall survival rate of 48 months compared to 43 months for the IV chemotherapy patients group. The percentages of patients completing the course were rather low; i.e. 32% from the IP patients group and 25% for the IV patients group. Armstrong *et al*. (2006) formulated two regimens; (i) IV [paclitaxel +

cisplatin] and, (ii) IV paclitaxel and IP [paclitaxel + cisplatin] to treat patients with optimally debulked Stage III OC. The IV alone regimen produced an overall survival of 49.7 months and the combined IV + IP regimen produced an overall survival rate of 65.6 months. The total number of patients was 415 while 83% of the IP patients group had completed the course of IP treatment and 42% for the IV patients group.

In a large clinical study carried out by Markman *et al*. (1992), 600 patients with small-volume residual Stage III OC (largest diameter disease after debulking $\leq$ 2cm) were randomised to receive either IV or IP cisplatin, both at 100 mg/m^2. With a median of approximately four years from study entry, patients receiving IP cisplatin showed a significant improvement in survival (median: 49 months) compared to IV cisplatin (median: 41 months). Patients with IP cisplatin also experienced less neutropenia and hearing loss. These were due to the lower systemic toxicity in IP cisplatin compared to IV cisplatin. This study suggested that IP cisplatin can increase the effectiveness of chemotherapy on small-volume residual OC.

Rothenberg *et al*. (2003) used IP cisplatin and IV paclitaxel as primary treatments in 68 patients with optimally debulked Stage III OC. The median survival time using IV chemotherapy was 41-52 months and the 2-year survival rate was 65-70%. Whilst for IP chemotherapy, the median survival time was 49-63 months and the 2-year survival rate was 70-80%. Based on the survival rates information from the studies presented above, it can be concluded that IP administration of chemotherapeutic agents are capable of producing higher survival rate compared to IV administration.

There are many reasons for patients being unable to complete the treatment of either IV or IP course but these factors will not be discussed here. However, in particular, Walker *et al*. (2006) investigated the reasons for IP failures and reported that up to two-third of the patients suffered from problems caused by the catheter. Half of them suffered complications related to the indwelling catheter devices and the rest experienced abdominal pain causing the patients to refuse the treatment. Further examples are given below (Markman, 1992; Willemse and Vries, 2003):

i. Subcutaneous installation of a catheter leads to higher risk of infection and fever.
ii. IP therapy involved delivering large volume of medication solution into the peritoneum of the patient. This causes abdominal pain, nausea and vomiting.

iii. The development of intra-abdominal adhesions, may be promoted by IP therapy which increase the risk of subsequent abdominal surgery.
iv. Other incidents included inflow obstruction and bowel injury.

IP administration can also lead to peritonitis (inflammation of the peritoneum), which prevents the use of higher drug doses. A number of authors have improved the problem by pretreating the patient with local anaesthetics before IP treatment; e.g. Use of lidocaine to lessen the pain during IP course (Zylberberg *et al*., 1996). Table 2.3 provides a summary of the advantage and disadvantages of IP administration.

Table 2.3: Advantages and disadvantages of IP chemotherapy (Willemse and Vries, 2003).

Advantage	Disadvantage
i. Higher therapeutic effect	i. Complications of IP catheter:
ii. Lower systemic toxicity:	- Infection
- Renal	- Perforation
- Neural	- Bleeding
- Bone marrow	- Pain; fibrous adhesions causing insufficient IP fluid and drug distribution or, local pain or irritation due to cytotoxic agents.

Other non-clinical related problems associated with IP treatment include the cost of performing the operation and clinicians are lack of familiarity with the technique. The instillation and replacement of a catheter requires skill and expertise (Armstrong *et al*., 2006 and, Markman and Walker, 2006). However, the beneficial pharmacology of IP therapy encourages promising outcomes and is increasingly been used. Evidence are demonstrated by the literatures cited above. The underpinning concepts of IP therapy is the direct delivery of medication to the disease site where ovarian cancer is confined to the peritoneal cavity. This criterion suits a microsphere delivery system which could offer a localised effect.

The drug-loaded microspheres can be directly delivered to the peritoneal cavity by a single injection. Over time, as the biodegradable microspheres degrade they are resorbed by the body and further releasing their drug content. No surgical removal is required and no complicated installation is required such as the instillation of a catheter system. These microspheres could also help to increase the exposure of tumour surface to cytotoxic drug via (1) their small and free flow spherical nature which helps *in situ* distribution and (2) the microspheres offer a high surface area for drug diffusion. Further elaboration on the microsphere drug delivery system will be discussed in Chapter Three.

Studies have been reported in the literature regarding the efficiency of cisplatin-loaded microsphere delivery system. Tamura *et al*. (2002) formulated three different cisplatin-loaded microspheres using PLGA and two PLA with different molecular weights. The platinum profile in plasma shown on Figure 2.4 is the concentration of cisplatin measured based on its platinum content after subcutaneous (s. c.) administration of the PLGA/PLA microspheres in male Donryu rats.

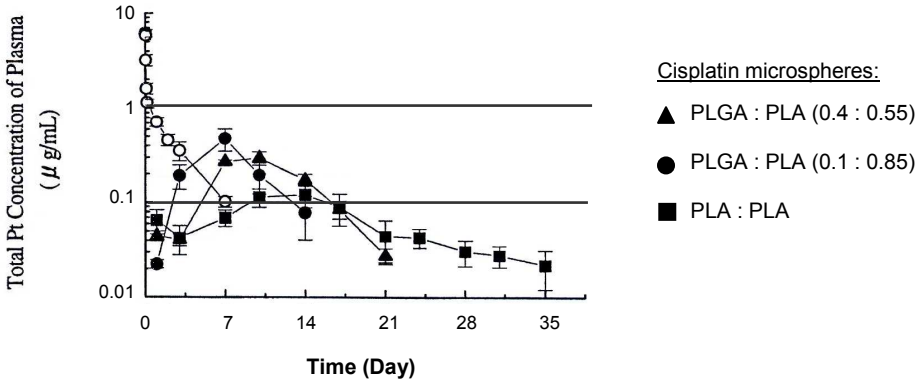

Figure 2.4: The plasma platinum concentration after s.c. administration of cisplatin-loaded microspheres of different formulations (close symbols) and cisplatin solution (open symbol) (adapted from Tamura *et al*., 2002).

For comparison, Tamura *et al*. (2002) also dissolved cisplatin in saline solution and followed the same microspheres administration into the rats at a dose of 5 mg/kg rat. Tamura *et al*. (2002) claimed that their results using IP administration exhibited the same concentration profile as the s. c. administration. It can be seen in Figure 2.4 that the cisplatin microspheres formulations exhibited the typical sustained drug release for two to four weeks as appose to one week from cisplatin solution.

A pilot study in 1993 was carried out with 13 patients receiving cisplatin-loaded microspheres (Hagiwara *et al*., 1993). Nine of these patients were suffering from gastric cancer, two with colon cancer and two with pancreatic cancer. The route of administration was IP injection of cisplatin-loaded microspheres; twelve patients received 100 mg of the formulation and one received 200 mg. At different time, ascites fluid and blood samples were collected from each patients. Figure 2.5 shows the corresponding cisplatin concentrations, measured based on its platinum content. In all cases, the cisplatin concentrations in ascites fluid were higher than those present in blood plasma. Their final observation noted that eight (62%) patients responded completely, four (31%) partially and one (8%) did not respond to the treatment. This resulted in a response rate of 92% towards IP administration of cisplatin.

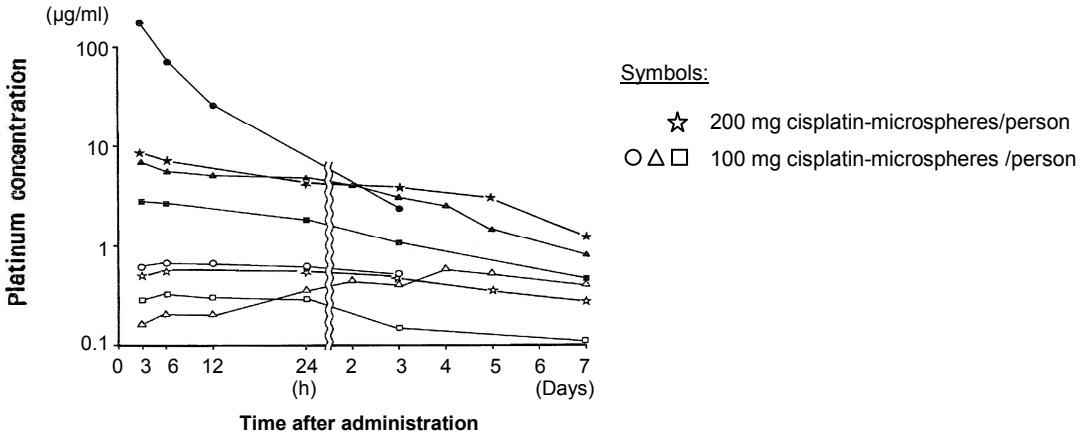

Figure 2.5: Platinum concentrations in ascites fluid (close symbols) and blood plasma (open symbols). Each symbol represents a patient (adapted from Hagiwara *et al*., 1993).

Results from Hagiwara *et al*. (1993) showed that the absorption of cisplatin into the blood plasma was low and this translated to a reduced systemic toxicity. The concentration remained high in the peritoneal cavity and this improved the therapeutic effect of IP therapy. Further example of involving clinical studies was reported by Fujiyama *et al*. (2003). The authors developed biodegradable microspheres loaded with cisplatin for local therapy in patients with thyroid carcinoma with poor diagnosis. Results showed that the treatment demonstrated antitumour effects without side effects during the treatment period, and a survival period of ≥ 1 year. Fujiyama *et al*. (2003) also found that the cisplatin-microsphere system demonstrated effectiveness in local injection therapy in patients with cancerous peritonitis or who were intolerable to surgery. After establishing the rational for developing a microsphere drug delivery system for IP chemotherapy, the following section studies the pharmacology profile of the model chemotherapy drug, cisplatin.

2.3 Single Agent Therapy – Cisplatin

Early clinical trials using cisplatin at standard dose (50 – 150 mg/m^2) have demonstrated the safety and efficacy of IP therapy. Cisplatin is one of the most active agents used for the treatment of OC (Rothenberg *et al*., 2003 and Markman 2006). After IP administration, the large molecular weight of cisplatin produces a peritoneal-to-plasma concentration ratio of 20 which result in a high level of intrinsic activity against OC (Howell *et al*., 1982 and Markman *et al*., 2004). Meanwhile, the therapeutic index of IP cisplatin can be further increased through the use of concurrent IV sodium thiosulfate, which

protects the kidneys from the cytotoxic effect of the drug. This circumvention enables the body to tolerate with a higher dose of IP cisplatin and thus dose escalation is permitted (Howell *et al*., 1982). From the principle of IP therapy, one can improve cancer response rate if the delivery of the anticancer drug to the cancer can be increased. With such a profile, cisplatin has been commonly used as a single agent to treat OC and because its profound availability for dose escalation which may increase cancer response rate (Bristow *et al*., 2002 and Gildy, 2008). These criteria make cisplatin a suitable model drug for this work.

2.3.1 Pharmacology Profile

Cisplatin (cis-diaminedichloroplatinum), with a molecular formula of $PtCl_2H_6N_2$, is a heavy metal complex containing a platinum atom at the centre of the molecule. It is surrounded by two chloride atoms and two ammonia molecules in the *cis* position, as indicated in Figure 2.6. The molecular weight of cisplatin is 300.05 and it has a water or saline solubility of 2 mg/ml.

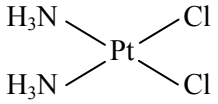

Figure 2.6: Molecular structure of cisplatin. It has two ammonia groups (NH_3) and chloride atoms (Cl) joining to the centre platinum atom in the *cis*-position.

The clinical benefits of cisplatin as an anticancer agent have now been recognised for over 30 years. To his surprise, Rosenberg discovered cisplatin in 1965 while investigating the effect of electric currents on bacteria (Rosenberg *et al*., 1965). A few years later cisplatin quickly reestablished itself as a chemotherapeutic agent after it was found to inhibit the growth in *Eschericia coli* (Rosenberg *et al*., 1969). Early clinical studies by Higby *et al*. (1974) found that cisplatin exhibited anti-tumour activity in testicular teratoma, while Wiltshaw and Kroner (1976) found similar behaviour in relapsed ovarian cancer.

The cisplatin concentration in plasma decays monoexponentially with a half-life of about 30 minutes following a two, six or seven hours infusion of 100 mg/m^2 dose. The total body clearance and volume of distribution at steady-state for cisplatin are about 15-16 l/h/m^2 and 11-12 l/m^2 respectively. About a quarter of the IV dose is excreted through the kidneys in the first 24 h. Total cisplatin (free and bound) has a prolonged half-life of 2 to 3 days. Cisplatin does not bind to protein but the platinum within its molecule can remain bound to protein in tissues for a long time (Rixe *et al*., 1996 and, van Zutphen and Reedjik 2005). The key

elements in the effects of cisplatin on DNA are (1) its controlled hydrolysis within a cell, (2) specific binding at adjacent guanine bases in DNA which leads to; (3) specific distortion of DNA, changing its interactions with proteins, leading to either repair of the damage, or cell killing by apoptosis.

The mode of action of platinum agents is through irreversible binding to DNA. Upon entering a cell, they will become aquated. In the case of cisplatin, it loses chloride or oxalate ions, gains two water molecules and becomes positively charged. This subsequently enables them to interact with nucleophilic molecules within the cell, including DNA, RNA, and proteins. Due to its unique chemical structure, the chlorine atoms of cisplatin are more subject to chemical displacement reactions by nucleophiles, such as water or sulfhydryl groups, than to enzyme-catalysed metabolism. When binding to DNA, the aquated platinum species binds preferentially to the highly nucleophilic N-7 position of the purine bases guanine and adenine in a DNA molecule (Reedijk, 2003). Three different types of binding can form on purine bases of DNA: monoadducts, intrastrand crosslinks, and interstrand crosslinks as illustrated in Figure 2.7. All crosslinks result in distortion of the DNA which then interferes with the cell multiplication (Rabik and Dolan, 2007).

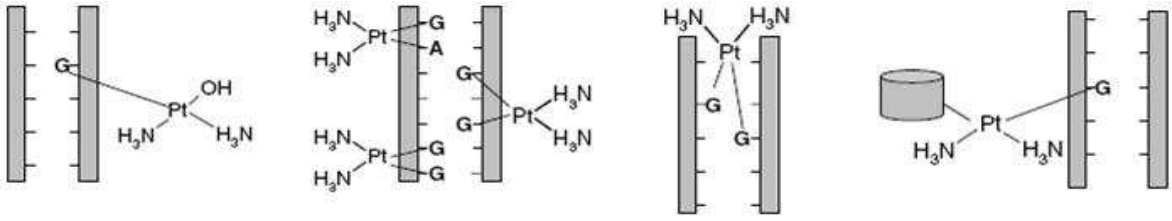

DNA Monoadduct | Intrastrand Crosslinks | Interstrand Crosslink | DNA-Protein Crosslink

Figure 2.7: Platinating agent adducts on DNA. Platinating agents are able to react with DNA to form monoadducts, intrastrand crosslinks (1,2-d(GpG), 1,2-d(ApG), 1,3- d(GpXpGp)), interstrand crosslinks (G-G), and DNA–protein crosslinks (adapted from Rabik and Dolan, 2007).

CHAPTER 3: CONTROLLED RELEASE SYSTEM

In Chapter Two we discussed the condition of ovarian cancer and due to its confinement in the peritoneal cavity; a local and direct delivery of cytotoxic drugs to the site can be introduced. This chapter discusses the suitability of a controlled release system with an emphasis on the model forms of the developed systems. The techniques used to develop the controlled release systems for this thesis are also discussed.

3.1 Controlled Release System

The key challenge with drug administration is that the plasma drug level should remain at the desired therapeutic level; above which may represent a toxic level, below which the therapeutic is no longer effective (Illum, 1987). A controlled release occurs when a carrier successfully captures a bioactive agent in such a way that the active agent is released from the carrier in a predesigned manner. The release of the agent may be constant or cyclic over a period, or it may be triggered by the environment or other external events.

Depending on the application, this system can be tailor-made to perform within hours to months or up to years. These systems can take the form of either soluble polymers, implants (to which the drug may be attached by some form of suitable biodegradable linkages) or biodegradable micro/nano-particles (in which the drug is entrapped). An impeccable reality of which a controlled release system is an ideal candidate system to be explored for this thesis is the Special Programme for Vaccine Development initiated by the WHO in the 1980s (Bloom, 1989). In parallel to improving conventional drug delivery, increasing attention is being paid to developing polymeric carriers for controlled delivery. Reason being that most principles developed for this strategy are versatile and adaptable.

The most indispensable attribute of a biodegradable material is its biocompatibility (i.e. no part of the polymer induces inflammatory responses in blood or tissues), and its degradation products can be metabolised and excreted by natural pathways (Shive and Anderson, 1997). Hence, biodegradable polymers have since been stemming in the biomedical application. In recent years, controlled drug delivery formulations and the polymers used in these systems have become much more sophisticated and materials have been developed to be target-specific; i.e. specific cell, tissue, or site (Gupte and Ciftci, 2004).

3.2 Use of Biodegradable Polymers

The primary criteria for a polymer to be used for controlled drug delivery formulation are such that the material has an appropriate physical structure, good stability and be readily processable (Yeo and Park, 2004). There is a broad range of biodegradable polymers available and the most widely studied belong to the polyester family. For example, polylactide acids (PLA) polyglycolide acids (PGA) and their copolymers, which in fact are approved by the US Food and Drug Administration (FDA). These polymers are particularly attractive due to their versatile degradation kinetics which can be preprogrammed. Clinically, for at least 20 years PGA and PLA have been applied for orthopaedic fixation, reconstruction and allogenic/autogenic bone surgery (Winet *et al*., 1995 and 1997). Not only because they are absorbed and revision surgery is unnecessary, but they are also non-proteinaceous and thus antigenic response is avoided.

3.2.1 Polylactide and Polyglycolide

Polylactide (PLA) and polyglycolide (PGA) are aliphatic polyesters of poly(α-hydroxy acids). These polymers and their associated copolymers are perhaps one of the most common biodegradable polymers known and have been used in drug delivery, bone osteosynthesis and tissue engineering (Middleton and Tipton, 2000). Compared to PGA, PLA has an extra chiral methyl group which gives rise to L or D-PLA (levorotary or dexorotary), or a racemix of DL-PLA.

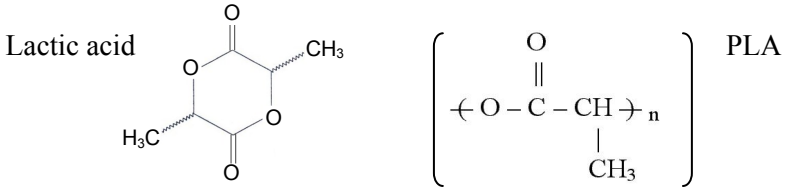

Figure 3.1: Molecular structure of lactic acid and PLA (adapted from Lakeshore Biomaterials, 2005).

The extra methyl group also makes PLA more hydrophobic than PGA due to steric hindrance of the methyl group. Consequently, the ester bond of PLA is less accessible for hydrolysis compared to PGA, making PLA has greater degradation resistance than PGA. The crystallinity of PLA usually governs their end uses. L-PLA is semi-crystalline as they have regular repeating units that enable the chains to fold into dense regions called crystallites. These act as cross-links giving the polymer higher tensile strength, low elongation and higher modulus, as well as higher resistance to degradation. These features make L-PLA suitable for

load-bearing applications such as orthopaedic fixations and sutures. On the other hand, D-PLA is an amorphous polymer having a random distribution of both isomeric forms of lactic acid and is unable to arrange into an organised crystalline structure (Hasirci *et al*., 2001). Therefore D-PLA is more suitable to be use in drug delivery applications that require a fast degradation rate.

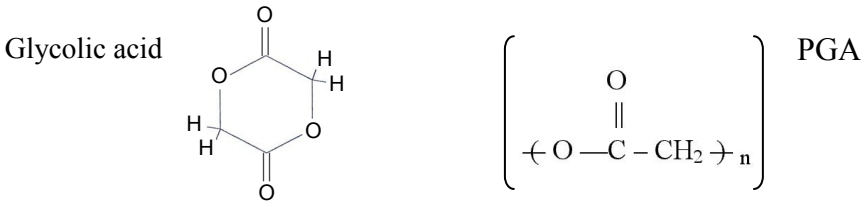

Figure 3.2: Molecular structure of glycolic acid and PGA (adapted from Lakeshore Biomaterials, 2005).

PGA is a highly crystalline polymer due to its relatively short chain length and polar properties which also give rise to a high melting point and low solubility in organic solvents. PGA is commonly used as biodegradable suture material in the 1970s and it continued to evolve in the biomedical polymer applications such as being synthesised with PLA to form polylactide-co-glycolide.

Both PLA and PGA degrade by hydrolysis of the ester bond linkage to yield their original monomers, L- or D-lactic acid from PLA and glycolic acid from PGA, which are common by-products of various metabolic pathways in the body (Jalil and Nixon, 1990). This cycle is the second stage of three major stages in carbohydrate catabolism, between the process of glycolysis and oxidative phosphorylation; a breakdown process of glucose to carbon dioxide.

3.2.2 Polylactide-co-glycolide (PLGA)

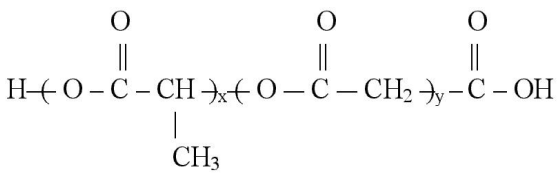

Figure 3.3: Molecular structure of PLGA; x = PLA, y = PGA (Freiberg and Zhu, 2004).

The molecular structure of PLGA is shown in Figure 3.3. Polylactide-co-glycolide (PLGA) are synthesised via random ring opening copolymerisation of monomers PLA and PGA. The polymerisation process usually requires a catalyst such as tin(II) 2-ethylhexanoate. During

this copolymerisation, successive monomeric units of lactic and glycolic acids are linked together by ester linkages, yielding a linear aliphatic polyester. The ratio of lactic/glycolic acids can be altered and for instance, 50:50 PLGA. The first number indicates the molar percentage of lactic and the second for glycolic acids.

The copolymer of PLGA extended their properties from their monomers PLA and PGA. Table 3.1 is the physical properties of PLA, PGA and PLGA. PLGA with different copolymer ratios have varying glass transition temperatures and degradation rates. Since PLGA have longer chains, they generally have lower crystallinity and are more amorphous than PGA or PLA. Copolymer PLGA is more susceptible to hydrolysis and degrades faster than their monomers, due to the disruption of the regularity of the polymer chain by the glycolide monomer (Park, 1995). Figure 3.4 is adapted from Middleton and Tipton (2000) in order to illustrate the relation between copolymer ratio and degradation rate.

Table 3.1: Physical properties of PLA, PGA and PLGA (Middleton and Tipton, 2000).

Polymer	Morphology	Glass Transition Temperature, T_g (°C)	Complete Resorption (months)
PGA	Semi-crystalline	35 - 40	6 to 12
L-PLA	Semi-crystalline	60 - 65	>24
DL-PLA	Amorphous	55 - 60	12-16
75:25 DL-PLGA	Amorphous	50 - 55	4 to 5
65:35 DL-PLGA	Amorphous	45 - 55	3 to 4
50:50 DL-PLGA	Amorphous	45 - 55	1 to 2

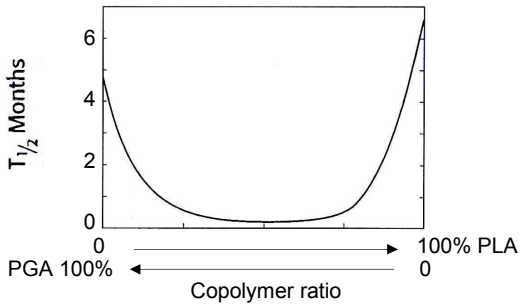

Figure 3.4: Half-life of PLA, PGA and PLGA copolymers (Middleton and Tipton, 2000).

PLGA undergoes random scission degradation (Cha and Pitt, 1990 and, Jalil and Nixon, 1990). PLGA is an attractive material for drug delivery systems because of its potential to offer different degradation rates by varying the lactide/glycolide acids ratio (Walter *et al.*, 2001). This feature is advantageous for applications requiring specific degradation kinetics ranging from weeks to months. Similar to PLA and PGA, PLGA is also biocompatible and is

hydrolytically degraded into natural metabolites: lactic and glycolic acids which are eliminated from the body through the Kreb's cycle (Gunatillake and Adhikari, 2003).

Degradation of a polymer can occur via mechanisms known as unzipping or random hydrolytic scission (Kiss and Vargha-Butler, 1999). In this case, aliphatic polyester PLGA undergoes hydrolytic degradation via random chain scission at ester linkages (Spenlehauer *et al*., 1989), such as illustrated in Figure 3.4. Random scission of the polyester backbone leads to the initial production of insoluble oligomeric fragments of carboxylic acid end groups, which can further catalyse the degradation. As degradation proceeds, soluble oligomers and monomers are formed and released. At later stage, mass loss of the polymer will occur (Loo *et al*., 2005). Figure 3.5 shows the degradation of PLGA.

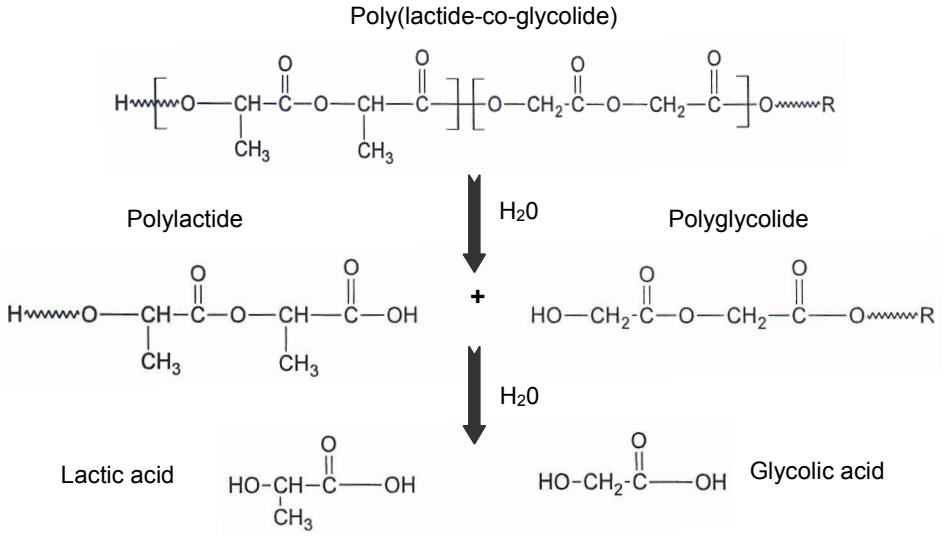

Figure 3.5: The degradation of PLGA occurs through hydrolytic scission at the ester linkage of the main chain. The final degradation products are their monomer; the lactic and glycolic acids.

3.3 Biocompatibility of PLA and PLGA

The importance of biocompatibility in determining the therapeutic usefulness of biomaterials is well recognised to ensure the safety and efficacy of the devices (Park, 1995 and Anderson, 1994). In controlled delivery, implantation of biodegradable polymeric products circumvents the need for surgical removal after complete release of the active agent. The circumvention potentially reduces pain, cost and risk of infection (Hasirci *et al*., 2001). Sandstrap *et al*. (1999) demonstrated that it was possible to obtain reasonable accordance between *in vitro* and *in vivo* results using PLGA microsphere systems in rats for the release

of nifedipine, while PLGA polymer has already been well characterised and approved for application in humans by the FDA (Waeckerle-Men and Groettrup, 2005).

Other credible studies have also proven the biocompatibility of PLGA in the brain (Kou *et al*., 1997) and central nervous system (Menei *et al*., 1999). Jackson *et al*. (2004) formulated paclitaxel-loaded PLGA films and characterised them for potential application as perivascular "wraps" to prevent restenosis. *In vivo* analyses on Wistar rats with no adverse reaction were reported in their work. Ogura and Kimura (1995) used biodegradable microspheres for targeted drug delivery to the retinal pigment epithelium. Both 50:50 and 75:25 PLGA were used for subretinal delivery in rabbits. Retinal pigment epithelium was demonstrated to phagocytose the biodegradable microspheres. No adverse cellular or tissues reactions were noted in these studies.

Massey *et al*. (2004) conducted investigations into the resorption rates and biocompatibility characteristics of PLA and 50:50 PLGA tympanostomy tubes in a guinea pig. Tympanic membranes of all animals following tube degradation were intact with minimal scarring and no signs of persistent foreign body response. The histological analysis showed that implantation of resorbable tubes was not accompanied neither by secondary infection, otorrhea, permanent perforation, nor followed by excess tympanosclerosis or localised or diffuse membrane atrophy. They concluded that these tubes were substantially equivalent to other FDA-approved tympanostomy devices with regard to safety and biocompatibility in the guinea pig model examined. They further suggested that by combining this approach with controlled release technology, an improved clinical performance can be expected.

An important consideration when evaluating biocompatibility in terms of tissue response to biodegradable implants is the biologic activity of the loaded drug or therapeutic agent, especially if it has cytotoxic, anti-inflammatory or wound healing characteristics. Moreover, the variation in inflammatory and foreign body giant cell responses can be affected by the implant form, different routes of administration of the implant as well as different implant sites in tissues or organs (Spenlehauer *et al*., 1989).

A study carried out on a controlled release system containing gentamycin exhibited a significant increase in the Phase I inflammatory response due to the cellular cytotoxicity of gentamycin when present at high concentrations (Anderson and Shive, 1997). Cisplatin loaded PLGA microspheres in rats also caused an increase in inflammatory reaction

compared to cisplatin-free microspheres. These are examples of the localised response to the released drug. However, the benefits gained from using this system far outweighed the slight increase in the localised inflammatory reaction (Ike *et al*., 1992 and Itoi *et al*., 1996).

These studies signified the importance in considering the inherent cytotoxicity of the drug or therapeutic agent when evaluating the biocompatibility of biodegradable systems. Otherwise, the histological observation of enhanced or prolonged acute and chronic inflammatory and foreign body reactions may be mistakenly attributed to the polymer or contaminants in the polymer. Sections 3.1 to 3.4 have justified the suitability of PLGA as the model polymer for this thesis. Preliminarily work also showed that this polymer is easily processable. Examples of commercially available products listed in Table 3.2 further confirm the biocompatibility profiles of PLA, PGA and PLGA and their versatile applications.

Table 3.2: Examples of the various forms of PLA, PGA and PLGA used in biomedical applications.

Product name & Manufacturer	Material & Form	Medication	Application
Nutropin® Depot Genentech Inc.	PLGA, microspheres	Somatropin	Growth failure
Zolade® Astra Zeneca Pharmaceuticals, LP	PLA, rod implant	Goserelin acetate	Prostate cancer, endometriosis
Trelsta® Depot Pharmacia & Upjohn Company	PLGA, microspheres	Triptorelin pamoate	Prostate cancer
BVS BVS, Abbot	PLA, stent	Everolimus	Coronary artery disease
CYPHER® Cordis, Johnson & Johnson	PLA, stent	Sirolimus	Coronary artery disease
TAXUS® Boston Scientific	PLA, stent	Paclitaxel	Coronary artery disease
Tissue Fixation Screw DePuy Orthopaedic Inc.	P-L-LA, screw/pin	-	Orthopaedics fixations
Interference Screw Instrument Makar	85:15 PLGA, screw	-	Orthopaedics fixations
SD Sorb Suture Anchor Dynamics	82:18 PGA, screw	-	Orthopaedics fixations
Dexon® Davis and Geck	PGA, suture	-	Surgical suture
Vicryl® Ethicon	PLGA, suture	-	Surgical suture

A number of PLGA or PLA microsphere systems are clinically available. Example is such as Lupron Depot®, manufactured by TAP Pharmaceutical Products Inc., which can be subcutaneously or intramuscularly administered. Lupron-PLA microsphere was reported to have an approximately 10 % of drug loading, and releases leuprolide, an GnRH analogue at

for treating prostate cancer. The following section will discuss the model forms of the devices developed for this thesis.

3.4 Microspheres for Controlled Delivery

Polymeric microparticle for drug delivery can be classified as colloidal carriers (Illum, 1987), which includes not only micro- and nano-spheres, but also liposomes, emulsions and materials of biological origin such as low density lipoproteins. Small spherical devices, made of biodegradable polymers could potentially accommodate reasonable drug loadings can be used to deliver drug in a continuous and controlled fashion (Freitas *et al*., 2005). Owing to their micron sizes, they can be ingested or injected. These devices practically act as a reservoir releasing their content at a relatively slow rate over a prolonged time allow less frequent administrations, thereby increasing patient compliance and reducing discomfort, protection of the therapeutic compound within the body, and maintaining a more-constant drug level in the blood (Freiberg and Zhu, 2004).

In some cases, particulate carriers have been devised for protecting the active molecules against the host; e.g. blood, lymph and digestive juice (Niwa *et al*., 1993). By controlling drug input with a modified release dosage form, it is possible to maintain the plasma drug concentration at the desired level with minimal fluctuations, meanwhile, providing a prolonged therapeutics effect with a reduced incidence of side effects. An efficient delivery strategy will also lead to cost efficiency (Akhtar and Agrawal 1997). Various parenteral microparticles drug delivery systems have been developed based on biodegradable polyesters polymers (Johansen *et al*., 2000; Birnbaum and Brannon-Peppas, 2003).

The delivery of chemotherapeutic agents using polymeric microspheres has become one of the most popular areas of research because of the possibilities of reducing toxicities and localising the drug delivery (Liggins *et al*., 2000 and Wang *et al*., 2005). Site-specific delivery offered by microparticulate system can also improve the biological effects of poorly water-soluble drugs with low bioavailability and short lives (Akhtar and Agrawal, 1997 and Hussain *et al*., 2002). The above examples have demonstrated the advantageous features of microsphere systems. To summarise, employing a microsphere delivery system could potentially offer to accomplish the purposes listed below:

i. A prolonged controlled release (i.e. controlled release of the therapeutic agents)

ii. Offers protection (i.e. host the entrapped drugs to increase their bioavailability)
iii. Localised effect (i.e. direct delivery to a target/specific site by injection etc.)
iv. Amplification of adjuvant effect (i.e. spherical depots offer high surface areas for drug diffusions therefore increase the contact between the drugs and target site.)

There are various methods for preparing microspheres and for examples, solvent evaporation, organic phase separation, spray-drying or supercritical fluid technology amongst which has been widely applied to tailor made the targeted systems. Spray-drying method is widely employed in the pharmaceutical industry and has been investigated by several researchers as a method for formulating biodegradable microparticles (Freitas and Muller, 1998 and Yoo *et al*., 1999). Considering the laboratory condition and availability of facility, a traditional single emulsion method based on the solvent evaporation was employed in this thesis to produce the drug-loaded microsphere system.

3.4.1 Production of Microspheres

Solvent evaporation and phase separation are probably the commonest techniques used to prepare microspheres due to the simplicity of its preparation mode. A range of mechanisms involved in the preparation process are subjects of investigations by a number of authors such as Rafati *et al*. (1997), Yang *et al*. (2001), Freitas *et al*. (2005), Mainardes and Evangelista, (2005). From preliminary experiments, it was decided that solvent evaporation technique will be used as the main technique for this thesis. The reasons are:

i. This technique permits small working volumes, which is cost effective for multiples trials and experiments.
ii. The procedures involved in this technique are easy to manipulate therefore allowing different production conditions to be investigated.
iii. This technique is rapid and the whole production process is not lengthy.

The two main methods of the solvent evaporation technique are single and double emulsions methods. The element that distinguishes between single and double or multiple emulsions is the hydrophobicity of the drugs used. For single emulsion, because the method involves an aqueous emulsion, the drug being encapsulated in the microspheres are limited to those that have low water solubility. A simple definition of an emulsion is the dispersion and stabilisation of one liquid within another to which it is immiscible.

3.4.2 Solvent Evaporation – Single Emulsion Method

Sansdrap and Moës (1993), and Freitas *et al*. (2005) have presented the microencapsulation technique using this method. The process involves emulsification of a polymer solution-containing drug (either dissolved or in suspension) into a second, immiscible liquid phase containing an emulsifier to form a dispersion of drug-polymer-solvent droplets. The solvent is removed from the dispersed droplets by applications of heat, vacuum, or by evaporation as the drug-loaded microsphere solidifies. They can then be separated by filtration or centrifugation, washed, and dried. The process can be basically divided into four stages:

i. Dissolution or dispersion of the drug often in an organic solvent containing the matrix forming polymer.
ii. Emulsification of this organic phase in a second continuous (frequently aqueous) phase immiscible with the first one.
iii. Extraction of the solvent from the dispersed phase by the continuous phase, which is accompanied by solvent evaporation, transforming the droplets into solid spheres.
iv. Harvesting and drying of the solid spheres.

3.4.3 Solvent Evaporation – Double Emulsions

A typical procedure for a double emulsion method is illustrated in Figure 3.6. This system is suitable for hydrophilic compound and compound with low solubility in the organic solvent (used to dissolve the polymer).

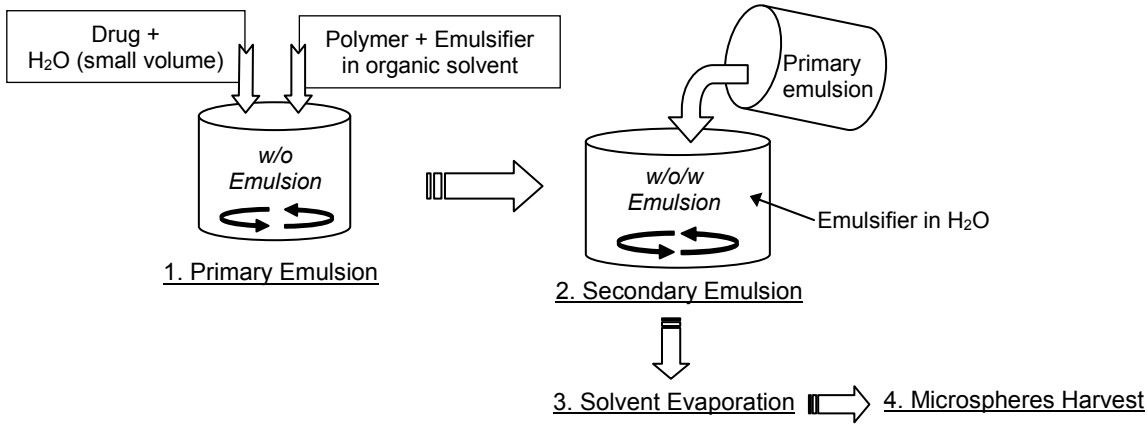

Figure 3.6: Schematic diagram of a w/o/w emulsion process. The primary w/o is formed by homogenising a polymer solution and a drug solution (usually aqueous). This emulsion is then added to a larger aqueous volume containing emulsifier to form the w/o/w emulsion.

The drug is first dissolved in water and emulsified in an organic phase containing the polymer and an emulsifier; forming the primary w/o emulsion. This emulsion is then

dispersed in another aqueous phase containing more emulsifier. Complication with this type of emulsion could occur when the primary emulsion is not sufficiently stabilised and the droplets containing the dissolved drug are lost to the aqueous phase in the secondary emulsion.

Primarily, the solvent of choice must be immiscible or only slightly soluble in the continuous phase (i.e. water). Most importantly, the solvent must has a lower boiling point than that of the water phase. If dissolution of the drug in the polymer solution is desired, then the ability of the solvent to dissolve the polymer and drug needs to be considered. Table 3.3 describes the basic criteria for selecting the working solvent.

Table 3.3: Important criteria for dispersed and continuous phase solvents (Watts *et al*., 1990).

Dispersed Phase Solvent	Continuous Phase
Ability to dissolve chosen polymer	Immiscibility with the continuous phase solvent.
Ideally, the solvent should be able to dissolve the drug.	Inability to dissolve polymer.
Immiscibility with the continuous phase solvent.	Low solubility toward drug.
Lower boiling point than continuous solvent phase.	Higher boiling point than dispersed phase solvent.
	Allows easy recovery and clean-up of microsphere

Preliminary work involving microspheres production was carried out using solvent ethyl acetate. Ethyl acetate is classified as a Class 3 solvent by the International Conference on Harmonisation (ICH Q3C (R3), 2005). It is less toxic than the commonly used dichloromethane (DCM) in PLGA microsphere production. Ethyl acetate has a high boiling point, i.e. 77^{o}C, and preliminary work showed that the nascent droplets required more than four hours to solidify. Collection before this resulted in non-uniform and misshapen microspheres. DCM was replaced as the working solvent for this work for its lower boiling point; i.e. 40 °C which would aid solvent removal during solvent evaporation stage in microsphere production. DCM is a class 2 solvent according to ICH Q3 (R3).

3.5 Hollow Fibres for Controlled Delivery

The development of hollow fibres started in the 1970's. Pitt and Schindler (1979) developed subdermal delivery system based on tubular implant made of poly(ε-caprolactone). Different

post-treatments were performed on the tubular implant in order to modify the porosity and the connectivity of the interior pores. Pitt *et al*. (1979) found that the dense structure of the implant required further adjustment to offer a better drug release kinetic. Few years later, Eenink *et al*. (1987) produced PLA hollow fibre with porous structure using a dry-wet spinning process based on the phase separation technique.

By applying different spinning conditions, Eenink *et al*. (1987) found that the property of the fibre can be modified to favour better drug release rates. The drug release rate appeared to be dependent on the fibre wall structure, and a porous structure was concluded by Eenink *et al*. (1987) to be necessary for better control in drug release. Since then, various drugs-loaded fibre systems have shown promising results including a predictable first order release kinetic (Dunn *et al*., 1982 and 1987; Eenink *et al*. 1987).

Zilberman (2007) developed bioresorbable PLGA fibres loaded with paclitaxel and the product demonstrated good mechanical properties. With a desired drug release profile, Zilberman (2007) concluded that they are ideal for scaffolds for tissue regeneration applications and other basic medical implants. PLGA hollow fibres have been developed as scaffolds for tissues engineering for their unique structures (Morgan *et al*., 2007 and Ellis and Chaudhuri, 2007).

Similar to microsphere production, the fibre production parameter can be altered to predetermine their final property for specific application. Tailor-made hollow fibre membranes with controllable structures improve their biomedical applications based on their mass transfer property, which controls the transport of permeate species (Perepechkin and Perepechkina, 1999).

The hollowness of the hollow fibre offers an opportunity to load additional drug dosage into the device. While drug can be encapsulated within the wall of the hollow fibre, in this case, it is intended that drug solution and drug-loaded microsphere to be loaded into the lumen of the fibre. This requires investigation into the behaviour of the new combined system. The studies of drug release from these systems are presented in Chapter Nine.

Preliminary work has been carried out to produce hollow fibre-patch and the final product is shown in Figure 3.7. The ultimate purpose of developing this drug-loaded fibre patch is that the device can act as a self-releasing device. For instance, after surgical removal of a tumour,

a chemotherapy drug-loaded fibre patch can be attached to the peritoneum in order to kill residual cancerous materials (Gilby, 2008). Different drugs loadings in the fibre wall and lumen can also be formulated for a co-delivery system. For the objective of this thesis, the development of hollow fibres and their drug release characteristics require an understanding of the membrane structure formation. This set the purpose for the next section and the concept will be applied to the production of PLGA hollow fibre.

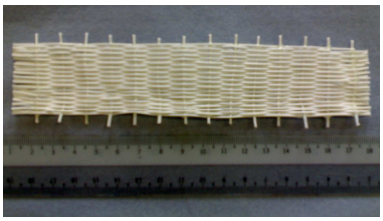

Figure 3.7: A "woven" 75:25 PLGA hollow fibre patch.

3.5.1 Production of Hollow Fibre

The hollow fibres developed in this thesis take the characteristic of a porous-asymmetric membrane. Synthetic membranes with asymmetric structures have very thin (0.1 to 1 μm) skin layer on a highly porous sublayer of 100-200 μm (Bungay *et al*., 1986). The phase inversion technique is a common method employed to produce asymmetric membranes. Phase inversion is a process whereby a polymer is transformed in a controlled manner from a liquid to a solid state (Mulder, 2000). The phase inversion of polymer to form a membrane can be achieved in a number of ways and by convention, Drioli and Nakagaki (1997) summarised three main methods as following:

i. Thermogelation of a two-component mixture - a process in which the cooling of a two component mixture from a temperature where both components form a homogenous phase, to a temperature where two phases will form, one phase will be the solid forming porous system.

ii. Evaporation of a nonsolvent from a three component mixture - a mixture of polymer, a solvent and nonsolvent will have: (1) a region where there will be homogenous phase and (2) a region of composition where two distinct phases will form. By starting from a composition in the homogenous region and evaporating the solvent, the system moves into the two phase region forming a liquid and a solid phase. This results in the formation of a solid phase with porous structure. The two-phase region is known as the miscibility gap in a ternary phase diagram (Figure 3.8).

iii. The third method is the mechanism through which the addition of non-solvent to a two mixture system causes precipitation. This method is known as the immersion precipitation and it is the method employed in this thesis.

Immersion precipitation achieves the phase inversion by immersing a solvent/polymer mixture cast in the desired shape into a nonsolvent coagulation bath. The behaviours of these three components can be related using a ternary phase diagram (Figure 3.8). One of the liquids will be rich in polymer the other lean in polymer. The addition of the nonsolvent to the two component mixture (a polymer and a solvent) rapidly moves the mixture from a homogenous phase to the miscibility gap. This is because of the exchange between solvent and nonsolvent. At the point where the miscibility gap is reached, a polymer rich phase and a polymer lean phase are formed. As the solvent/non-solvent exchange continues, the polymer rich phase reaches a point where it can be considered as solid.

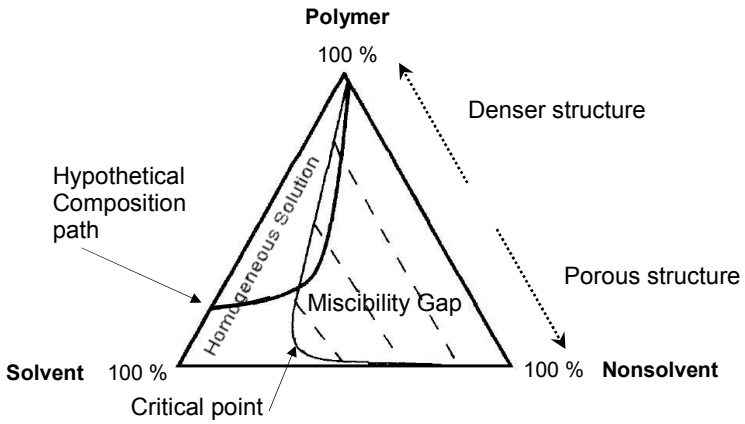

Figure 3.8: Ternary phase diagram relating the three components; polymer, solvent and nonsolvent to the structure formation of hollow fibre membrane (adapted from Chung, 1997).

The immersion precipitation can be characterised using thermodynamics principle because the process begins with a demixing process. The initial procedure for hollow fibre formation is to prepare a homogeneous (thermodynamically stable) polymer solution. This will often correspond to a point on the polymer-solvent axis. The demixing process is the addition of a nonsolvent into the polymer solution that causes the solution to become thermodynamically unstable. During the demixing, if the solvent/nonsolvent exchange is very rapid, the composition path will enter the miscibility gap almost immediately after immersion. When the miscibility gap is entered at compositions above the critical point, nucleation of the polymer-lean phase occurs. Phase separation is thus initiated via the nucleation and growth of a polymer-lean phase.

In a slow or delayed demixing, the composition of the solution remains in the homogeneous region for a certain period of time. During this the composition in the polymer solution gradually shifts to higher nonsolvent concentration until finally the miscibility gap is entered. The solvent/nonsolvent exchange continues as the demixing process continues. Eventually, both the compositions of the polymer-rich -lean phases will move towards the polymer-nonsolvent axis.

The rapid and delay demixing result into two different types of membrane structures. Rapid demixing usually produces thin and less dense skin layer but with open structure in the sublayer. Delay or slow demixing usually produces thick and denser skin layer with less open or interconnect sublayer (Bungay *et al*., 1996). The lower porosity in the skin layer compared to the porosity of the sublayer can be related to the high polymer concentration in the interfacial layer between the polymer solution and the nonsolvent at the instant of demixing.

For semi-crystalline polymer or amorphous polymers, gelation is a common phenomenon for solidification process (Mulder, 2000). When gelation occurs, a dilute or more viscous polymer solution is converted into a system of infinite viscosity. In semi-crystalline polymers, gelation is often initiated by the formation of microcrystallites. For amorphous polymers, it often involves a sol-gel transition. A sol-gel transition occurs where the solution gels. The addition of a nonsolvent induces the formation of polymer-polymer bonds and gelation occurs at a lower polymer concentration.

A work by Kong and Li (2001) investigated a range of effects in the production of hollow fibre membranes. They found that water permeation rate increases and solute rejection decreases as the polymer concentration is reduced. This is translated to a condition of higher flux and porosity. Barth *et al*. (2000) suggested that the following parameters could affect the final performance of the hollow fibre:

i. Composition of polymer solution (polymer, solvent, additives etc)
ii. The non-solvent or the mixture of non-solvents,
iii. The temperature of the polymer solution, the coagulation bath or the environment,
iv. The amount of dry phase inversion before wet phase inversion and the humidity, and among others.

Barth *et al*. (2000) conducted their investigations using polysulfone (PSF) polymer, N-methyl-pyrrolidone (NMP) as solvent, and water or acetone as nonsolvent. Their studies

concluded that the phase inversion process leads to the development of long finger-like cavities beneath the surface of the membrane. These became smaller when the concentration of PSF was increased in the casting solution. In another work by Deshmukh and Li (1998) revealed that the coagulation rate in hollow fibre has a great effect on the structure of the membrane produced. Rapid coagulation results in large finger-like cavities whereas slow coagulation results in a porous sponger like structure.

For this thesis, the hollow fibre is developed for its structural characteristic which may be beneficial to drug release kinetic. An example of the cross sectional structure of a hollow fibre is shown in Figure 3.9. These structural characteristics are associated with high mass transfer resistance (Zhang and Cussler, 1985; Yang *et al*., 2001b and Tai, 2007) and could act as a barrier to rapid drug release. The dense "finger-like" structures adjacent to the skin layers were anticipated to provide additional control in drug release thereby prolonging the drug release period. More detailed morphology characterisation of PLGA hollow fibre will be presented in Sections 5.3 and 6.4.

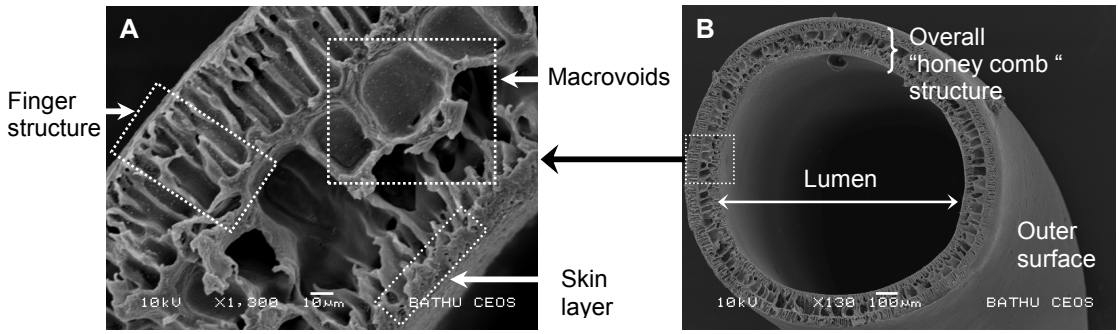

Figure 3.9: Cross section of a 72:25 PLGA hollow fibre prepared using the phase inversion technique. (A) Detailed fibre wall structure and (B) Cross sections of the hollow fibre.

CHAPTER 4: MATERIALS AND METHODS

This chapter describes the methodology applied to develop the drug-loaded PLGA microspheres (Section 4.1), hollow and solid fibres (Section 4.2). Sections 4.3 and 4.4 describe the methods used to determine drug concentration, drug loading and encapsulation efficiency. Section 4.5 describes the *in vitro* drug release analysis while Section 4.6 describes characterisation of PLGA microspheres followed by characterisation of PLGA hollow and solid fibres in Section 4.7.

4.1 The Development of Drug-Loaded Microspheres

4.1.1 Materials

HPLC grade dichloromethane (DCM) used as solvent and polyvinyl alcohol (PVA) used as emulsifier were purchased from Fisher Scientific, UK.

Table 4.1: Biodegradable polymers purchased from Lakeshore Biomaterials, Inc., USA.

Polymer	Grade	Molecular Weight & Inherent Viscosity	Abbreviation
50:50 Poly(DL)lactide-co-glycolide	GMP	51 k Da, 0.57 dL/g	50:50 PLGA
65:35 Poly(DL)lactide-co-glycolide	GMP	118 k Da, 0.79 dL/g	65:35 PLGA
75:25 Poly(DL)lactide-co-glycolide	GMP	113 k Da, 0.75 dL/g	75:25 PLGA

** All PLGA are with carboxylic acid end-capped to improve degradability.*

Table 4.2: Anaesthetic and chemotherapy drugs used for the production of drug-loaded PLGA devices.

Model Drug	Grade	Supplier	Abbreviation
Lidocaine (anaesthetic)	GMP	Spodefell Ltd., UK	LID
Cisplatin (chemotherapy)	USP 27	Lianyungang Unionrun Foreign Trade Co. Ltd., China.	CPt

4.1.2 Equipment

Table 4.3: List of equipment used in microspheres production.

Equipment/Instrument	Manufacturer	Functions
Homogeniser (IKA-Ultra-Turrax® T25)	Janke & Kunkel GMBH & Co. KG., Germany	Creation of single or double emulsions for microspheres production
Centrifuge (IEC CL10)	Thermo Electron Corporation, UK	Harvest of microspheres

4.1.3 Production of Microspheres – Single Emulsion Method

The desired concentrations of drug and polymer were prepared into DCM and left mixing on a roller mixer for at least three days to ensure thorough mixing. Typically, 10 g of the drug/polymer solution was injected into 100 ml of PVA solution and homogenised in order to produce a uniform w/o emulsion (Figure 4.1A and B). After that, the nascent microspheres were transferred to magnetic-stirring for solvent evaporation for 3 h at 750 rpm as the microspheres solidify (Figure 4.1C). Examples of working concentrations are such as 10 % (w/w) polymer, drug-to-polymer ratio of 1:2 and 0.5 % (w/w) PVA. Investigations into the effects of these parameters are presented in Section 5.1.

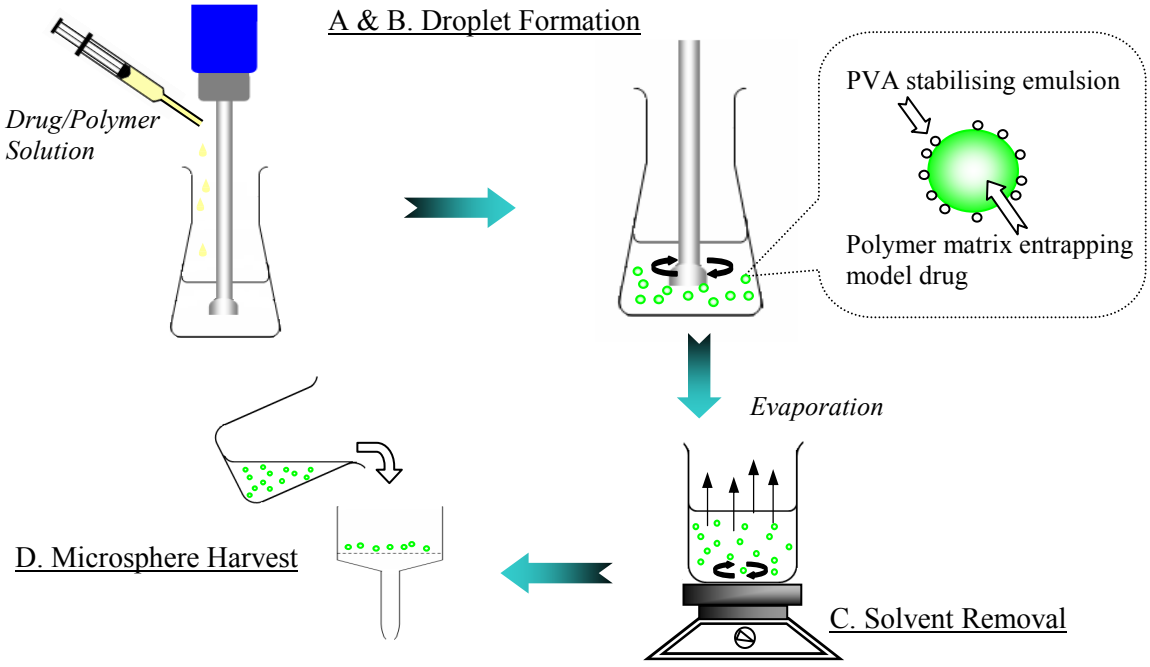

Figure 4.1: The production of microsphere: (A) Drug/polymer mixture is injected into PVA solution using a syringe with 17G needle and (B) undergoes homogenisation. (C) The nascent microspheres are transferred to magnetic stirring. (D) The harvesting step involves a vacuum filtration system.

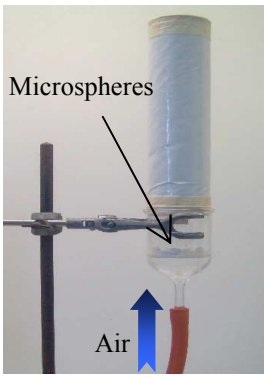

Figure 4.2: The filtered microspheres are placed in a sintered glass funnel in which a mild current of air is passed through to dry the microspheres.

After the magnetic stirring, the resulting microspheres (as suspension in PVA solution) were transferred to 50 ml centrifuge tubes for centrifugation at 1000 rpm for 3 min. The supernatant (i.e. PVA solution) was replaced with 50 ml fresh distilled water and underwent centrifugation again. Lastly, for harvesting step; the microspheres were filtered (Figure 4.1D) and washed once with distilled water, collected and air dried (Figure 4.2).

4.2 The Development of Drug-Loaded Hollow and Solid Fibres

4.2.1 Materials

Polymers and drugs used for manufacturing drug loaded hollow and solid fibres were as listed in Tables 4.1, 4.2 and 4.3 respectively. Solvent used in this case was HPLC grade 1-methyl-2-pyrrolidone (NMP), purchased from Sigma-Aldrich, UK. NMP is highly miscible with water and this criterion is necessary to achieve the phase inversion effect.

4.2.2 Equipment

Table 4.4: List of equipment used in hollow and solid fibres production.

Equipment/Instrument	Manufacturer	Functions
Syringe Pump (KDS 100)	KD Scientific Inc., USA	Delivery of polymer/drug solution during spinning process.
Micropump (REGLO-Z)	ISMATEC SA, Labortechnik, Switzerland	Delivery of internal coagulant during spinning process.
Motorised Roller (AEG AM63NT4)	Spaggiari Trasmissioni S.P.A., Italy	Collection of nascent fibres during spinning process.

4.2.3 Spinning of Hollow and Solid Fibres – Phase Inversion Technique

The desired concentrations of drug and polymer were prepared into NMP and left mixing on a roller mixer for at least three days. Distilled and tap water were used as the internal and external coagulants respectively. Prior to spinning, the drug/polymer dope was degassed in a desiccator for 1-2 h using a vacuum pump to remove gas bubbles. Figure 4.3A shows the spinning apparatus used to spin PLGA hollow fibre and Figure 4.3B shows the solid fibre spinning system. All spinning work was carried out at room condition.

For spinning of hollow fibre, 100 ml of drug/polymer dope was collected into a syringe and mounted onto a syringe pump. The dope was then extruded into a tube-in-orifice spinneret, with a simultaneous flow of the internal coagulant through the central tube in the spinneret.

This produces a lumen in the centre of the nascent hollow fibre. The extruded nascent hollow fibre from the spinneret then passed through a water bath (external coagulant) in which NMP diffused into the aqueous phase and the nascent hollow fibre continue to solidify. The air gap between the spinneret and water level was fixed at 10 cm. The nascent hollow fibre was gently driven into a washing tank by a motorised roller, at a typical speed of 5 rpm. A suitable rotation rate is important to prevent mechanical dragging of the fibre. The fibre was immersed in the washing tank for at least 24 h as the nascent fibre solidified before they were collected for drying.

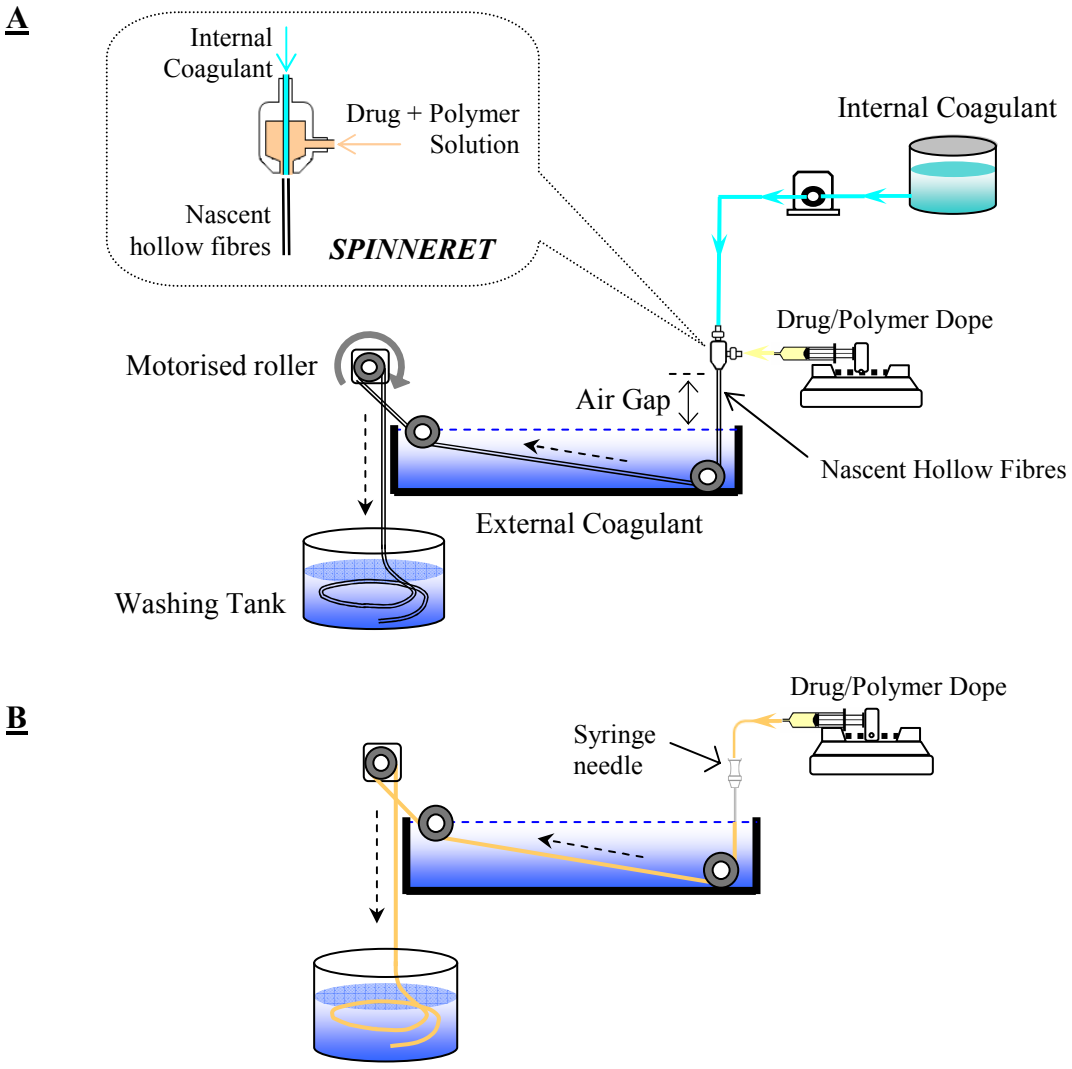

Figure 4.3: Schematic diagrams (A) Hollow fibre spinning system. The internal coagulant or bore liquid flow rate was usually maintained at 1 - 2 ml/min. (B) Solid fibre spinning system. The spinneret was replaced with a needle (17G) to extrude polymer/drug solution with a rate of 2-3 ml/min.

For spinning of solid fibre, a spinneret was not used and the polymer/drug solution in this case, was extruded through a syringe needle (17G) directly into the water bath such that the

needle tip was just reaching the surface of the water bath as illustrated in Figure 4.3B. The collection and washing of solid fibres remained the same as in hollow fibre production.

4.3 Determination of Drugs Concentrations in PLGA Devices

4.3.1 Anaesthetic Drug Concentration Determination

Lidocaine concentration was determined using a Cecil 3000 Series uv spectrophotometer (Cecil Instrument, UK) with wavelengths, λ = 262.5 nm. Drug solutions with desired concentrations were prepared by dissolving the drug crystals in phosphate buffer saline and subsequent dilution with the buffer. The calibration curve of known drug concentrations with corresponding absorbances for lidocaine is shown in Figure 4.4.

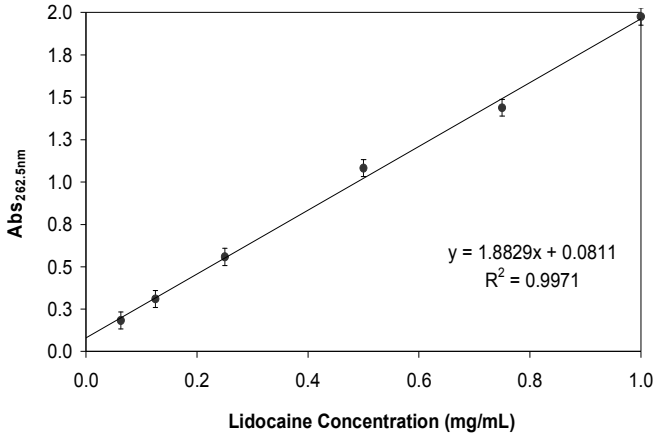

Figure 4.4: Calibration curve with lidocaine concentration ranged from 0.05 to 1.0 mg/ml.

4.3.2 Chemotherapy Drug Concentration Determination

Cisplatin concentration was measured based on the platinum content in the drug molecule using a Model 3110 atomic absorption spectrometer (AAS) (Perkin Elmer Ltd., UK), equipped with a platinum cathode lamp set at a λ = 265.9 nm. The platinum content in the sample was measured directly by aspirating the sample solution into the AAS at a rate of 1.0 ± 0.2 ml/min for 20 sec. The cisplatin content was determined using the calibration curve shown in Figure 4.5 constructed using standard platinum solution. Platinum standard solution (1 g/l) in 2M HCl was purchased from Sigma-Aldrich, UK.

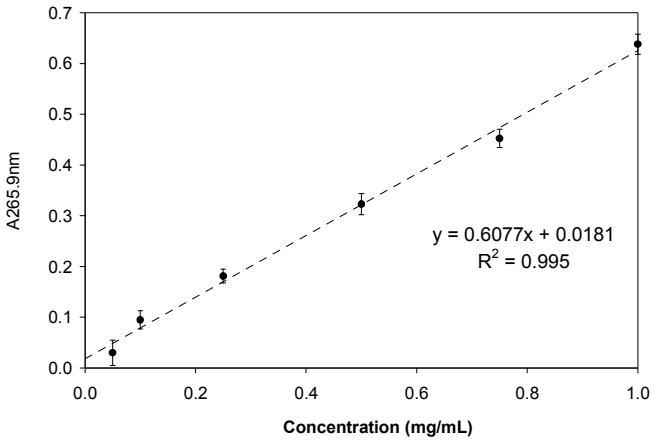

Figure 4.5: Calibration curve with cisplatin concentration ranged from 0.05 to 1.0 mg/ml.

4.4 Drug Loading and Encapsulation Efficiency

Typically, 5 ml of DCM was used to dissolve a 0.20 g of lidocaine-loaded sample and the mixture was left for complete dissolution overnight. After that, 5 or 10 ml of 0.1M H_2SO_4 solution was added to extract the drug and left overnight. The aqueous phase was then collected and measured according to the method described in Section 4.3.1. 0.1M H_2SO_4 solution was used to normalise absorbance readings while all the drug loaded samples were measured against blank samples. The drug loading (DL) and encapsulation efficiency (EE) were estimated using Equations 4.1 and 4.2 respectively.

$$\text{DL (\%)} = \frac{\text{Total Drug Encapsulated (mg)}}{\text{Total Sample Used (mg)}} \times 100\% \quad (4.1)$$

$$\text{EE (\%)} = \frac{\text{Total Drug Encapsulated (mg)}}{\text{Total Drug Used in Preparation (mg)}} \times 100\% \quad (4.2)$$

Acid digestion was used to process cisplatin-loaded samples. Nitric acid (HNO_3) and hydrochloric acid (HCl), used as aqua regia were purchased from Fisher Scientific, UK. A 0.20 g of cisplatin-loaded sample was digested with 4 ml of aqua regia (1:3, HNO_3:HCl) and dried at 85^{o}C for 45 min to just dryness. The drying duration and temperature were altered in order to produce solution-least residue for further processing. Depending on the sample, this procedure was repeated once or twice in order to achieve complete sample digestion to yield an absolute platinum content. 5 or 10 ml of 2M HCl were then added and the solution was aspirated to the AAS for the determination of cisplatin concentration (Section 4.3.2). The DL and EE were estimated using Equations 4.1 and 4.2 respectively.

4.5 *In vitro* Incubation of PLGA Devices

For both *in vitro* drug release and degradation analyses, all samples were incubated in a shaking water bath (Grant Instrument, UK) maintained at 37.0 ± 0.5 ^{o}C, with a back-forth shaking of 150 rpm for up to thirty days. 0.1 M phosphate buffered saline solution (PBS) was prepared from ready-made tablets purchased from Oxoid Ltd., UK.

4.5.1 *In vitro* Drug Release Analysis

Approximately 0.20 g of sample was immersed in 10 ml of PBS (pH 7.4) and incubated in the condition described above. For hollow or solid fibres, each sample constituted fifteen 8 cm fibres were immersed in 15 ml of PBS. The total weight of twenty fibres was approximately 0.20 g. Control samples were prepared in a similar way but using blank microspheres or hollow/solid fibres. The frequencies of absorbance measurements and PBS refreshing may vary during the first day depending on the released drug concentration. Typically, initial measurements were taken hourly for the first six hours and later at twelve hour intervals or daily. Drugs concentrations were determined using methods described in Section 4.3 and normalised against the blanks accordingly.

4.5.2 *In vitro* Degradation Analysis

Sample preparation for PLGA microspheres, hollow and solid fibres were the same as in Section 4.5.1. In order to monitor the degradation of PLGA samples, samples were collected at tenth, twentieth and thirtieth days for SEM imaging (Section 4.6.2) and mass loss analysis using Equation 4.3:

Percentage mass loss due to degradation, $\% M_{Loss} = [(M_o - M_n) / M_o] \times 100\ \%$ (4.3)

M_o and M_n are the weights of the sample before and after degradation respectively.

4.6 Characterisation of PLGA Microspheres

4.6.1 Particle Size Analysis

Particle size was measured using a Mastersizer X (Malvern Instruments, UK) with a laser diffraction with range lens of 300 mm, a laser obscurity between 12 and 25%. Briefly, in a laser diffraction particle analyser, a beam of laser light is projected through an aperture to the sample particles and as a result, the incident light is diffracted and scattered onto a lens. This lens focuses the scattered light onto a detector array and using Mie theory (which solves Maxwell's equations for the boundary conditions of a spherical particle), the particle size

distribution is inferred from the collected diffracted light data. Each sample was analysed a total of 2000 times by the system to give a mean particle size.

The measurement system for PLGA microspheres was based on the wet dispersion in which the sample is suspended in a compatible solvent that is also transparent to the laser beam. A sample (~0.1 g) was prepared into a glass vial containing 2 ml of cyclohaxane and lechitin (1 mg/ml) and sonicated for 5 min in order to produce a homogeneous suspension. After that, a few drops of this suspension were added to the sample chamber equipped with a magnetic stirring bead. The latter feature prevents the suspension from precipitating whereas lechitin helps to stabilise the suspension.

4.6.2 Scanning Electron Microscopy (SEM)

In order to examine the surface morphologies of PLGA devices, small amount of sample was evenly sprinkled (for microspheres) or placed (for fibres) onto a carbon adhesive disc mounted onto an aluminium stub. Samples were coated with a thin layer of gold for 5 min in an Edwards Sputter-coater S150B and viewed using a JEOL JSM 6310 electron microscope operating at a typical 10k V accelerating voltage, 20^{o}C and 10^{-5} Torr. For assessing the internal structure of PLGA microspheres, a cryo-fractioning technique was used. A basic protocol for cryo-fractioning sample preparation is illustrated in Figure 4.6.

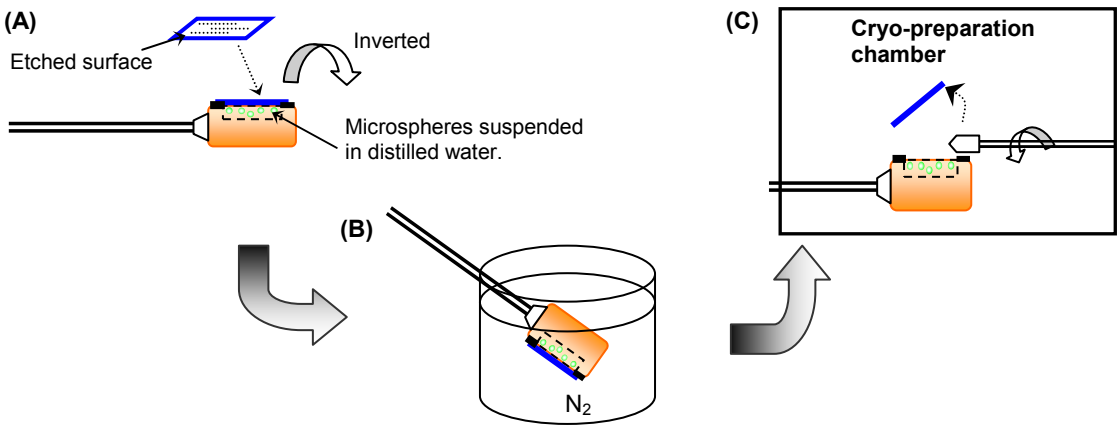

Figure 4.6: Sample preparation involves in cryo-fractioning of microspheres prior to SEM imaging.

A cup-shaped sample holder was filled with a suspension of microspheres in distilled water and covered by a thin rectangular sheet of scratched aluminium (Figure 4.6A). The sample holder aperture was sealed by anchoring each end of the aluminium rectangle to a piece of sticky carbon adhesive disc. The whole apparatus was inverted to prevent the sinking of

microspheres, and then plunged into liquid N_2, "plunge freezing" (Figure 4.6B). In quick repetition, the sample holder was introduced into the cryo-preparation chamber which was maintained under vacuum and -165^{o}C (Figure 4.6C). The scratched aluminium rectangle was then removed with a cold blade causing fracturing of the ice crystal at the specimen surface. The specimen was then transferred into the SEM chamber and mounted onto a stage at -170^{o}C. The stage temperature was then raised to -80^{o}C in order to sublime the ice slowly hence revealing the fractured microspheres. After that, the specimen was transferred back into the preparation chamber, for gold-coating and ready for imaging.

4.6.3 Confocal Laser Scanning Microscopy (CLSM)

In order to examine the distribution of drug within the microsphere, CLSM was used. PLGA microspheres were prepared according to method described in Section 4.1.3, but with trifluoromethyl umbelliferone (4-TFMU) premixed to the polymer solution. PLGA-to-4TFMU of ratio of 1:1 was used. A small amount of sample was placed between two glass slides with minimal mineral oil added to hold the cover slides in place. The sample containing-slides were then mounted onto the microscope sample stage. The distribution of entrapped 4-TFMU in PLGA microspheres were observed using a Carl Zeiss LSM 510 (Germany) microscope equipped with Argon photon laser (laser power, 10-75%) with excitation wavelength, λ = 488 nm. The pinhole size was varied from 169 to 1000 μm. Image viewing and processing were performed using LSM 510 software. 3 dimensional (3D) projection is generated using a series of 2 dimensional (2D) micrographs.

4.6.4 Disc Making

This experiment was conducted in order to assess microspheres swelling due to hydration using a hydraulic press (Specac Ltd., UK). Stainless steel evacuable pellet die was used to compact PLGA microspheres into a disc under a hydraulic pressure of 1-3 tonnes. The resulting disc; 7 mm in diameter and approximately 3 mm in thickness was then treated in PBS and incubated in the condition described in Section 4.5.

4.7 Characterisation of PLGA Hollow and Solid Fibres

4.7.2 Scanning Electron Microscopy (SEM)

The morphology of both hollow and solid fibres were observed using SEM. The specimen preparation and imaging conditions were similar those described in Section 4.6.2.

4.7.3 Gas Permeation Analysis

Gas permeation analyses were conducted on hollow fibres in order to assess the permeability of the PLGA hollow fibres. The analysis generates information on mean pore size and effective surface porosity. The apparatus set up is illustrated in Figure 4.7A. A bubble metre was used to measure the volumetric flow rate of permeate gas through the fibre module.

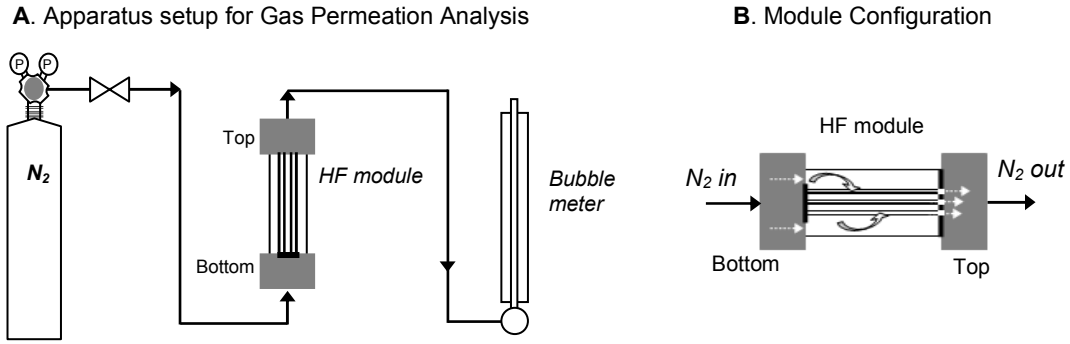

Figure 4.7: (A) The apparatus set up for gas permeation analysis on PLGA hollow fibres. The N_2 is fed into the bottom of the hollow fibre (HF) module and the permeate gas is connected to a bubble meter. (B) Configuration of HF module.

The module containing the hollow fibres was prepared by sealing one the end of the hollow fibre using Epoxy® resin while the other end remained open. The open end fibre was fixed to the top of the module, as illustrated in Figure 4.7B. This configuration allows the gas to permeate through the fibre wall into the lumen and the permeate gas from the lumen subsequently travels into a vertical bubble meter from its bottom.

Measurements were carried out under operating pressure ranged from 1 to 2 M Pa. Time measurements were recorded for the bubbles created by the permeate gas to travel along a predetermined distance along the bubble meter. The time was then used to calculate the gas permeation flux. The gas permeation flux was calculated using the Equation 4.4 and plotted against mean pressure. The gradient and intercept from the plot equal to P_o and K_o respectively in Equation 4.5. The mean pore diameter can thus be calculated. Equation 4.6 was to calculate the effective surface porosity.

Gas permeation flux, $J = NA / P_{in}$ (4.4)

Mean pore diameter, $\bar{r} = \left(\frac{16}{3}\right)\left(\frac{P_o}{K_o}\right)\left(\frac{8RT}{\pi MN_2}\right)^{0.5} \mu_{N2_2}$ (4.5)

Effective surface porosity, $\frac{\varepsilon_p}{L_p} = \frac{8\mu_{N2}RTP_o}{\bar{r}^2}$ (4.6)

Where N is the molar flow rate of N_2 (mol/s), A is the membrane surface area (m^2), P_{in} is the pressure inside hollow fibre (2.01 M Pa), P_o is the gradient of plot (mol/s.Pa^2.m^2), K_o is the intercept of plot (mol/s.Pa^2.m^2). R is the universal gas constant (8.31 kJ/k/mol.K), M is the molecular weight of N_2 (2.7 x 10^{-2} kg/mol), μ_{N2} is the viscosity of N_2 (1.78 x 10^{-5} Pa.s), and T equals 298 K.

4.8 Data Analysis

For comparison between two means, independent *t-test*, two tailed with $p < 0.05$ was used to test the significant in the differences. Where more than two means were involved, analysis of variance (ANOVA-single factor, $p < 0.05$) was used instead. Single or non-linear regressions, and model fittings were done using software *R* and *Solver* from the *Microsoft'*s *Excel* with least squares method. Graph/plot representation shows the means from $n = 3$ or 5 with standard deviations.

CHAPTER 5: THE DEVELOPMENT OF PLGA DEVICES

This chapter reports the development of PLGA devices. The objectives were to establish the production conditions for producing PLGA microspheres and hollow/solid fibres. Section 5.1 presents the results and findings for PLGA microspheres production. The investigation into the production of PLGA hollow and solid fibres is presented in Section 5.2. More details of each development work are described in each section.

5.1 The Development and Production of PLGA Microspheres

This section is divided into two subsections. Section 5.1.1 studies the effects of homogenisation conditions, PVA and PLGA concentrations on microsphere size based on the single emulsion-solvent evaporation method. Section 5.1.2 presents the work involving the double emulsion-solvent evaporation method. For ease, 50:50 PLGA microsphere will be abbreviated as 50:50MS henceforth, similarly for 65:35 and 75:25 PLGA microspheres.

5.1.1 Single Emulsion Method - Effects of the Homogenisation Conditions, PVA and PLGA Concentrations on Microsphere Size

For each experiment, 10 g of polymer solution was homogenised in 100 ml of PVA solution. After that, the nascent spheres were transferred to magnetic stirring. Lastly, the resultant spheres were filtered, washed and air-dried. Detailed procedure for single emulsion method is previously described in Section 4.1.3. Table 5.1 tabulates the experimental condition for each investigation. Different homogenisations time and speed, concentrations of PVA and 50:50 PLGA were employed to produce 50:50MS. Five batches of microspheres for each experiment were produced and analysed for their sizes using laser diffraction method (Sections 4.6.1) and their morphologies using SEM imaging (Section 4.6.2).

Table 5.1: Experimental conditions employed in the studies of the effects of homogenisation conditions, PLGA and PVA concentrations on the size of 50:50 PLGA microspheres.

50:50 PLGA (% w/w)	PVA concentration (% w/w)	Homogenisation Time (min)	Homogenisation Speed (rpm)
15	1	15	6500
	3		
	5		
	10		
15	0.5	5	6500
		10	
		15	
		20	
15	0.5	15	6500
			9500
			13500
5	0.5	15	6500
8			
10			
15			

5.1.1.1 Results and Discussion

The formation of PLGA microspheres is illustrated in Figure 5.1. During the single emulsion method, the PLGA containing-DCM solution was homogenised into a PVA containing-water phase. An emulsion is thus formed because of the semi-immiscibility of the organic solution. The aqueous phase now contains multiple oil droplets or nascent microspheres. Possible coalescence between the droplets of emulsion is prevented by the presence of an emulsifier such as PVA. As the solvent diffuses out from these droplets, these nascent spheres solidify to form solid spheres. The latter process is described as solidification due to solvent diffusion. The dissolved solvent eventually evaporates at the air-liquid interface.

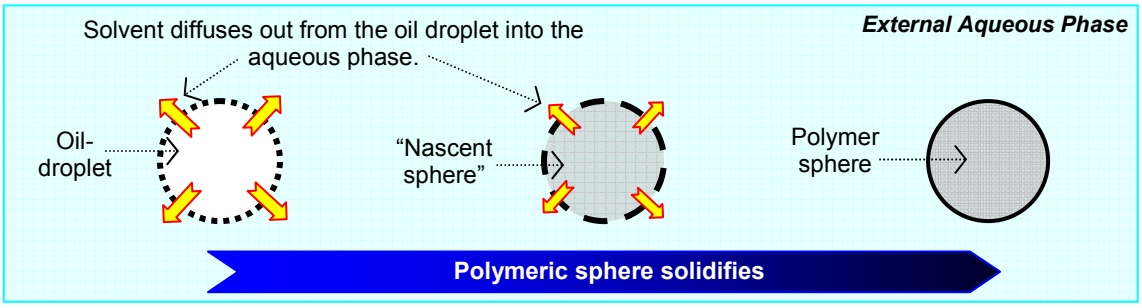

Figure 5.1: The mechanism of sphere formation from an oil-droplet to nascent sphere to polymeric sphere.

Classically, emulsifiers are amphiphilic compounds that have a hydrophilic (i.e. head group) and a lipophilic end (i.e. tail) and Figure 5.2 illustrates the functioning of an emulsifier. The emulsifier molecules organised themselves such that their tails adjoin in the organic droplet and their head in the opposite direction. Thus, a stabilised emulsion is formed and the coalescences between droplets are prevented. In this case, the PVA molecules are thought to absorb onto the surfaces of the oil/polymer droplets, and serving the same purpose as an emulsifier. Increase in emulsifier concentration will increase the stability of the emulsion (Cui *et al*., 2005). In the single emulsion method, a higher emulsifier concentration will result in a larger excess of emulsifier that adsorbs on the surface of the organic droplets. The end result is a decrease in the microsphere sizes (Sansdrap and Moës, 1993 and Boisdron-Celle *et al*., 1995).

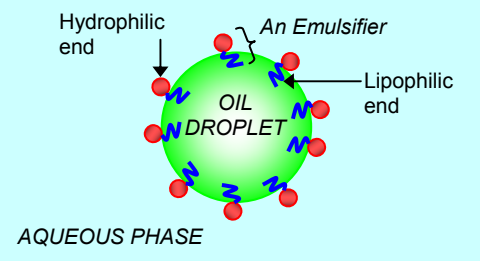

Figure 5.2:
The figure shows the functioning of an emulsifier stabilising an oil droplet in an aqueous phase.

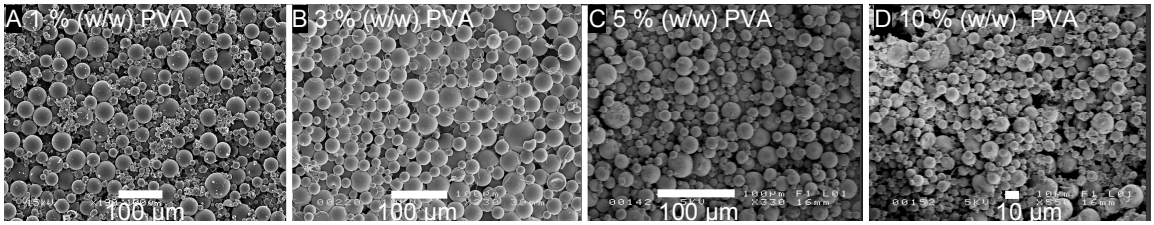

Figure 5.3: 50:50MS produced using (A) 1; (B) 3; (C) 5 and (D) 10 % (w/w) PVA.

Figure 5.3 shows the 50:50MS produced using different PVA concentrations. By visual comparison, 50:50MS produced using 10 % (w/w) PVA is probably the smallest amongst the others whereas 1 % (w/w) PVA produced the largest 50:50MS. The size distributions tend to be smaller for 50:50MS produced using 5 and 10 % (w/w) PVA. While SEM images show the surface morphology the microspheres, laser diffraction technique (Section 4.6.1) was used to estimate the particle size distribution. With particle size analysis, three diameter percentiles or percentage (%) undersize were produced for each sample. They are referred as the majority fraction (90%), minority fraction (10%) and, the 50% fraction which is also the median of the particle size. It is commonly referred to as the 50th percentile, D50 or D[v, 0.5]. The "v" denotes a volume distribution. The three percentiles or undersizes will be described as the D[v, 0.9], median size and the D[v, 0.1] henceforth.

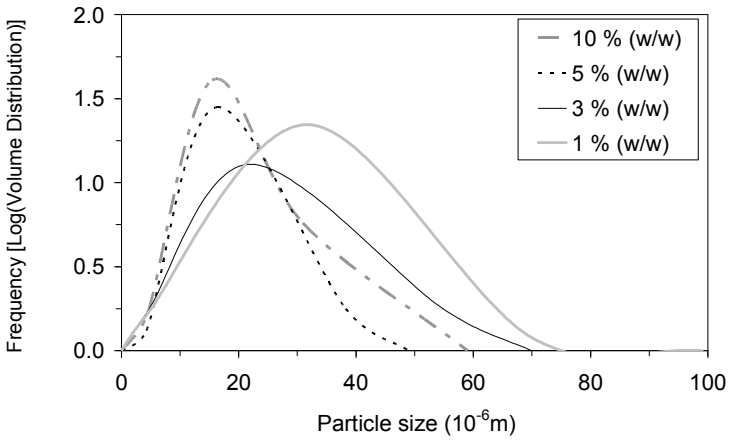

Figure 5.4: Results showing the effect of PVA concentration on the size distribution of 50:50MS.

Figure 5.4 shows the effect of PVA concentration on the size distribution of 50:50MS. D[v, 0.9] size of the 50:50MS produced using 1 % (w/w) PVA was ≤69.89 μm. The median size was ≤32.05 μm and the D[v, 0.1] size was ≤4.01 μm. As previously concluded by Freiberg and Zhu (2004), the amount of emulsifier is a primary factor to control sphere size. From Figure 5.4, the smallest diameter percentile of the four 50:50MS produced using four different PVA concentrations were statistically similar (*t*-test, $p<0.05$). These sizes ranged from 4.01 to 4.53 μm. The D[v, 0.9] sizes of the four 50:50MS demonstrated a decreasing trend with increasing PVA concentration. The same can be observed on their median sizes. The lower PVA concentration was found to produce larger particle sizes and distribution. Table 5.2 shows the variations in each data set. The decrement in the D[v, 0.9] size was the most pronounced between 50:50MS produced using 1 % (w/w) and 3 % (w/w) PVA.

Table 5.2: The size distribution of 50:50MS produced using PVA concentrations of 1, 3, 5 and 10 % (w/w).

PVA concentration (% w/w)	Diameter Percentile		
	D [v, 0.9]	D [v, 0.5]	D [v, 0.1]
1	69.89 ± 19.53 μm	32.05 ± 13.38 μm	4.01 ± 2.57 μm
3	54.84 ± 18.51 μm	21.95 ± 11.89 μm	4.42 ± 2.87 μm
5	38.25 ± 12.74 μm	16.31 ± 7.49 μm	4.30 ± 1.86 μm
10	30.92 ± 8.95 μm	15.47 ± 7.92 μm	4.53 ± 1.26 μm

Similar trend was observed in a work by Jalil and Nixon (1990) where there was a sharp drop in diameter when the emulsifier was increased from 1 to 2 %. Beyond this concentration there was little change in sphere size due to no emulsifier could be adsorbed at the sphere surface. Scholes *et al*. (1993) found that a PVA concentration of above 10 % had no effect on sphere sizes. Görner *et al*. (1999) also reached to the same conclusion and they also found

that polymer concentration (at constant surfactant concentration) is more dominant in governing the microsphere sizes. Through the understanding of the principle of an emulsifier, there exists an optimum concentration where above this point no more emulsifier could be adsorbed at the sphere surface. Further increase in the emulsifier concentration will not affect the sphere sizes. This could help to explain the decreasing size distribution with the increased PVA concentration as seen on Figure 5.4 and Table 5.2. In contrast, a lower PVA concentration probably led to insufficient surface adsorbing emulsifier and allowed a higher degree of coalesces between oil droplets. As a result, these nascent droplets/spheres solidified to yield larger spheres.

Regarding the residual PVA in the final product, a work conducted by Zambaux *et al*. (1998) showed that by using a 5 % (w/v) PVA solution, a single washing procedure led to particles containing ~20 % (w/w) PVA whereas three washing decreased the PVA content to ~10 % (w/w). Although increasing washing repetition could improve the situation but when drug encapsulation is involved, it could lead to higher tendency of drug loss. Furthermore, when ≥ 5 % (w/w) PVA was used, much smaller spheres were produced (Table 5.2) and caused problems during filtration in the microsphere harvesting stage. The filter membrane was sometimes damaged, causing fibres to remain within the final product.

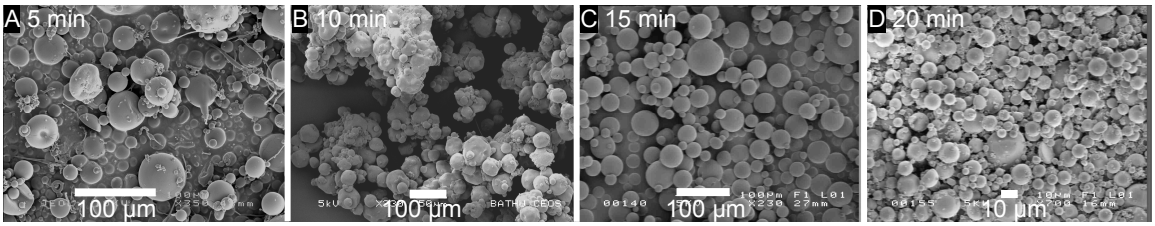

Figure 5.5: 50:50MS produced with homogenisation time of (A) 5, (B) 10, (C) 15, and (D) 20 minutes.

Figure 5.5 shows the 50:50MS produced with different homogenisation times. The 50:50MS produced with homogenisation times of 5 and 10 minutes resulted in none uniform spheres. Polymeric aggregates and strands are also present in the final products (Figures 5.5A and B). Increasing the homogenisation time to 15 minutes improved the sphericity of the resultant spheres, as shown in Figure 5.5C. Figure 5.5D shows that 20 minutes of homogenisation time produces much smaller 50:50MS. Based on the SEM images, it can be deduced that there exists a minimum time required to thoroughly homogenise the organic volume in the aqueous phase. It is often been predicted that increasing the time of homogenisation helps to produce a more stable microsphere system. This is because the more thorough shear force

created by the homogenisation to form the emulsion. This subsequently leads to an improved spheres uniformity and symmetry from the stabilised emulsion.

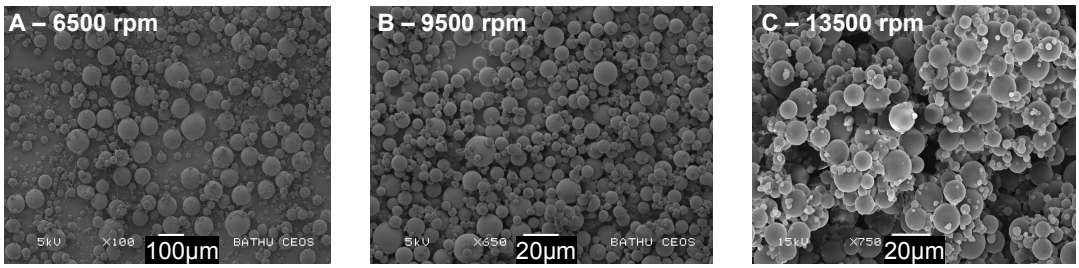

Figure 5.6: 50:50MS produced with homogenisation speed of (A) 6500; (B) 9500 and (C) 13500 rpm's.

Figure 5.6 shows the SEM images of 50:50MS produced using different homogenisation speeds. Figure 5.6A shows that a 6500 rpm homogenisation speed produced large 50:50MS with a wide size distribution. Further increase in homogenisation speed to 13500 rpm produced 50:50MS of approximately 20 µm in diameter (Figure 5.6C). Studies have shown that microsphere size decrease with increasing stirring rate since increase in stirring rate produces finer emulsions through stronger shear forces and increased turbulence (Jalil and Nixon, 1990). Ruan *et al*. (2002) also demonstrated that stronger emulsification strength resulted in smaller particles.

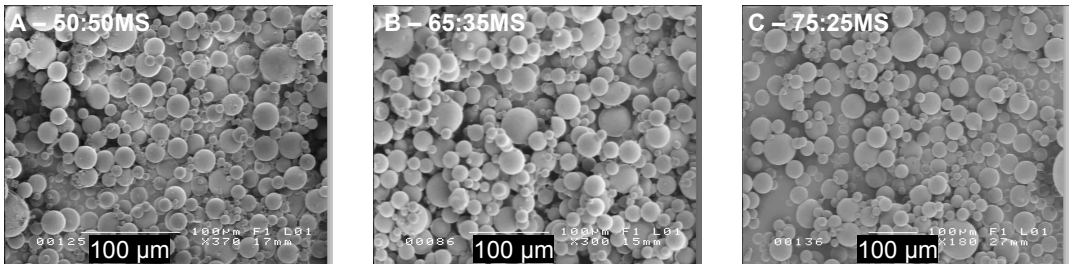

Figure 5.7: The resultant 15 % (w/w) of (A) 50:50MS; (B) 65:35MS and (C) 75:25MS.

In addition to the 50:50MS produced using different polymer concentrations, 65:35 and 75:25 PLGA were also used to repeat the experiment under the same condition. Examples of 15 % (w/w) of 50:50MS, 65:35MS and 75:25MS are shown in Figure 5.7. 75:25MS tend to have the largest spheres, followed by 65:35MS and 50:50MS, probably due to the higher inherent viscosities of 75:25 and 65:35 PLGA (Table 4.1). This suggests that the higher lactide acid ratio is, the larger spheres could be produced (Yan *et al*., 1994). Figure 5.8 further compares the size distributions of 15 % (w/w) 50:50MS, 65:35MS and 75:25MS.

(A) 50:50MS

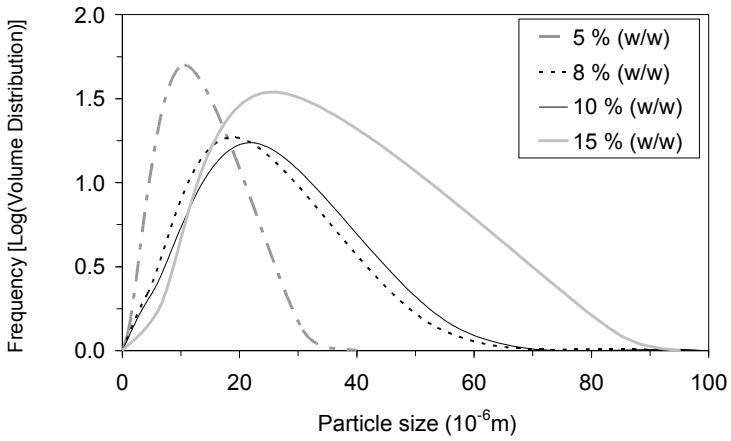

(B) 65:35MS

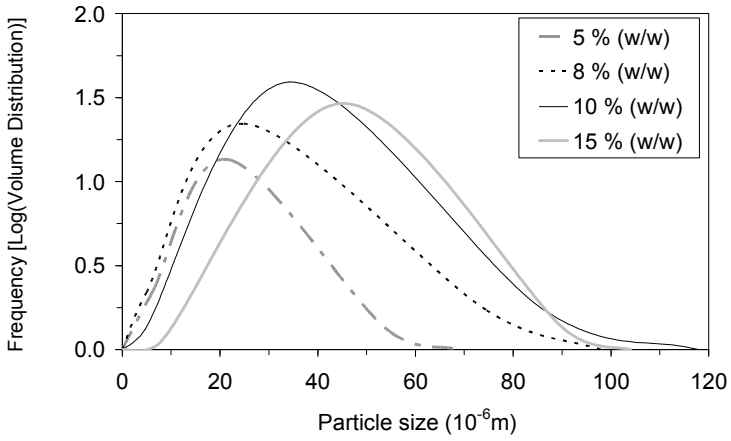

(C) 75:25MS

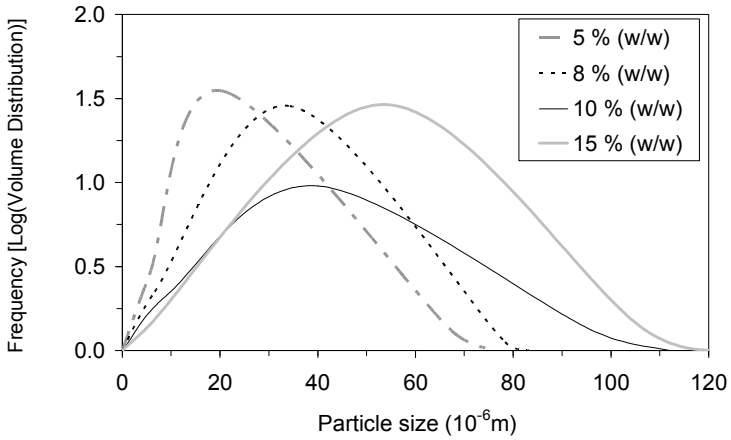

Figure 5.8: The size distributions of (A) 50:50MS, (B) 65:35MS and (C) 75:25MS produced using 5, 8, 10 and 15 % (w/w) polymer concentrations.

As seen in Figure 5.8A, 50:50MS of lowest polymer concentration (5 % w/w) yields the smallest spheres; with D[v, 0.9] being ≤30.78 μm, median size being ≤10.60 μm and D[v, 0.1] size being ≤1.06 μm. There is an increasing trend in D [v, 0.9] size of 50:50MS when the polymer concentration was increased from 5 to 15 % (w/w). Only the median sizes of 8 % (w/w) and 5 % (w/w) 50:50MS were found statistically different (*t*-test, $p < 0.05$).

From Figure 5.8B, by comparing the D[v, 0.9] size, 5 % (w/w) 65:35MS has the smallest size of ≤ 54.02 while 15 % (w/w) 65:35MS has the largest spheres of ≤ 90.43 μm. Similar to 50:50MS, the D[v, 0.1] of 65:35MS did not show any relationships to its polymer concentration. Both the D[v, 0.9] and median sizes of 65:35MS demonstrated an increasing trend with increased in polymer concentration.

Figure 5.8C shows the 75:25MS size distribution with different polymer concentrations. As expected, the lowest polymer concentration generally produced the smallest spheres while the opposite was observed for higher polymer concentration. 15 % (w/w) 75:25MS has the largest spheres compared to 65:35MS and 50:50MS. This may be attributed to the higher lactic acid ratio in the PLGA which has a higher as-reported inherent viscosity in Table 4.1 (Section 4.1). This condition produces a system with higher viscosity while at constant homogenisation effect, the shear force generated by the homogenisation is not sufficient to break the more viscous phase into smaller droplets. Therefore, they remained in larger sizes, forming larger nascent spheres and finally larger solid spheres. However, there seemed to be no clear trend for the D[v, 0.1] fraction in any case. Further comparisons on the sizes of PLGA microspheres are studied and results are tabulated in Tables 5.3 to 5.5.

Table 5.3 compares the sizes for the D[v, 0.1] sizes of the three PLGA microspheres. There is lack of a clear trend across different PLGA and polymer concentration. In some cases, the size distributions are similar. These size ranges are not within the targeted range therefore will not be further discussed. The very large variation in sizes may have caused by the imperfection in homogenisation effect. During the production process, different regions of the vessel may have varied mixing dynamics and affected the movement of the droplets. Stagnant region would promote the coalescence of the droplets. It was also found that the products occasionally attached to the vessel walls. Attempts to recover these microspheres for analysis may have contributed to the problem.

Table 5.3: The sizes of the D[v, 0.1] fraction of 50:50MS, 65:35MS and 75:25MS.

Concentration (% w/w)	D [v, 0.1]		
	50:50 PLGA	65:35 PLGA	75:25 PLGA
5	1.06 ± 0.83 μm	6.15 ± 1.10 μm	5.55 ± 2.43 μm
8	4.31 ± 1.14 μm	4.94 ± 1.81 μm	6.67 ± 1.70 μm
10	5.02 ± 1.85 μm	4.66 ± 2.26 μm	9.28 ± 3.58 μm
15	5.95 ± 1.92 μm	8.00 ± 3.69 μm	4.59 ± 1.34 μm

Table 5.4: The median sizes of 50:50MS, 65:35MS and 75:25MS.

Concentration (% w/w)	D [v, 0.5]		
	50:50 PLGA	65:35 PLGA	75:25 PLGA
5	10.60 ± 3.92 μm	21.55 ± 5.88 μm	20.30 ± 9.11 μm
8	19.41 ± 4.63 μm	24.83 ± 6.68 μm	34.26 ± 6.91 μm
10	22.53 ± 3.99 μm	34.14 ± 9.35 μm	42.40 ± 12.06 μm
15	26.01 ± 3.74 μm	44.98 ± 10.98 μm	53.51 ± 11.54 μm

Table 5.5: The sizes of the D[v, 0.9] fraction of 50:50MS, 65:35MS and 75:25MS.

Concentration (% w/w)	D [v, 0.9]		
	50:50 PLGA	65:35 PLGA	75:25 PLGA
5	30.78 ± 9.01	54.02 ± 10.89	67.33 ± 25.67
8	53.73 ± 16.29	74.57 ± 18.28	78.34 ± 15.62
10	58.07 ± 14.19	86.43 ± 26.57	95.99 ± 12.63
15	84.21 ± 28.16	90.43 ± 12.68	107.13 ± 29.83

Table 5.4 shows the median sizes 50:50MS, 65:35MS and 75:25MS. In some cases, overlapping deviations of samples indicate the insignificant differences in the size. Table 5.5 shows that there are increasing trends across the PLGA in the D[v, 0.9] sizes. At a same concentration, 50:50 PLGA has the lowest viscosity as apposed to 65:35 and 75:25 PLGA which offers lower resistance for homogenisation. Hence, finer droplets was formed and yielded smaller spheres. This trend is common in the literatures (Yan *et al*., 1994 and Ghaderi *et al*., 1996).

The same could be used to explain when the polymer concentration is increased. The higher polymer concentration forms more volumes of "droplets" and this higher volume increases the frequency of collisions between these droplets. Thus, a higher concentration results in more fusions of these semi-formed particles and produces larger particles. Also, higher polymer concentration will yield higher viscosity and it requires a higher shear force to "break" these viscous droplets. Boisdron-Celle *et al*. (1995) obtained an almost linear trend between sphere size with 50:50 PLGA concentrations while keeping other parameters constant. In their studies, 13.5% (w/v) polymer yielded spheres of ~90 μm and 5.5% (w/v) yielded spheres of ~20 μm. In general, Figure 5.8 concurred with these authors where spheres sizes tended to increase with polymer concentration.

5.1.2 Investigation of Double-Emulsion Solvent Evaporation

The objective of this section was to establish a double-emulsion method to produce drug-loaded PLGA microspheres. Extensive efforts have been shown by numerous authors to improve the microsphere delivery system for both lipophilic and hydrophilic drugs and these works served as a foundation for the development work herein. The selection criteria comprised:

i. The similarity in materials (e.g. drugs and polymer) – this similarity provides guidance in developing a method to encapsulate hydrophilic drugs in PLGA microspheres. In retrospect, insights into alternative production recipes such as different emulsifiers or solvents could be gained.
ii. The different procedures – numerous authors have formulated production procedures in order to accomplish their objectives and each was proclaimed advantageous. With a collection of procedures, their feasibilities are studied and developed to an optimum method.
iii. The selected works were collected over in the past twenty years. This indicates how the technique has evolved throughout the years including newly developed techniques used to characterise the microspheres.

The various adapted methods are detailed in Table 5.6. Modifications were made accordingly in order to suit the production process. After preliminary trials, each experiment was repeated twice and drug loading were determined using the method described in Section 4.4. The concentration of fluorouracil was determined using uv-spectrophotometer (λ = 262 nm). Each method was compared on the basic of drug loading, quality of resultant spheres and the feasibility to perform the procedures. The structure of the following Result and Discussion section is organised such that a text of discussion is presented prior to SEM results. A summary of major studies findings are presented in Table 5.7.

Table 5.6: Experimental double-emulsion methods adapted from the literatures. *HG = Homogenised; MG-S = Magnetic stirring*

Authors	Experimental Condition		
	First Emulsion	**Second Emulsion**	**Final Stage**
Ogawa *et al*. (1988)	[1g 5-FU in 10% (w/v) gelatin] homogenised in [4 g 75:25 PLGA in 7.5 ml DCM] at 6500 rpm, 5 min	First emulsion HG into [400 ml 0.5% PVA] at 6500 rpm, 15 min	Mixture transferred for MG-S at 500 rpm, 2h, 30^{o}C
Chen and Lu (1999)	[1 g 5Fu] homogenised in [0.5 g 50:50 PLGA in 6.5 ml acetone] at 13500 rpm, 5 min	First emulsion mixed into[50 ml mineral oil with 8% SPAN 80] by MG-S at 1500 rpm, 15min	Mixture transferred for MG-S at 800 rpm, 4h
Perez *et al*. (2000)	o/w method: [1 g 5Fu and 0.8 g 75:25 PLGA] in [10 ml DCM] mixed with magnetic stirring at1500 rpm, 10 min	First emulsion mixed into [250 ml 0.25% PVA] by MG-S at 500 rpm, 3h	
	w/o/w method: [1 ml 0.05 mg/ml 5Fu and 0.8 g 75:25 PLGA] sonicated in [10 ml DCM] mixed for 30 sec	First emulsion mixed into [250 ml 0.25% PVA] by MG-S at 1200 rpm, 5 min	
Niwa *et al*. (1993)	[0.2 g 50:50 PLGA and 0.1 g 5Fu] homogenised in [0.5 ml DCM + 25 ml acetone + 5 ml methanol] at 13500 rpm, 10 min	First emulsion mixed into [100 ml 4% PVA] by MG-S at 500 rpm, 3.5h	
Hussain *et al*. (2002)	[0.5 ml 0.05 g/ml 5Fu] sonicated in [0.05 ml 4% PVA] for 10 min	First emulsion HG into [0.5 g 75:25 PLGA in 5 ml DCM] at 13500 rpm, 5 min MG-S [160 ml 4% PVA + 0.9% NaCl] at 1000 rpm, 3h	
Messaritaki *et al*. (2005)	[0.01 g PVA] homogenised in [2 ml 5Fu (0.05g/ml)] at 13500 rpm, 1 min	First emulsion HG into [2 ml 5Fu & PVA + 3 ml 8% 75:25 PLGA] at 13500 rpm, 15 min.	Second emulsion mixed into [100 ml 4% PVA + 0.9% NaCl] by MG-S at 500 rpm, 3h
Zambaux *et al*. (1998)	[1 ml 0.05 g/ml 5Fu] homogenised in [4 ml 8% 75:25 PLGA] at 13500 rpm, 10 min	First emulsion HG into [8 ml 4% PVA] at 13500 rpm, 5 min	Mixture mixed into [150 ml 0.1% PVA] by MG-S at 500 rpm, 2h
Spenlehauer *et al*. (1989)	[0.5 g 5Fu] sonicated in [8.4 ml DCM] for 10 min	First emulsion HG into [1g 75:25 PLGA] at 6500 rpm, 10 min Transferred to [250 ml 4% PVA + 0.9% NaCl] MG-S at 250 rpm, 4h	
Yan *et al*. (1994)	[1 ml 0.05 mg/ml 5Fu] mixed into [0.2 g 75:25 PLGA in 10ml DCM] using homogenisation (13500 rpm, 2 min), or vortexing (5 min), or sonication (5 min)	First emulsion mixed into [100 ml 5% isopropanol in 20 ml 1% PVA] by MG-S at 500 rpm, 30 min	

5.1.2.1 Results and Discussion

Ogawa *et al*. (1988) devised a method to encapsulate hydrophilic drug in PLA or PLGA microspheres using gelatin as the emulsifier in the inner water phase based on a water-in-oil-in-water (w/o/w) emulsion method. 10% (w/v) of gelatine, as opposed to 20% (w/v) quoted in the literature was used herein because it was found very problematic to dissolve the high concentration gelatine. Ogawa *et al*. (1988) also cooled the working solution to 15^{o}C during the production process but this was found to cause instant gelling. For this reason, gelatin partially retained its "gel" form and is visible in the final product (Figure 5.9). This procedure was found to be problematic especially during the product recovery. Figure 5.9 shows that the sizes of the resultant microspheres ranged between 1 to 10 μm. This small size is thought to cause by the concentrated gelatine. Residual gelatine also formed "linkages" between microspheres as can be seen in Figure 5.9.

Chen and Lu (1999) optimised an o/w method to encapsulate carboplatin in 50:50 PLGA microsphere. The mineral oil used in this experiment was found troublesome (e.g. highly viscous) for processing from preparation to cleaning. During the production process, the nascent spheres constantly attached to the vessel wall which caused problems to product recovery. The harvesting procedures involved triplicate washing with heptane and a further stirring in cold heptane before they were collected. The product recovery from this procedure was low and aggregates of polymer are present in the final product (Figure 5.10). This procedure was found not to be robust and drug loading determination was problematic due to the interference by undesirable residual materials.

Perez *et al*. (2000) produced poly-ε-caprolactone microspheres containing both lipophilic and lydrophilic. This single emulsion (o/w) procedure produced microspheres with varied degree of sphericity and a small amount of larger particles (Figure 5.11A). Polymeric aggregates were observed to be present in the final product produced using the w/o/w method (Figure 5.11B). In comparison, the o/w method produced microspheres with better morphology and results show no significant difference in drug loading (*t*-test, $p < 0.05$).

According to Niwa *et al*. (1993), methanol is admixed to the organic phase to dissolve 5Fu and the addition of acetone would lead to drastic decrease in sphere size. The higher the acetone to DCM ratio, the more rapidly acetone diffuses into the aqueous phase, causing rapid polymer deposition on the outer surface of droplets. Preliminary trials showed low productivity. Modifications were made such that sequential addition of solvent to the

polymer and drug solutions was incorporated into the procedure. The final procedure yielded large amount of polymer remnants (Figure 5.12).

Hussain *et al*. (2002) intended to formulate a co-delivery of antisense oligonucleotide and fluorouracil (5Fu) using PLGA microspheres. Useful remarks from this literature are such that the morphology of microspheres was not affected by either separate or simultaneous encapsulation of two drugs. This was also the case for encapsulation efficiencies. From Figure 5.13, the microspheres produced have smooth surface and good sphericity but are highly porous. The low PLGA concentration may have contributed to the formation of small particles. The high speed magnetic stirring (1000 rpm) may have promoted increased rate of solvent removal thereby yielding these porous spheres.

A work by Messaritaki *et al.* (2005) was intended for NMR and confocal microscopy studies of the burst release mechanism from PLGA microspheres loaded with 5Fu. This w/o/w procedure roduced highly porous spheres and with varied degree of sphericity while polymer aggregates are also present in the final product. Figure 5.14 shows that the surface pores are clearly visible on the sphere and are as large as 1 μm. The resultant microspheres produced using the method adapted from Zambaux *et al*. (1998) have similar characteristics to the microspheres shown in Figure 5.14. This similarity indicates that a w/o/w method will produce porous microspheres.

Spenlehauer *et al*. (1989) achieved the w/o emulsion by continuously stirring the suspension at 250 rpm for 4 h before harvesting the product. This was unusual compared to other work. Normally, an emulsion is first formed, then the nascent microspheres are transferred to magnetic stirring for a much longer period. Figure 5.16 shows that this procedure produced microspheres with a large size distribution and partially deformed spheres/capsules. The large size distribution was expected because of the low speed of stirring (i.e. 250 rpm). The formation of very small spheres may due to the high PVA concentration (i.e. 4%).

Yan *et al*. (1994) conducted studies to study the effects of different mixing methods on the morphology of protein-loaded PLGA microspheres using by w/o/w emulsions. Their work showed that different mixing techniques (e.g. sonication, homogenisation, vortex mixing) produced microspheres with different structures. In this experiment, it was found that the vortex mixer was not efficient to form a stable emulsion. Figure 5.17 shows the highly

porous microspheres produced from this procedure. It is attributed that the high porosity was a result of addition of isopropanol which increased the rate solvent removal.

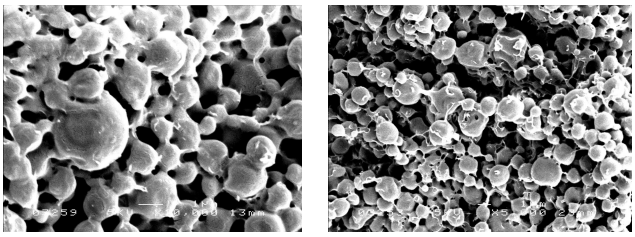

Figure 5.9: Resulting microspheres produced using method adapted from Ogawa *et al*. (1988).

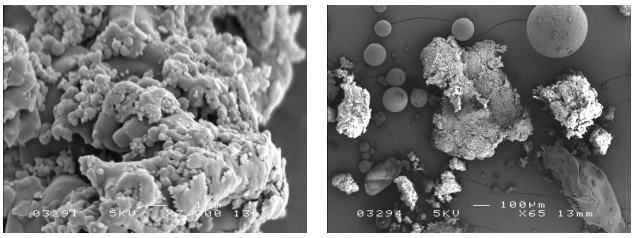

Figure 5.10: Resulting microspheres produced using method adapted from Chen and Lu (1999).

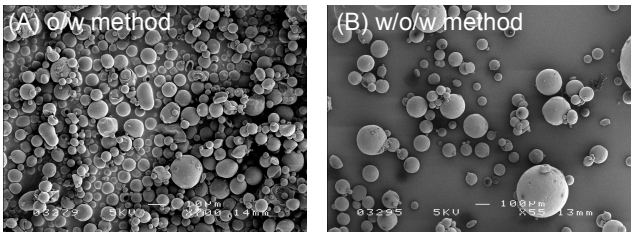

Figure 5.11: Resulting microspheres produced using (A) o/w emulsion and (B) w/o/w methods adapted from Perez *et al*. (2000).

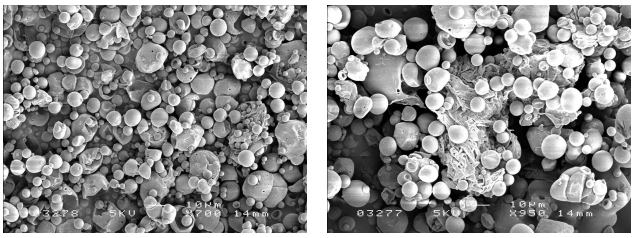

Figure 5.12: Resultant microspheres produced using w/o/w emulsion method adapted from Niwa *et al*. (1993).

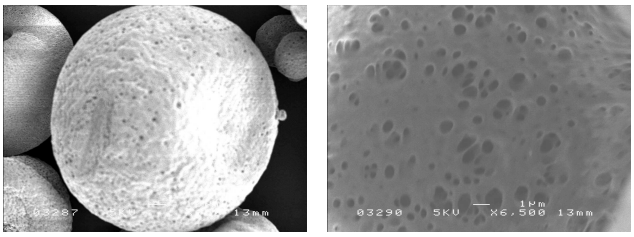

Figure 5.13: Resultant microspheres produced using method adapted from Hussain *et al*. (2002).

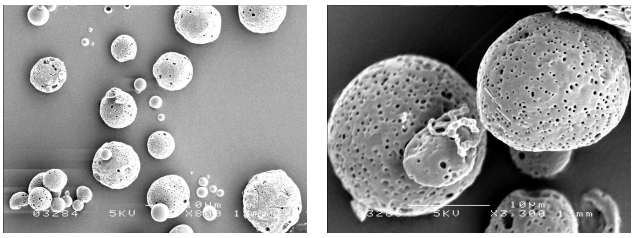

Figure 5.14: Resultant microspheres produced using method adapted from Messaritaki *et al.* (2005).

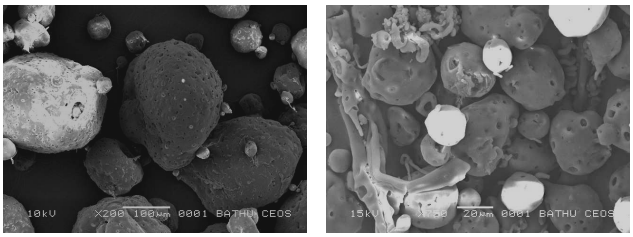

Figure 5.15: Resultant microspheres produced using method adapted from Zambaux *et al*. (1998).

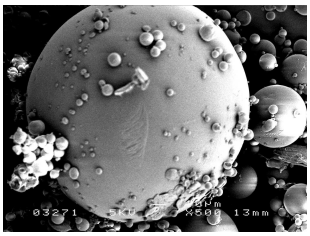

Figure 5.16: Resulting microspheres produced using method adapted from Spenlehauer *et al*. (1989).

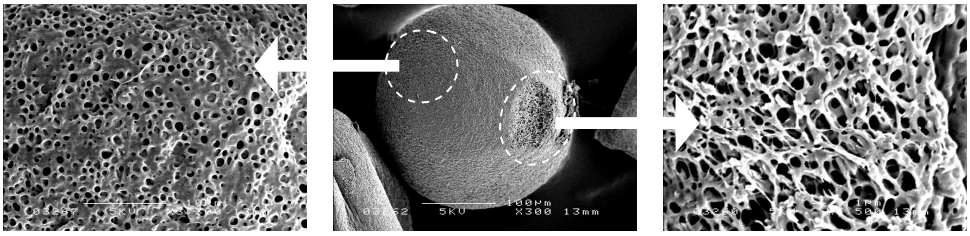

Figure 5.17: Resultant micro spheres produced based on procedures adapted from Yan *et al*. (1994).

The above findings demonstrated the advantages and disadvantages of each adapted procedure. For this work, it was observed that a single emulsion method tended to produce PLGA microspheres with a smooth surface, whereas a double emulsion method tended to produce PLGA microspheres with a porous surface. The latter was especially true when additional solvent was added to the system to promote faster solvent removal. The robustness of these procedures were assessed and it was found that a double emulsion method of this sort required detailed consideration to ensure good productivity.

In general, it was found much easier to carry out the procedures for single emulsion and the whole production period was also shorter. Most of the works adapted from the literature they were conducted on small scales. In this regard, most of the experiments reported herein were scaled up with a factor of five or ten. This has in turn altered the fluid dynamic of the system. Therefore result deviations from the adapted literature were anticipated. *In vitro* drug releases from these microspheres were measured and results are shown in Appendix III. Findings show that these drug releases were rapid, probably due to their low drug loading or high surface porosity. Table 5.7 summarises the concluding remarks for experiments in this section.

The major advantage offered by the model drugs used in this thesis is their dried-powder form. This enables a larger amount of working concentration in comparison to drug solution. Preliminary experiments with a single emulsion method using cisplatin and lidocaine demonstrated good reproducibility. Since the starting drug concentration can be processed in grams, as apposed to milli-grams in commercially available drug solution, a better drug

loading can be achieved compared to those reported in Table 5.7. For these reasons, the double emulsion method will not be employed for further development work.

Table 5.7: A summary of the findings from Section 5.1.2 and concluding remarks. The figures in bracket are calculated drug loading from the final product. Data represent mean ± standard deviation, $n = 3$.

Method by Author	Size range & Consistency	Morphology of Product	Remarks	Drug Loading
Ogawa *et al*. (1998)	1-10 μm Consistent	▪ Spherical ▪ Reasonably uniform	▪ Gelatin is problematic for processing and, ▪ Difficult to be removed, remained in samples forming linkages.	4.33 ± 2.31 %
Chen and Lu (1999)	50-300 μm Poor	▪ Spherical but hardly uniform ▪ Presence of large amount of polymer remnants	▪ Mineral oil and Span 80 are problematic; forming viscous solution and difficult for processing and cleaning. ▪ Viscous solution hinders effective homogenisation.	6.21 ± 3.56 %
Perez *et al*. (2000)	10-200 μm Moderate	▪ Capsules & spherical ▪ Reasonably uniform	▪ Reasonable good microspheres & microcapsules produced. ▪ w/o/w method produced spheres with a small number of visible but small and pores.	5.02 ± 3.51 %
Niwa *et al*. (1993)	10-20 μm Moderate	▪ Microcapsules & spherical ▪ Moderate uniformity	▪ Microspheres and irregular particles produced. ▪ Polymer aggregates largely present in final product.	3.44 ± 2.01 %
Hussain *et al*. (2002)	50-200 μm Low consistency	▪ Microcapsules & spherical ▪ Moderate uniformity	▪ Low uniformity microspheres & microcapsules produced. ▪ Very visible porous surface, pores bigger than 2 μm.	5.18 ± 2.44 %
Messaritake *et al*. (2005)	10-50 μm Moderate	▪ Mostly microcapsules ▪ Not uniform	▪ Reasonable good microcapsules produced. ▪ Very visible porous surface.	4.37 ± 2.14 %
Zambaux *et al*. (1998)	10-50 μm Poor	▪ Microcapsules & spherical ▪ Low uniformity	▪ Microcapsules produced. ▪ Very visible porous surface.	2.21 ± 1.03 %
Spenlehauer *et al*. (1989)	10-150 μm Moderate	▪ Spherical and smooth ▪ Uniform	▪ Reasonably good microspheres produced. ▪ Smooth surface	7.02 ± 4.20 %
Yan *et al*. (1994)	50-100 μm Poor	▪ Microcapsules ▪ Not uniform	▪ Very large particle with highest visible porous structure. ▪ Presence of polymer aggregates.	7.25 ± 2.55 %

5.2 The Development and Production of PLGA Hollow and Solid Fibres

This section presents the production of PLGA hollow and solid fibres using a wet spinning method based on the phase inversion technique. The large amount of PLGA required to spin each batch of hollow fibre is a concern to cost of production. Therefore, the investigation work was carefully devised based on the works by previous researchers in the Department, namely; Ellis, (2005), Tai (2007) and Shearer (2008). The spinning work and apparatus were fundamentally similar to the previous system. However, the spinning conditions were tested accordingly to accomplish the aim of this thesis. See Table 5.8 for details. Since the viscosity and polymer concentration of the PLGA dope used in this work were in general, lower than those to make commercial membrane, a syringe pump was used to deliver the polymer dope. This extrusion method provides better control of the flowrate of the dope. Meanwhile, in order to aid the solvent diffusion process and decrease the immersion time, the desired fractions of nascent fibres were cut into 20 cm in length during the immersion stage. Decreasing the aqueous immersion period would help to reduce drug leakage and loss. For ease, 50:50 PLGA hollow fibre will be abbreviated as 50:50HF, and 50:50 PLGA solid fibre as 50:50SF. Similar abbreviation will also be used for fibres made of 65:35 and 75:25 PLGA.

5.2.1 Method

50:50, 65:35 and 75:25 PLGA were used to spin both hollow and solid fibres according to the method and conditions described in Section 4.2. The spinning apparatus is shown previously in Figures 4.3 and 4.4 respectively. Prior to spinning, the polymer dope was degassed for 1-2 h. Table 5.8 describes the spinning conditions for hollow and solid fibres. Occasionally, the flowrates of both the bore liquid and polymer dope required slight adjustments in the beginning of the process when the system was approaching equilibrium.

Table 5.8: The spinning conditions for 50:50, 65:35 and 75:25 PLGA hollow and solid fibres.

Spinning Condition	Hollow Fibre	Solid Fibre
Polymer used	20 % (w/w) 50:50, 65:35 and 75:25 PLGA	
Solvent used	1-methyl-N-pyrrolidone (NMP)	
Polymer extrusion rate (ml/min)	2.5 ± 0.5	4.0 ± 1.0
Spinneret	Yes	No
Bore liquid flow rate (ml/min)	2.0 ± 0.5	No bore liquid used
Air gap (cm)	10.0 ± 0.5	No air gap
Speed of collection motor (rpm)	7 ± 2	10 ± 2

The PLGA hollow fibre 'membrane' developed in this work were characterised using gas permeation (Section 4.7.3) to obtain mean pore size and effective surface porosity, as well as by SEM imaging for morphology. Because these membranes were intended to be encapsulating drugs or loaded with drug solution for the purpose of drug delivery, as opposed to a traditional separation application, further membrane characterisation, i.e. flux or rejection analysis, were not applicable and therefore not carried out. These analyses will not realistically characterise the transport and spaces occupied by the entrapped drug.

5.2.2 Results and Discussion

The shape of the hollow fibre is determined by pushing the polymer dope under pressure through a spinneret. A spinneret is a device which two or more fluids can be fed with one central flowing fluid and the other flowing concentrically around the central flow. In this work, a tube shaped stream of viscous polymer solution flows from the nozzle of the spinneret, and within this stream the bore liquid flows. Figure 5.18 is the cross sectional view of the tube-in-orifice used in this work. The bore liquid, also termed as the internal coagulant facilitates the phase inversion process at the lumen of the hollow fibre. The external coagulation bath facilitates phase inversion of the outer surface of the fibre.

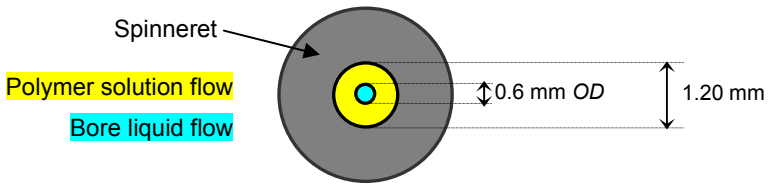

Figure 5.18: Cross sectional view of the spinneret with a tube-in-orifice used in this work.

Prior to the spinning of hollow fibres using PLGA, practice runs were carried out using polysulfone and a set of spinning condition was devised for preliminary PLGA experiments. A number of process variables of the spinning condition were tested, such as the air gap, polymer concentration, polymer solution and bore liquid flowrates were varied and examples of results from these investigations are shown in Table 5.9. The conditions used to spin these PLGA hollow fibres are given in the table. Table 5.9 also summarises the defects observed on the relevant hollow fibres and their causes. The distinctive structures of the fibre wall produced by the different spinning conditions are clearly visible in the SEM images. These structural characteristics are closely associated to the physical property of hollow fibre membranes such as molecular weight cut off (MWCO) and porosity.

Table 5.9: Results of hollow fibres spun using different spinning conditions. *HFM = Hollow Fibre Membrane*

Cross Section SEM images of Hollow Fibre	Spinning condition	Defects on Hollow Fibres:	Cause of Defects:
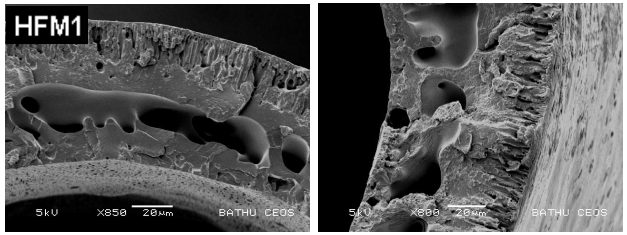	▪ Air gap: 15 cm ▪ Polymer solution flowrate: 5 ml /min ▪ Bore liquid flow rate: 0.5 ml/min ▪ Polymer concentration: 25 % (w/w)	▪ Irregular macrovoids. ▪ Very dense structure. ▪ Very dense inner skin layer.	▪ High polymer concentration. ▪ Small air gap. ▪ Low bore liquid flowrate.
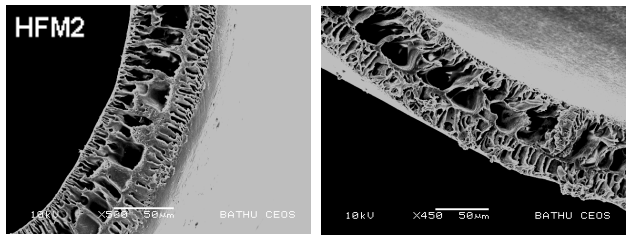	▪ Air gap: 15 cm ▪ Polymer solution flowrate: 2 ml /min ▪ Bore liquid flow rate: 2 ml/min ▪ Polymer concentration: 20 % (w/w)	▪ Regular and consistent macrovoids. ▪ Visible finger structures. ▪ Rather thin fibre wall.	▪ Large air gap.
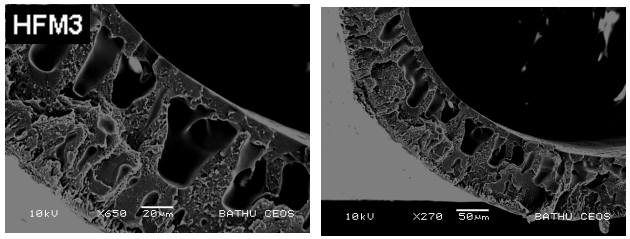	▪ Air gap: 10 cm ▪ Polymer solution flowrate: 3 ml /min ▪ Bore liquid flow rate: 1 ml/min ▪ Polymer concentration: 25 % (w/w)	▪ Very large macrovoids. ▪ Dense structure. ▪ Thick skin layer.	▪ High polymer concentration. ▪ Inadequate bore liquid flowrate.
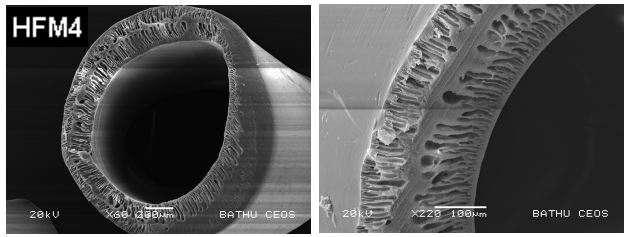	▪ Air gap: 10 cm ▪ Polymer solution flowrate: 2 ml /min ▪ Bore liquid flow rate: 5 ml/min ▪ Polymer concentration: 30 % (w/w)	▪ Dense structure. ▪ Limited macrovoids. ▪ Longer finger structure.	▪ High polymer concentration. ▪ Low bore liquid flowrate.

Previously, a work by Wen and Tresco (2006) showed that a reduction in MWCO of the membrane was caused by an increase in the flowrates of polymer solution and bore liquid. This was attributed to increased shear stresses within the spinneret, and between the bore liquid and the fibre lumen. The increased stress aligns the polymer molecules which allows for tighter packing within the polymer molecules on the surface, and leads to formation of a dense skin layer (Chung and Hu, 1997). This effect is reflected in the SEM images of HFM1 and HFM4 fibres presented in Table 5.9.

The effect of increasing polymer concentration will decrease the MWCO of the membrane. This is due to an increased viscosity which leads to an increase in shear stress in the spinneret. The higher polymer concentration also means that more space will be taken up by the polymer in the fibre structure, and this leads to a formation of denser structure with reduced porosity (Wen and Tresco, 2006). This explains the dense structures of HFM1, HFM3 and HFM4 where 25 and 30 % (w/w) were used to produce these hollow fibres.

Denser structure formed by higher polymer concentration also caused by a condition where the molecules are more tightly packed in the spinneret before the molecules can relax once they leave the spinneret (Qin *et al*., 2001). The higher air gap tended to reduce the wall thickness of the hollow fibre. This effect could be seen by comparing hollow fibres spun using 15 cm air gap (i.e. HFM1 and HFM2) and 10 cm air gap (i.e. HFM3 and HFM4). This is because the air gap increases longitudinal stress which acts to pull apart adjacent polymer chains (Chung and Hu, 1997).

The findings and the spinning condition of HFM2 presented in Table 5.9 enabled a final spinning condition to be established and is tabulated in Table 5.8. Typically, a polymer and bore liquid flowrates of approximately 2 ml/min with an air gap of 10 cm were used to spin a 20 % (w/w) PLGA hollow fibre. A “preset” stage was required to adjust both the flowrates of the bore liquid and polymer solution when the nascent hollow fibre was first emerging from the orifice of the spinneret. This stage usually takes 5-10 minutes before an equilibrium condition is reached and then the speed of the collection motor can be set. In all cases, only hollow fibre formed during the equilibrium stage was used for subsequent studies in order to obtain fibre of consistent quality.

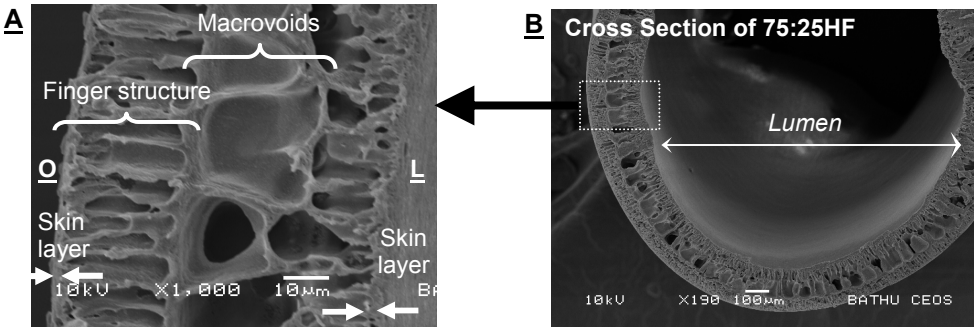

Figure 5.19: (A) The morphology of the fibre wall of 20 % (w/w) 75:25 PLGA hollow fibre. (B) A cross section of the 20 % (w/w) 75:25HF. *O = Fibre outer surface, L = Inner surface at the fibre lumen*

Figure 5.19 shows the morphology of the fibre wall of 75:25HF. There are two skin layers; one at the outer surface and another at the lumen of the hollow fibre (Figure 5.19A). These skin layers are the result of the instantaneous demixing during the phase inversion process. The skin layers surrounding the hollow fibre and its lumen are instantly formed at the solvent/nonsolvent interface due to a rapid solvent exchange. The skin layers enveloped a layer with finger-like structure and adjacent to this structure, large cavities or macrovoids forming a sublayer in the fibre core. The formations of these structures are discussed below.

Two types of membranes structures are discussed by Drioli and Nakagaki (1986); namely, the "sponge-like" and the "finger-like" structures. They are formed during the rapid phase inversion in a coagulation bath and subsequent solidification form the membrane structure. During phase inversion, the mixed solution of rapidly changing composition forms the two separate phases. At a particular point (when its composition crosses into the miscibility gap), the solvent leaches out from the solution. A microporous structure within the polymer-rich phase is formed with the cavities formed by the influx of nonsolvent. The former phase eventually reverts to being entirely solid as the solvent migrates out.

Bungay *et al*. (1986) suggested that a fast precipitation tends to give larger finger structures whilst slow precipitation will results in a more sponge like structure. The type of solvent can affect the rate of precipitation. A non-compatible solvent will take longer to exchange with nonsolvent and will thus spend more time within the structure. Hence, the finger structure will be fewer and smaller because precipitation is slower. A compatible solvent will exchange with nonsolvent more rapidly and finger-like structures will be numerous and large as precipitation is fast.

The finger structure propagates rapidly with a thin (skin) precipitated layer of polymer preventing direct contact with the nonsolvent. Increasing the initial polymer concentration will lead to a higher polymer concentration at the skin/polymer interface. This implies a higher volume fraction of polymer and consequently, a denser skin layer will be formed with a lower porosity. This is due to a lower solvent exchange flux.

The macrovoid formation originates from the demixing effect. The formation of macrovoids takes place through two stages: (1) initiation, (2) propagation or growth. Most of the macrovoids start to develop just beneath the skin layer, initiated by some of the nuclei which are formed directly underneath this layer. Initially, the dispersed droplets formed between the polymer-rich phase and the interface of the solution/nonsolvent interface consist of a mixture of solvent and nonsolvent with very little polymer. These droplets then develop further until the surrounding continuous phase solidifies. Figure 5.20 illustrates the formation of macrovoids.

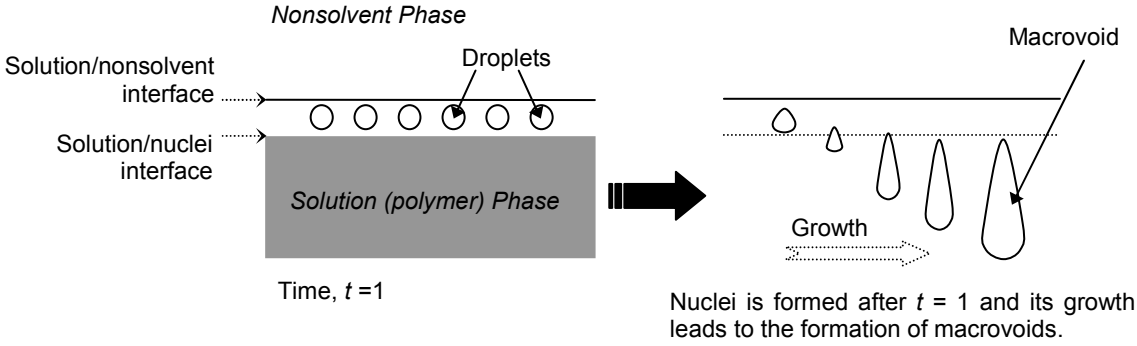

Figure 5.20: Schematic representation of the growth of macrovoids during instantaneous demixing and as the solvent exchange proceeds.

The diffusional flow of solvent from the surrounding polymer solution initiated the growth of the nuclei in the polymer-lean phase. The first droplet of the polymer-lean phase being formed at time; say $t = 1$, the polymer solution in front of the droplets is still homogenous and remains stable, i.e. no new nuclei is formed. At the same time, diffusion of solvent and nonsolvent occur into the first nuclei. In this way the growth of a macrovoid occurs and this growth continues until the polymer concentration in the macrovoid at the solution interface becomes so high that solidification occurs. The coalescence of the droplets before solidification is responsible for the formation of large cavities and porous structures.

The porosity of the hollow fibre governs its permeability and for control drug release, the diffusion of medium across the fibre is important. Specifically, the permeability of a

membrane is determined by the morphology of the skin layer; including pore size, pore density and/or distribution, the thickness of the skin layers, and among others (Mulder, 2000). For membrane application, pore size usually determines the selectivity (i.e. MWCO) and the pore density and thickness of skin layers determine the flux of mass transfer (Drioli and Nakagaki, 1986).

In general, the influential factors in spinning condition discussed in Section 3.5.1 also apply as factors influencing the membrane permeability. For instance, a decrease in permeability can be caused by increases in polymer concentration and polymer solution flowrate. This is due to the increase of polymer volume fraction at the interface thereby creating a higher resistance for the solvent/nonsolvent exchange. This is similar to a delay in demixing resulting in a denser structure. Decrease in air gap also leads to decrease in permeability (Mulder, 2000). On the other hand, the increase in the flowrate of the bore liquid will increase the permeability of a membrane because of the enhanced solvent/nonsolvent exchange rate at the interface of between the lumen surface and the bore liquid. This parallels to the effect of rapid demixing forming a porous structure (Wen and Tresco, 2006).

The results from gas permeability analysis (Section 4.7.3) conducted on 20 % (w/w) 50:50HF, 65:35HF and 75:25HF are shown in Figure 5.21. The plot indicates that the effective surface porosity tends to increase as the lactide acid in the PLGA increases. In term of mean pore diameter, 65:35HF tends to have the larger size. Statistic analysis (ANOVA, $p < 0.05$) suggests that there were no significant differences in both the mean pore diameter and effective surface porosity between 50:50HF, 65:35HF and 75:25HF. This is reflected on the overlapping deviations in each result.

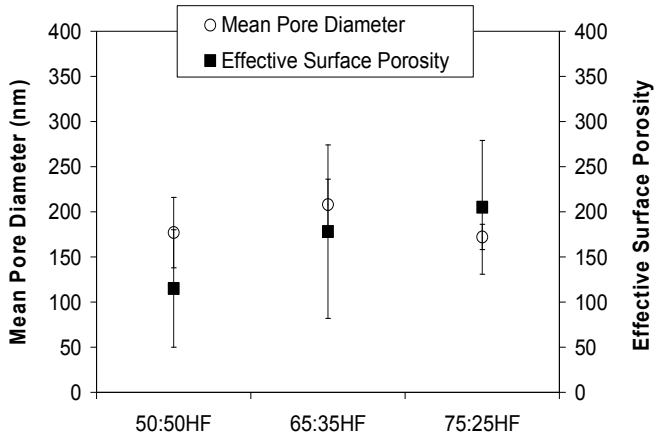

Figure 5.21: Gas permeation analyses showing the mean pore diameter and effective surface porosity of 20 % (w/w) 50:50HF, 65:35HF and 75:25HF.

The similarity in results observed in the plot is not unexpected because of the constant spinning conditions and the same polymer concentration used. It should not be mistaken that the effective surface porosity is a function of mean pore size. This is because the varied structure across the fibre wall and the core structure could be the dominant factor in governing the effective porosity instead of the overall mean pore size (Kong and Li, 2000 and Tai, 2007). The overall structure across the fibre wall comprises the skin layers, macrovoids of various sizes, a sponge-like sublayer of various thicknesses and porosities, all can affect the effective porosity (Drioli and Nagakagi, 1986).

Based on the optimum condition established for spinning hollow fibre, the final spinning condition of solid fibres was developed. In this case, there were less spinning parameters involved. Attempts to maintain a constant polymer concentration at 20 % (w/w) was plausible leaving only the flowrate of the polymer solution and the speed of the collection motor required adjustment accordingly. The successful PLGA solid fibre formed with structure of consistent quality is shown in Figure 5.22. The finger-like microcavities in the fibre wall are visible in Figure 5.22A. Figure 5.22B shows the skin layer and structure near the outer surface of the solid fibre. Since a spinneret was not used and with no bore liquid, the characteristic of hollowness is not seen in a solid fibre. The formations of the skin layer and finger structure from the phase inversion are similar to those in hollow fibre.

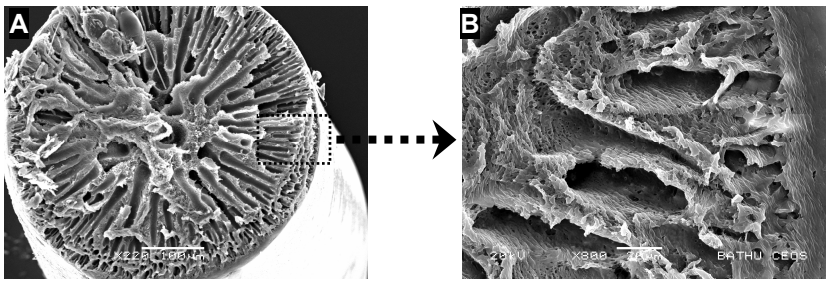

Figure 5.22: SEM images of 20 % (w/w) 75:25 PLGA solid fibre. (A) Cross section showing the finger structure and (B) skin layer at the outer surface.

More detailed morphological characterisation of PLGA hollow and solid fibres will be presented in Sections 6.3 and 6.5 respectively. The estimated internal (*ID*) and outer (*OD*) diameters of 50:50HF, 65:35HF and 75:25HF are tabulated in Table 5.10. The *OD* of 50:50SF, 65:35SF and 75:25SF were also measured. These results further suggest that under the same spinning condition, the physical property of the hollow fibres is very similar.

Table 5.10: The measured *ID* and *OD* of 50:50, 65:35, and 75:25 PLGA hollow and solid fibres.

PLGA Hollow/Solid Fibre	Outer Diameter (Average ± Standard Deviation) µm	Internal Diameter (Average ± Standard Deviation) µm
50:50HF	688 ± 83	477 ± 66
65:35HF	751 ± 95	524 ± 75
75:25HF	852 ± 84	630 ± 88
50:50SF	676 ± 73	-
65:35SF	715 ± 63	-
75:25SF	764 ± 78	-

5.3 Conclusion

1. The objective in Section 5.1 was to establish a standard procedure to produce PLGA microspheres for this work. A typical requirement is to process a 10 g of polymer solution in 100 ml of PVA solution. Adequate residence time and speed during the homogenisation stage are required in order to thoroughly homogenise the total volume of organic phase and form a suitable size emulsion. The organic droplets-emulsion solidifies to produce microsphere of desire sizes. The required PVA concentration is such as to produce a stable emulsion containing the nascent microsphere of desirable sizes and good sphericity upon solidification.

2. The main parameters in the single emulsion, oil-in-water (o/w) were investigated and the final optimum condition is such as: 15 min of homogenisation time, 0.5 % (w/w) PVA concentration, and 6500 rpm of homogenisation speed for processing a typical 15 % (w/w) polymer solution.

3. Results from the investigation into double emulsion methods demonstrated that the procedures involved were laborious and associated with low productivity. Since the model drugs are available in solid form, this enables a higher starting drug concentration which is necessary to ensure better drug loading. For this reason, a double emulsion method will not be developed in this work. All drug-loaded microspheres will be produced using single emulsion with the condition determined in (2) above.

4. The principle of phase inversion technique (Section 3.5) was studied closely and applied to spinning of both hollow and solid fibres. Preliminary experiments preset a condition for the spinning of PLGA hollow fibre and further adjustments were tested before a final spinning condition was established. The final spinning condition for the production of PLGA hollow fibre are such as: 10 cm as the air gap, 2 ml/min as the starting bore liquid flowrate, 3 ml/min as the starting polymer solution extrusion rate and 5 rpm as the starting speed for collection motor. Once the spinning system has reached equilibrium, the latter three rates required adjustment accordingly.

5. Using the established spinning condition determined in (4) above, results show good quality hollow fibres were produced. Hollow fibres made of PLGA with different copolymer ratios exhibited consistent fibre wall structures. Cross section examination of hollow fibres reveals the unique finger-like structure across the fibre wall. Uniform and thin skin layers, macrovoids with consistent geometry were also obtained.

6. Based on the spinning condition of PLGA hollow fibre, the spinning of PLGA solid fibre was established. Solid fibres made of PLGA with different copolymer ratios were successfully produced with consistent fibre wall structure. The elongated finger structure is observed across the solid fibre wall.

CHAPTER 6
MORPHOLOGICAL CHARACTERISATION OF PLGA DEVICES

This chapter studies the morphology of PLGA devices before and after *in vitro* degradation by means of SEM imaging and mass loss measurement. Section 6.1 presents the morphological characterisation of PLGA microsphere and Section 6.2 follows their *in vitro* degradation by means of SEM imaging. Similarly, Sections 6.3 and 6.4 study the morphologies of PLGA hollow fibre before and after degradation respectively. The morphological characterisations of PLGA solid fibre before and after degradation are presented in Sections 6.5 and 6.6 respectively.

6.1 Morphological Characterisation of PLGA Microspheres

50:50, 65:35 and 75:25 PLGA were used to produce blank microspheres based on the single emulsion method described in Section 4.1.3. Briefly, 10 g of 15 % (w/w) polymer solution was homogenised at 6500 rpm in 100 ml of 0.5 % (w/w) PVA for 15 min. After that, the nascent microspheres were transferred to magnetic stirring for 3 h. Finally, they were washed, filtered and air dried. Five batches of each PLGA microsphere were prepared for this and subsequent degradation studies. For ease, 50:50 PLGA microsphere will be abbreviated as 50:50MS henceforth, similarly for 65:35 and 75:25 PLGA microspheres.

6.1.1 Morphology of PLGA microspheres

The surface morphologies of 50:50MS, 65:35MS and 75:25MS produced using the single emulsion method are shown in Figures 6.1 (A1), (A2) and (A3) respectively. Their overall smooth surfaces are seen on the images obtained with higher magnifications (Figures 6.1-A2, B2 and C2). The smooth condition is thought to be a result of rapid solvent diffusion and polymer deposition during the phase inversion process. This scenario is very similar to the rapid demixing between solvent and nonsolvent previously described in Section 3.5.

The formation of microsphere will be illustrated in Figure 6.3 later. Sometimes, imperfect effects from homogenisation or unstable emulsion can cause the nascent spheres to coalesce. As a result, deformations to the sphericity of the final product are observed, as indicated in Figures 6.1 (A1) and (C1).

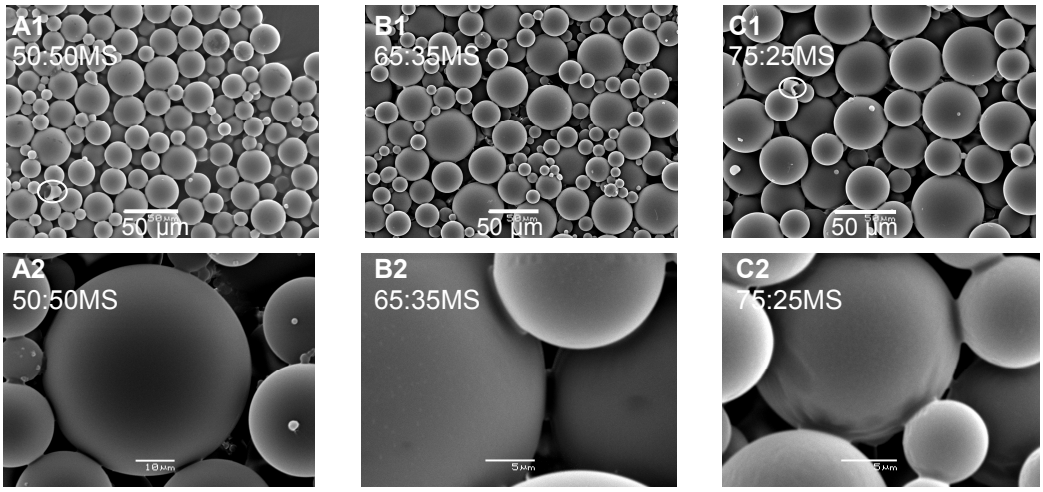

Figure 6.1: SEM images of 50:50MS (A1 & A2), 65:35MS (B1 & B2) and 75:25MS (C1 & C2) produced using the single emulsion method at polymer concentration of 15 % (w/w).

Attempts to magnify the PLGA specimen was found problematic due to the heat sensitivity of PLGA. When the magnification is increased, the heat generated by the electrons projected onto the PLGA specimen tends to destroy the specimen. Likewise, magnification could not be repeated on the same area. Figure 6.2 shows the heat-damage 75:25MS specimen. Due to these circumstances, the typical acceleration voltage used for SEM imaging on PLGA specimen was maintained at 10-15 kV. The bright regions/bands observed on the SEM images are caused by the electron charging of residual moisture.

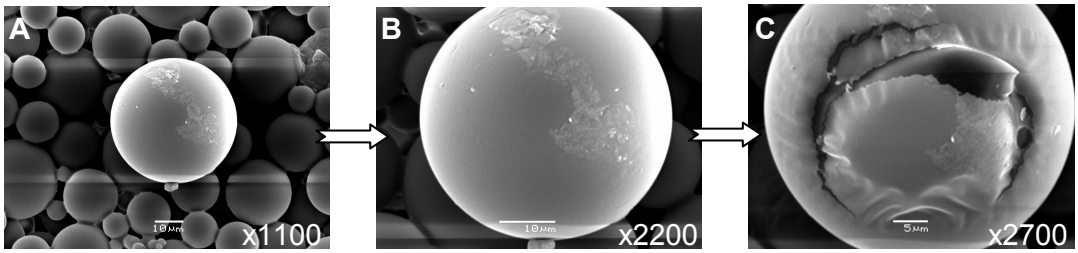

Figure 6.2: SEM images showing heat sensitivity of 75:25MS during magnification.

6.1.2 SEM Cryo-Fractioning

This section presents the results that reveal the interior of PLGA microsphere. The basic cryo-fractioning protocol is given in Section 4.6.2. Understanding the internal structures of biodegradable microspheres will aid the understanding of their drug release kinetics (Yang *et al*., 2001 and, Kim and Park, 2004).

As aforementioned, the smooth outer surface of the microsphere is a result of rapid solvent deposition. During the emulsion process, the organic droplets or nascent spheres experience

solidifying effect as a result of solvent diffusion. This initial rapid solvent diffusion is driven by the largest concentration gradient present at the interface between the organic droplets and the aqueous phase. At this instant, the outermost layer of the droplet will solidify first forming a layer enveloping the nascent interior (Crotts and Park, 1995). Consequently, the nascent spheres will solidify from the periphery towards the centre. A higher polymer concentration will produce a denser outermost layer due to a more rapid solvent diffusion (Yang *et al*., 2000). Figure 6.3 illustrates a possible scenario of the formation of nascent microsphere during the phase inversion process.

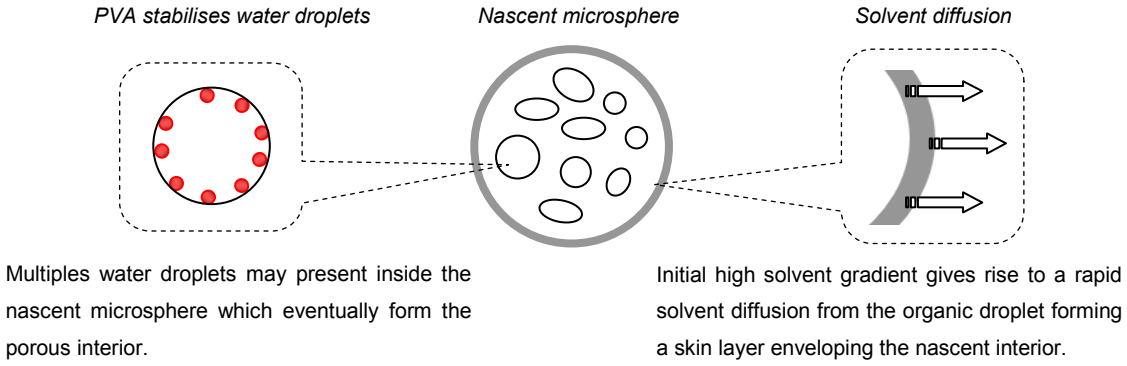

Figure 6.3: A simplified initial solvent diffusion events during the formation of a skin layer enveloping the nascent interior, which contains multiple water droplets.

The diffusion of the remaining solvent out from the nascent microspheres to the aqueous phase may give rise to a porous interior. This is because of the partial water immiscibility of DCM which permits the influx of water into the nascent spheres, and the presence of a PVA-stabilised water emulsion. An increase in concentration of the aqueous phase will increase the volume of water droplets-emulsion, forming more water pockets. Upon solidification, these pockets will form particles with interior of higher porosity. Since the nascent sphere solidifies inwards from its periphery, there is a tendency that the water-emulsion will be driven towards the centre of the microspheres. This situation can form microspheres with larger cavities at their centres. The above mechanisms are used to explain the porous interior of 75:25MS shown in Figure 6.4.

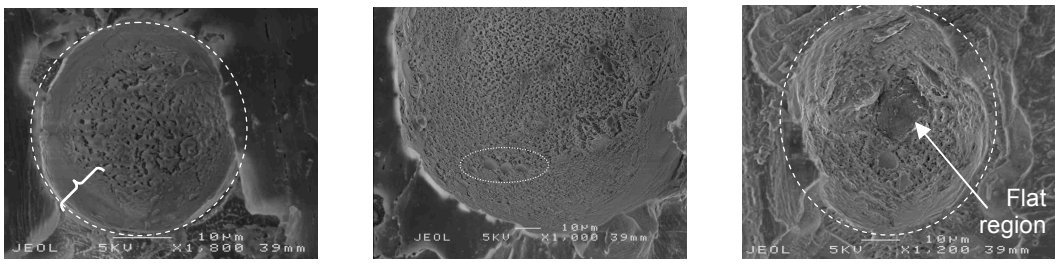

Figure 6.4: SEM images of cryo-fractured 75:25MS.

Figure 6.4A shows a 75:25MS of ~35 μm in size whereas Figure 6.4B shows a 75:25MS of ~110 μm in size. The microcavities in the porous interiors of these 75:25MS are approximately ~1 nm in size. Figure 6.4A indicates a "skin" layer enveloping the sphere while a flat region is observed in Figure 6.4C. During contact with N_2 freezing, it is possible that the rather weak porous structure expanded due to ice crystallisation. As this expansion takes place, the adjacent structure shrinks. If this occurs across a local region, it could form a flat region. Figure 6.4 (B) and (C) also show the present of a small number of macrocavities. These may be a result of the formation of random size water droplets-emulsion. With a less viscous 65:35 and 50:50 PLGA polymer solutions, higher interior porosity can be expected because of the higher influx of water into the nascent spheres during phase inversion.

While a number of 75:25MS were successfully fractured, little fractured 50:50MS and 65:35MS were obtained. Figure 6.5 illustrates a possible scenario during the cryo-fractioning of specimen. The initial assumption was that a larger sphere would aid the fracturing process. This is because of the larger surface of the larger sphere would be strongly held by the surrounding ice crystal.

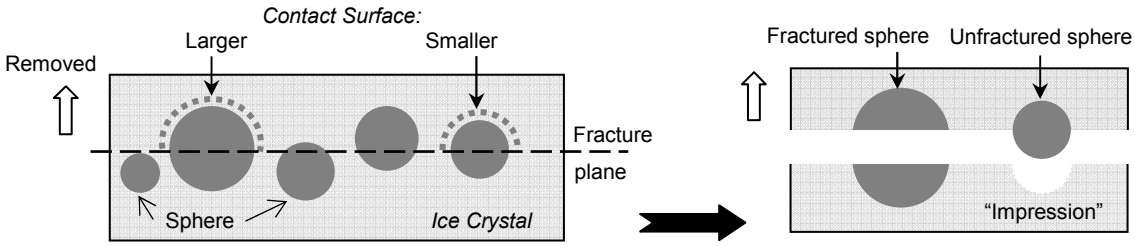

Figure 6.5: Possible scenario during sample preparation for cryo-fracturing. Larger sphere offers a larger surface area to be held by the ice crystal while the opposite applied for a smaller sphere.

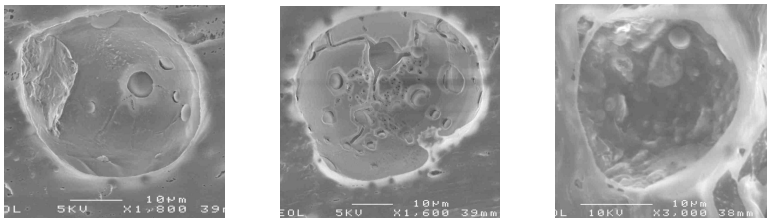

Figure 6.6: SEM images showing the "impression" resulted from the removal of a sphere.

Owing to the minute sizes of the specimen, it is impossible to distribute the spheres between the fracture plane, while the fracture plane is a random position due to the nature of the procedure. For these reasons, the whole sphere was removed leaving an empty space (Figure 6.6). To attempt to improve the fracturing effect, further modification was made to the basic protocol procedure and details are included in Appendix IV. Figure 6.7 shows the fractured

75:25MS using the modified procedure. These specimens were first freeze-dried, and then fixed onto Araldite® resin followed by sectioning using a microtome. The freeze drying may have altered the internal structure of the 75:25MS because their exposed interiors seen in Figure 6.7 are different from those in Figure 6.4. Close-up images of 75:25MS (Figure 6.7B) indicate that their internal morphology were dense with no visible cavities.

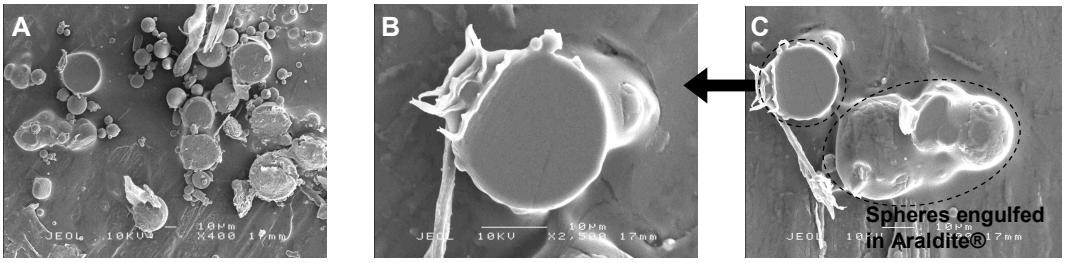

Figure 6.7: SEM images of fractured 75:25MS using a modified cryo-fractioning procedure.

All the microspheres used in this section were produced using the same condition therefore it was anticipated that they would have similar characteristic. Based on the results in Figures 6.4 and 6.7, two critical conditions must be distinguished:

i. In the basic protocol, the spheres were prepared based on the condition described in Section 4.6.2. They did not undergo any overnight freeze-drying.
ii. In the modified procedure, the specimen was freeze-dried overnight prior to cryo-fractioning.

Freeze drying can affect molecular mobility of PLGA by altering the excess structural energy in the glassy particle. Glassy materials, including amorphous or semi-crystalline polymer at temperatures below their glass transition (T_g) are thermodynamically unstable. These materials are to be regarded as solidified supercooled liquids, whose properties such as free volume, enthalpy and entropy are greater than they would be in the equilibrium state (Allison, 2008a). In the metastable glassy state, the physical and mechanical properties of such materials change with time as the glass attempts to achieve equilibrium by slow changes in molecular configurations. Molecular mobility in the glassy state allows the glass to relax toward the equilibrium liquid state in a process referred as structural relaxation.

Molecular mobility in PLGA may lead to structural changes, such as the closure of surface pore and structural relaxation in glassy PLGA microparticles is characterised by volume reduction (density increase) and can affect the dynamic behaviour of the amorphous PLGA microspheres (Allison, 2008a). PLGA microparticle can exhibit pore closure in increased

humidity environment (Bouissou *et al*., 2006) and incubation in solution (Ali *et al*., 1993). Messaritaki *et al*. (2005) discovered that the freeze drying had detrimental effect on the permeability of PLGA microsphere. A non-freeze-dried PLGA microsphere has much larger pore density than the freeze-dried sphere.

Owing to the structural instability of glassy-PLGA microspheres, all the PLGA microspheres used in this thesis were standardised to undergo air drying according to the method described in Section 4.1.3 and they were freshly prepared prior to each experiment. Unconditioned storage of PLGA microspheres may lead to irreversible aggregation of the microspheres. Bouissou *et al*. (2006) reported that at high humidity and temperature higher than the polymer's T_g, interparticulate bridges were formed due to high degree of molecular mobility of the PLGA chains. For the shortcomings encountered in the cryo-fracturing process, it is suggested that:

i. Figure 6.4 is more suitable to be used to predict the internal morphology of the single emulsion-PLGA microspheres produced in this thesis.
ii. Subsequent freeze-drying of 75:25MS can alter the internal structure of 75:25MS due to polymer aging or structural relaxation.

6.1.3 Distribution Of Entrapped Agent in PLGA Microsphere

This section studies the distribution of entrapped agent in microsphere which can mimic the distribution of the entrapped drug in PLGA microspheres. This information can be related to the drug release pattern of PLGA microsphere (Rigby *et al*., 2004 and Messaritaki *et al*., 2005). The objective was achieved by using a fluorescent compound, 4-trifluoromethyl umbelliferone (4-TFMU) as the entrapment agent and observation under confocal laser scanning microscopy (CLSM). 75:25MS entrapped with 4-TFMU were produced using the method described in Section 4.6.3. Confocal micrographs showing 75:25MS entrapped with 4-TFMU are shown in Figure 6.8.

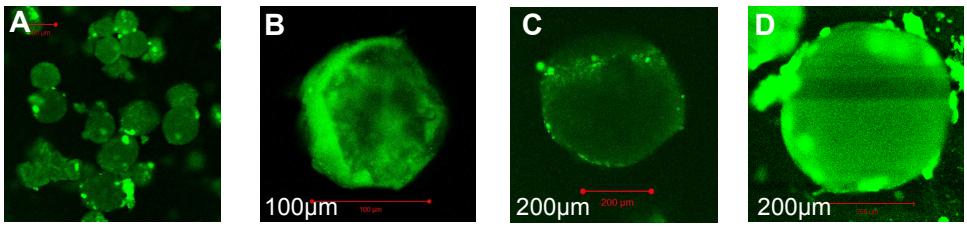

Figure 6.8: Confocal micrographs focused at equatorial plane showing (A) multiple 75:25MS and (B) to (D) singular 75:25MS entrapped with 4-TFMU.

Figure 6.8A shows multiples 75:25MS while singular 75:25MS are shown in Figure 6.8 (B) to (D). Figures 6.8 (B) and (C) indicate a heterogeneous distribution pattern of the entrapped 4-TFMU based on the varied fluorescence intensities. By "stacking" sequential 2D micrographs collected at different planes depth through the specimen, the spatial distribution of entrapped 4-TFMU in 75:25MS can be studied.

The 3D projections of 75:25MS entrapped with 4-TFMU are shown in Figures 6.9 and 6.10; with orthogonal views of the sphere and sequential 2D micrographs focused at different depth planes. The depth of the image plane is indicated on the top left corner of the micrograph; i.e., 0 μm indicates the image plane was at the periphery of the sphere; 1 μm indicates the image plane was 1 μm into the sphere from its periphery.

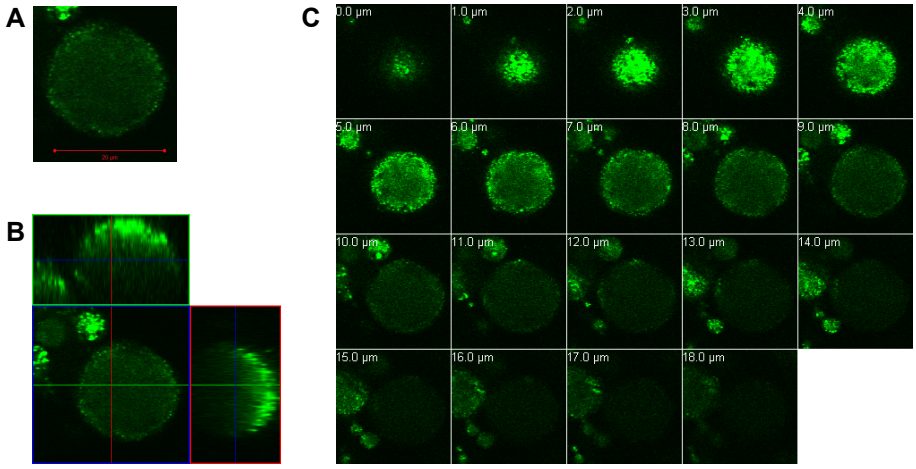

Figure 6.9: Confocal micrographs showing the cross sections of a 75:25MS entrapped with 4-TFMU, (A) at equatorial plane, (B) orthogonal views and (C) cross sections at different plane depth.

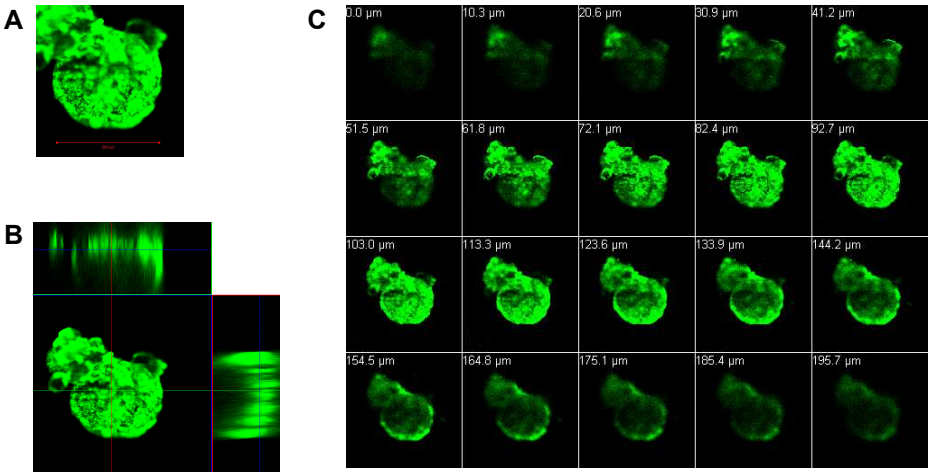

Figure 6.10: Confocal micrographs showing the cross sections of a 75:25MS entrapped with 4-TFMU, (A) at equatorial plane, (B) orthogonal views and (C) cross sections at different plane depth.

Figure 6.9 shows a 75:25MS of size ~20 μm. From Figure 6.9C, it can be seen that the spatial distribution of 4-TFMU varied across the sphere. For instance, with the increasing intensity from plane distance of 0 μm to 4-5 μm, this indicates an increase in concentration of entrapped agent across these planes. Figure 6.10 shows a number of smaller spheres are located at top left quadrant of the main sphere. Referring to the equatorial plane of the sphere, the 4-TFMU at this plane is highly concentrated (i.e. high intensities).

The distribution of 4-TFMU in sphere shown in Figure 6.10 indicates similarity to the one shown in Figure 6.9. Findings in Section 6.1.1 indicated that the 75:25MS has porous interior and this may permit water transport. Hence, regions filled with 4-TFMU could vary in intensity over time due to probable water transport within the porous the interior.

Figures 6.9 and 6.10 show that the spatial heterogeneous distribution of 4-TFMU in 75:25MS. The amorphous regions in PLGA are thought to hinder a homogeneous distribution of the entrapped agent (Sastre *et al.,* 2004). An imperfect entrapment can arise from an unstable emulsion during the production process. This instability leads to the coalescence of droplets and cause the drug to heterogeneously distribute in the microsphere (Perez *et al.*, 2000). Emulsion instability is also seen previously in Figure 6.4 where macrocavities are observed in the interior matrix.

6.2 Degradation of PLGA Microspheres

This section studies the *in vitro* degradation of 50:50MS, 65:35MS and 75:25MS in PBS. The same samples produced in Section 6.1.1 were used in this study. *In vitro* degradation was carried out by incubating the samples in a shaking water bath with a back-forth shaking (150 rpm) maintained at 37^{o}C. Details of degradation analysis can be found in Section 4.5. At ten, twenty and thirty days intervals, samples were collected for SEM imaging.

Hydrolysis has been widely accepted as the main degradation pathway for PLGA polymers (Metha *et al*., 1994; Hauesberger and DeLuca, 1995 and Lu *et al*., 1999). Typically, the term degradation refers to a chemical process resulting in the reduction of the average molecular weight. As the incubation progresses, erosion will take place and it is a physical process whereby mass is lost from the sample by solubilisation of polymer chains and their removal from the vicinity. It will be shown that the PLGA microspheres produced in this thesis

underwent bulk degradation pathway and their mass loss profiles are associated with lag phases. The degradation states of 50:50MS, 65:35MS and 75:25MS over a period of thirty days are shown in Figure 6.11.

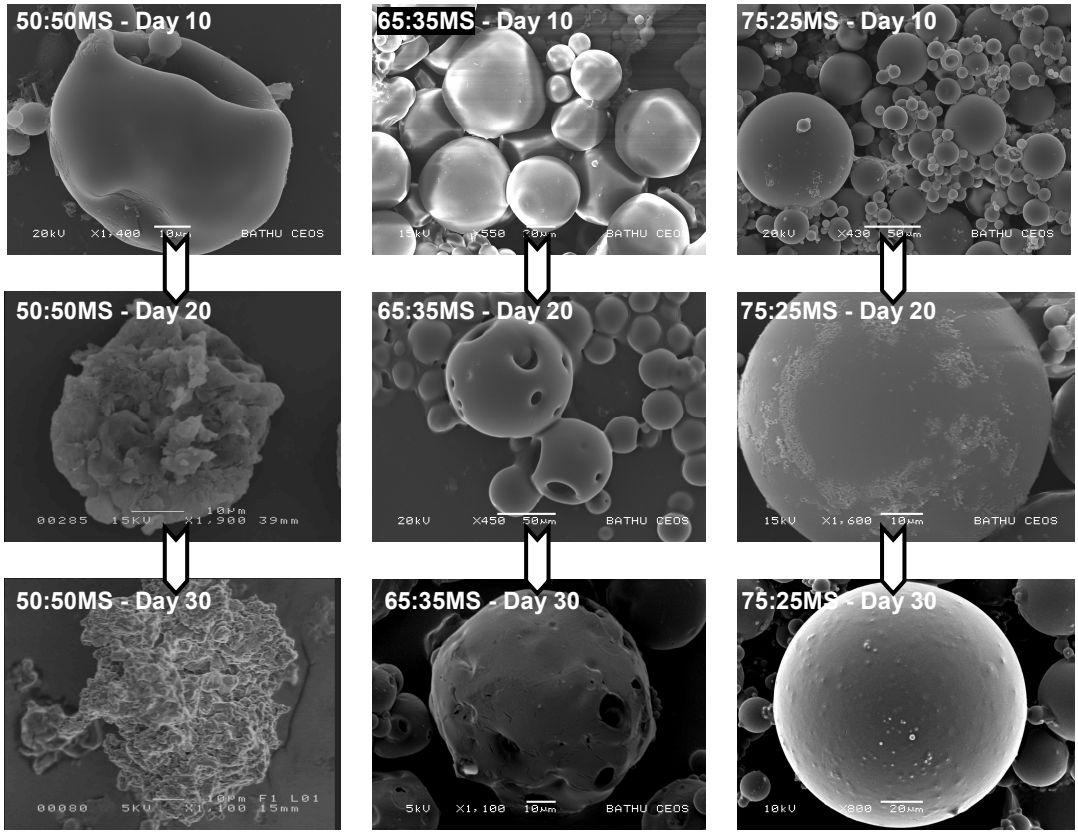

Figures 6.11: SEM images showing the morphological changes experienced by 50:50MS, 65:35MS and 75:25MS after 10, 20 and 30 days of incubation in PBS.

After ten days in PBS, 50:50MS had deformed and swelling/shrinking can be observed. After twenty days, the surface of 50:50MS had collapsed with small fractions of polymeric debris formed at its surface. After thirty days, it was increasingly difficult to distinguish a degraded 50:50MS from polymer debris. The degradation of 65:35MS after ten days exhibited a small degree of deformation and it could also be a result of hydration that caused 65:35MS to swell. After twenty days, pores can be partially observed on 65:35MS. The formation of these surface pores on 65:35MS is thought to be caused by degradation effect on the polymer. Unlike 50:50MS, 65:35MS did not degrade to substantial matrix disintegration and its morphology is retained after thirty days.

As the degradation process is hydrolytic, water uptake into the polymer has an important effect on the rate of polymer degradation. Amorphous PLGA permits water influx and initially, water diffuses into the microspheres and attacks the chemical bonds in the

amorphous region, cleaving the long PLGA chain (Zweers *et al*., 2004). As this progresses, polymer remnants will formed such as those seen in the twenty days degraded 50:50MS. Kiss and Vargha-Butler (1999) concluded that the glycolide content can significantly increase the hydrolysis rate of PLGA. Lactide with its pendant methyl group tends to sterically hinder water and makes it more hydrophobic than glycolide. Hence, 50:50MS is observed to degrade faster due to its highest glycolide ratio, which is more prone to hydrolytic attack.

Throughout the incubation period, 75:25MS demonstrated better resistance to degradation and retained its spherical form the best comparing to 50:50MS and 65:35MS. After ten days, no distinct effect of degradation is observed on 75:25MS. After twenty days, 75:25MS partially show small degree of roughness on its surface. Attempts to magnify on these areas were inconclusive because of the heat-sensitivity of the PLGA specimen. After thirty days, 75:25MS is still intact but with increased microscopic swelling across its surface.

PLGA undergoes bulk erosion due to faster water diffusion into the polymer matrix is than polymer degradation (Lu *et al*., 1999). Since the diffusion of water into the matrix is faster than polymer degradation, the whole matrix undergoes degradation and eventually erosion. The two principle mechanisms of polymer degradation are illustrated in Figure 6.12. The distinct differences between the two mechanisms is that surface erosion causes the sample to reduce in size while for bulk degradation, the sample experience less size reduction but undergoes more pronounced morphological changes. Surface erosion of polymers occurs with a constant rate while in bulk degradation; such as PLGA, it involves more complicated events because they do not show constant erosion velocity (Göpferich and Langer, 1995; Park, 1995 and Göpferich, 1996).

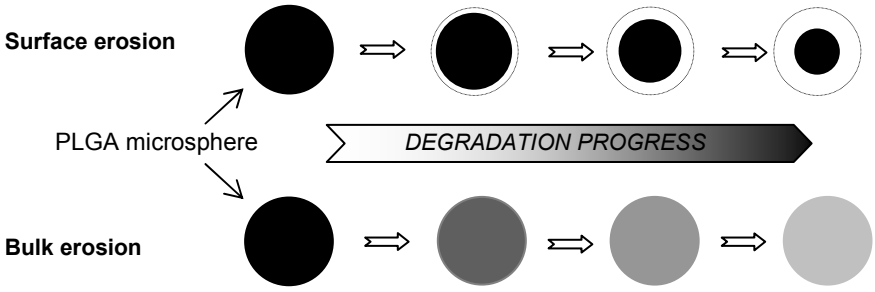

Figure 6.12: The mechanisms of surface and bulk erosions. *The colour intensity symbolises the degree of erosion; with the darkest as undegraded and lightest as most eroded.*

Based on Figure 6.11, it is evident that 50:50MS and 65:35MS exhibit the characteristics of bulk erosion. Initially, Spenlehauer *et al*. (1989) suggested that PLGA microspheres undergo

homogenous degradation with both equal rates of degradation in core and surface. Later it is discovered that PLGA microspheres can proceed heterogeneously throughout the device (Li *et al*., 1990 and Therin *et al*., 1992). This is caused by an autocatalysis situation. The degradation of PLGA will produce byproducts with carboxylic acid chain ends in the system. Figure 6.13 shows the formation of acidic products as a result of hydrolysis at the ester linkages in the PLGA chain.

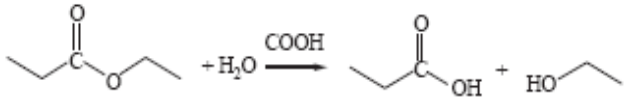

Figure 6.13: Hydrolysis of ester bonds in biodegradable polyesters (Loo *et al*., 2005).

The acidic byproducts could autocatalyse the ester hydrolysis. For those that are formed in the interior and are insoluble oligomers, they remained relatively trapped (de Jong *et al*., 2001). This results in a decrease in local pH which could promote interior degradation of the matrix. The soluble oligomers and those located near to the surface can leach out from the matrix through the diffusing medium. Meanwhile, the hydroxyl ions from the buffer provide a neutralisation effect on the carboxylic end groups located at the surface (Dong *et al*., 2005). Hence, the surface undergoes a relatively slower degradation compared to the interior.

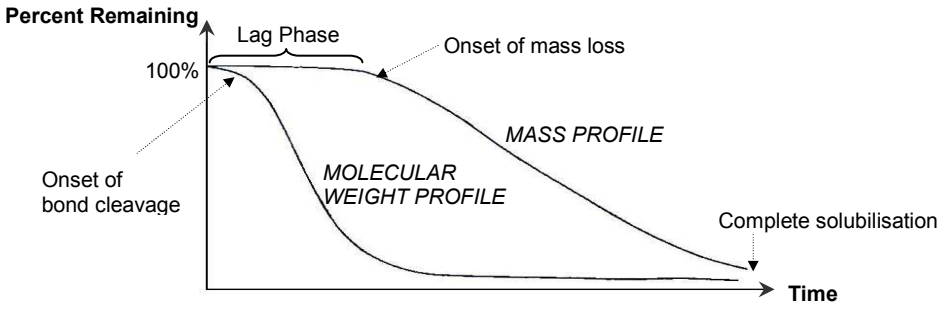

Figure 6.14: Theoretical molecular weight decrease and mass loss of PLGA during degradation (Hausberger and DeLuca, 1995).

A theoretical molecular weight decrease and mass loss during bulk degradation of PLGA is adapted from Hausberger and DeLuca (1995) and shown in Figure 6.14. During degradation, an almost immediate and rapid decrease in molecular weight can be observed as susceptible bonds in the PLGA chains are cleaved. This leads to the formation of chains of small fragments as the degradation products. The onset of mass loss corresponds to a point when a critical molecular weight is reached due to the continual bond cleavage. Appreciable mass loss will only begin when the degraded small fragments begin to obtain a critical molecular

weight (Hausberger and DeLuca, 1995 and Metha *et al*., 1994). After this only will the solubilisation of low molecular weight degradation products begun. Hence, a lag phase is present on the mass loss profile as indicated in Figure 6.14.

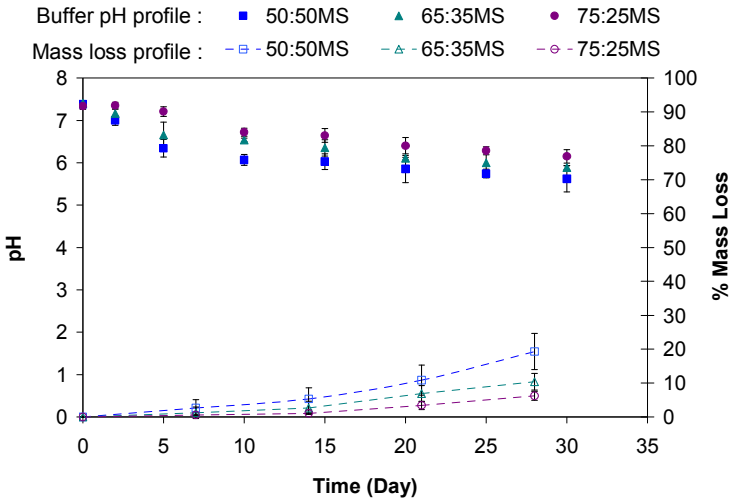

Figure 6.15: The degradation profiles of 50:50MS, 65:35MS and 75:25MS.

The pH and mass loss profiles of 50:50MS, 65:35MS and 75:25MS during the incubation in buffer were measured and are shown in Figure 6.15. The decrease in pH suggests the release of acidic products from degradation of PLGA samples. The buffer pH of 50:50MS was the lowest after thirty days of degradation. This suggests the greater susceptibility of glycolide to hydrolytic degradation. The removal of glycolic acid has been reported to be as twice as fast as that of lactic acid from 50:50 PLGA sample (Göpferich, 1996). Meanwhile, Siepmann *et al*. (2004) reported that the sizes of microspheres did not strongly affect the degradation of the matrix. However, the buffer pH's of the three PLGA samples at Day 30 were not significantly different from each other (ANOVA, $p < 0.05$).

The initial more prominent decrease in buffer pH of 50:50MS and 65:35MS may due to the initial release of degradation products near the microsphere surface. Meanwhile, the buffer influx may have given rise to a neutralisation effect. Time also required for the degraded byproducts formed in the interior to leach out. Combination of these conditions minimise the decrease in buffer pH at later stage.

Appreciable mass loss of 50:50MS was only noticeable after approximately a week, and two weeks for 65:35MS and 75:25MS. This may be because the degraded mono/oligomers had not reached critical molecular weights and the soluble byproducts were only formed at later

stage. These two conditions might have delayed the onset of mass loss. The lag phase may also due to the time required by the polymeric microspheres to become hydrated (Metha *et al*., 1994). The degraded products formed in the interior also depend on the presence of a medium for transport or to leach out into the buffer. The lag phase in mass loss of 50:50 PLGA microspheres could be as long as two weeks (Dunne *et al*., 2000).

At the end of thirty days, the changes in both the buffer pH and mass loss of 75:25MS and 65:35MS were not as extensive as for 50:50MS. Only the mass loss of 50:50MS was significantly different from that of 75:25MS (ANOVA, $p < 0.05$). This is attributable to the greater degradation resistance of 75:25 PLGA. During degradation of PLGA in buffer, the matrix shifts from glassy state to a rubbery state and is independent of the microsphere size (Siepmann *et al*., 2004). The increasing mass loss in 50:50MS is attributable to the continual attack in its amorphous region as the polymer state rapidly shifts to a rubbery state. The rubbery state permits higher water diffusion through the matrix and further promotes the hydrolytic attack on the PLGA chain, causing further mass loss.

6.3 Morphological Characterisation of PLGA Hollow Fibres

This section presents the morphology of PLGA hollow fibre produced based on the phase inversion method described in Section 4.2.3. For ease, 50:50 PLGA hollow fibre will be abbreviated as 50:50HF henceforth; similarly for 65:35 and 75:25 PLGA hollow fibres. The outer surfaces of 50:50HF, 65:35HF and 75:25HF are shown in Figure 6.16. They are relatively smooth with no visible pores. These pore-less surfaces are a result of the rapid polymer precipitation during the phase inversion. A small degree of unevenness on the surface of 50:50HF may be caused by the amorphous property of 50:50 PLGA as apposed to the more crystalline 75:25 PLGA, which show a denser and smoother outer surface. Mechanical dragging or friction between the orifice and the nascent hollow fibre can also cause uneven polymer deposition during the spinning process.

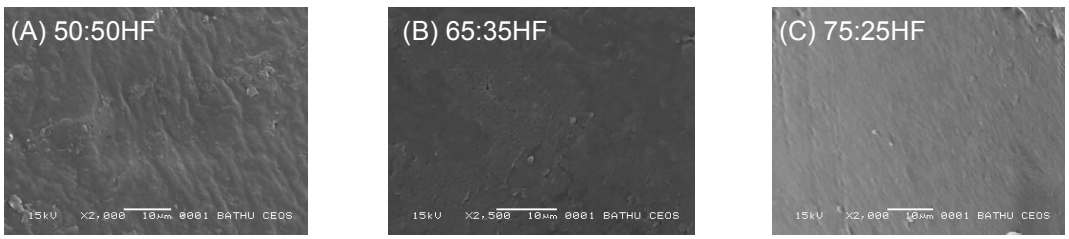

Figure 6.16: The outer surfaces of 20 % (w/w) (A) 50:50HF, (B) 65:35HF and (C) 75:25HF.

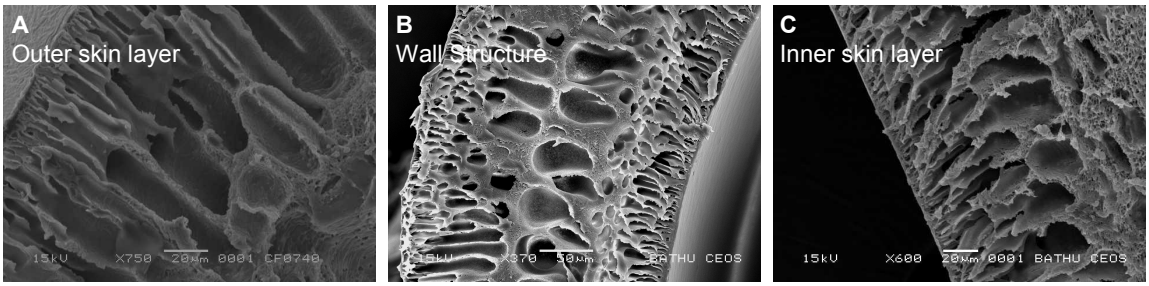

Figure 6.17: Detailed cross sectional views of the fibre wall structure of 20 % (w/w) 75:25HF.

Figure 6.17 shows the cross section details of 75:25HF. The overall "honey-comb" structure can be seen across the fibre wall as indicated in Figure 6.16B. Both the outer and inner skin layers with adjacent finger-like microcavities can be seen (Figure 6.16A and D, respectively). Throughout the phase inversion process, air pockets were formed initially and upon solidification, transformed to the finger-like microcavities and macrovoids structures. The long and elliptical finger cavities are due to diffusion of solvent into the aqueous phase. These different sublayers form the asymmetrical property of the hollow fibre membrane, which also give the fibre its mechanical support.

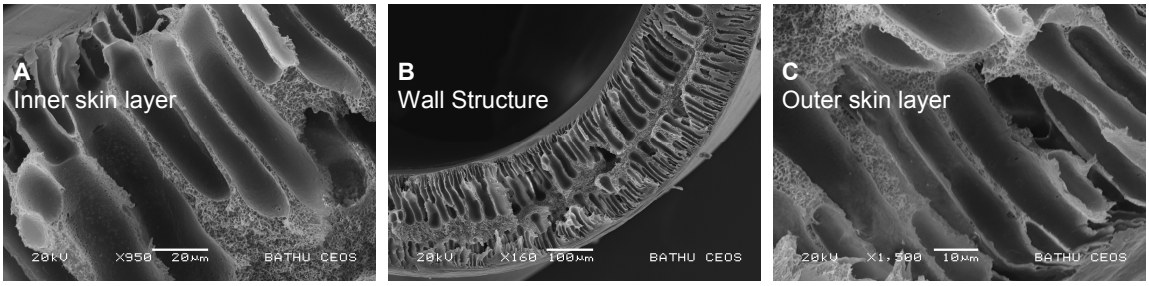

Figure 6.18: Detailed cross sectional views of the fibre wall structure of 20 % (w/w) 65:35HF.

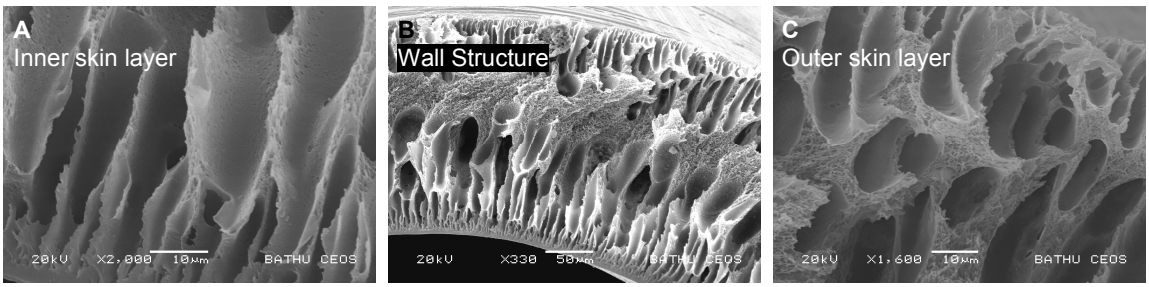

Figure 6.19: Detailed cross sectional views of the fibre wall structure of 20 % (w/w) 50:50HF.

The cross sections of 65:35HF and 50:50HF are shown on Figures 6.18 and 6.19 respectively. In all cases, the finger-like microcavities are visible across the fibre walls between the skin layers. The skin layers are formed during the contact between the polymer solution and water. The diffusion of solvent is rapid and this produces layers with denser

structures compared to the centre of the fibre. The slower diffusion of the remaining solvent from the nascent hollow fibre gives rise to the macrovoids at the fibre core.

6.4 Degradation of PLGA Hollow Fibres

This section studies the *in vitro* degradation of 50:50HF, 65:35HF and 75:25HF. The same batches of PLGA hollow fibres produced in Section 6.3 were used in this study. *In vitro* degradation was carried out by incubating the samples in a shaking water bath with a back-forth shaking (150 rpm) maintained at 37^{o}C. More details of degradation analysis can be found in Section 4.5. At ten, twenty and thirty days intervals, fibres were randomly collected, sectioned and prepared for SEM imaging. The degradation conditions of 50:50HF, 65:35HF and 75:25HF are shown in Figures 6.20 to 6.22. Figure 6.20 shows the degradation of 50:50HF incubated in PBS for ten, twenty and thirty days.

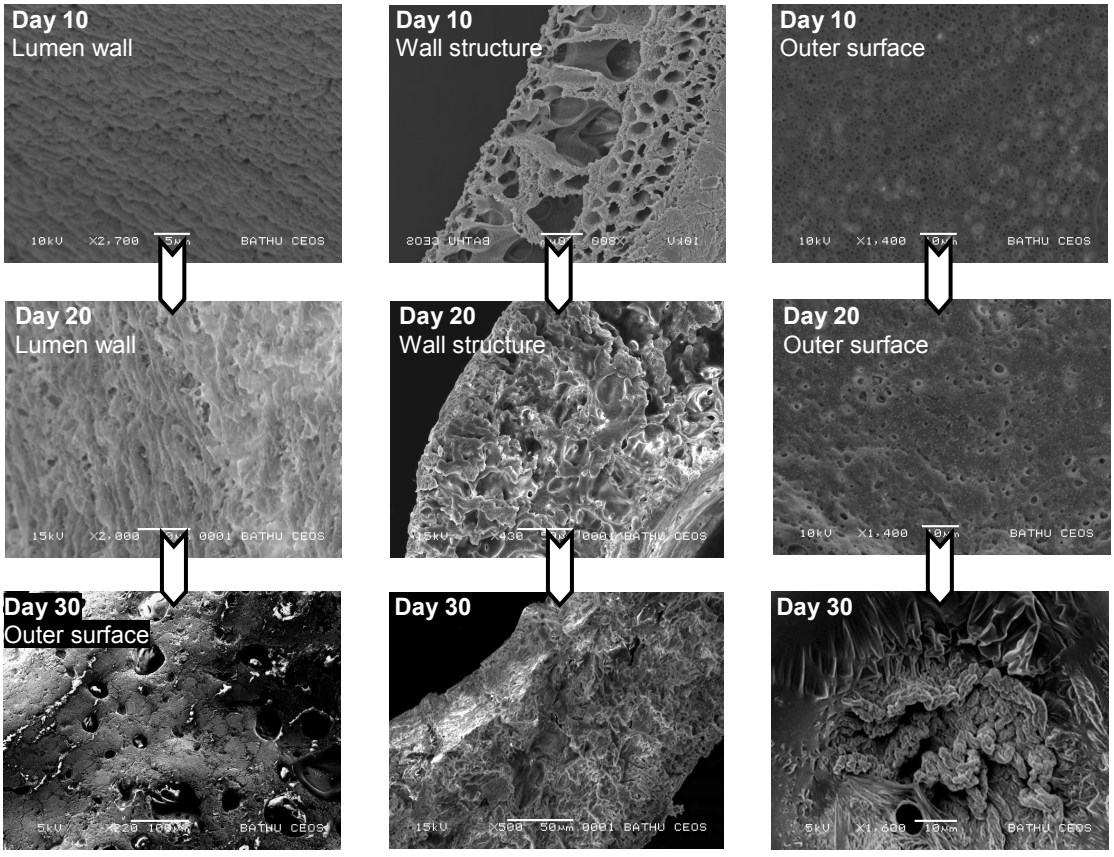

Figure 6.20: SEM images of degrading 50:50HF after 10, 20 and 30 days of incubation in PBS.

The honeycomb structure across the fibre wall of 50:50HF at Day 10 was still intact but its macrocavities had markedly increased in size. Numerous pores can be observed on its outer

surface. These conditions show that degradation effect will lead to an increase in the fibre porosity. Figure 6.20 shows that 50:50HF with the most glycolide content is highly susceptible to hydrolytic degradation. The glycolic acid in the PLGA chain was suggested by Göpferich (1996) could be more susceptible to hydrolytic attack. At Day 30, 50:50HF had disintegrated into polymeric debris. The thirty days degraded 50:50HF showed the entanglements of polymer chain most likely constituted by the remaining polylactide.

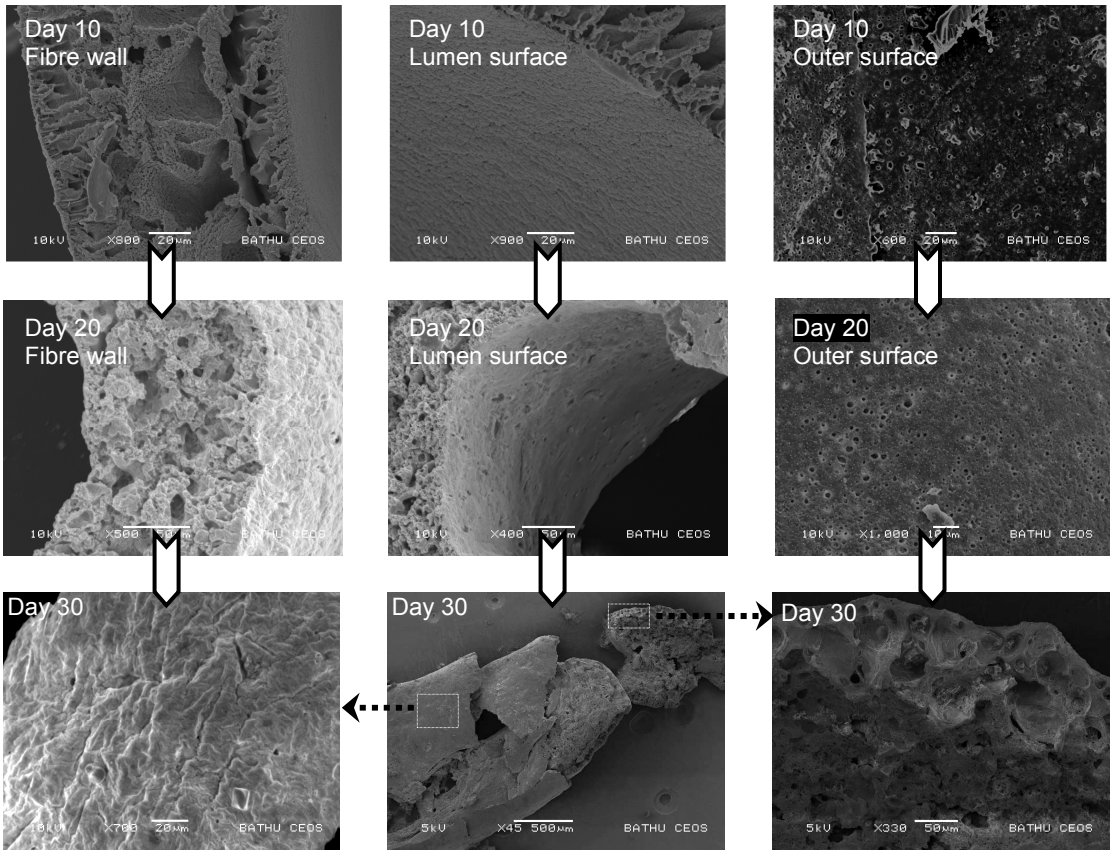

Figure 6.21: SEM images of degrading 65:35HF after 10, 20 and 30 days of incubation in PBS.

Figure 6.21 shows the degradation conditions of 65:35HF incubated in PBS for ten, twenty and thirty days. The fibre wall at Day 10 still retains the honeycomb structure but is highly porous. Pores formation had also begun on the outer surface of 65:35HF at Day 10. Degradation effect becomes noticeable by comparing the lumen surfaces of 65:25HF at Days 10 and 20. At Day 20, the degraded 65:35HF lost its honeycomb structure in the fibre wall. Similar approach from 50:50HF is applied here where the amorphous regions in the PLGA permitted hydrolytic attack and the breakage of mono- or oligo-mers disrupted the polymer chain. As a result, disintegration to the physical state of the thirty days degraded 65:35HF is clearly visible.

The thirty days degraded 65:35HF confirms the occurrence of autocatalytic effect where its outer surface condition is better than its disrupted interior. As previously discussed, the fast water diffusion leads to hydrolytic attack in the fibre interior. With the formation of insoluble byproducts and the skin layers that restrict mass transfer, minimises medium transport. Hence, the accumulation of acidic products might have promoted autocatalytic degradation. Meanwhile, the formation of degradation products at/near the fibre surface are likely to be neutralised by the bulk fluid and thus, degradation is suppressed.

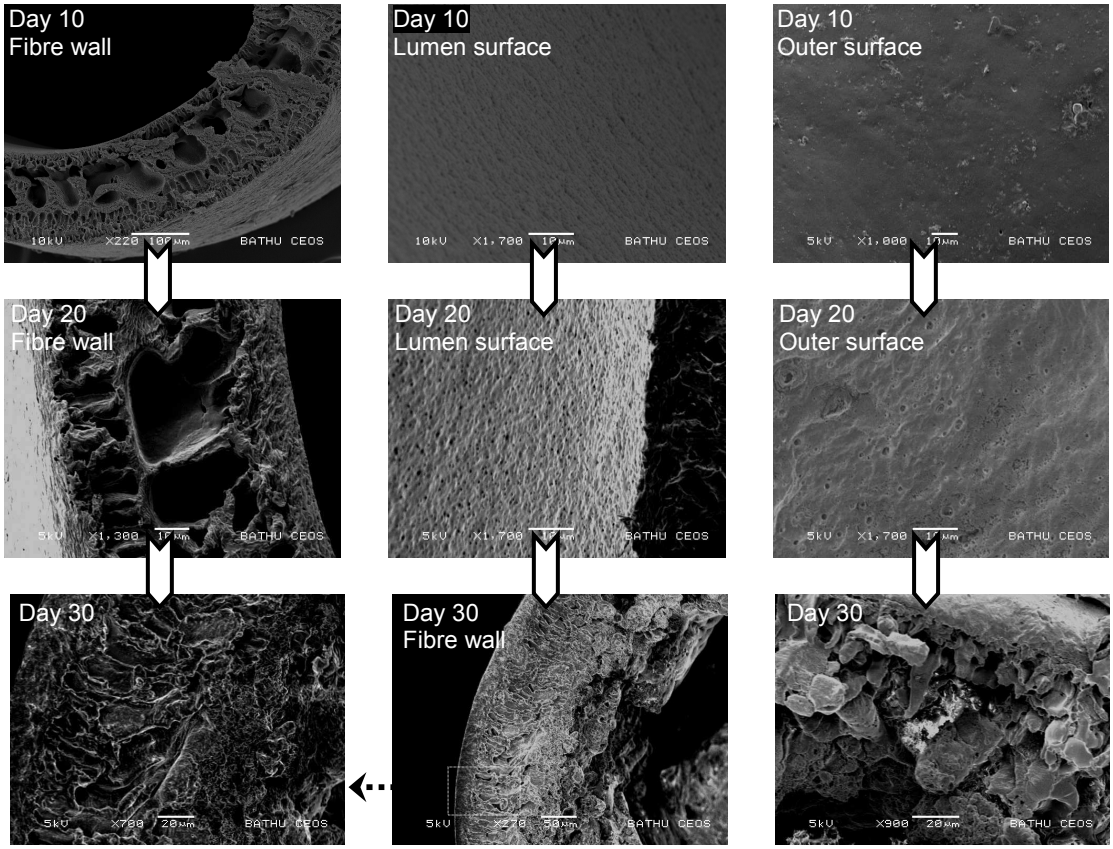

Figure 6.22: SEM images of degrading 75:25HF after 10, 20 and 30 days of incubation in PBS.

Figure 6.22 shows the degradation conditions of 75:25HF incubated in PBS for ten, twenty and thirty days. At Days 10 and 20, the fibre wall structure of 75:25HF did not undergo any distinct degradation but pores are visible on their lumen surfaces. After Day 30, 75:25HF still retain its fibre integrity but its honeycomb structure had started to collapse. As previously discussed, the presence of an extra chiral methyl group on the lactide unit reduces the chemical reactivity of the ester groups through steric hindrance (Göpferich, 1996). The removal of mono- or oligo-mers from the PLGA main chain also increases the mobility of the remaining molecules. Polymer backbone movements may have produced the structural changes observed in the thirty days degraded 75:25HF.

In general, the degradation states of PLGA hollow fibres demonstrated the expected trend; where 50:50HF with the highest glycolic acid ratio experienced the fastest degradation rate. In contrast, 75:25HF demonstrated high degradation resistance. This trend concurred with the previous results from PLGA microspheres. By studying the degradation states of PLGA hollow fibres, it is confirmed that PLGA hollow fibres undergo bulk degradation erosion.

In terms of the structure of the devices, hollow fibres have a more open structure for contact with water compared to microspheres, i.e. the lumen of the hollow fibre and its open end fibre wall structure. These conditions allow for higher water influx into the fibre. However, as aforementioned, the denser structures at the skin layers of the hollow fibres are associated with high mass transfer resistance. This effect is reflected on the thirty days degraded 65:35HF where polymeric disruption was less severe at the surface compared to the interior.

The initial formation of insoluble degradation products and the restricted mass transfer at the skin layers, promoted autocatalytic effect at the fibre interior. Since hollow fibre is a larger and thicker structure compared to microsphere, the degree of heterogeneous or bimodal degradation in hollow fibre would be greater (Grizzi *et al*., 1993).

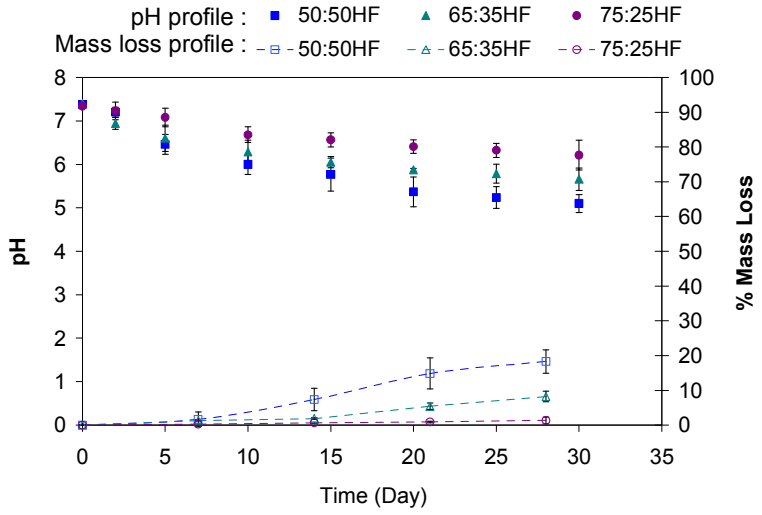

Figure 6.23: The degradation profiles of 50:50HF, 65:35HF and 75:25HF.

The mass loss and buffer pH profiles of 50:50HF, 65:35HF and 75:25HF were measured over a period of four weeks and results are shown in Figure 6.23. From statistic analyses (ANOVA, $p < 0.05$), only the buffer pH and mass loss of 50:50HF were significantly different from 75:25MS. There were significant differences between 65:35HF from 50:50HF and 75:25HF. The lag phase for 50:50HF is observed to be approximately two weeks and

after this, the mass loss tends to increase linearly. The mass losses of 63:35HF and 75:35HF are lower in comparison. Figure 6.20 shows that 50:50HF underwent severe degradation effect and the porosity of its structure was increased. The increased porosity may have eased the release of degradation byproducts and this is reflected by the decreasing buffer pH of 50:50HF seen in Figure 6.23. The increased porosity also promoted buffer penetration and diffusion. As a result, degradation continued causing the mass loss to increase further.

The decrease in buffer pH of 65:35HF and 75:25HF was not as great as for 50:50HF. The small changes in buffer pH may due to the less degradation effects occurring in the former two. Since 65:35HF and 75:25HF have higher lactic acid compositions in their polymers, they would have higher degradation resistances.

6.5 Morphological Characterisation of PLGA Solid Fibres

This section presents the morphology of PLGA solid fibres produced using the phase inversion technique described in Section 4.2.3. 20 % (w/w) 50:50, 65:35 and 75:25 PLGA were used to produce blank solid fibres. For ease, 50:50 PLGA solid fibre will be abbreviated as 50:50SF henceforth; similarly for 65:35 and 75:25 PLGA solid fibres. The surface conditions of 50:50SF, 65:35SF and 75:25SF are shown in Figure 6.24. Similar to PLGA hollow fibres, these solid fibres have smooth and rigid surfaces. The rapid polymer deposition during the phase inversion produces these properties.

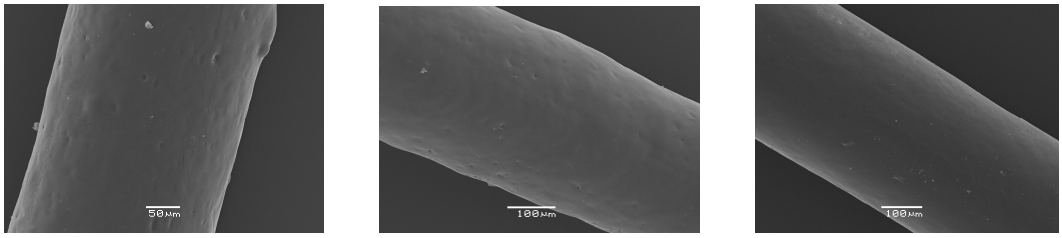

Figure 6.24: The surface conditions of 20 % (w/w) (A) 50:50SF, (B) 65:35SF and (C) 75:25SF.

The morphology of the cross sections of 75:25SF, 65:35SF and 50:50SF are shown in Figure 6.25. The cross sectional structures of 50:50SF, 65:35SF and 75:25SF show the typical finger-like microcavities structures enveloping by skin layers. Unlike hollow fibre, solid fibre has no lumen. The longer solvent diffusion path from the fibre core contributes to the extended finger structure during the phase inversion process.

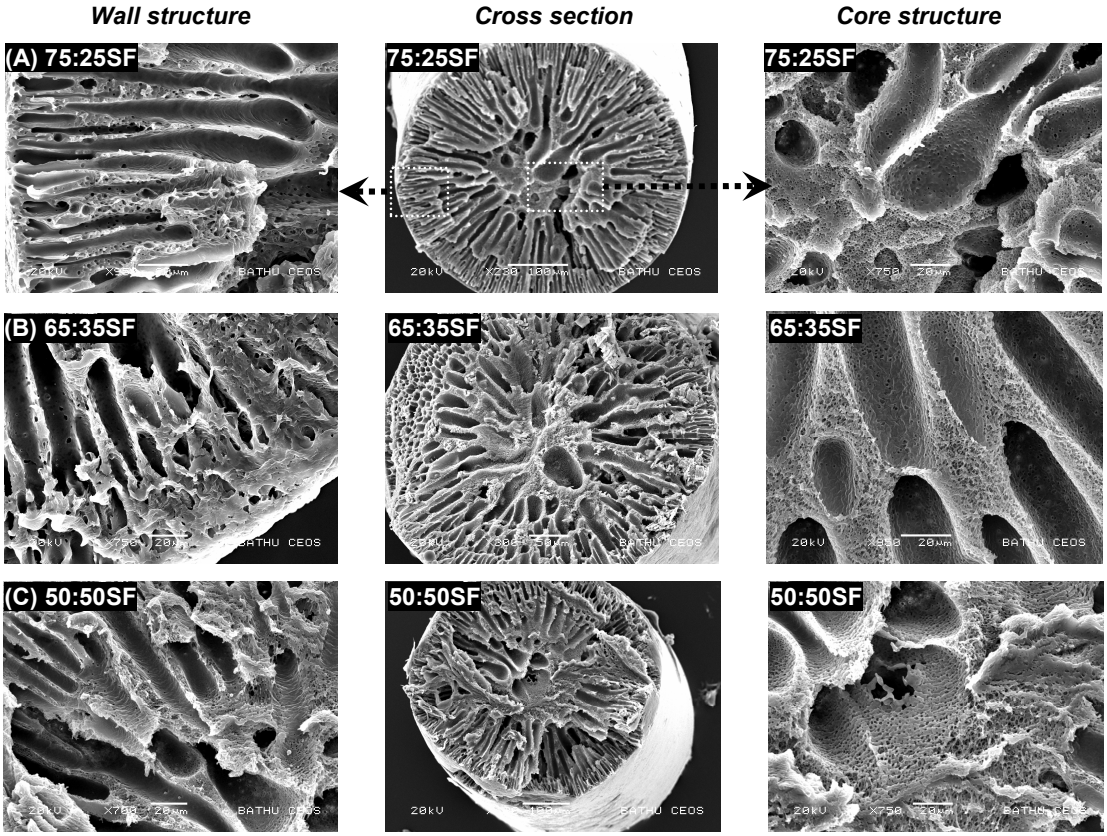

Figure 6.25: The cross sectional views of 20 % (w/w) (A) 75:25SF, (B) 65:35SF and (C) 50:50SF.

6.6 Degradation of PLGA Solid Fibres

This section studies the *in vitro* degradation of 50:50SF, 65:35SF and 75:25SF. The same batches of PLGA solid fibres produced in Section 6.5 were used in this study. *In vitro* degradation was carried out by incubating the samples in a shaking water bath with a back-forth shaking (150 rpm) maintained at 37^{o}C. Details of degradation analysis can be found in Section 4.5. At ten, twenty and thirty days intervals, fibres were randomly collected, sectioned and prepared for SEM imaging.

The degradation states of 50:50SF after ten, twenty and thirty days of incubation in PBS are shown in Figure 6.26. As incubation progresses, the degree of unevenness and swelling on the surface of 50:50SF developed over time. Swelling effect on 50:50SF is clearly visible at Day 10. Meanwhile, the fast degrading 50:50SF lost the finger structure of its fibre wall. The development of surface pore is visible from Day 20 to Day 30 as 50:50SF. Cavities are observed to be developing at the core of 50:50SF at Day 10. As degradation progressed, these cavities continued to grow in size and depth, after twenty and thirty days in PBS.

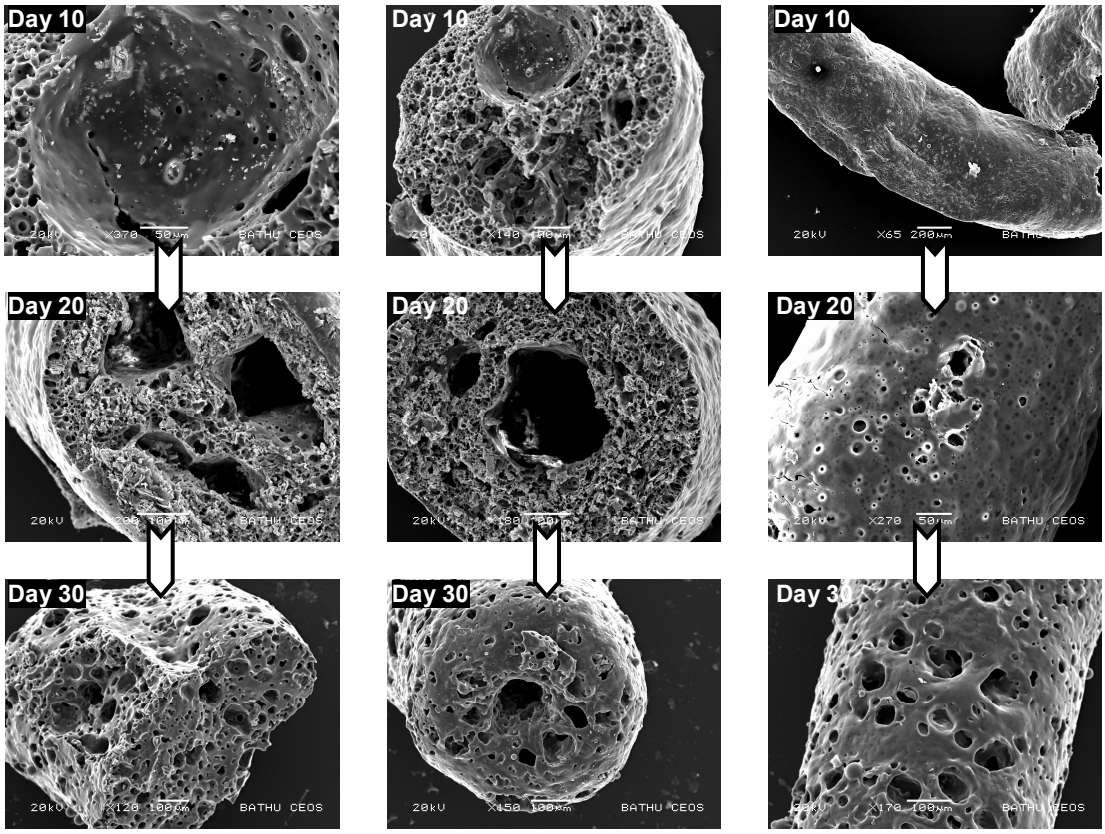

Figure 6.26: 20 % (w/w) 50:50SF after 10, 20 and 30 days of incubation in PBS.

The presence of interior autocatalysis is thought to contribute to the hollowness of the cavities. Unlike hollow fibre, solid fibre without lumen offers no passage to transport any degraded byproducts. Findings in Section 6.4 showed that PLGA can undergo heterogeneous degradation where the inner matrix experience different rates of degradation compared to the matrix surface. The 50:50SF sample was incubated at 37^{o}C and subjected to constant shaking while immersion in buffer led to hydrolytic degradation. Under these conditions, the unevenness on the fibre surface may also caused by the distortion to the polymer chain as a result of degradation, heat or motion effects from the incubation.

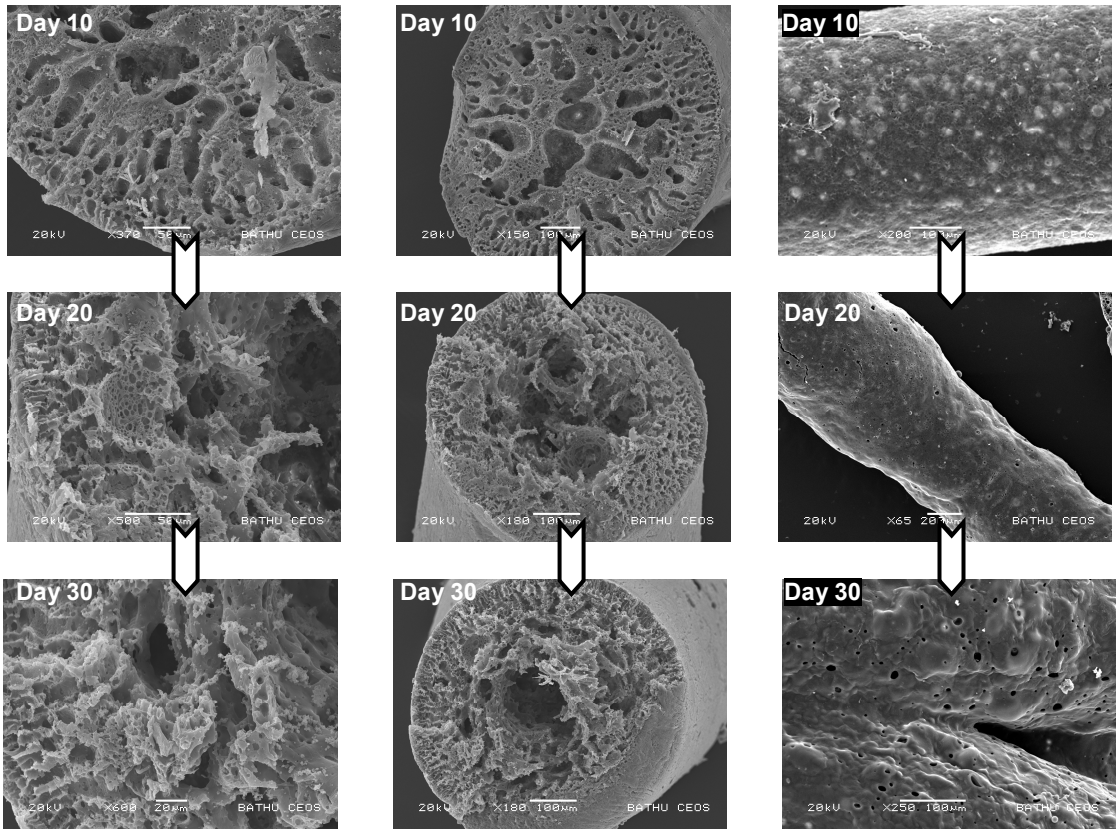

Figure 6.27: 20 % (w/w) 65:35SF after 10, 20 and 30 days of incubation in PBS.

Figure 6.27 shows the ten, twenty and thirty days degraded 65:35SF. The finger structure is partially visible at Day 10 and the swelling on the fibre can also be observed. The swelling confirms the uptake of water by polymeric solid fibre. Among the finger structure, larger cavities had also started to develop at the core of 65:35SF on Day 10. At Day 20, the cavities at the core continued to develop and the polymeric disintegration due to degradation is becoming more evident. Degradation continued and at Day 30, these cavities had grown in size and depth.

With the swelling effect, the interior of the fibre becomes more hydrated as the polymer shifts to a rubbery state. This hydration subsequently may have promoted interior hydrolytic degradation. The accumulation of the degraded byproducts in the fibre core matrix can produce a local acidic environment which autocatalyse the degradation. The degraded polymer remnants at the core matrix can be seen at Day 30.

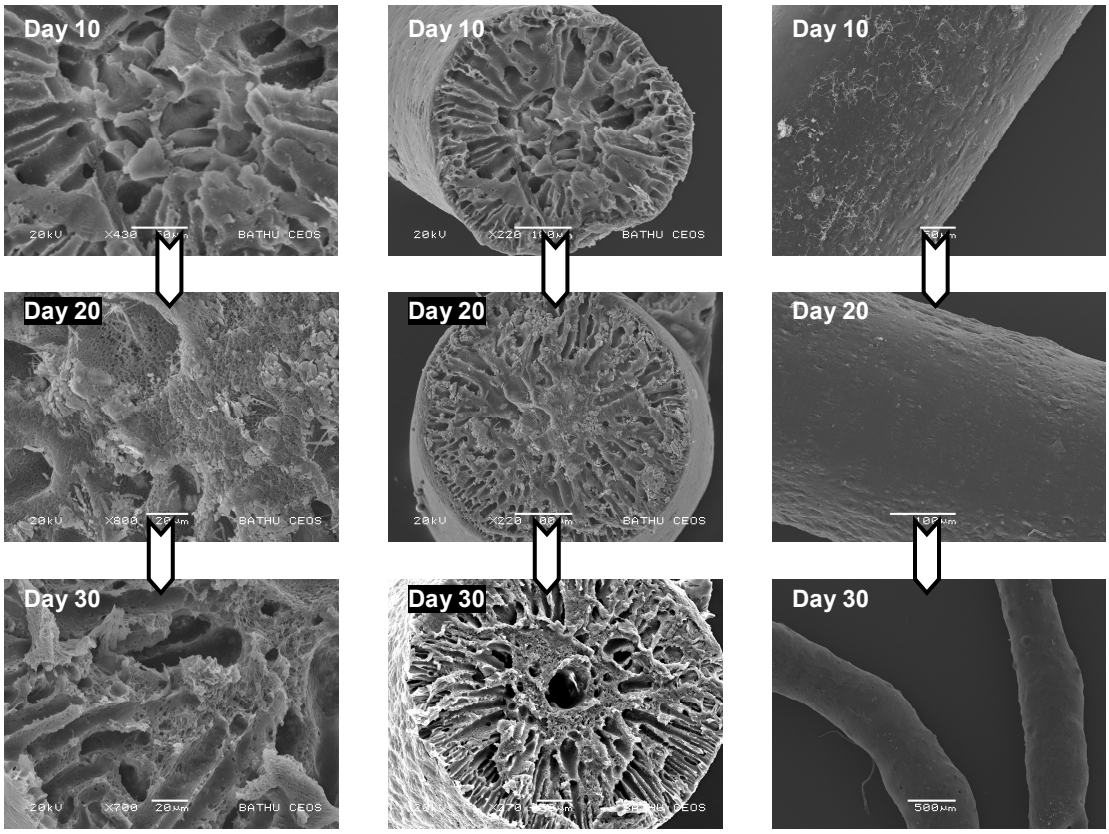

Figure 6.28: 20 % (w/w) 75:25SF after 10 and 20 days of incubation in PBS.

Figure 6.28 shows the ten, twenty and thirty days degraded 75:25SF. In general, the structural changes in 75:25SF was minimal compared to 50:50SF and 65:35SF. The finger structure of 75:25SF can be clearly identified throughout the incubation period. This scenario is attributable to its higher lactide content which have high resistance against hydrolytic attack.

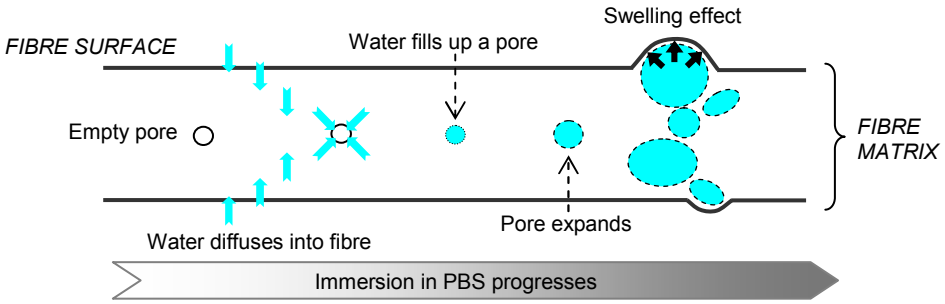

Figure 6.29: A simplified illustration of the swelling-expansion events in a porous fibre matrix. Bold arrows indicate hydrolytic attack.

The polymer swelling/shrinking in solid fibre is thought to be similar to those observed in microspheres. A hypothetical pore expansion is illustrated in Figure 6.29 to envisage the different swelling degrees experienced by PLGA solid fibre. Considering a single void or

pore is gradually becoming hydrated, the pore/void will expand. This expansion takes place in all direction and continues towards the outer layer of the fibre. The fibre porous structure comprises non-uniform cavities of various sizes and dimensions. Therefore these pores/cavities will expand at different rates. These conditions are suggested to be the cause of the unevenness of the fibre surface.

Regions with different water permeability; i.e. glycolic vs. lactic acids regions, may also evolve over time as degradation takes places. This could further alter the structural expansion in the fibre. At the swollen surface, the surface tension at the hemispheres stresses the polymer chain and with the breakage of oligomers, monomers or glycolide from the region, polymeric disintegration leads to the formation of surface pores.

The degraded PLGA solid fibres at the end of thirty days are observed to retain better structural integrity compared to PLGA microspheres, especially in the case for 50:50 PLGA. The much larger structure of solid (and hollow) fibre offers smaller surface area for contact with buffer compared to the submicron microsphere. This factor reduces the degradation effect on solid fibre. Similar to hollow fibre, the dense structure at the skin layer of solid fibre restricts medium transport. Therefore buffer influx is minimised and degradation is also reduced in the interior. This condition may also minimise the transport of degradation products, and interior autocatalytic degradation would be more severe in solid fibre compared to hollow fibre. As result, large cavities were developed at the core of the fibre due to more severe autocatalysed degradation.

The mass loss and changes in buffer pH during the degradation of 50:50SF, 65:35SF and 75:25SF were measured and results are shown in Figure 6.30. The development of large cavities at the core of 50:50SF from Day 10 onwards (Figure 6.26) can be validated by the continual decrement in its buffer pH which was caused by the release of degradation acidic products. The lag phase in mass loss of 50:50SF is approximately two weeks. Prior to the onset of mass loss, the interior autocatalysis reaction gradually increased the interior porosity. After two weeks, the degradation products leached out into the buffer as the formation of surface pore took place. At this stage, it is thought that 50:50SF had degraded to a critical degree where a network of pores within the polymeric matrix has formed, which allows the release of monomers and oligomers (Burkersvoda *et al*., 2002). This caused appreciate mass loss and drop in buffer pH. The increased porosity permitted higher

hydration rate and medium transport therefore degradation rate also increased. As a result, the mass loss of 50:50SF continued to increase.

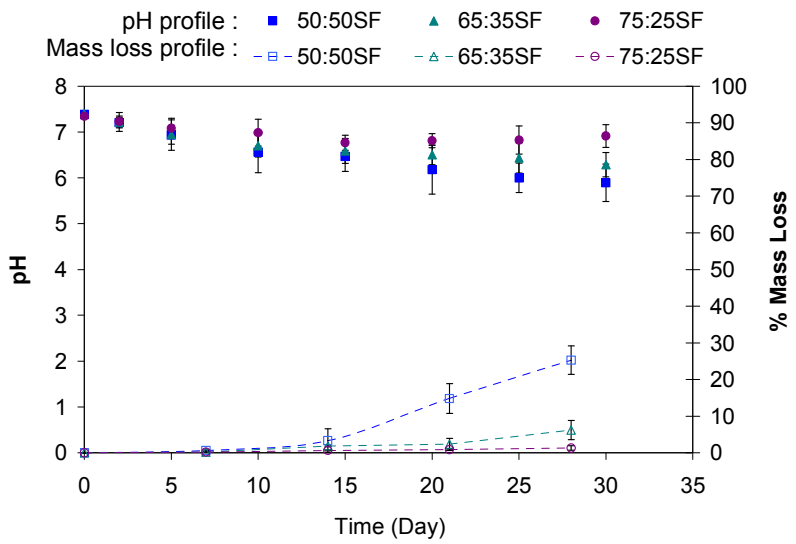

Figure 6.30: The degradation profiles of 50:50SF, 65:35SF and 75:25SF. Fill symbols = pH profile. Open symbols = mass loss profile.

Figure 6.27 shows that 65:35SF experienced greater erosion than 75:25SF. This is reflected in the decrease in buffer pH of 65:35SF compared to the buffer pH of 75:25SF. While the surface degradation of 65:35SF and 75:25SF were experiencing neutralisation effect from the buffer, the degradation effect was reduced. Coupled with the delay in pore formation, less acidic products were formed and released into the buffer. Thus, decrease in buffer pH was not as prominent as in 50:50SF. This concurs with the relatively small mass loss experienced by 65:35SF and 75:25SF. Statistic analyses (ANOVA, $p < 0.05$) suggested that only the buffer pH and mass loss of 50:50SF were significantly different from those of 75:25SF.

6.7 Conclusion

1. Degradation of PLGA devices is thought to be initiated by hydration during the immersion in buffer. The amorphous property of PLGA permits buffer influx into the polymer matrix.

2. For PLGA polymer, the mechanism of degradation is assumed to be hydrolysis. The mode of action of hydrolytic attack is through the random scission at the ester linkage

in the polymer main chain. The final degradation product is the monomers of the copolymer; namely lactic and glycolic acids.

3. For PLGA microspheres, hollow and solid fibres, the degradation pathway on these devices assume the bulk degradation characteristic. This is evident in the degradation studies where the degrading PLGA devices underwent obvious morphological changes.

4. Devices made of 75:25 PLGA experienced the least effect of degradation because of its highest lactide content compared to 65:35 and 50:50 PLGA. This is thought to benefit from the extra chiral methyl group in the lactic unit which enhances its chemical stability towards hydrolytic attack. 50:50 PLGA which has the least lactide ratio demonstrated the opposite characteristic. 50:50 PLGA experienced the fastest degradation rate due to its higher glycolide ratio.

5. Autocatalytic degradation is observed to occur in PLGA devices. This is attributable to the accumulation of the degradation products with carboxylic end groups. Degraded product at the surface of the device can be removed from the vicinity by buffer. For those that trapped deeper in the matrix or interior of the devices, their accumulation would result in a decrease in local pH and hence, autocatalyse the degradation. This is evident for the case of PLGA hollow and solid fibres where their core or fibre wall structures experienced higher degree of polymeric disintegration compared to their outer surfaces.

6. Comparing the degradation rates between microsphere, hollow and solid fibres, microsphere degrade the fastest. This is because the submicron particles have higher surface area therefore offer greater medium influx rate. Thus, a higher hydration rate and faster degradation are observed. For hollow fibre, its lumen provided extra surface area for medium transport compared to solid fibre. This leads to better release of degradation products and thus autocatalysis was not as severe as those observed in solid fibre. The degrading solid fibre show core disruption and larger cavities were developing at the core as degradation progressed.

7. The unique finger structures formed during the phase inversion technique of hollow and solid fibres are also thought to indirectly resist hydrolytic degradation. This is because of the denser structures near the skin layers are associated with high mass

transfer resistance. This minimises buffer influx and hydration that cause hydrolytic degradation.

8. From the literature, the swelling of polymeric matrix shifts the system from glassy state to rubbery state. Medium diffusion is assumed to be faster in the rubbery state. Thus, swelling of PLGA devices is thought to have promoted hydration and swollen devices undergo faster degradation. The morphological conditions of the three PLGA devices shown in SEM images evidently demonstrate that these devices experienced swelling.

9. In terms of mass loss, devices made of 50:50 PLGA exhibit the highest and fastest mass loss. This is attributed to its higher glycolide ratio, which is more prone to degradation. A lag phase of approximately two weeks is observed in the mass loss profile of 50:50 PLGA hollow and solid fibres. In the case of 50:50MS, the lag phase was observed to be approximately a week.

10. The mass loss of 50:50 devices at the end of four weeks varied between 20 to 30%. For devices made of 65:35 PLGA, the mass loss is approximately 10% and 5% for devices made of 75:25 PLGA at the end of four weeks. The onsets of mass loss of the latter two were delayed for more than two weeks.

11. The decrease in buffer pH is the highest for devices made of 50:50 PLGA due to their greater susceptibilities to hydrolytic degradation. This led to the formation of more acidic degradation products and once leached into the buffer, the buffer pH is subsequently lowered.

CHAPTER 7
STUDIES OF CONFINED WATER IN PLGA MICROSPHERES

This chapter studies the transport of free water imbibed within pores of PLGA microspheres using nuclear magnetic resonance (NMR). The approach is to follow the movement of free water to probe structural information of the sample. Quantitative analyses such as mean pore size, pore size distribution and volume can be obtained from available techniques such as mercury porosimetry and gas adsorption. The former uses a mercury intrusion-extrusion mechanism while the latter uses nitrogen adsorption-desorption.

Mercury porosimetry also requires absolutely dry sample and this technique forces mercury into the pores or voids by applying pressure (Strange *et al*., 1993 and Strange, 1994). Mercury will not replace any liquid already in the pores or voids, unless additional pressure is applied to displace the liquid (Ek *et al*., 1995). Since the analysis usually undergoes two pressure levels (one lower and one higher), concern is then raised where high pressure might possibly deform a pore (Landry, 2005). Difficulty also encountered in discriminating between interior pores and voids between small porous cellulose beads (Ek *et al*., 1994). In addition, for solids which are susceptible to swelling, pore structures may be different in dry and wet states.

Gas adsorption subjects the sample to *in situ* heating (i.e. $\geq 100^{o}$C) or degassing for long periods (i.e. $\geq$ 12h) in order to produce an absolutely dry sample. Subsequent analyses utilise weight measurements and, ad- and desorption isotherms to generate pores information. Heating to $\geq 100^{o}$C is beyond the T_g of PLGA and it has been a major problem to obtain absolutely dry PLGA microsphere. PLGA microspheres were found to be extremely light and encourage static; thus accurate weight measurements, as required by these methods could be problematic. Transferring PLGA microsphere into a specific sample chamber also hinders accurate measurements.

The samples used for this work were incubated in water and that means predrying is required for the above analyses. This may affect the pore structure due to redeposition of dissolved compound present in the fluid within pores structure (Collins *et al.*, 2007). In this case, possibly the degradation byproducts. PLGA was selected for this work because of its hydrolytic-degradation and an aqueous environment is ideal to mimic an *in vivo* condition.

From the issues associated with sample handling and the fragility of PLGA microspheres, a non-invasive method and a method which can deal with "wet" samples is sought. NMR enables the determination of diffusion coefficients for mobile species that can be related to pore information. This method requires the sample to be saturated with a probe liquid; water in this case, which makes it a good simulation system to explore the pore structural evolution of degrading PLGA microspheres in aqueous environment.

7.1 Pulse Field Gradient (PFG) NMR

NMR is sensitive to the chemical and physical environments of a molecule and, for this reason this technique can characterise motion in liquid phase system (Hollewand and Gladden, 1995). Pulsed field gradient (PFG) NMR is a method used to study the self-diffusion of liquids by facilitating the measurement of root mean square (r.m.s.) displacement of the self-diffusing molecules (Callaghan, 1991). This measurement is responsive to the structure of over a scale comparable to r.m.s. displacement of molecules during the measurement duration ranged from milliseconds to seconds. In this case, the mobile species; ^{1}H nucleus within the self-diffusing water is used to monitor the movement of free water.

Free water molecules are always in Brownian motion (Hansen *et al*., 2005). While self-diffusing water in bulk has a free diffusion, the diffusion of imbibed or confined liquid is restricted by the wall of the pore. The relationship for the molecular mean square displacement, $\overline{r^2}$ and the molecular self-diffusion coefficient, D_o is given by the Einstein equation:

$$\overline{r^2} = 6D_o\Delta \tag{7.1}$$

with Δ as the diffusion time (Veith *et al*., 2004). By varying the diffusion time, the diffusing molecules can indicate the connectivity of the pore space. This connectivity is characterised by a geometrical quantity termed as tortuosity (Hürlimann *et al*. 1994). The tortuosity will be defined shortly below.

Since the 1960's, Stejskal and Tanner (1965) had used PFG NMR experiments to measure molecular self-diffusion using the attenuated spin echo under the influence of a magnetic gradient. Spin echo refers to the refocusing of a precessing nuclear spin magnetisation by a 180^o pulse of a resonant radio frequency. The pulse sequence used for this work is the pulsed

field gradient spin echo (PFGSE), such as illustrated in Figure 7.1. Consider that a radio frequency (r. f.) pulse has been applied to a nucleus, the nucleus will be excited and undergoes relaxation by emitting an echo. The signal generated from the pulse decays with time due to spin-spin relaxation.

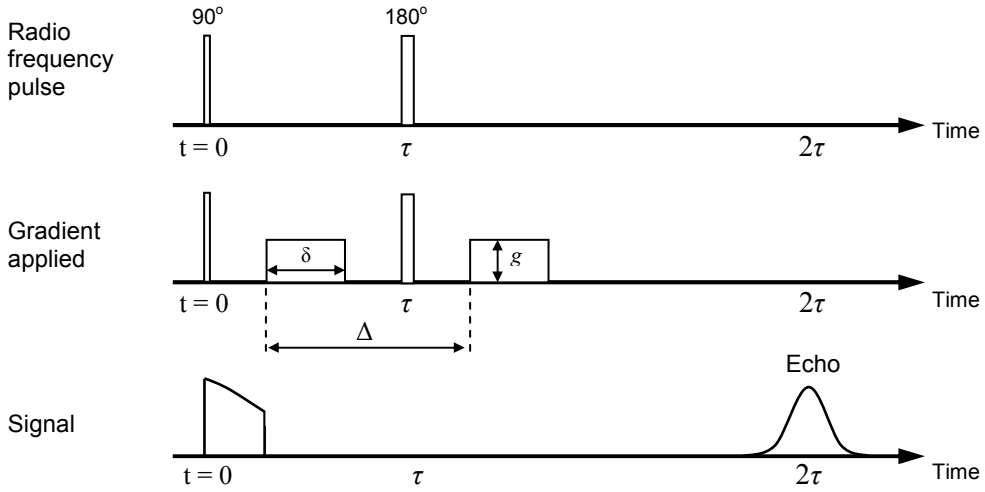

Figure 7.1: A pulsed field gradient spin echo (PFGSE) NMR sequence with a gradient, *g* used and the attenuated echo signal emitted after a 180° dephasing-pulse is applied (Hollewand and Gladden, 1995).

For a group of nuclei present, inhomogeneity in the magnetic field gradients causes different spins to precess at different frequencies and as a result, these spins will be out of phase with each other. This inhomogeneity led-to-dephasing can be re-phased by applying a 180° pulse. If a r. f. pulse is applied for a τ period of dephasing, an echo of the r. f. pulse will be emitted at time 2τ. With a magnetic field gradient applied after the initial r. f. pulse, the relaxation of a nucleus will then be dependent on its position in the magnetic field. If the nucleus is diffusing during the measure period, then the 180° will not be able to position the nucleus back in phase with the others because of its different precessing frequency. The echo signal is therefore reduced or attenuated.

PFG NMR utilises the above features to measure the diffusion coefficient of a molecule. After a defined time, diffusion coefficient; *D*, of the measuring species can be obtained by observing the positions of the molecule before and after its random diffusion, each labelled with a field gradient respectively. The echo attenuation, *R* is defined as the ratio of the echo intensity in the presence of the gradient to the echo intensity obtained in the absence of a gradient; i.e. I/I_o (Hollewand and Gladden, 1995). For free Brownian self-diffusion, where the random motion of the molecules is assumed to follow Gaussian behaviour, the echo attenuation has the functional form given by:

$$R = \frac{I}{I_o} = e^{-\gamma^2\delta^2 g^2(\Delta - \frac{\delta}{3} - \frac{\tau}{2})D} = e^{-D\theta} \tag{7.2}$$

where γ is the gyromagnetic ratio of the observed nucleus; g is the applied PFG strength; δ is the time of the applied PFG; Δ is the diffusion time; τ is the correction time for the phasing and dephasing between bipolar gradients and D is the diffusion coefficient (Kerssebaum, 2002). For simplicity, the term $\gamma^2 \delta^2 g^2 [\Delta - (\delta/3) - (\tau/2)]$ will be abbreviated as θ.

A single diffusing system will give rise to a linear log-attenuation plot of ln (I/I_0) vs. θ, with a gradient that equals the diffusion coefficient, D of the diffusing species. Deviations from this linearity can arise from regions of the sample possessing different diffusion coefficients; i.e. multi-component diffusion environment (Hollewand and Gladden, 1995). For the microsphere experiment herein, it was anticipated that there would be two water components; free water in bulk and water imbibed in microsphere (Messaritaki *et al*., 2005). Hence, considering a two separate diffusion components present, the model now becomes:

$$I = I_0[p.e^{-\theta D_1} + (1-p).e^{-\theta D_2}] \tag{7.3}$$

where D_1 is the diffusion coefficient of free water in bulk and D_2 is the diffusion coefficient of water imbibed within pores. p is the fraction of free water while $(1 - p)$ is the fraction of imbibed water.

For water that is imbibed within pores or cavities, their diffusion are restricted by the size of the pores/cavities (Callaghan *et al*., 1983). The restricted diffusion in cavities can be related to the radius of the cavity:

$$R = \sqrt{5D\left(\Delta - \frac{\delta}{3}\right)} \tag{7.4}$$

where R is the cavity radius, D is the diffusion coefficient, Δ is the diffusion time and δ is the length of the gradient pulse. Pore diameter, d is $2R$. For Equation 7.3 to valid, Δ had to satisfy the conditions in relation to pore size and diffusion time (Callaghan *et al*, 1983)**.**

For all diffusion to be restricted, Δ must be sufficiently large compared to the pore size. Reason being that a long diffusion time allows the water molecules to reach to the restriction bounded by the pore surface. Hence, they are under restricted diffusion and from Einstein equation (Equation 7.1); $\Delta \gg \overline{r^2}/6D$. Contrarily, if Δ is too short; i.e. $\Delta \ll \overline{r^2}/6D$, the diffusion time is insufficient for the molecule to diffuse across the pore, then the measured diffusion coefficient represents the free diffusion because the molecules will not reach to the boundary of the pore (Ek *et al*., 1994 and Hürlimann *et al*., 1994).

The effective diffusion of the imbibed water in a porous solid is related to its molecular self-diffusion coefficient by:

$$D_{eff} = \frac{D_o \varepsilon}{\kappa} \tag{7.5}$$

D_{eff} is the effective diffusion coefficient; D_o is the molecular self-diffusion coefficient; κ is the tortuosity and ε is the voidage of the solid (Hürlimann *et al*., 1994). Equation 7.5 shows that the higher the tortuosity is, the lower the D_{eff} is, due to lower r.m.s. displacement. Since the NMR signal measurement is observed based on the intensity that is proportional to volume, which in turn comprises the voidages density. Therefore, the diffusion coefficient measured by PFG NMR, D_{PFG} can be related to D_{eff} by:

$$D_{eff} = \varepsilon . D_{PFG} \tag{7.6}$$

By equating Equation 7.5 and Equation 7.6,

$$\kappa = \frac{D_o}{D_{PFG}} = \frac{D_1}{D_2} \tag{7.7}$$

Where $D_o = D_1$ = diffusion coefficient of free water and, $D_{PFG} = D_2$ = diffusion of imbibed water (Hollewand and Gladden, 1995). The tortuosity or the connectivity of the porous network can thus be studied. A high κ value usually indicates a complex network system.

7.1.1 Method

Blank PLGA microspheres were prepared using a single emulsion method described in Section 4.1.3. Approximately 0.3 g of sample was immersed in 2 ml of distilled water and then transferred into a 5 mm *ID* NMR tube. ^{1}H NMR with PFGSE sequence experiments were conducted using a 400 MHz Bruker spectrometer at probe temperature 298 K. The measurement of diffusion coefficient of water was conducted using diffusion ordered spectroscopy (DOSY) program. DOSY follows the intensity of the spin echo signal based on the movement or displacement of a species from one point to another; this movement alters the intensity of the signal. ^{1}H DOSY NMR data was obtained for ^1H_2O alone in order to determine the ^1H_2O peak position and diffusion coefficient for free water.

The values of Δ, δ and τ used were 0.05 s, 0.002 s, and 0.001 s, respectively. For each measurement, eight datum points (16 scans / datum) were collected at different PFG strengths ranged from 67.40 to 3203.0 Gaussian per meter (G/m). Each measurement yielded a set of eight intensities (I_{real}); each corresponded to the eight different PFG strengths. I_{calc} was generated by fitting these I_{real} to Equation 7.4 using *solver* from *Microsoft Excel* with least-squares method. The echo attenuation; $R = I / I_o$ is a relative parameter.

Findings in Section 6.1.2 showed that 75:25MS tends to have porous interior and their interior pores were in the order to 1 nm. As aforementioned, in order to obtain a restricted diffusion, the diffusion time, Δ has to be sufficiently large. Based on Equation 7.1 and a Δ value of 0.05 s, the corresponding r.m.s. displacement was ~26 μm. This value exceeds the pore size but not larger than the microspheres used in this experiment.

7.1.2 Results and Discussion

Figures 7.2 (A) and (B) show the goodness of fit for Equation 7.4 used to estimate the diffusion coefficient of imbibed water, D_2 and fraction of free water, p. The calculated intensities (I_{calc}) are in good correlation to the I_{real} where R^2 are very close to unity.

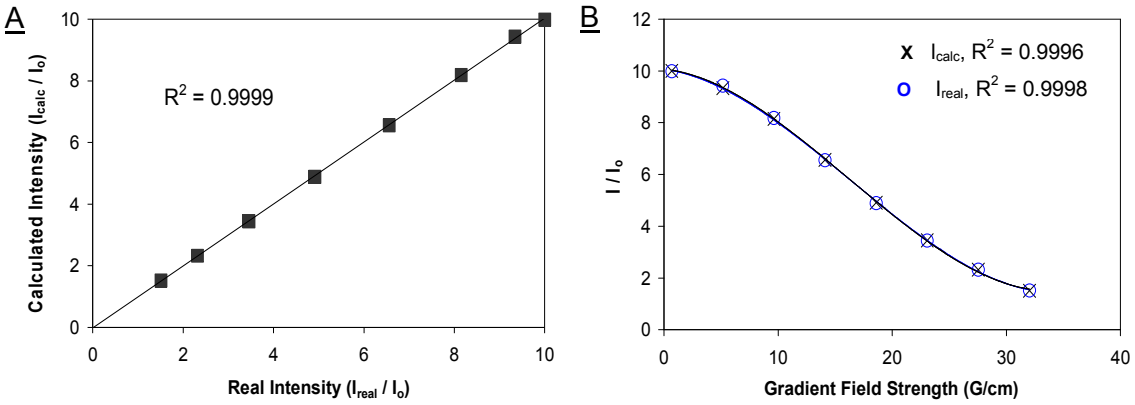

Figure 7.2: (A) Plot of calculated intensities, I_{calc} against real intensities, I_{real}. (B) Comparison of the calculated intensity (I_{calc}) and real intensity (I_{real}) against different PFG strengths.

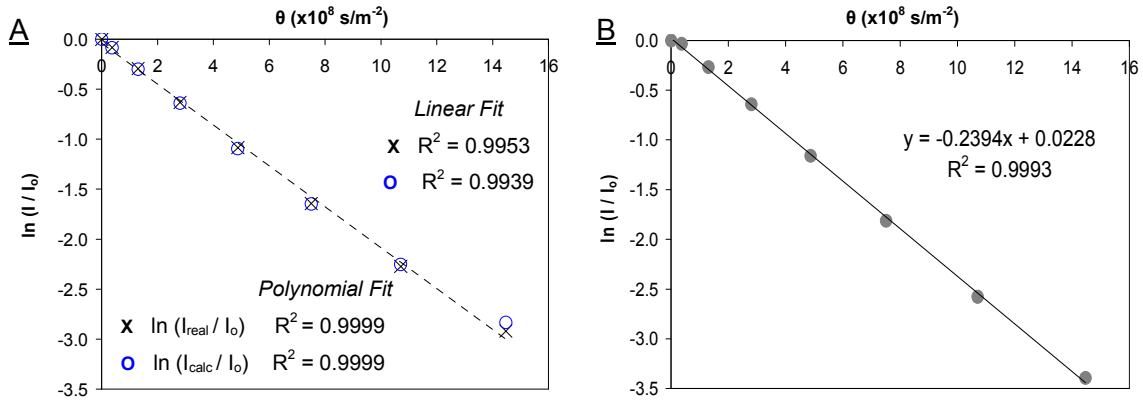

Figure 7.3: (A) Example of a log-attenuated intensity plot based on the two D's component model Equation 7.4. (B) Log-attenuated intensity plot used to estimate the diffusion coefficient of free water.

Figure 7.3A is an example of log-attenuated plot based on the data measured using PLGA microsphere sample. The polynomial trendline yielded higher values of R^2 and thus

indicating that the system contained more than one diffusion component as suggested earlier. By using water and one *D* component model (Equation 7.3), the diffusion coefficient of free water, D_1 can be determined from the gradient of the log attenuated plot shown in Figure 7.3B. The D_1 for free water was found to be 2.22 m^2/s. Mitra *et al*. (1995) reported a value of 2.3 x 10^{-9} m^2/s while the Bruker Biospin Handbook suggested a value of 2.299 x 10^{-9} m^2/s at 298K (Wolff, 2005).

Swelling of the device is common for PLGA microspheres (Matsumoto *et al*., 2006), and PLGA rod implants (Witt *et al*., 2000). Figure 7.4A shows the 65:35MS-discs produced using method described in Section 4.6.4. These images prove that 65:35MS underwent hydration and the disc had swollen after ten and twenty days immersion in water. Figure 7.4 (B) and (C) show the fragility of PLGA microsphere towards high pressure disc-pressing. The partially deformed 65:35MS could lead to a hydration gradient across the disc.

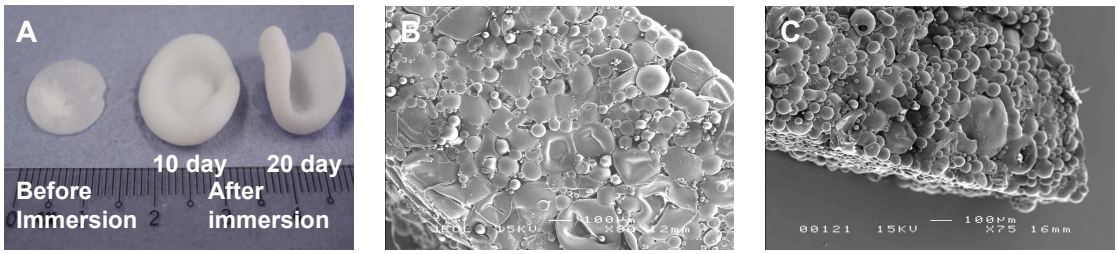

Figure 7.4: (A) 65:35MS-disc before and, after 10 days and 20 days immersion in water. (B) and (C) SEM images of 65:35MS-disc.

The effects of water uptake (i.e. hydration) by PLGA microspheres are proposed below:

i. Hydration occurs via two phases, water diffusion through amorphous region of the polymeric microsphere and water penetration through surface micropores. This hydration process will increase the fraction of imbibed water $(1 - p)$. Prior to this, the microspheres may be partially filled with residual water from the production process.
ii. Increase in imbibed water $(1 - p)$ would result in an increase in D_2.
iii. When a cavity or pore undergoes hydration, it expands and leads to swelling. As a result, the microsphere can increase in size (Figure 7.4A).
iv. Through interconnecting channels, water can travel from one pore to another. Different regions within a microsphere can experience different hydration rate due to water transport.

With repeated experiments using different batches of microspheres, it was found that PLGA microspheres are associated with both intra- and inter-variations within production batches.

In order to minimise these variations, the sample remained in the same tube was used throughout the experiment. The result presented herein is batch-specific and PFG-NMR was used to explore the pore swelling mechanism. Occasionally, unobtainable data were due to faulty DOSY measurements. The diffusion coefficient of imbibed water, D_2 estimated from two D's component model measured over a period of one hundred days is shown in Figure 7.5. These results were obtained from a same batch of microspheres and will be denoted as Batch 1 (B1). The corresponding fraction of imbibed water $(1 - p)$ is shown in Figure 7.6. The hourly measurements during the first ten hours are shown in Appendix V.F.

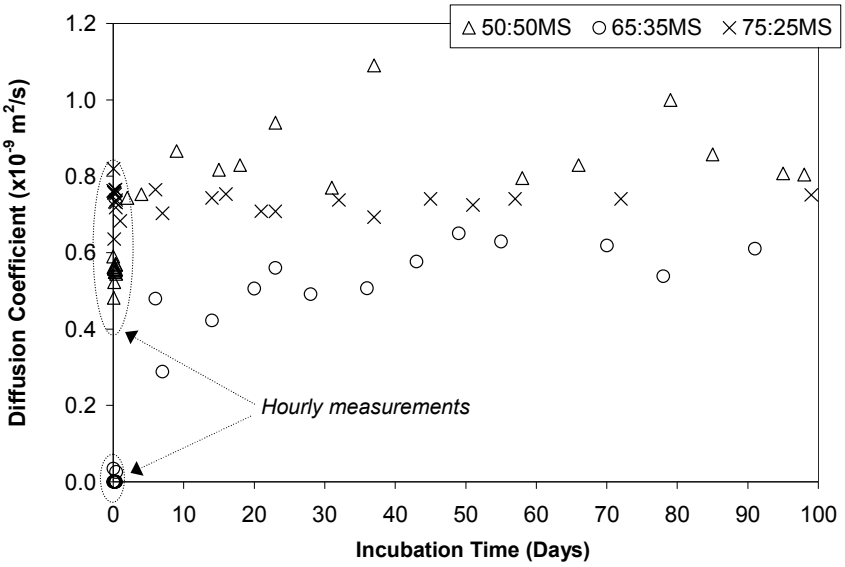

Figure 7.5: The diffusion coefficient of imbibed water, D_2 of 50:50MS (△), 65:35MS (○) and 75:25MS (×).

Figure 7.5 shows the measured D_2's were smaller than the free water diffusion; D_1 of ~2.2 x10^{-9} m^2/s, and this suggests restricted water diffusion. The very low values of D_2 of 65:35MS during the initial hourly measurement suggested a low volume of imbibed water, and is reflected on its low $(1 - p)$ shown in Figure 6.7. With an assumption that the D_2 of 65:35MS on the fifth day is an outlier, there is an increasing trend until the twenty-first day. Thereafter a decrease in D_2 for about fifteen days before it increases again on the forty-fifth day. From the fiftieth day onwards, D_2 of 65:35 remain relatively constant. The increasing trend in D_2 of 65:35MS in the first twenty five days could be attributed to the increasing hydration rate which leads to swelling. This can be validated by an increasing trend in its fraction of imbibed water seen in Figure 7.6.

There is a clear increase in D_2 of 50:50MS over the first twenty days and thereafter the values tend to fluctuate at a magnitude of 0.8 x 10^{-9} m^2/s. The D_2 measured on the thirty-fifth

day has a value of 1.09 x 10^{-9} m^2/s and its corresponding fraction of imbibed water has the value of unity (result not shown on Figure 7.8). This is attributed to a faulty measurement thereby generating this outlier. Unlike its D_2 trend, the fraction of imbibed water of 50:50MS is observed to decrease after the first day and then increases again until the thirtieth day. After that, the $(1 - p)$ tend to fluctuate at a magnitude of 0.4. This fluctuation may due to (1) intermittent swelling and shrinking, (2) different rates of hydration in empty pores and, (3) the commencement of interior degradation that altered the structural volume.

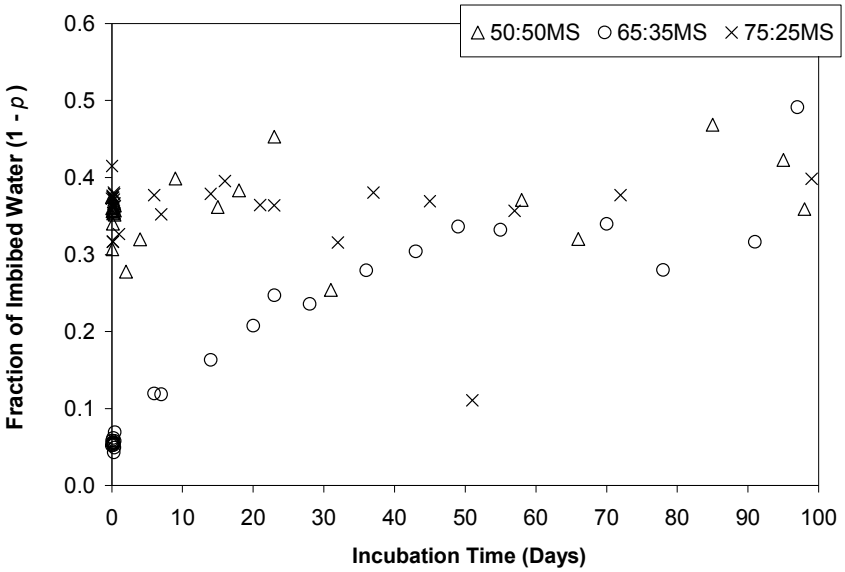

Figure 7.6: The fraction of imbibed water $(1 - p)$ in 50:50MS (△), 65:35MS (○) and 75:25MS (×).

During the initial hourly measurements, the D_2's and fractions of imbibed water of 50:50MS and 75:25MS shown on Figure 7.5 are well above those of 65:35MS, suggesting the former two experienced higher rates of hydration. The D_2 of 50:50MS begun with a lower value than of 75:25MS but after four days, it surpasses the D_2 of 75:25MS. A possible scenario is that; initially, the pores in 50:50MS were the smallest and then water started to diffuse into these pores. This is highly possible due to the more amorphous regions in 50:50 PLGA. As a result, pore expansion and swelling increased the fraction of imbibed water.

50:50MS has the most amorphous region which permits higher water diffusion and thus higher hydration rate. In this sense, the glycolide acid content decreases the hydrophobicity of PLGA. Here, it is suggested that the least hydrophobic and degradation resistance 50:50MS give rise to a higher water diffusion compared to 65:35MS and 75:25MS. As a result, 50:50MS is more prone to swelling. Hence, D_2 increases with $(1 - p)$ because of the higher hydration rate experienced by 50:50MS.

The rather constant values of D_2 of 75:25MS indicate that the internal structure of 75:25MS was highly intact. The fraction of imbibed water in 75:25MS is also observed to be relatively constant. These conditions would agree with the less hydrophilic 75:25 PLGA which minimises hydration due to its extra chiral group.

Figures 7.5 and 7.6 were reproduced and presented in Figure 7.7 in order to show the initial results of twenty days. The very low D_2 values of 65:35MS during the first ten hours of measurement corresponded with less than 10% of imbibed water; i.e. $(1 - p) < 0.1$, as shown in Figure 7.7B. There was an increment in D_2 of 50:50MS after the first ten hours and this suggests that the water diffusion increases during this period of time. This is attributed to the higher hydration rate of 50:50MS which leads to swelling and thus, the imbibed water was able to move more freely in enlarging pores. The relatively constant D_2's of 75:25MS indicates minimal pore swelling.

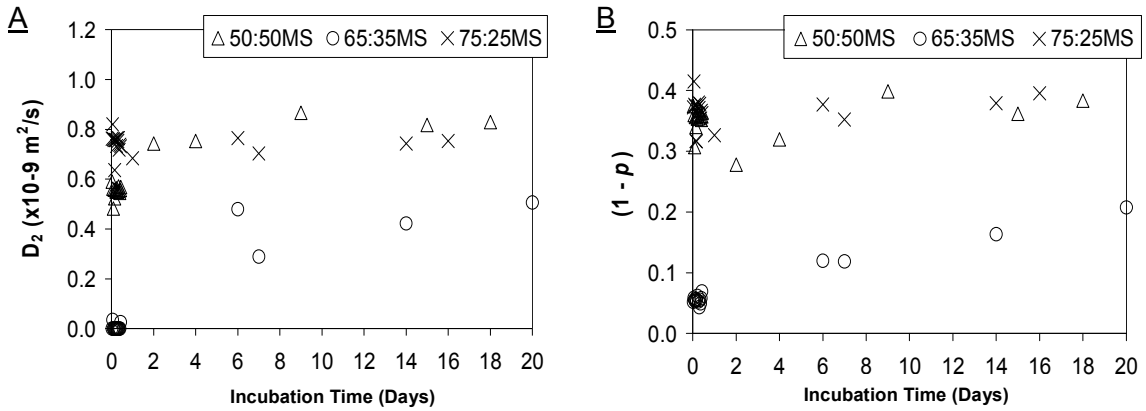

Figure 7.7: Reproduction of Figures 7.6 and 7.7 on the first twenty days of measurement. (A) The diffusion coefficient of imbibed water, D_2 of 50:50MS, 65:35MS and 75:25MS. (B) The fraction of imbibed water, $(1 - p)$ in 50:50MS, 65:35MS and 75:25MS.

The experiment was repeated with two different batches of PLGA microspheres; denoted as Batch 2 (B2) and Batch 3 (B3) produced using the same method and condition as B1. Results were plotted on the same graphs in order to study the repeatability of the work. Measurement was planned for thirty days in conjunction with the degradation experiment reported in Section 6.2. Random measurements were still carried out in order to confirm the behaviour of the system at later stages.

Figure 7.8 shows the diffusion coefficients of imbibed water in 50:50MS, 65:35MS and 75:25MS from B2 and B3. The corresponding fractions of imbibed water in 50:50MS,

65:35MS and 75:25MS from B2 and B3 are shown in Figure 7.9. Occasionally, the estimated p had the values of unity, resulting D_2 of zero values. On the other hand, when D_2 approaches D_1 (i.e. 2.22 x 10^{-9} m^2/s), their corresponding $(1 - p)$ values were unity. These values were not shown in Figure 7.9 because majority of the results concentrated at low values and the y-axis was focused to reflect them.

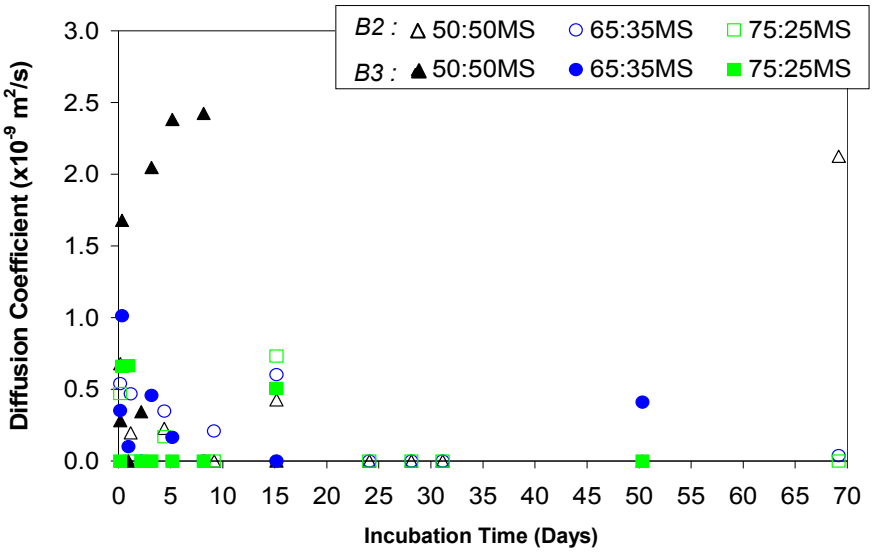

Figure 7.8: The diffusion coefficient of imbibed water, D_2 of 50:50MS (△, ▲), 65:35MS (○, ●) and 75:25MS (□, ■) from Batch 2 (B2, open symbols) and Batch 3 (B3, close symbols) microspheres.

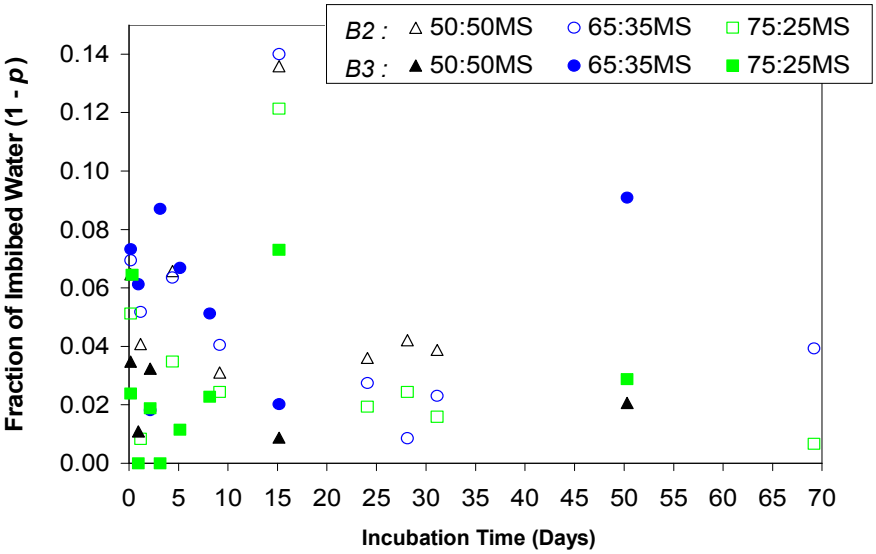

Figure 7.9: The fraction of imbibed water, $(1 - p)$ of 50:50MS (△,▲), 65:35MS (○,●) and 75:25MS (□,■) from Batch 2 (B2, open symbols) and Batch 3 (B3, close symbols) microspheres.

From Figure 7.8, the measured D_2 values from B2 and B3 microspheres were approximately halved of those of D_2 from B1 microspheres, with the exception for the 50:50MS. The D_2

results from B2 and B3 microspheres seemed logical because their corresponding fractions of imbibed water are also much smaller than those observed in B1 microspheres.

50:50MS from B3 demonstrated an increasing trend in D_2 during the first ten days. Due to faulty NMR data acquisition, no data could be processed thereafter. It corresponding fraction of imbibed water did not concurred with this trend. The fraction of imbibed waters measured on the third, fifth and eighth days had the value of unity (data points not shown) and this could be explained by the increasing D_2 from the fifth day to the eight day. The highest D_2 value during this period is 2.42 x 10^{-9} m^2/s, which matches the value of free water and therefore the measured D_2 is no longer under restricted diffusion.

65:35MS from both B2 and B3 show a decreasing trend in D_2 values during the first ten day and their corresponding $(1 - p)$ in Figure 7.9 indicate agreement. This trend is opposing the trend exhibited by 65:35MS from Batch 1. 75:25MS from B2 and B3 also demonstrate decreasing trends in both their D_2 and $(1 - p)$. The very low D_2 detected could be the diffusion within the polymer matrix. By comparing the results of $(1 - p)$ shown on Figures 7.9 and 7.6, microspheres from B2 and B3 had much less imbibed water with fractions of $\leq$ 0.15. B1 microspheres had almost doubled this amount. This explains the smaller D_2 values from B2 and B3 microspheres than those from B1.

Overall the results from the three different batches PLGA microspheres suggest the presence of inter-batch variations. Very often the D_2 results tend to exhibit "sinusoidal" pattern and this is interpreted as the intermittent swelling and shrinking of the pores within these microspheres. This is a common characteristic of polymeric microspheres which are capable of hydration. Fujiyama *et al*. (2003) presented cross sectional SEM images of degrading PLGA/PLA microspheres. Interior structural collapse is shown by these authors and at different degradation time, this structure alternated between dense and porous natures. Swelling is thought to have caused local cavities or pores expansion and minimises the spaces between the adjacent cavities. The pore sizes of swollen cellulose beads after immersion in water could sometimes doubled its initial sizes (Ek *et al*., 1995).

In the event of water diffusing from one pore to another, i.e. from bigger pores to smaller pores or vice versa. While the water in a bigger pore leaves to fill a smaller pore, the "swollen" bigger pore decreases in size while the smaller pore expands as water gradually fills up. These lead to temporary changes in pore sizes where pore expands and shrinks due

to water migration between pores. So far results indicate these events are random. It could also be that initially, the pores nearest to the microsphere surface experience a more frequent hydration/swelling effect. As immersion proceeded, the inner part of the spheres becomes increasingly hydrated. The presence of interconnecting channels of different sizes can affect the mobility of water. Section 7.2 will show that these interconnecting channels also swell and shrink over time. This could further affect the hydration rates in the main pores. The different crystalline and amorphous regions of polymeric PLGA microsphere would also affect water diffusion within the polymer matrix.

The PFG-NMR measurement could be indeterminately detecting water molecules located near the wall of the pores or diffusing near the surface of the pore wall. Callaghan *et al*. (1979) had observed a reduction in the diffusion coefficient of water and concluded it is caused by the occasional binding of water at the pore surface layers. There could be a nano-sized layer water surrounding the interior pore surface (Callaghan *et al*., 1983). The Brownian motions of these water molecules persisted within this layer and showed higher r.m.s. displacement. This layer of water exists only nearest to the pore surface due the OH-bond interactions between the water and pore wall that leads to a fraction of the water next to the pore wall no longer fully free. Section 7.2 will further discuss the nano-sized water layer located at the pore surface.

In addition, the tortuosity effect also arises from the changes in local dimensionality. Structural heterogeneities have been shown to influence both steady-state and transient diffusion (Hollewand and Gladden, 1993, and Rigby *et al*., 1996). Callaghan *et al*. (1979) suggested a two-third reduction in diffusion coefficient for lamellar or slit-shaped and, a-third reduction for cylindrical or capillary geometry pores. While monitoring the adsorbed liquids in porous glasses with pore sizes ranged 0.8-50 nm, Kärger *et al*. (1983) found that stabilisation of liquid molecules by the pore wall might be responsible for the reduction in diffusivity in small pores. Fukuda *et al*. (1989) also agreed to the same conclusion where decreased in diffusivity was observed from the effects of smaller pores (4 - 45 nm) samples. In conjunction to these studies, findings in Section 6.1.3 showed that microcavities in 75:25MS are ~1 nm in size.

By obtaining the diffusion coefficient of the imbibed water (D_2) from Equation 7.3, the r.m.s. displacement of water and the pore diameter, d can be estimated using Equations 7.1 and 7.4 respectively. The results of 50:50MS, 65:25MS and 75:25MS from Batches 1, 2 and 3,

plotted against incubation time are shown in Appendix V.A. A summary of the overall trends observed on the pore size evolutions of the PLGA microspheres over the period of twenty days is presented in Table 7.1. The tortuosity results estimated using Equations 7.3 and 7.7 are also shown in Appendix V.B. Only results up to twenty days are shown because changes were more prominent during this period. The tortuosity in PLGA microspheres vary randomly over time but 75:25MS tend to show the smallest fluctuation in its tortuosity factor.

Table 7.1: Summary of the overall trends observed for the pore size evolutions exhibited by 50:50MS, 65:35MS and 75:25MS from different batches.

PLGA microspheres	Overall trends observed for Pore sizes Evolutions		
	Batch 1	Batch 2	Batch 3
50:50MS	Increase – constant Small increase on Day 1 to 2; constant thereafter.	Sinusoidal Decreases on Day 1, thereafter gradual increase.	Sinusoidal Increases within Day 1, decreases after Day 1, increases thereafter.
65:35MS	Increase – constant Gradual increase over 6 days; constant thereafter.	Increase – constant Increases after Day 1; constant thereafter	Sinusoidal Slight increase on Day 1; decreases thereafter.
75:25MS	Constant Small degree of fluctuation.	Sinusoidal Decreases from Day 1 to 5, increases thereafter.	Constant Slight decrease.

The pore evolution in PLGA microspheres often exhibit intermittent swelling and shrinking. The expansion of one pore, or a few pores in a region may "push" the surrounding pores and cause them to shrink. If the overall shrinkage is dominant, then a reduction in fraction of imbibed water was observed. This effect will also be reflected in a decrease in water displacement or pore size. Comparing the overall trends exhibited by 75:25MS to 50:50MS and 65:35MS, 75:25MS of all batches demonstrated the least fluctuation in results.

For comparison purposes, the pore sizes from PLGA microspheres are collected to assess the degree of pore swelling. Figure 7.10 shows the swollen pore diameters calculated using Equation 7.4 for 50:50MS, 65:35MS and 75:25MS from B1, B2 and B3. The swollen pore was taken as the largest pore observable from each sample and is not time-specific The initial pore size is the pore size measured at the first time point. Comparing the initial pore sizes of 50:50MS, 65:35MS and 75:25MS, their sizes are not significantly different from each other (*t*-test, $p < 0.05$). This indicates that the single emulsion method employed in this thesis produces microspheres with interior pores of similar magnitudes and is independent of the different copolymer ratios.

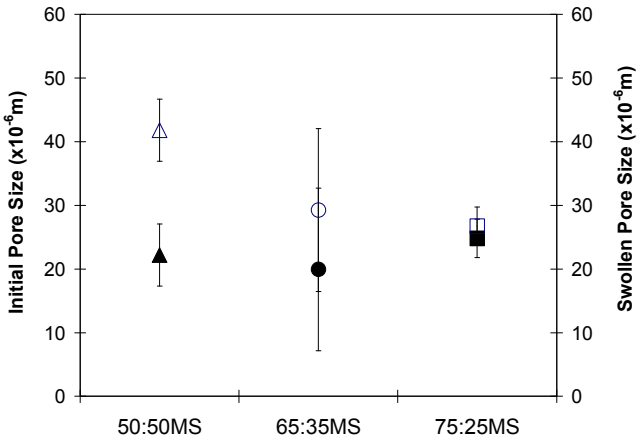

Figure 7.10: The average pore sizes of 50:50MS, 65:35MS and 75:25MS from B1, B2 and B3. Fill symbols = initial pore size measured at the first time point; open symbols = largest (swollen) pores.

The pore swelling in 50:50MS is the greatest and its swollen pore is significantly larger than its initial pore size (*t*-test, $p < 0.05$). 65:35MS and 75:25MS did not experience significant pore swellings. Comparing the swollen pore sizes, only the swollen pore of 50:50MS is significantly larger than the swollen pore of 75:25MS (ANOVA, $p < 0.05$). 75:25MS of all batches experienced the least swelling effect. This is contributed to its structural integrity of 75:25 PLGA. In contrast, 50:50MS experienced the most swelling effect. This is due to its highest glycolide acid ratio which provides more amorphous region for water diffusion. Thus hydration and swelling is greater in 50:50MS.

7.2 NMR Cryoporometry

NMR cryoporometry is a technique used to determine pore size distribution in a porous media by studying the melting point depression of a confined liquid (Mitchell *et al*., 2008). It will be explained shortly that the pore size and melting point have a reciprocal relationship. Similar to PFG NMR, NMR cryoporometry measures the signal from the ^{1}H within the liquid molecule. The property of a confined liquid will deviate from its bulk state because the confinement has introduced new liquid molecules-solid wall interactions and surface-to-volume ratios (S_v). While S_v is affected by the size of a pore, the spin–spin relaxation time of the NMR signal is long for a liquid and short for a solid (Strange *et al*., 1993 and Hansen *et al*. 1996). This enables differentiation between a molten liquid and a frozen liquid as a function of temperature during freezing.

Gas adsorption and mercury porosimetry characterise porous media based on studies of the equilibrium conditions between liquid and gas phases arise from capillary effects. These methods transform volume/pressure data into volume/pore size data. Cryoporometry generates the same sort of data but based on heat/temperature data from the studies of solid/liquid equilibrium. Similar to capillary phenomena, hysteresis is also observed for freezing and melting transitions in cryoporometry experiments (Denoyel and Pellenq, 2002, and Denoyel *et al*., 2004).

The development of NMR cryoporometry is fuelled by the theories from J. W. Gibbs, J. Thomson, W. Thomson (later Lord Kelvin) and J. J. Thomson, whom among the pioneers to realise the different mechanisms involved in a non-equilibrium phase transitions experiencing by a confined material. Their experimental findings showed that variables such as geometry can affect the basic property of the matter such as its vapour pressure. In particular, they established that the bulk melting point varies inversely with crystal size. A pore of size x will melt at a temperature $T_m(x)$ lower than the bulk melting point T_m, which is inversely proportional to x. As expressed in Mitchell *et al*. (2008), the Gibbs-Thomson equation that relates the melting point depression, ΔT_m for a small crystal of size x is:

$$\Delta T_m = T_m - T_m(x) = \frac{4\sigma_{sl} T_m}{x \Delta H_f \rho_s} \tag{7.8}$$

where T_m is the normal bulk melting point, $T_m(x)$ is the melting point of pore of size x, σ_{sl} is the surface energy of the solid-liquid interface, ΔH_f is the enthalpy of fusion, ρ_s is the density of the solid. Assuming all parameters in the equation to be independent of temperature and pore dimension (Hansen *et al*., 1996), then Equation 7.8 can be simplified to:

$$\Delta T_m = \frac{k}{x} \tag{7.9}$$

where k is the melting point depression constant associated to the absorbate's thermodynamic property (Strange, 1993).

The numerical constant "4" in Equation 7.8 is derived for cylindrical pores. Equation 7.8 is a basic model that assumes the pore structure has the same geometry throughout the sample. Micro- and mesoporous materials can have pores or voids of different geometry; i.e. slit-shaped, cylindrical or spherical etc. In real samples, the influence of pore geometry must be taken into account because the geometry is often not perfect. For instance, the pores may be interconnected or of mixed geometry. The model then requires new approach taking into

account the confinement's structure and properties. Webber *et al*. (2008) further formulated k into multiples of constants such that;

$$k = k_g \,.\, k_s \,.\, k_i \tag{7.10}$$

k_g is a geometric constant dependent on the interfacial shape, k_s is a constant involving parameters specific to the crystalline solid of solid-liquid system and k_i is an interfacial energy term. The calibration of these constants is beyond the scope of this thesis and an appropriate value for PLGA-water system will be adapted from a selected literature.

A temperature gradient was anticipated to be present along and across the measuring sample. This temperature gradient is minimised by using a set of susceptibility plugs. The plugs raised the sample to within the receiver coil and at the same time, reduced the sample length. Not only these plugs help to provide insulation for the sample, they also permit liquid expansion and prevent the NMR tube from rupturing during freezing. Figure 7.11 shows the ensemble of a sample tube. The NMR experimental condition herein is developed by Perkins *et al*. (2008) and they suggested a temperature deviation of 0.2 K to be expected.

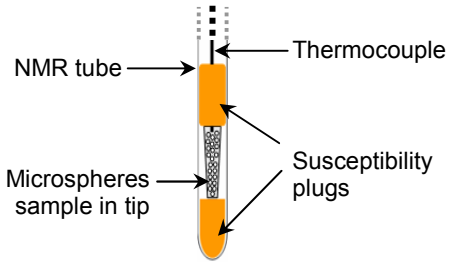

Figure 7.11: An ensemble of a sample prepared using susceptibility plugs and thermocouple for NMR cryoporometry analysis.

7.2.1 Method

Blank PLGA microspheres were prepared according to the method described in Section 4.1.3. Approximately 1 g of microspheres "stock" sample was immersed in 5 ml of distilled water and incubated at 37^{o}C in a shaking water bath (Section 4.5). At specific time interval, a small amount of microspheres was collected using a tip. The top part of the tip was trimmed in order to fit into a NMR tube. The trimmed tip was then inserted into a NMR tube and positioned between a set of susceptibility plugs. A thermocouple used to assess temperature was inserted through the top susceptibility plug to the depth of just reaching the sample (Figure 7.11). Fresh sample was prepared from the "stock" for each measurement. Cryoporometry analysis was conducted using the same NMR system described in Section 7.1 but with liquid nitrogen as a mean to control the temperature ranged between 225 K and 273 K. The temperature was varied step-wise (0.5 or 1 K/step) with a 10 minutes equilibration

time in between changes. The small step change was necessary to ensure temperature stability. The sample was subjected to consecutive cycles of freezing, melting and refreezing, abbreviated as F/M/rF cycles. E.g. The temperature was reduced step-wise from room temperature (c.a. 298 K) to 225 K, then raised to 273 K and reduced again to 225 K.

The variation of NMR signal intensity (*I*) during the F/M/rF cycles was measured as a function of temperature (*T*) was plotted as the *IT* curve. The reasons for using water as a probe fluid are that the water molecules are small enough to enter the minute cavities within the sample and no part of the sample is soluble in water. Allen *et al*. (1998) found that repeated freezing-thawing often changes the structure of porous materials while the growth of ice crystal can cause deterioration to the sample. For these reasons, each analysis was done on fresh sample.

7.2.2 Results and Discussion

The principle of cryoporometry requires the understanding of the mechanism of freezing and melting transitions. In order for a new phase to appear; i.e. from liquid to solid, an interface must exist. For most real cases, suspended impurities or imperfectly wetted surfaces provide an interface on which the growth of a new phase is initiated. These elements enable heterogeneous nucleated-freezing (Scherer, 1998). In the absence of these elements, a new phase is developed from a small, localised embryo formed within the bulk metastable liquid. This is known as homogeneous nucleation, and it is only activated when a free energy barrier to form the embryo of critical size is overcome, beyond which the new phase grows spontaneously (Debenedetti, 1996).

In the case of suspended solids, such as PLGA spheres, they present as a small degree of distribution that provide additional nucleation sites (Chellaiah and Viskanta, 1989). Two common freezing mechanisms in porous media are: freezing initiated by nucleation in pores, or by solid-front penetration through pores which are in contact with the frozen bulk (Swainson and Schulson, 2001 and Beurroies *et al*., 2004). The former is associated with homogeneous nucleation while the latter occurs via heterogeneous nucleation. Here, the freezing in pores is thought to be heterogeneously nucleated by the presence of bulk ice surrounding the microspheres, and penetration of ice front into the interior of the microspheres (Hansen *et al*., 2005 and Petrov *et al*., 2006). Figure 7.12 depicts a scenario for the PLGA microspheres used herein.

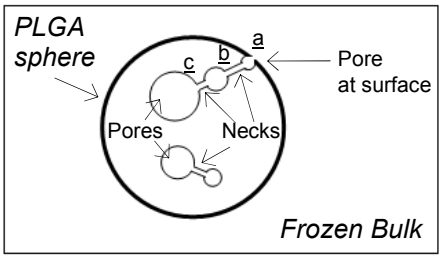

Figure 7.12: A depicted PLGA-sphere with a porous network. Pores are interconnected through necks, both varied in size but the latter is assumed to be smaller than the main pores.

The interior pores are connected through "necks" which are smaller in size and they ensemble the typical ink-bottle pores. Brun *et al*. (1977) proposed that the ingress of solid front (ice) from frozen bulk into the pores is the mechanism responsible for pore freezing. This mechanism will be illustrated later with the F/M/rF cycles obtained from PLGA microspheres. With excess liquid saturating the microsphere, once the bulk liquid is frozen, further freezing in the pores occurs by ice ingress through pores which are in contact with the frozen bulk. For example, pore *a* is in direct contact with the frozen bulk, ice front ingresses into the microsphere through the necks from *a* to *b* to *c*.

In order to overcome nucleation barrier that may delay freezing, Brun *et al*. (1977) suggested to freeze the system with excess liquid and at a low enough temperature to obtain a frozen bulk. Following that, the temperature is increased to a point just below the bulk melting temperature to study melting in pores. Subsequently, freezing cycle is initiated again. By doing so, the solid phase will always exists at the entrance of the pores and can act as nuclei for freezing inside pores, which can eliminates the nucleation barrier as assumed earlier. Thus, for the experiment herein, after the first cooling cycle (Freezing 1), the Melting cycle was aimed to melt only the confined ice while the bulk remained frozen. After that, the temperature was decreased again (Refreezing); these constituted the F/M/rF cycles.

The resulting F/M/rF cycles show that the signal intensities of the latter two cycles were very close to the signals of the background noise and were unable to clearly indicate any phase changes. This scenario may due to a very low volume of confined water which failed to produce significant signal during the melting cycle. It is also possible that 75:25MS used herein has pores of magnitudes such that their corresponding melting points are very close to the bulk melting temperature. For these reasons mentioned, only the freezing curves will be used to explore the pore characteristic in 75:25MS.

The measured NMR intensity is temperature dependent due to Boltzman's effect. The Maxwell–Boltzmann statistics shows that the ratio of NMR proton spins, with upper- and lower-energy states are temperature dependent (Mitchell *et al*., 2008). The measured

intensity, SI (T_K) at absolute temperature, T_K can be corrected relative to the signal intensity, SI (273 K) at 273 K based on the Curie Law using Equation 7.11:

$$\frac{SI(T_K)}{SI(273K)} = \frac{273}{T_K} \tag{7.11}$$

The measured intensities of cryoporometry experiments were corrected using Equation 7.11 and the results show that the temperature effect was minimal to the measured intensities. Therefore Equation 7.11 was not crucially required to correct the intensity data.

For comparison purposes, the F-cycle for 75:25MS immersed in water for various days are shown on the same plot (Figure 7.13). Individual *IT* curve for the F/M/rF cycles will be shown from Figures 7.14 to 7.17. In some cases, the values of I/I_o are observed to be higher than unity. This is attributed to the varying I_o. Since I was detected based on the presence of molten water in molten phase and indicative to its volume in bulk, over time, the bulk water diffuses into the microspheres and thus reduces the prior measured I_o.

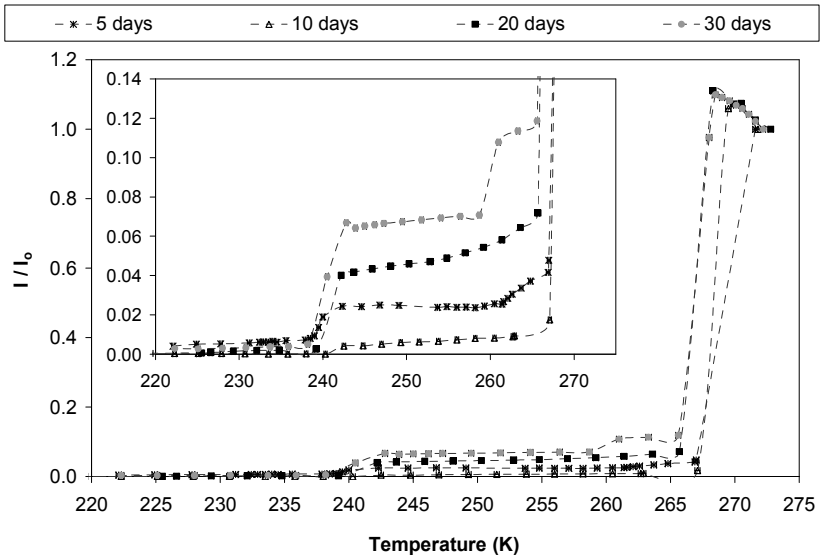

Figure 7.13: *IT* curves for the F-cycles of 75:25MS after immersion in water for 5, 10, 20 and 30 days. Inset: A refocus on the lower scale of I/I_o.

Referring to the significance decrease in signal intensities shown on Figure 7.13, the bulk liquid was frozen at 266-267 K (denoted as T_{Fo}). The F-cycle of five days immersion 75:25MS exhibits a diminutive step just after 260 K and at another at ~240 K. The F-cycle from ten days 75:25MS exhibits a clear step close to T_{Fo} and another at ~241 K. The F-cycle from twenty days 75:25MS exhibits a gradual decrease in I/I_o below T_{Fo} and a step at ~240 K. The thirty days 75:25MS exhibits the most distinct pattern where a clear and prominent

step close to T_{Fo} can be seen followed by another at ~240 K. The secondary freezing temperatures seen in Figure 7.13 suggest an "ink-bottle" geometry pores are present in 75:25MNS. These F-cycles indicate similarity to results from Khokhlov *et al.* (2007) using samples with ink-bottle pore geometry.

Since the measured intensity is proportional to the volume of water present, the decrease in intensity shown on the refocus *IT* curve suggests that bulk water constituted almost 90% of the total volume detected and ~10% water were imbibed in 75:25MS. After the bulk freezing point, the occurrence of second or third freezing points is attributed to the solid (ice) front penetration into the subsets of pores within the partially frozen microspheres.

Owing to their high S_v, liquid confined in pores crystallises (or freezes) and melts at temperatures well below their bulk melting points (Christenson, 2001). Compared to bulk, this high S_v ratio introduces excess energy for the solid. Thereby, shifts the liquid-solid equilibrium towards the liquid state (Petrov and Furó, 2006). Hence, molten liquid is still present in the porous microspheres even below the normal freezing point of water. As aforementioned, the freezing of water in pores occurs via the ingress of ice crystals from the frozen bulk into the interior pores (Khokhlov *et al.*, 2007 and Perkins *et al*., 2008) and this causes the delay in complete freezing of water present in the system, as seen on Figure 7.13.

Figure 7.14 shows the F/M/rF cycles subjected on 75:25MS after five days of immersion in water. The plot focused on the lower scale of I/I_o in order to show the small variations in I/I_o with temperature. After Freezing 1, the frozen sample was subjected to subsequent Melting but the temperature was raised only to the point below the bulk melting (i.e. $\leq$ 273K) while the bulk remained frozen. Following that, Refreezing was initiated. Following the Freezing 1 curve, the bulk liquid was first frozen at ~267 K. Second and third freezing transitions occurred at ~258.5K (T_{N1}) and ~239K (T_{N2}) respectively. For convenience, the notations such as 'N1' and 'N2' are used to describe the relative temperatures to T_{Fo}; i.e. T_{N1} is closer to T_{Fo} while T_{N2} is further away from $T_{Fo.}$ With both the F/M cycles, it shows that the confined water in 75:25MS underwent supercooling.

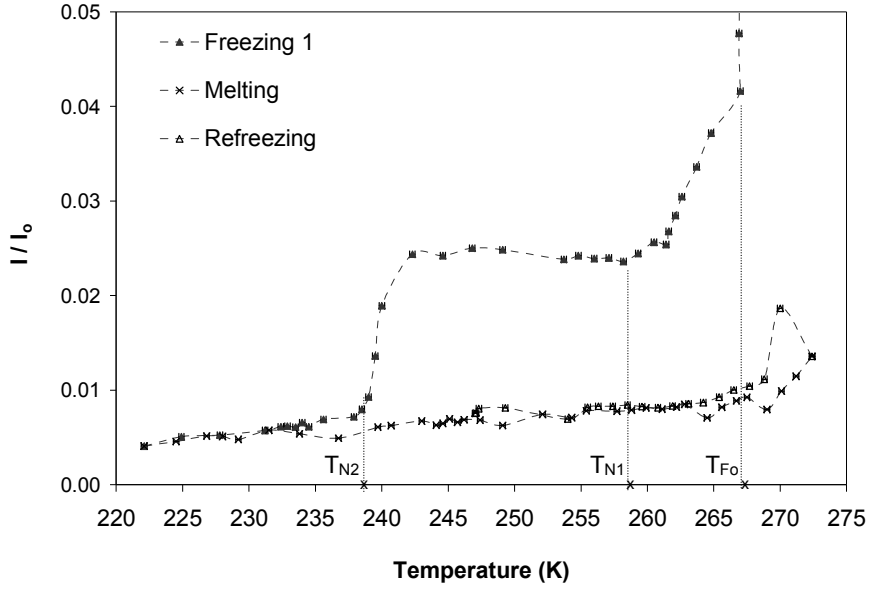

Figure 7.14: *IT* curves for F/M/F cycles of 75:25MS after 5 days immersion in water.

It is also evident that the F/M cycles shown in Figure 7.14 did not retrace one another thereby suggesting the presence of hysteresis. This is largely due to the delayed in freezing nucleation (Janssen *et al*., 2004). By referring to Figure 7.14, the mechanism whereby the freezing of water confined in pores occurs by ice ingress from the frozen bulk through the interconnecting channels can be demonstrated.

After the bulk liquid freezes at T_{Fo}, from the intensity detected, it indicates that molten and confined liquid are still present in the system. While the microspheres are surrounded by a frozen bulk, ice crystals started to ingress into the microspheres via the pores at the surface. The ice front will first freeze the water in the connecting channels. The ice front in the channels then ingress into the pores and consequently freezes the liquid confined in the main pore. The presence of confined liquid leads to supercooling and shifted the actual freezing point. The pore size is more reliably determined using the melting temperature by raising the temperature after the primary freezing cycle. The F-cycle is therefore used to predict the size of the neck through which the ice front ingresses through.

For porous media, the hysteresis is thought to have originated from the pores of varying cross sections and networks. It is the connection through a smaller channel to a bigger main cavity that gives rise to pore blocking effect, or known as the ink-bottle mechanism. This mechanism occurs when a narrow channel is preventing the further ingress of the solid phase. After reaching T_{Fo}, the ice front will not be able to ingress into smaller pores until the

thermodynamical condition favouring this penetration is achieved. Consequently, a second or third freezing point is detected at a much lower temperature. The following are suggested by Petrov and Furó (2006) to explain the freezing/melting hysteresis;

i. As far as bulk liquid is concerned, homogenous nucleation causes uncontrollable delay on cooling. The bulk liquid becomes supercooled until homogeneous nucleation initiates freezing.
ii. Freezing by solid ingress within the interior pores may be heterogeneously nucleated by the surrounding bulk ice but this solid ingress is delayed by pore-blocking effect.
iii. There present a free-energy barrier for solid ingress which separates metastable states of a confined material from stable ones.

This sort of analysis is advanced from the studies of capillary condensation and vaporisation which are parallel to those of melting and solidification/freezing respectively (Beurroies *et al*., 2004 and Denoyel *et al*., 2004). With the delayed in freezing, Figure 7.14 shows that the 75:25MS used herein are indeed:

i. Porous and hydration enables water to be imbibed in these pores.
ii. The presence of hysteresis suggested these pores are made of ink-bottle geometry. The ink bottle effect is thought to delay the freezing of confined water.
iii. Since melting curves could not be explored, the freezing curves can only used to estimate the size of the neck. The presence of second and third freezing points indicated a bimodal system; 75:25MS used herein was potentially inherited with necks of one or two different sizes.

Referring to Figure 7.14, when the temperature reaches T_{N1}; this point corresponds to the freezing of the water in the interconnecting necks of size, x_{N1}. Further cooling to T_{N2} freezes the water in the neck of size x_{N2}. From the Gibbs-Thomson equation (Equation 7.9), the neck with size x_{N1} is bigger than the neck with size x_{N2} because the latter occurs at a lower temperature. Further F/M/rF cycles obtained from 75:25MS after ten, twenty and thirty days of immersion in water are shown in Appendix V.C. These cycles exhibit great likeliness to Figure 7.14, with secondary freezing temperatures suggesting the presence of smaller necks.

The same mechanism observed in liquid freezing can be expected for melting of liquid in porous media inherited with ink-bottle pores (Beurroies *et al*., 2004). Since the water confined in pores will not freeze before the water in its connecting necks, likewise, the

melting will also begin in the neck before the frozen confined water. For melting transition in small pores, in most cases, nuclei of the liquid phase are present at all relevant temperature.

Booth and Strange (1998) studied the freezing and melting cycles of cyclohexane in silicas using NMR. They observed a melting point below the bulk's melting point but in the confined ice crystal, there were two distinct components of the transverse relaxation time. The short relaxation time (comparable to the crystal phase in the bulk) was attributed to the ice crystal in the inner core of the pore and the long relaxation time was attributed to the liquid-like layer between this crystal and pore wall, the so-called "bound-layer". It is thought that melting begins from this liquid-like phase layer. Denoyel and Pellenq (2002) also agreed to this phenomenon suggesting that surface melting occurs at the end of the metastable range and the only condition is that the pore wall is preferentially wetted by the liquid rather than by the solid phase (ice).

Overloop and van Gerven (1993), Morishige and Kawano (1999) among others also observed the presence of a bound layer located adjacent to the pore wall which remained liquid-like structure when the inner fluid had frozen, such as illustrated in Figure 7.15. This phenomenon is observed regardless the geometry and size of the pores. Based on these studies, the melting mechanism in pores or necks is thought to begin from the surrounding wall inwards to the core of the ice crystal. Morishige and co-workers repeatedly found that the freezing of this bound layer was a continuous process and it persisted over a range of temperature (Morishige and Nobuoko, 1997 and, Morishige and Kawano, 1999).

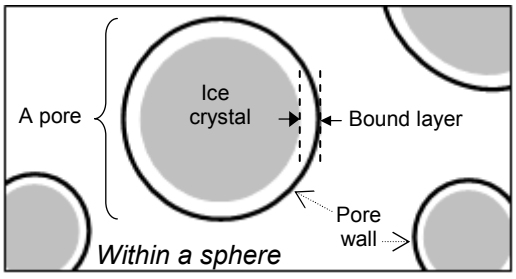

Figure 7.15: Within frozen liquid confined in a pore, there exits of a 'bound layer' located between the frozen inner core and pore wall. The ice crystal formed at the inner core is thus enveloped by a layer of unfrozen water adjacent to the pore surface.

Since the early 1980s, Buttet *et al*. (1982) and Myles (1982) have shown that the decrease in freezing temperature for water in the inner region of the pore is consistent with the Gibbs-Thompson equation but the pore diameter, x is replaced by (x-x_{bw}) where x_{bw} is the thickness of the bound water. Webber *et al*. (2001) also reached to the same conclusion. Hansen *et al*. (1996) found that this thickness was within experimental error and its variation with material type was only marginal. Thus, x_{bw} can be treated as a constant but this assumption only valid

for pore with dimension bigger than x_{bw}. This layer also appears to be temperature dependent (Petrov *et al*., 2007). This bound layer can cause problem when it produces signal extending to low temperature which can be misinterpreted as very small pores (Aksnes *et al*., 2001).

Results from experiments conducted on 50:50MS were presented below where the results of 65:35MS are included in Appendix V.C. The F-cycles subjected on 50:50MS after immersion in water for various days are shown on Figure 7.16. The sampling time point of 50:50MS was based on hourly basis in view to a more rigid sample before degradation had altered its internal structure which might complicate results interpretation. The F-cycle from 50:50MS after two hours immersion in water did not exhibit any clear step below T_{Fo} (266 K) but close observation suggests that there may be a small step present at ~260 K. Based on the enlarged plot (shown in inset), the F-cycle of six hours water-immersed 50:50MS exhibits a step at ~258 K. The F-cycle from 50:50MS after fifteen hours immersion in water exhibits a clear step at ~255 K. Thereafter fluctuation occurred at a magnitude close to the background signal and no further interpretation will be derived. For the thirty hours immersed 50:50MS, a step tends to appear at ~266 K and another at ~236 K.

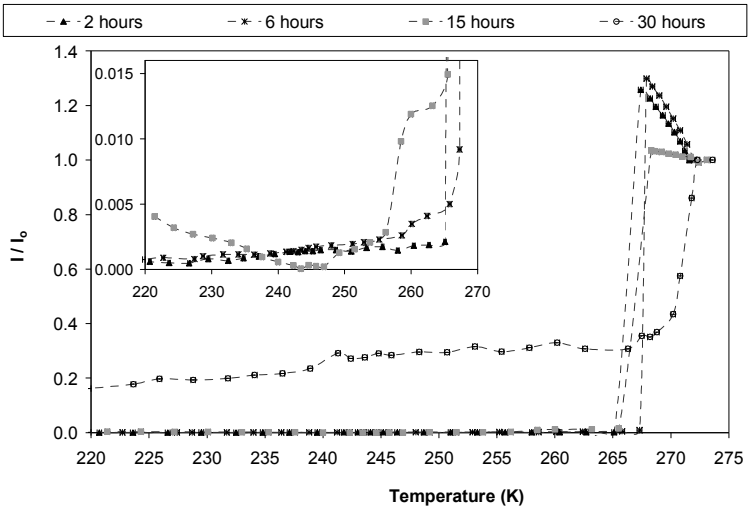

Figure 7.16: *IT* curves for freezing cycles of 50:50MS after 2, 6, 15 and 30 hours immersion in water. Inset: A refocus on the lower scale of I/I_o.

The F-cycles shown in Figure 7.16 demonstrate the difficulty of interpreting precise information purely based on the *IT*-curve. The information of interest, in this case, the pore size distribution can be quantitatively determined by studying the distribution of these freezing of temperatures. From the Gibbs-Thompson equation, the measurement of melting or freezing of confined liquid produces a temperature distribution that depends on the pore size distribution. Since the liquid volume is related to the measured intensity, the *IT* curves

represented the pore volume as a function of temperature (Strange *et al*, 1993). The pore volume, *V(x)* is a function of pore diameter *x* and the volume of pores with diameter between ($x + \Delta x$) is $(dv/dx)\Delta x$. If the pores are filled with liquid, the melting temperature of the liquid $T_m(x)$ is related to the pore size distribution by;

$$\text{With } \frac{dV}{dx} = \frac{k}{x^2}\frac{dV}{dT} \tag{7.12}$$

From Equation 7.9; $x = k / \Delta T_m$, and substituting into Equation 7.12;

$$\frac{dV}{dx} = \frac{k}{(k/\Delta T_m)^2}\frac{dV}{dT} = \frac{\Delta T^2}{k}\frac{dV}{dT} \tag{7.13}$$

From the gradient of the *IT* curves; $\frac{dI}{dT} \approx \frac{dV}{dT} = \frac{I_{T_1} - I_{T_2}}{T_1 - T_2}$ (7.14)

Substituting 7.13 into Equation 7.13;

$$\frac{dV}{dx} = \frac{\left[273.15 - \left(\frac{T_1 + T_2}{2}\right)\right]^2}{k} \times \frac{I_{T_1} - I_{T_2}}{T_1 - T_2} \tag{7.15}$$

Note that 237.15 K is used herein as the normal freezing temperature for water and not the freezing point measured on melting curve obtained from specific sample. Reason being the presence of supercooling which shifted the actual freezing point. The pore size distribution can then be determined using the measurement *dV/dx* provided *k* is known for the liquid use. A range of *k* values for water as probe liquid measured using different silica beads are available in the literatures; i.e. 52 K nm (Hansen *et al*., 1996; Morishige and Kawano, 1999) and 58 K nm (Webber *et al*., 2001). Hansen *et al*. (2005) used particles made of polystyrene crosslinked with divinylbenzene for cryoporometry and found a *k* value of 42 K nm. In work involving PLGA microspheres by Petrov *et al*. (2006), they assumed a *k* value of 50 K nm.

In cryoporometry, the problems with polymeric microspheres are the influences of swelling and degradation, both which will alter the physical structure and property of the measured sample. The influence of these variations needed to be accounted for in the *k* calibration. For this thesis, a *k* value of 50 K nm will be used to estimate the magnitude of the neck sizes based on the freezing curves. The measurements of *dV/dx* as a function of pore size distribution are presented in Figures 7.17 and 7.18. A summary of the estimated neck sizes and their corresponding freezing temperature are presented in Tables 7.2 and 7.3.

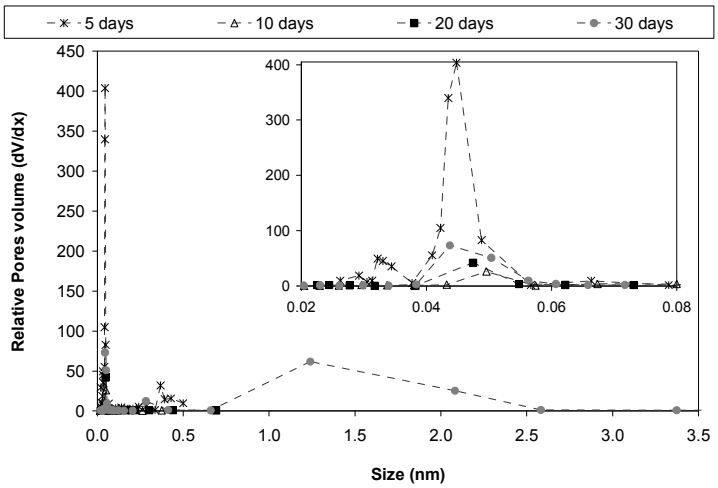

Figure 7.17: The measurement of *dV/dx* as a function of pore size distribution for 75:25MS immersed in water for 5, 10, 20 and 30 days. Inset: Refocus on the lower scale of pore size distribution.

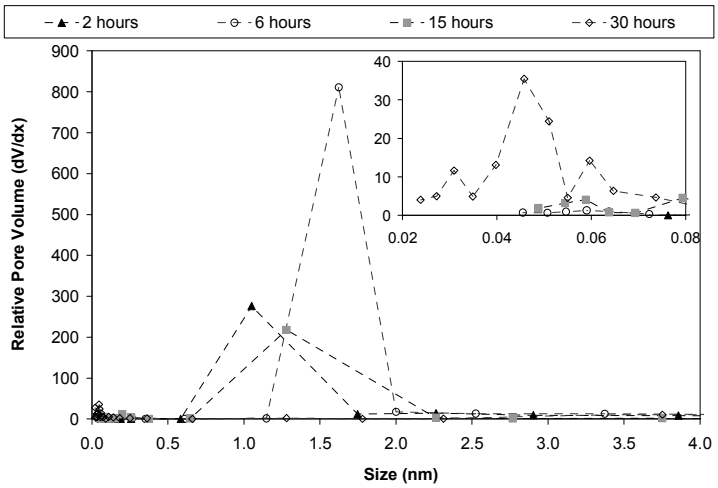

Figure 7.18: The measurement of *dV/dx* as a function of pore size distribution for 50:50MS immersed in water for 2, 6, 15 and 30 hours. Inset: Refocus on the lower scale of pore size distribution.

Table 7.2: The estimated freezing temperatures and necks sizes of 75:25MS after immersion in water.

Immersion in water (Day)	First Freezing Transition		Second Freezing Transition	
	Temperature, T_{N1} (K)	Neck size, x_{N1} (nm)	Temperature, T_{N2} (K)	Neck size, x_{N2} (nm)
5	261.4	0.36	239.5	0.05
10	-	0.05	240.3	0.05
20	-	0.05	239.2	0.05
30	265.6	1.24	238.2	0.043

Table 7.3: The estimated freezing temperatures and necks sizes of 50:50MS after immersion in water.

Immersion in water (Hour)	Estimated Temperature (K)	Estimated Neck size (nm)
	T_{N1}	x_{N1}
2	265.1	1.05
6	267.3	1.62
15	265.5	1.28
30	238.9	0.05

As been anticipated, necks with bigger sizes have higher freezing temperatures. This is because a liquid confined in smaller pore requires a lower temperature to freeze, according to the Gibbs-Thompson equation. For the necks present in 75:25MS, only the five and thirty days samples show a bimodal necks system. The appearance and disappearance of the smaller necks in 75:25MS could have caused by the swelling and shrinking effects. Hansen *et al*. (2005) discovered a complicating situation in which changes could appear in the porous network upon the addition of water. During their sample preparation, the drying process caused the pores to partially shrink, and in extreme cases, collapsed. In subsequent measurement, some of the larger pores that collapse during the earlier drying reappeared after water immersion.

The evolutionary of swelling-shrinking are seen in PFG-NMR experiments. In 75:25MS, although pores of size x_{N1} were not detected on the tenth and twentieth days, they may reappear at different stages. The expansion of smaller space within the polymeric matrix could also be forming new necks, while the swollen necks transforming into larger cavities/pores and disappeared from the detection.

For 50:50MS, they are observed to have unimodal necks pore system. Again, the intermittent polymer swelling and shrinkage may have give rise to the increase and decrease in their neck size. Due to the amorphous nature of 50:50 PLGA, 50:50MS undergoes high rate of hydration and this leads to greater effect of swelling. After fifteen hours immersion in water, a much smaller neck size; i.e. 0.05 nm was detected. This neck could be a newly expanded space due to polymeric swelling, or a neck that is experiencing shrinking effect. Results from PFG-NMR experiment show that 50:50MS can be experiencing more prominent swelling effect between the first and second days (Batch 1 50:50MS, Figure 7.7A). Thereafter pore swelling becomes more random. These characteristics provide reasoning to suggest the appearance of second necks in 50:50MS at much later stage.

7.3 Conclusion

1. Findings from Chapter Six and Figure 7.4 are used to confirm that PLGA microspheres undergo swelling. Swelling is initiated by water uptake of microspheres; i.e. hydration.

2. Following are the proposed swelling effects on PLGA microspheres:
   i. Swelling causes the pore to expand and increase in size. As a result, the microsphere will eventually increase in size.
   ii. The hydrated and swollen pores would offer more paths for water displacement and this promotes self-diffusion of water. Consequently, an increase in the diffusion coefficient of imbibed water can be expected.
   iii. Within a sphere, pores are thought to be interconnected. Since these connecting channels are still part of the polymeric matrix, they will also experience swelling. The expansions in these channels ease the migration of water from one pore to another.

3. By measuring the diffusion coefficients of imbibed water in PLGA microspheres using PFG NMR, the estimated pore sizes increased and decreased over time. This phenomenon is attributable to the evolution pores swelling and shrinkage. 50:50MS with the highest glycolide acid ratio is most hydrophilic and easily wetted and so more susceptible to swelling.

4. It is predicted that solvent evaporation with single emulsion produces microspheres with interior pores of similar sizes regardless the different ratio of lactide to glycolide ratios. This could be validated by the similar initial pore sizes of 50:50MS, 65:35MS and 75:25MS. It was found that 50:50MS experienced significant pore swelling while 65:35MS and 75:25MS did not. The significant pore swelling observed in 50:50MS could be a result of interior autocatalytic.

5. NMR cryoporometry experiments subjected 75:25MS and 50:50MS to a series of freezing, melting and refreezing cycles. The results from freezing curves led to the following findings:
   i. Homogenous nucleation initiates freezing in the bulk liquid. This produces a frozen bulk surrounding the suspended microspheres.

ii. The surrounding bulk provides nucleation site for heterogeneous freezing in microspheres where the confined liquid freezes via ice ingress through the pores at the surface of the microspheres which are in contact with the frozen bulk.

iii. The inheritance of pores with ink-bottle geometry causes a delay in freezing due to pore-blocking effect. The liquid confined in a pore will not freeze before the liquid filling the connecting necks. Pore blocking effect also leads to hysteresis.

iv. The same behaviour was expected for the melting transition of liquid in microspheres. Melting begins in the frozen liquid in the connecting necks before the frozen liquid confined in pores.

6. The Gibbs-Thompson equation shows that for a pore size of x, its melting temperature, $T_m(x)$ is inversely proportional to the size of the pore. NMR cryoporometry is expected to show a decrease in $T_m(x)$ due to increase in pore size resulted from pore swelling. From the Melting and Refreezing cycles obtained from 75:25MS, the I/I_o values in all cases were very low and occasionally close to the background noise signal. This scenario was thought to cause by the insufficient melting of frozen water to produce a significant change in signal intensity in addition to the low fraction of confined water. Therefore, the melting curves could not be explored to predict the pore size. Instead, the freezing curves were used to predict the neck size through which ice front ingress deeper into the microspheres.

7. The freezing curves measured as a function of temperature shows that the 75:25MS used was inherited with pores of ink-bottle geometry and bimodal neck system. The dV/dx vs. size distribution plots show that the neck sizes shifted over time possibly due to swelling mechanism. Evolutionary swelling and shrinkage causes the necks of bigger sizes to disappear from been detected on the freezing curve but reappeared at later stages.

8. It is possible that 50:50MS will only develop to a bimodal neck system after two days of immersion in water. The F-cycles shown in Section 7.2 indicate that 50:50MS were inherited with unimodal neck system but further experiment (shown in Appendix V.C) show that a second neck was detected on the F-cycle after longer period of immersion. Apart from suggesting that these necks were capable of

extensive shrinkage, it is also possible that new necks may be forming; i.e. swelling continued to expand spaces between polymer matrixes forming new necks while the initial necks expand to becoming a pore.

9. With their amorphous nature and susceptibility to hydrolytic degradation, the above strongly suggested that PLGA microspheres used in this thesis undergo swelling. Polymer swelling is caused by hydration, since it is almost impossible to control the water transport inside a microsphere, pore swelling so far is considered as a random rate process, as well as pore shrinking. Other factor contributing to this random effect is the varied amorphous and crystalline regions in the polymeric PLGA microspheres.

CHAPTER 8: *IN VITRO* CISPLATIN RELEASE PROFILES

8.1 Cisplatin-Loaded PLGA Microspheres and Solid Fibres

The ultimate application of the developed system is for the intraperitoneal treatment of advanced ovarian cancer. Cisplatin (CPt) was selected as the model drug for this work because it has a proven activity in ovarian cancer. The objective of this chapter was to study the *in vitro* drug release profiles of CPt-loaded microspheres and solid fibres. Their drug release profiles were studied by using simple rate release kinetic models.

According to Lao *et al*. (2008), modelling of drug release from surface degrading systems would be easier because the drug is release concurrently with the layer-by-layer degradation starting from the outermost surface. In contrast, complication arises from bulk degrading PLGA which does not progress at a constant velocity across the sample. Faisant *et al*. (2002) conveniently categorised the mathematical modelling approaches for degradable devices into two groups: (1) empirical models that assume first or zero order process controlling the overall drug release; (2) models considering specific physicochemical phenomena, such as diffusional, mass transfer or chemical reaction such as degradation and autocatalytic effects.

For this work, two empirical models, first and zero order kinetics, and a simplified Higuchi model were used to fundamentally characterise the CPt release profiles of PLGA samples. The models adapted from Koester *et al*. (2004) are shown below:

Higuchi Model: $Q_t = k_H.t^{0.5}$ (8.1)

First order kinetic: $\ln Q_t = \ln Q_i + k_F.t$ (8.2)

Zero order kinetic: $Q_t = Q_i + k_z.t$ (8.3)

Q_i and Q_t and are the amounts of drug at time, $t = 0$ and $t = t$ respectively. k_H is the Higuchi dissolution constant, k_F and k_z are the first and zero orders rate constants respectively. The conditions and assumptions associated with Equations 8.1 to 8.3 are described in Table 8.1.

For zero order kinetic, the equation is commonly used to describe drug dissolution from several types of modified release pharmaceutical dosage forms such as those that involved an osmotic system (Costa and Lobo, 2001). A zero order kinetic model is useful for system that requires prolong pharmacological action. For first order kinetic, it can be used in porous matrices system that contains water soluble drug maintained in a sink condition (Mulye and

Turco, 1995). The pioneering model first proposed by Higuchi was to describe the dissolution of drug in suspension from ointment and it is valid throughout the measurement period except when the total depletion of the drug is reached.

The Higuchi model can be further developed for drug release from spherical homogenous matrix systems and planar or spherical system having a granular (heterogeneous) matrix (Higuchi, 1962 and 1963). The model can be used to study the release of water soluble and low soluble drugs incorporated in semi-solid and/or solid matrixes. This model is expressed in Equation 8.4:

$$Q_t = \sqrt{\frac{D\varepsilon}{\tau}(2C - \varepsilon C_s)C_s t} \tag{8.4}$$

Where Q_t is the amount of drug release in time t by surface unit, C is the initial concentration of the drug, ε is the matrix porosity, τ is the tortuosity factor, C_s is the drug solubility in the matrix/exipient media and D is the diffusion constant of the drug molecules in that liquid. Equation 8.4 can be simplified and written as Equation 8.1 to characterise the drug release using a single integral value, which is essentially the effective diffusion coefficient of the dissolution component. The simplicity of Equation 8.1 can offer a good description for drug release profiles but sometimes conflicts with the more complex conditions.

Table 8.1: Conditions and assumptions of the Higuchi, first and zero order kinetics models.

MODEL	CONDITIONS	ASSUMPTIONS	Note
Zero Order	▪ Same amount of drug is released by unit time.	▪ Drug dissolution from matrix that does not disaggregate. ▪ Area of matrix remains constant. ▪ No equilibrium condition is achieved.	(i) (ii) (iii)
First Order	▪ The amount drug released is proportional to the amount of drug remaining in its interior. ▪ The amount drug released by unit of time is diminishing.	▪ The matrix is inert, insoluble, nonswellable towards the drug and medium. ▪ Area of matrix remains constant. ▪ Medium influx and drug dissolution in the medium rapidly occur when come into contact.	(iv) (ii) (v)
Higuchi Model	▪ Drug release is a diffusion process based on Fick's first law. ▪ Drug released is square root time dependent.	▪ System is not surface coated. ▪ Matrix does not undergo significant alteration in the presence of water. ▪ Dissolution of drug is instantaneous. ▪ Drug release rate is controlled by the rate of drugs diffusion and solubility within the device.	(vi) (ii) (v)

Notes no. (i) to (vi), see text for discussion.

The degradation studies in Chapter Six provide reasoning for the applicability of Equations 8.1 to 8.3. Notes no. (i) to (vi) are discussed below:

(i) The degradation effect of 75:25 PLGA was not as extensive as for 50:50 PLGA and 65:35 PLGA. Therefore, the zero order kinetic could be applied on 75:25 PLGA. For faster degrading 50:50 and 65:35 PLGA, zero order kinetic may be applicable during the initial period before prominent degradation effect sets in.

(ii) Similar to (i). It is assumed that initially the morphology and sizes of the PLGA devices do not alter significantly before prominent degradation. 50:50 PLGA devices are likely to experience morphological changes during the first week and a few days later, follow by 65:35 PLGA devices.

(iii) Drug diffusion is continual because buffer refreshment maintains a concentration gradient between the device and dissolution medium, i.e. sink condition.

(iv) So far little or no literature information has suggested the presence of any chemical interaction between cisplatin/lidocaine and PLGA. Therefore, the developed PLGA devices are assumed to be inert towards the model drugs.

(v) PLGA is amorphous therefore medium influx can take place and leads to drug transport. Cisplatin has a water solubility of 2 mg/ml therefore drug dissolution buffer can occur which leads to drug release.

(vi) No coatings were incorporated into the developed systems in this work.

Results show that Equations 8.1 to 8.3 are inadequate to provide good fit to CPt release profiles and a three compartmental model was further developed in order to improve model fitting. This model will be evaluated in the discussion section. For ease, CPt-loaded 50:50 PLGA microspheres will be abbreviated as CPt-50:50MS and CPt-loaded 50:50 PLGA solid fibres as CPt-50:50SF. Similarly for the microspheres and solid fibres made of 65:35 and 75:25 PLGA.

8.2 Production of CPt-Loaded PLGA Microspheres and Solid Fibres

CPt-loaded 50:50, 65:35 and 75:25 PLGA microspheres were produced using the method described in Section 4.1.3. A polymer concentration of 15 % (w/w) and a drug-to-polymer ratio of 1:2 were used. Briefly, 10 g of polymer/drug solution was homogenised in 100 ml PVA solution (0.5 % w/w) at 6500 rpm for 15 min. Then the nascent microspheres were transferred to magnetic stirring before they were harvested. CPt-loaded 50:50, 65:35 and 75:25 PLGA solid fibres were spun using the method described in Section 4.2.3 with a drug-to-polymer ratio of 1:2 and a 20 % (w/w) polymer concentration.

The resulting CPt-loaded microspheres were sieved into three different size fractions; between 90-75 μm, 75-53 μm, and 53-38 μm, in order to compare their drug release rates.

Five preweighed samples were prepared from each PLGA microsphere and solid fibre for *in vitro* drug release analyses. CPt concentration and drug loading were determined using methods described in Sections 4.3.2 and 4.4 respectively. *In vitro* drug release analysis was carried out by incubating the sample in a shaking water bath maintained at 37^{o}C. More details of the incubation conditions can be found in Section 4.5.

8.3 Results & Discussion

The drug loadings for CPt-loaded solid fibres and microspheres of different size fractions are shown in Figure 8.1. The drug loadings of PLGA solid fibres are in general higher than those of microspheres and this is thought to be because of the higher water miscibility of NMP. The faster solvent diffusion into the aqueous phase leads to a rapid phase inversion of the nascent solid fibre compared to the case of DCM with microsphere. A faster rate of solidification would decrease the residence time of drugs leakage and loss. Figure 8.1 shows that 75:25 PLGA tends to have higher drug loading compared to 50:50 and 65:35 PLGA. This trend is attributable to the higher lactic acid ratio in 75:25 PLGA which produces a more viscous solution and thereby exhibits a faster rate of solidification. PLGA with higher glycolic acid ratio would be more hydrophilic which permits higher diffusion of medium. Therefore drug leakage and loss are higher.

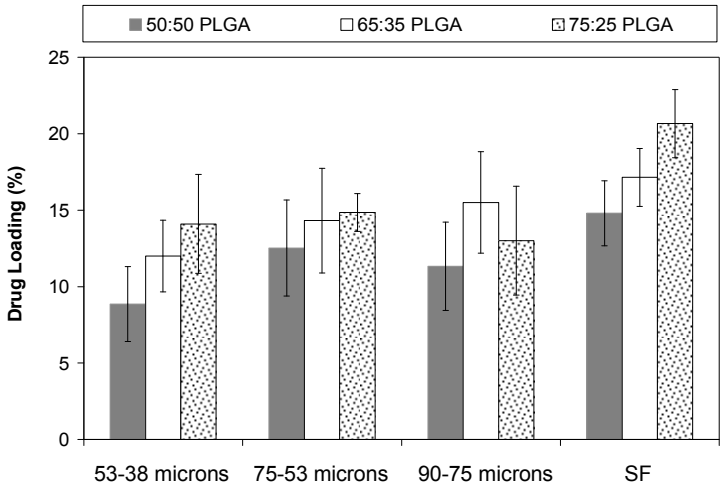

Figure 8.1: Drug loadings of PLGA solid fibres (SF) and PLGA microspheres of sizes 53-38 μm, 75-53 μm and 90-75 μm and solid fibres. Data represent mean ± standard deviation (n = 5).

Table 8.2: Statistical analyses comparing the drug loadings between PLGA solid fibres and microspheres.

	PLGA Sample	Significant Difference ANOVA – one factor ($p < 0.05$)
SF	75:25SF vs. 65:35SF	✓
	75:25SF vs. 50:50SF	✓
	50:50SF vs. 65:35SF	✗
MS vs. SF	50:50MS (38-53 μm) vs. 50:50SF	✓
	50:50MS (53-75 μm) and (75-90 μm) vs. 50:50SF	✗
	65:35MS (38-53 μm) vs. 65:35SF	✓
	65:35MS (53-75 μm) and (75-90 μm) vs. 65:35SF	✗
	75:25MS (38-53 μm) vs. 75:25SF	✓
	75:25MS (53-75 μm) vs. 75:25SF	✓
	75:25MS (75-90 μm) vs. 75:25SF	✓

Table 8.2 summarises the comparisons of drug loading between PLGA solid fibres and microspheres. Siepmann *et al*. (2004) suggested that drug loading increases with particle size due to a condition where bigger spheres offer bigger structure to accommodate more drugs. In terms of total surface area, smaller microspheres would have higher surface for drug leakage compared to bigger microspheres during the rapid phase inversion process. However, considering the volume of a small and a large nascent microspheres, the bigger the nascent sphere, higher the volume of solvent it contains. This would require longer residence time for solvent diffusion and solidification. In contrast, a smaller sphere with lesser solvent volume will solidify faster. The combinations of the above mechanisms may have contributed to the deviation in drug loading trend with regard to microsphere size, as seen in Figure 8.1.

Section 6.1.3 showed the spatial heterogeneous distribution of the entrapped agent in 75:25MS, due to reasons such as imperfect emulsification. This also indicates that for microspheres of similar sizes, the amount of entrapped drug could be different. As a result, the inhomogeneity of entrapment ratio of microspheres in a size fraction could be producing an "average" effect on the final drug loading and thus, affected the trend in overall drug loading.

The cumulative *in vitro* releases of CPt from 50:50SF and 50:50MS of three size fractions, namely; 90-75 μm, 75-53 μm, 53-38 μm over a period of twenty days are shown in Figure 8.2. The drug release profiles of 50:50 PLGA samples are fundamentally described as biphasic; Phase 1 is the initial faster drug release during the first day and a slower drug

release, and thereafter Phase 2. It will be shown later that the Phase 2 release is affected by different mechanisms that arise from the degrading PLGA devices. Phase 1 is associated with a rapid drug release known as the "burst release" and is common in PLGA microspheres. It has been reported that an instant cumulative CPt release as high as 20% (Itoi *et al*., 1996) and 25% (Fujiyama *et al*., 2003) occurred in PLGA microspheres.

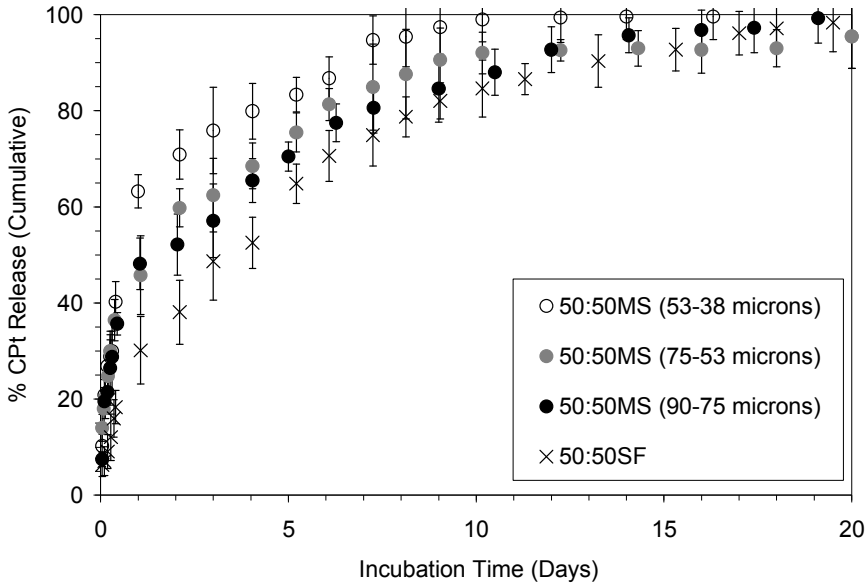

Figure 8.2: Percentage (%) cumulative release of CPt from 50:50MS with size fractions: 53-38 μm (○), 75-53 μm (●), 90-75 μm (●) and 50:50SF (×). Data represent mean ± standard deviation (n = 5).

The mechanisms contributing to the Phase 1 release are proposed below:

i. The presence of a large drug concentration gradient between microspheres and buffer at the first instant of buffer immersion. The large concentration gradient may provide a greater driving force for CPt to diffuse faster into the buffer.

ii. During polymer solidification, drug diffused towards the periphery of the nascent microspheres or solid fibres. This leads to entrapment of CPt in the periphery of the microspheres or solid fibres. During immersion in buffer, these samples become hydrated and CPt located in these peripheral layers is rapidly released.

iii. During the production processes, free CPt from leakage adsorbed on the surface of the microspheres or solid fibres. These CPt are then rapidly released into the buffer.

Previously in Chapter Seven, it was found that the pore size of 50:50MS (Batch 1) underwent hydration during the first few hours of measurement and then increased in size from the first to the second day. Pore swelling (Hopfenberg and Hsu, 1978) and buffer immersion (Siepmann *et al*., 2004) shift the physical state of the system to a rubbery state

which permits faster medium diffusion (Fan and Singh, 1989). Siepmann *et al*. (2004) also found that this shift was independent of microsphere size. Thus, the swelling susceptibility of 50:50MS is thought to be closely related to a rapid drug release. The rapid Phase 1 drug release observed in CPt-50:50MS during the first day correlates well to the pore swelling profile seen in Figure 7.7 (Section 7.1).

During the Phase 1 release, 50:50MS released 45-65% of their drug contents compared to ~30% from 50:50SF. Comparing the forms of solid fibres to microspheres, solid fibre is a cylindrical device whereas microspheres present as multiple submicron particles. In addition to swelling, these spherical devices also offer much higher surface area for drug diffusion. As a result, 50:50MS exhibits a higher drug release rate compared to 50:50SF. After approximately ten days, the drug release from 50:50SF converged to the drug release from 50:50MS of intermediate and largest size fractions. Meanwhile, 50:50MS of the smallest size fraction has reached to content depletion. The smallest size fraction 50:50MS has the largest surface area:volume ratio and it was anticipated that they would exhibit a faster drug release rate. See Table 8.3 for estimation of surface area:volume ratio.

Drug release from 50:50SF was slower because of its lower surface area and its dense wall structure. The release of drug from PLGA solid fibres is closely related to their skin layers formed during the phase inversion process. Figure 8.3A shows the finger-like structure of 50:50SF extended towards the outer surface of the fibre. The structure is denser towards the fibre outer surface (indicated as ‘s2’ in Figure 8.3A) compared to the structure at the fibre core (s1). The denser structure near the skin layer offers higher mass transfer resistance and limits medium transport compared to macrovoids. From previous discussion in Sections 3.5 and 5.2, this feature of skin layer could reduce drug release rate. This phenomenon is reflected in the slower drug release of 50:50SF (Figure 8.2).

Figure 8.3: SEM images of (A) the finger structure of undegraded 50:50SF. Region ‘s2’ has a denser structure compared to region ‘s1’ with microvoids. (B) and (C) twenty days degraded 50:50SF.

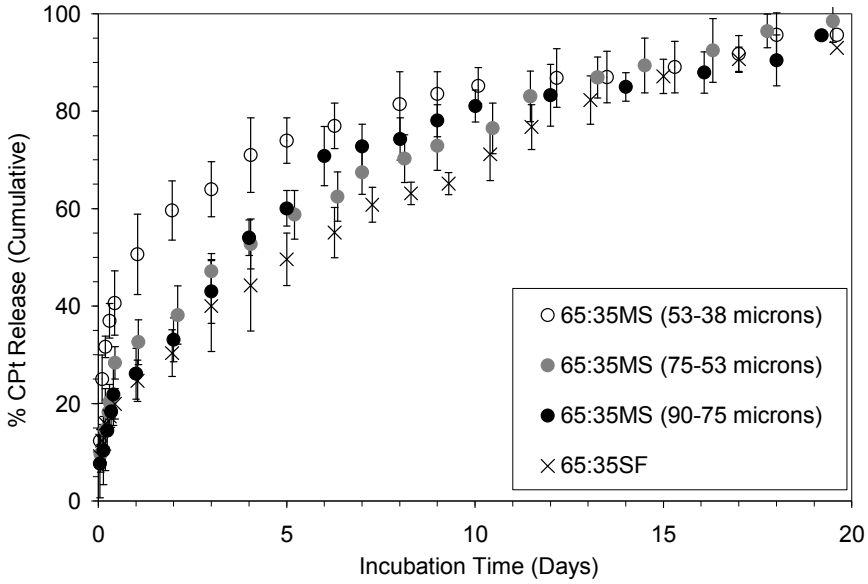

Figure 8.4: Percentage (%) cumulative release of CPt from 65:35MS with size fractions: 53-38 μm (○), 75-53 μm (●), 90-75 μm (●) and 65:35SF (×). Data represent mean ± standard deviation (n = 5).

Figure 8.4 shows the cumulative *in vitro* releases of CPt from 65:35MS of different size fractions; 90-75 μm, 75-53 μm, 53-38 μm, and 65:35SF over a period of twenty days. 65:35MS of the smallest size fraction clearly exhibits the fastest drug release rate compared to other size fractions and 65:35SF. For example, 65:35MS of the smallest size fraction released up to 40% of its drug content during the first day whereas 65:35SF did not reach to 40% drug release until Day 3. 65:35SF with its larger and dense fibre wall structures possess higher resistance to drug diffusion. These features of solid fibre caused CPt to require longer time to diffuse to the surface. Thus, drug release from 65:35SF is delayed and slower. After two weeks, the drug release from 65:35MS of all size fractions and 65:35SF tend to converge and proceed at the same rate towards the end.

The overall slower CPt release from CPt-65:35MS compared to CPt-50:50MS, can be related to a tendency of gradual pore swelling in 65:35MS (Figure 7.5, Section 7.1) over a period of approximately three weeks. The corresponding fractions of imbibed water were observed to be increasing over this period. This hydration profile obtained from PFG-NMR experiments mimics the CPt release from 65:35MS seen in Figure 8.4. The gradual hydration within 65:35MS provides medium for drug transport such that drug can be released into the buffer.

For CPt-loaded PLGA solid fibres, SEM images following the degradation of PLGA solid fibres in Section 6.6 showed that 50:50SF (Figure 6.26) degraded faster than 65:35SF

(Figure 6.27). For the degrading 50:50SF and 65:35SF, large cavities were formed at the centre of the fibres. Comparing their surfaces conditions, pores formation started after ten days and thereafter, the surface pores of 50:50SF increased in numbers and sizes faster than those of 65:35SF. The larger pores developed on the 50:50SF after twenty days in buffer may be the reason why a full drug release is observed after approximately eighteen days in Figure 8.2. The pores on the surface of 65:35SF were size-consistent and this may have led to near zero-order drug release while preventing uncontrollable release of the remaining CPt.

According to Fick's Law of diffusion, the driving force for drug diffusion is due to the presence of a concentration gradient between two points of measurement (Coulson and Richardson, 1999). In this case, the concentration of drug in buffer is lower than in the microsphere/solid fibre. Table 8.11 shows that the estimate surface area:volume ratio of smaller microspheres are higher than those larger ones. In comparison, Table 8.3 shows that the much larger solid fibre has much smaller surface area:volume ratio. See Appendix VI.I for sample calculations. Microsphere of larger size would exhibit a lower rate of drug release because of the longer diffusion path length across the larger microsphere. Vice versa, smaller microsphere will shorter path length would have a higher drug release rate.

Table 8.3: Estimate surface area:volume ratio of 15 % (w/w) PLGA microspheres in a 0.2 g sample.

PLGA	Size Fraction	Diameter (10^{-6} m)	Number of microspheres (10^{7})	Surface area of one microsphere (10^{-5} cm^2)	Volume of one microsphere (10^{-9} cm^3)	Total Surface Area:Volume ratio
50:50MS	D [v, 0.1]	6	114.93	0.11	0.11	100.00
	D [v, 0.5]	26	1.41	2.12	9.20	23.08
	D [v, 0.9]	84	0.04	22.17	310.38	7.14
65:35MS	D [v, 0.1]	8	48.49	0.20	0.27	75.00
	D [v, 0.5]	45	0.27	6.33	47.71	13.33
	D [v, 0.9]	90	0.03	25.45	381.75	6.67
75:25MS	D [v, 0.1]	5	239.10	0.07	0.05	127.66
	D [v, 0.5]	53	0.17	8.83	77.96	11.32
	D [v, 0.9]	107	0.02	35.97	641.51	5.61

Table 8.4: Estimate surface area:volume ratio of 20 % (w/w) PLGA solid fibres.

PLGA	Diameter (10^{-6} m)	Number of fibres	Surface area of one fibre (10^{-5} cm^2)	Volume of one fibre (10^{-9} cm^3)	Total Surface Area:Volume ratio
50:50SF	670	10	16.84	2.82	5.97
65:35SF	720	10	18.10	3.26	5.56
75:25SF	760	10	19.11	3.63	5.26

The CPt release profiles of 50:50 and 65:35 PLGA shown on Figures 8.2 and 8.4 indicate agreement to Fick's Law. In some cases, the microspheres of intermediate and largest size fractions exhibited similar release rates. The reasons causing the deviation from the Fick's law of diffusion are such as: (1) a spatial heterogeneous distribution of the entrapped agent in PLGA microsphere was shown in Section 6.1.3. Drug located in the outermost periphery of the microspheres are expected to be rapidly released, (2) the different local concentration of the drug within a microsphere which can influence the drug release pattern (Matsumoto *et al*., 2005), (3) while hindering a homogeneous drug distribution, the different amorphous regions in PLGA also affect the freedom of drug diffusion within the matrix, in addition to contributing to a rapid drug release (Sastre *et al.,* 2004).

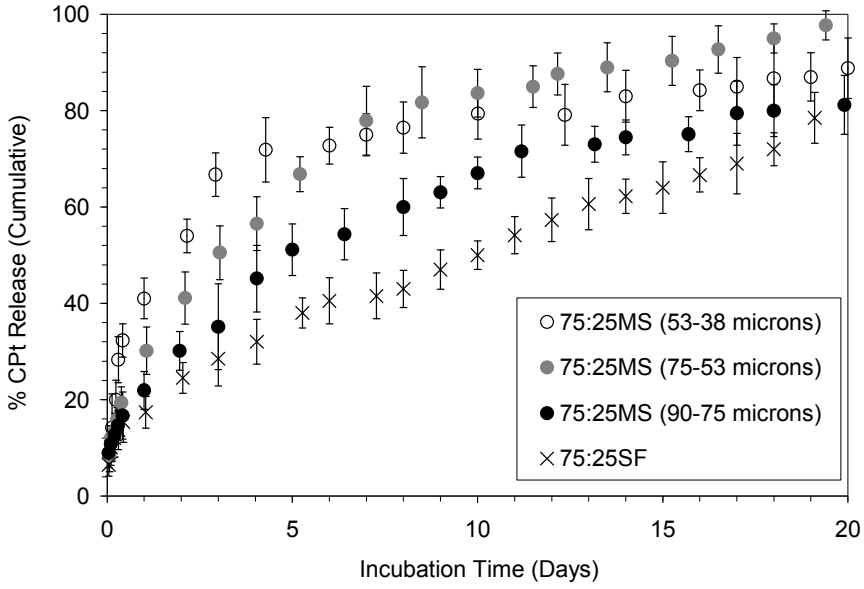

Figure 8.5: Percentage (%) cumulative release of CPt from 75:25MS with size fractions: 53-38 µm (○), 75-53 µm (●), 90-75 µm (●) and 75:25SF (×). Data represent mean ± standard deviation (n = 5).

Figure 8.5 shows the cumulative *in vitro* releases of CPt from 75:25MS of different size fractions; 90-75 µm, 75-53 µm, 53-38 µm, and 65:35SF over a period of twenty days. 75:25MS exhibits a higher overall release rate while the drug release from 75:25SF remains the lowest throughout the twenty days period. The 75:25MS of the smallest size fraction exhibits the highest release rate during the first week and followed by a slower release towards the end. In this case, CPt may be entrapped deeper in the matrix and longer time was required for these drugs to diffuse to the surface. After a week, 75:25MS of the intermediate size fraction exhibits a fast release and approaches to content depletion. In this case, most of the CPt may be located in the peripheral layer of the microsphere and a faster

continual drug release is observed. For 75:25SF, its degradation resistance restricted the surface pore formation (Section 6.6, Figure 6.28) which produces a slower drug release compared to 50:50SF and 65:35SF.

The overall time taken to reach to content depletion exhibited by 75:25 PLGA samples is longer compared to 65:35 and 50:50 PLGA. This could be attributed to the higher degradation resistance of 75:25 PLGA. The burst release is also more prominent in 50:50MS compared to 65:35MS and 75:25MS.

Findings in Section 7.1 showed that PLGA microspheres underwent swelling. During swelling of a microsphere, its glass transition temperature is lowered and the system shifts to a rubbery state. 50:50MS was found the most susceptible to swelling compared to 65:35MS and 75:25MS. The pore expansion in 50:50MS would promote medium transport and lead to an increase in drug diffusion. As a result, 50:50MS exhibits a faster drug release as oppose to 75:25MS which restricts pore swelling. The interior tortuosity of 75:25MS was also found to be constant (Figure 12.3, Appendix V.B). This constancy may have contributed to the near zero order release in the later stage of Phase 2 drug release.

Findings from Section 6.1.2 indicated the porous interior of PLGA microspheres used in this work while degradation changes their surface morphologies (Section 6.2). While the diffusion pathway for the entrapped drug may not be of forward channels, the tortuosity of these channels also changes over time (Section 7.1). Based on these results, it is thought that the diffusion of entrapped CPt and subsequent drug release are affected by the changing interior of the microspheres due to degradation and swelling effects. Local autocatalytic degradation will also alter the interior porosity of the device however its effect is theoretically difficult to be accounted for in drug release (Siepmann *et al*., 2004).

As the degradation progresses, disintegration of the polymeric structure continues to disrupt the finger structure (Section 6.6). The degraded solid fibre with increased structural porosity would eventually leads to a faster drug release. Results from PFG-NMR experiments showed that the tortuosity of PLGA microspheres changes over a period of thirty days (Figure 12.3, Appendix V.B). This characteristic is attributable to the evolutionary swelling and shrinking in the PLGA microspheres, due to hydration and water transport in the porous interior. Likewise, the similar polymeric solid fibres made of PLGA were also anticipated to

experience changes in their interior tortuosities, due to both swelling/shrinking and degradation effects.

Spenlehauer *et al*. (1988) presented a study on the effects of process conditions on the distribution CPt crystal in PLGA microsphere. The drug distribution system by Spenlehaeur *et al*. (1988) is suitable to be adopted because of the similarity in working polymer (PLGA), solvent (DCM), emulsifier (PVA), and single emulsion method. Spenlehauer *et al*. (1988) proposed five types of CPt distribution as illustrated in Figure 8.6. The characteristic of these distribution patterns are summarised in Table 8.5.

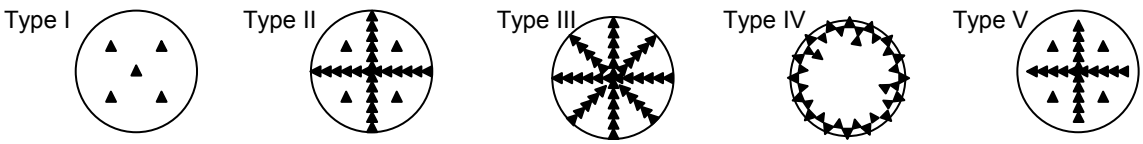

Figure 8.6: Different distribution patterns of cisplatin crystal within a microsphere. Black triangle represents cisplatin (Spenlehauer *et al*., 1988).

Table 8.5: The distribution patterns of cisplatin in PLGA microsphere (Spenlehauer *et al*., 1988).

Type	Characteristic of Distribution Pattern
I	Cisplatin are distributed in the polymer matrix with no contact between each other.
II	Large amounts of cisplatin present in the matrix. Some are in contact with each other and formed a network, which connects the cisplatin at the inner part of the microsphere to those nearer to the surface.
III	Similar to type II but no isolated cisplatin. All cisplatin are in contact with each other forming a dense network.
IV	Cisplatin are in contact with each other but they tend to locate at the surface layer of the microsphere.
V	Similar to Type II, but the cisplatin-network is located at the centre of the microspheres with not cisplatin at the surface layer. For example, no direct connection between the inner drug-network and the surface of the microsphere. Also depicted as a layer of polymer enveloping an inner drug network.

For the developed CPt-loaded microspheres herein, Type IV is an appropriate pattern to be adapted because Spenlehauer *et al*. (1988) suggested that centrifugation promoted this type of distribution. While a Type IV drug distribution pattern can be assumed initially, this distribution pattern would likely to change, and different distribution patterns could be assumed at different stages as drug release proceeded.

From the CPt release profiles of 50:50MS and 50:50SF shown in Figure 8.2, their Phase 1 releases are likely to associate with a Type IV drug distribution pattern resulted from a centrifugation effect. After that, the faster CPt release rate observed on 50:50MS may be characterised by a Type I distribution pattern because the drug loading was relatively lower in 50:50MS. The lesser amount of drug entrapped in the microsphere is unlikely to give rise to a dense crystal network. During buffer immersion, the medium transport promoted random diffusion and redistribution of CPt. With a fast degradation rate, CPt in 50:50MS had less chance to alter between drug distribution patterns as drug release was fast.

For 65:35MS, the CPt distribution may initially assume a Type IV distribution pattern and later changed to a Type II and/or Type I. After Phase 1 release, the CPt released from 65:35MS was slower compared to 50:50MS. A Type II distribution might have produced this slower release. Following this, with a higher resistance in degradation compared to 50:50MS, the drug distribution pattern changed to Type I. At this later stage, the drug diffusion continued and drugs entrapped deeper in the matrix were slowly released.

For 75:25MS, after Phase 1 release, a Type V of drug distribution may be used to characterise the system. The reason being that the highly degradation-resistant 75:25MS would have an intact interior which is more capable of entrapping the remaining CPt. Although 75:25MS was least affected by hydrolytic degradation, but medium transport continued to allow the outflow of drug. Apart from predicting the different drug distribution pattern, a hypothetical model of the drug release in parallel with a bulk degrading PLGA microsphere is illustrated in Figure 8.7.

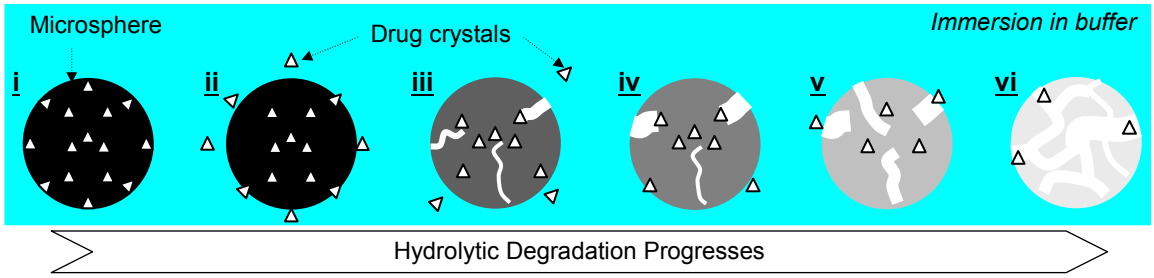

Figure 8.7: A hypothetical model of drug release from microspheres with a Type IV drug distribution.

The sequence of the drug release is envisaged as below:

i. Initially, Type IV drug distribution is assumed in the microsphere.
ii. The release of drug crystals located at the outermost peripheral of the microsphere. Since the microsphere has a porous interior, immersion in PBS enables buffer

penetration. This will initiate internal hydrolytic degradation. The presence of porous structure and buffer enable drug transport inside the microsphere.

iii. With bulk degradation, internal degradation will lead to changes in tortuosity. New microchannels will be formed and collapsed as a result of degradation.

iv - v*ii*. Degradation progresses and this increases the size of the microchannels which then offer higher freedom for medium and drug transports. Structural disintegration continues and the remaining drugs are released into the buffer.

Siepmann *et al*. (2004) followed the *in vitro* degradation of PLGA microspheres by measuring their molecular weights and showed that the size of microsphere did not affect the rate of degradation. Chapter Six concluded that the lactide:glycolide ratio was more prominent in governing the degradation rate of microsphere. Sections 6.2 showed that 75:25MS exhibits high degradation resistance. Hence, the effect of degradation on the release of CPt from 75:25MS is thought to be lesser compared to 50:50MS and 65:35MS.

A bulk degradation pattern for both PLGA hollow and solid fibres were also determined in Chapter Six. The core matrixes of these fibres are observed to degrade faster than their outer surface. This effect is thought to be promoted by the skin layers surrounding these fibres and also their much larger structure. Similar to PLGA microspheres, the hypothetical model described in Figure 8.7 could be used to predict the drug release from the bulk degrading fibres. The major difference is that the larger structure of the fibre is thought to offer a longer diffusion pathway and thus, slower drug release could be expected.

As described earlier, the drug release during the first day can be termed as Phase 1 and drug release thereafter as Phase 2. In preliminarily fittings, partitioning the *in vitro* drug release profiles into Phase 1 and Phase 2 show better models fittings using Equations 8.1 to 8.3. The Higuchi model, $Q_t = k_H.t^{0.5}$ (Equation 8.1) fits well to the experimental data for both microspheres and solid fibres during the Phase 1 drug release and examples of results are shown in Figure 8.8. The estimated Higuchi constants, k_H are presented in Table 12.4 (Appendix VI.C).

Based on these results, it could be suggested that the drug release from PLGA solid fibres and microspheres during the first day are diffusional-controlled and is proportional to the square root of time. The nature of bulk degrading PLGA where water diffusion into the device is fast, supports a possible diffusional drug release phase in PLGA depots. The

diffusional release during Phase 1 is thought to be associated with the 'burst effect' discussed earlier. Factors such as surface-adsorbed drugs, drugs located at/near surface, centrifugation effect that caused drugs to locate in the peripheral layer of the microsphere, and the swelling susceptibility of polymeric devices especially those made of 50:50 PLGA are thought to contribute to Phase 1 release.

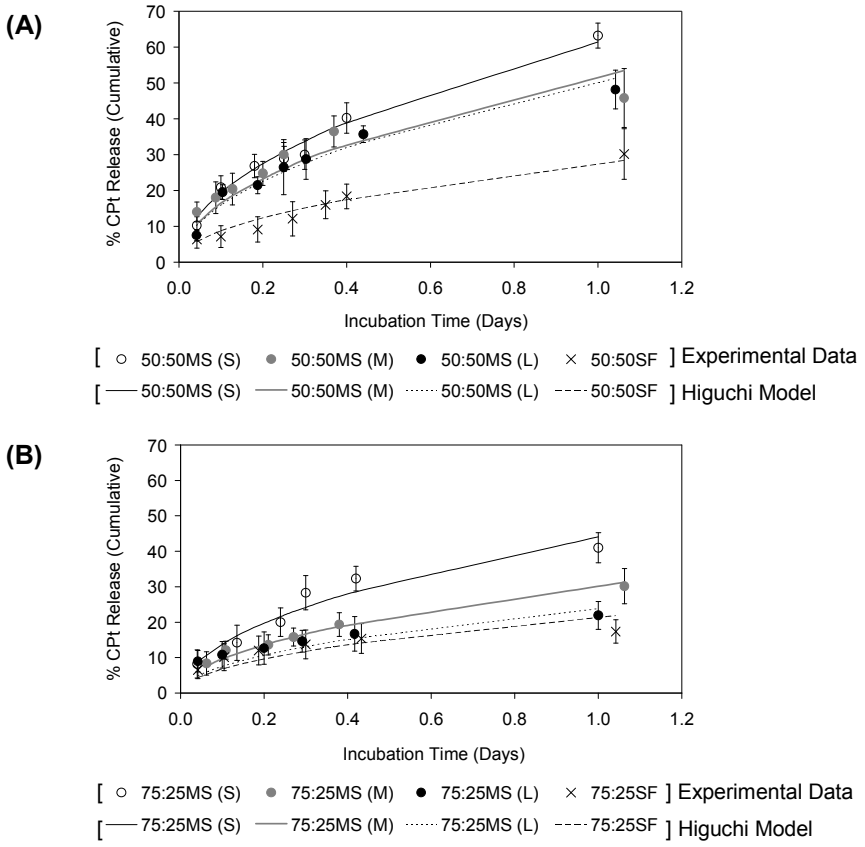

Figure 8.8: Fittings of Higuchi model to drug releases from (A) 50:50 and (B) 75:25 PLGA microspheres and solid fibres during Phase 1. *Size fractions: S = 53-38 μm, M = 75-53 μm and L = 90-75 μm.*

During Phase 1 drug release, microspheres of the smallest size fraction tend to exhibit the fastest drug release compared to microspheres of larger size fractions. This trend agrees to a Fickian's diffusion where smaller particles is associated with higher surface area:volume ratio, which offer higher surface area for drug diffusion. Similar observation is also applied for the slower drug release comparing solid fibre to microsphere.

Equations 8.1 to 8.3 were also fitted to the Phase 2 drug release and results are shown in Appendix VI.C. The Phase 2 drug releases of PLGA samples indicate partial similarities to Equations 8.1 to 8.3 with respect to different stages during the release period. This similarity may due to the existing conditions of the PLGA devices that fulfilled the assumptions of

these models described in Table 8.1. The structural evolution of these PLGA devices causes the system to deviate from the assumptions and therefore model Equations 8.1 to 8.3 were not longer valid in the new condition. Based on studies findings in Chapters Six and Seven, the deviations from the models are suggested to be caused by:

i. Degradation leads to the formation of surface pores on microspheres and hollow/solid fibres. The development of these pores, the bulk and heterogeneous degradations influenced the drug release rate as the diffusion passages for drug are altered over time.
ii. The pore swelling and shrinking in PLGA microspheres alter the interior tortuosity. These mechanisms will affect drug diffusion in the pore network, the rubbery state or amorphous regions in the matrix. Thus, the drug diffusion pathway is altered.
iii. In addition to (i) and (ii), the spatial heterogeneous distribution of the entrapped drug within a microsphere, subsequent drug release and the redistribution of the entrapped drug due to medium transport and subsequent drug release.
iv. Cryoporometry experiments in Section 7.2 showed that the pores in PLGA microspheres are made of ink-bottle geometry. The connecting necks were also found to undergo swelling and shrinking. It is also hypothesised the transformation of an expanding neck to a pore-like cavity, and the formation of new and smaller necks. In part to (iii) above, the random swelling/shrinking of necks could have effect of releasing the drug entrapped in the main pores.

Results show that CPt release from PLGA microspheres and solid fibres cannot be fully characterised by empirical models (Equations 8.1 to 8.3) with single parameters. It has been reported in the literature that PLGA microparticles can yield non-square root relation drug release profile (Le Corre *et al*., 1997 and Fujiyama *et al*., 2003). Simple empirical models such as averages or straight lines are useful for generalising trends in a system, but do not account for physical condition such as degradation effect of the PLGA drug releasing depots. Preliminary model fittings show that CPt release profiles of PLGA microspheres and solid fibres are at least biphasic. A biphasic drug release model for microsphere drug delivery is common in the literatures. Examples are such as the one developed by Batycky *et al*. (1997) which considers a burst release phase followed by a drug diffusion phase which occurs via interconnected pores.

More comprehensive model developed by Grassi *et al*. (2000) accounted the factors such as the sizes of the particles, the physical state and distribution of the entrapped drug within the

device including the dissolution and diffusion of the drug. Jalil and Nixon (1990a and 1990b) proposed a number of relevant mechanisms such as surface-drug desorption, drug diffusion through particle pores and various regions in the polymer matrix. It is common for a model to have specific components that are mechanism- and time-dependent during the release period (Liu *et al*., 2006 and Duarte *et al*., 2006). Sometimes, the contribution of these mechanisms could be difficult to be quantified (Polakovič *et al*., 1999).

Empirical models derived from the first order models are appropriate for use to study drug release from depots. A semi-mechanistic model is an empirical model which can be used to relate the parameters of the rate equation to physical condition of the depots. When a solid matrix containing a water soluble drug is introduced into an aqueous environment the drug will leach into the aqueous phase. The more that drug leaves the matrix means that the amount remaining for subsequent released is reduced. It can be assumed that the driving force for mass transfer is proportional to the difference between the outer surface concentration and the concentration of solute in a solute-rich region (Glueckauf and Coates, 1947).

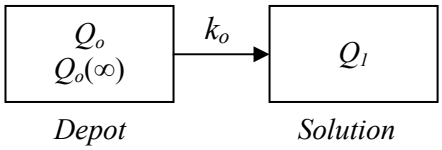

Figure 8.9: A two compartmental model showing the relationship between Q_o and Q_1.

Figure 8.9 shows a two compartmental model of drug release, where Q_o is the amount of drug remained in the depot after Q_1, the amount of drug is released in solution, which is dependent on the release constant, k_o. $Q_o(\infty)$ is amount of drug in the depot which will be released after a long time. The equation which predicts release of drug from a depot device (i.e. PLGA microsphere or fibre) can be derived from the rate equations using Laplace transformations (Mayersohn and Gibaldi, 1970). Here, drug released in the solution is related to the drug remained in the depot by:

$$\frac{dQ_1}{dt} = k_o.Q_o \tag{8.5}$$

where Q_o is the amount of drug remaining in the depot. Q_1 is the amount of drug released in solution from the depot. k_o is the rate of drug release. From Figure 8.9, it can be seen that he concentration of drug remaining in the depot, Q_o decreases at a rate:

$$\frac{dQ_o}{dt} = -k_o.Q_o \tag{8.6}$$

Transforming the differential Equations 8.5 and 8.6 using Laplace transformation gives:

$$s.\overline{Q_1} - Q_1(0) = k_o.\overline{Q_o} \tag{8.7}$$

$$s.\overline{Q_o} - Q_o(0) = -k_o.\overline{Q_o} \tag{8.8}$$

$\overline{Q_1}$ and $\overline{Q_o}$ are Q_1 and Q_o in Laplace space. Applying the initial conditions when $t = 0$ are: $Q_1(0) = 0$ and $Q_o(0) = Q_o(\infty)$. Rearranging Equation 8.8 gives:

$$\overline{Q_o} = \frac{Q_o(\infty)}{(s + k_o)} \tag{8.9}$$

Substituting Equation 8.9 into Equation 8.7 gives;

$$\overline{Q_1} = \frac{k_o.Q_o(\infty)}{s(s + k_o)} \tag{8.10}$$

An anti-Laplace transformation of Equation 8.10 gives:

$$Q_1 = Q_o(\infty).(1 - e^{-k_o t}) \tag{8.11}$$

A single exponential, also known as the linear driving force (LDF) model (Sircar and Hufton, 2000), is simple to implement and so is widely used (Messaritaki *et al*., 2005 and Machida *et al*., 2000). For some PLGA devices the initial burst of drug release can occur to a greater extent than predicted by a single exponential or mono-exponential equation. Evidence of this is indicated in preliminary fittings of Equations 8.1 to 8.3. More examples of these results are shown in Appendix VI.C. As the apparent rate of release changes the previous model is no longer applicable. As a result, a single exponential (Equation 8.11) shows poor fit to experimental data and examples are shown in Figure 8.11. Such an effect could be caused by redistribution of the drug within the depot, the decreasing amount of the remaining drug, or the structural changes in the degrading devices.

To attempt to improve the fit of model Equation 8.11, a second exponential term can be added to the model based on an approach of using a three compartmental model, as illustrated in Figure 8.10. The model now contains a releasing depot with two pools. Physically it means that a fraction of drug is released faster from a pool where the readily released drugs are located near/at the surface of the depot, while the second pool represents subsequent drug release preferably from those entrapped deeper in the matrix.

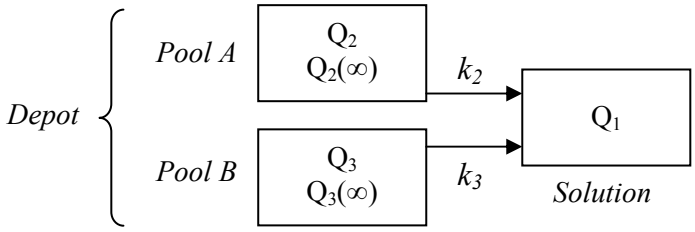

Figure 8.10: A three compartmental model showing the drug release from a two pools-releasing depot.

The amount of drug release in solution, Q_1 is related to Q_2 and Q_3 by:

$$\frac{dQ_1}{dt} = k_2.Q_2 + k_3.Q_3 \tag{8.12}$$

Where Q_2 and Q_3 are the remaining drug in the depot after drug of amount Q_1 is released into the solution. $Q_2(\infty)$ and $Q_3(\infty)$ are the amount of drugs remaining in Pools A and B, which will be released after a long time. k_2 and k_3 are the release rate constants of Pools A and B respectively. Using the same treatment applied in Equations 8.5 to 8.10; integrating and transforming the individual components of Q_1, Q_2 and Q_3, the final three compartmental-model describing the relationships between the amount of drug release and the remaining drug in a two pools-releasing depot is given by:

$$Q_1 = \left[Q_2(\infty).(1 - e^{-k2t}) \right] + \left[Q_3(\infty).(1 - e^{-k3t}) \right] \tag{8.13}$$

For details of derivation, see Appendix VI.D. Both Equations 8.11 and 8.13 were fitted to the CPt release profiles and examples of results are shown in Figure 8.11. The full set of result is presented in Appendix VI.F. The amount of remaining drugs; Q_2 and Q_3, rate release constants; k_2 and k_3 of model Equation 8.13 were estimated from fitting the model to CPt release profiles. Results are plotted in Figure 8.12. Summary of goodness of fit is presented in Table 8.6 and was compared based on the Akaike's Information Criterion (AIC) (Akaike, 1974) factor.

Adding parameters should always reduce the residual error of the model; a more complex model cannot be justified unless the improvement in predicting power justifies the reduction in degrees of freedom. The complete set of results of model Equations 8.11 and 8.13 fittings can be found in Appendix VI.F with examples of residual error plots in Appendix VI.G. A summary is tabulated in Table 8.6. In all cases, the AIC values of model Equation 8.13 are lower compared to those of Equation 8.11. The distribution of residual plots also shows random distribution between the zero-axis. These results validate the addition of a second exponential term.

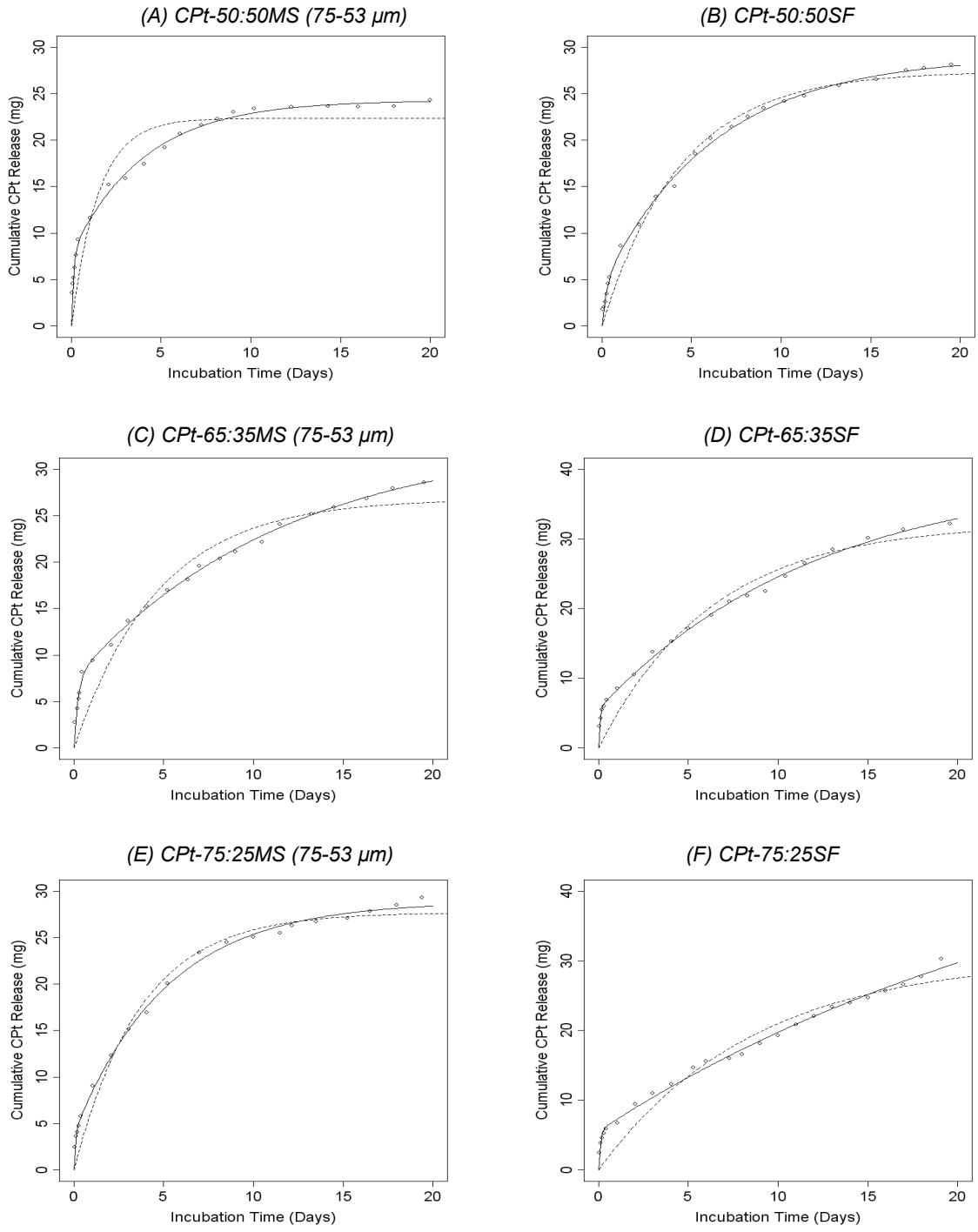

Figure 8.11: Examples of model Equations 8.11 and 8.13 fittings to CPt release profiles of PLGA solid fibres and microspheres of the intermediate size fraction (75-53 µm). (A) CPt-50:50MS, (B) CPt-50:50SF, (C) CPt-65:35MS, (D) CPt-65:35SF, (E) CPt-75:25MS (F) CPt-75:25SF. Solid lines represent biexponential Equation 8.13 and dashed lines represent monoexponential Equation 8.11.

Table 8.6: Summary of goodness of fit of model Equations 8.11 and 8.13 to CPt release profiles.

CPt-Loaded Device		Bi-exponential - Equation 8.13 Mono-exponential - Equation 8.11	AIC	Degrees of Freedom
CPt-50:50MS	53-38 μm	Bi-exponential	32.2835	15
		Mono-exponential	69.4570	17
	75-53 μm	Bi-exponential	39.9778	17
		Mono-exponential	103.254	19
	90-53 μm	Bi-exponential	27.1519	16
		Mono-exponential	97.9456	18
CPt-50:50SF		Bi-exponential	27.1519	16
		Mono-exponential	80.7240	20
CPt-65:35MS	53-38 μm	Bi-exponential	32.4188	16
		Mono-exponential	95.6021	18
	75-53 μm	Bi-exponential	33.2682	17
		Mono-exponential	103.0168	19
	90-53 μm	Bi-exponential	52.4364	14
		Mono-exponential	7.323e-06	16
CPt-65:35SF		Bi-exponential	2.204e-06	18
		Mono-exponential	36.3515	16
CPt-75:25MS	53-38 μm	Bi-exponential	99.1854	18
		Mono-exponential	51.6827	15
	75-53 μm	Bi-exponential	82.2888	17
		Mono-exponential	35.4511	16
	90-53 μm	Bi-exponential	81.077	18
		Mono-exponential	42.7116	17
CPt-75:25SF		Bi-exponential	50.5924	20
		Mono-exponential	112.9819	22

Based on results above, the bi-exponential Equation 8.13 is suggested to be more suitable to fit to the CPt release profiles compared to a mono-exponential model. This also implies that the developed PLGA solid fibres and microspheres can be described as a depot having two pools; the first pool contains a fraction of readily release drug is which located near/at the surface, and subsequent drug release is from the second pool with drug entrapped deeper in the depot. The parameters of Equation 8.13 are plotted in Figure 8.12.

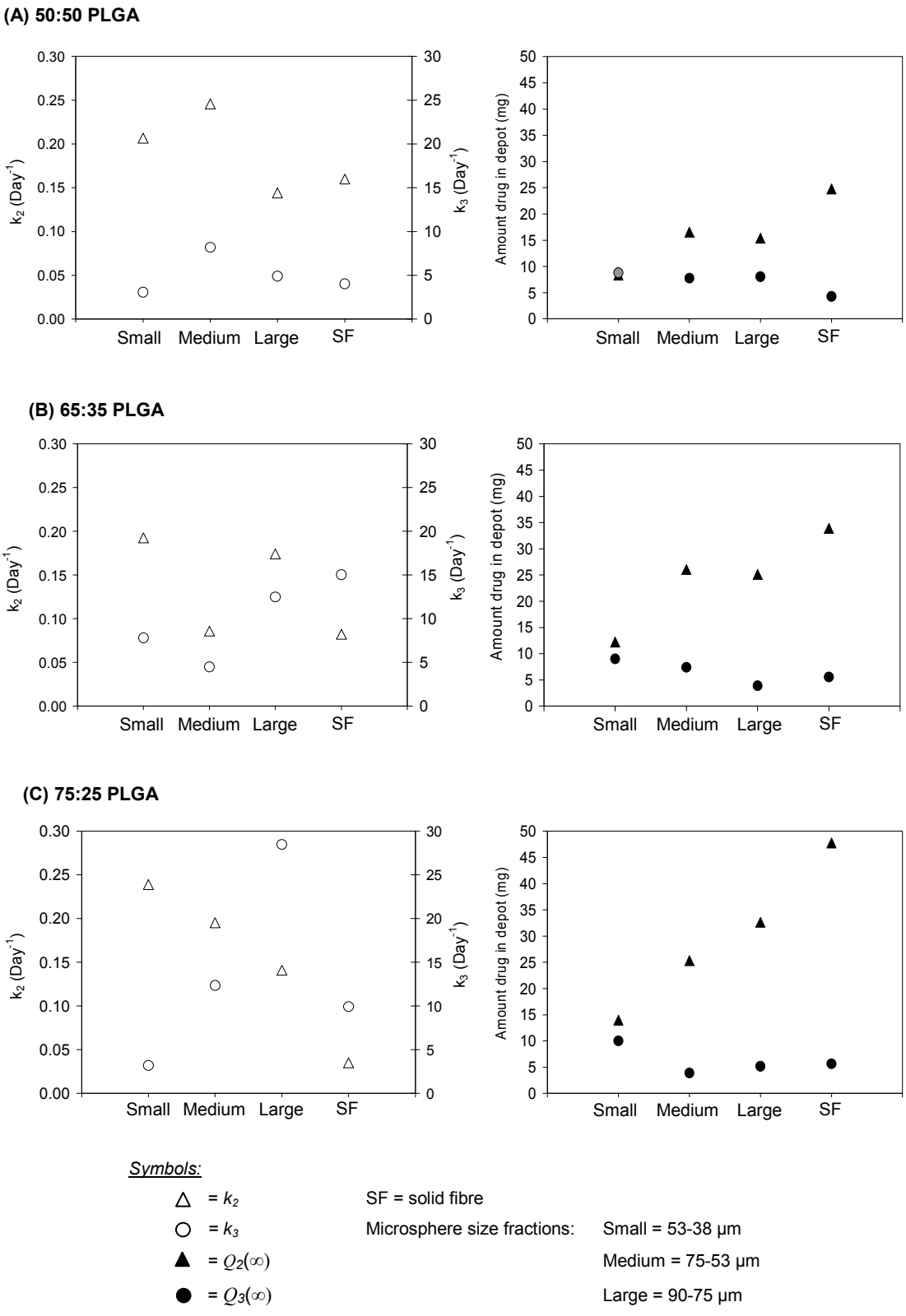

Figure 8.12: Estimate parameters of biexponential model Equation 8.13. k_2 and k_3 are the rate constants associated to Pools A and B respectively. $Q_2(\infty)$ and $Q_3(\infty)$ are the amount of drug in Pools A and B which will be released after a long time respectively.

Model Equation 8.13 is based on a condition of two pools being present in the depot. This is based on the observation of a faster initial drug release from "Pool A" which can be characterised using a Higuchi diffusional model. Subsequently, drug remaining drug in "Pool B" in the depot will be released. Hence, k_2 and k_3 are the rate constants of drugs release from Pools A and B respectively. Figure 8.12A shows that the k_2 values of CPt-50:50-MS and –SF are of similar magnitudes and likewise, for their k_3 values. The same observation can be made for CPt-65:35MS and -SF (Figure 8.12B).

In terms of the amount of remaining drugs in CPt-50:50MS/SF and CPt-65:35MS/SF; i.e. $Q_2(\infty)$ in Pool A and $Q_3(\infty)$ in Pool B, $Q_2(\infty)$ tends to increase with a decrease in surface area:volume ratio. On the other hand, $Q_3(\infty)$ tends to decrease with a decrease in surface area:volume ratio. As previously shown in Tables 8.3 and 8.4, larger structure is associated with smaller surface area:volume ratio. This result indicates that a larger structure holds more drugs in its fast release pool. The amount of drug in the fast releasing Pool A also tends to be higher than those in Pool B.

CPt-75:25MS and -SF exhibit different behaviour then CPt-50:50MS/SF and CPt-65:35MS/SF. The clear decreasing trend of k_2 is observed to be correlated to a clear increasing trend of $Q_2(\infty)$. This relationship can be translated to a condition where a larger structure could hold more drug in its fast release pool (i.e. Pool A) and its smaller surface area:volume ratio decreases the rate of drug release from this pool.

An observation can also be made where the sample with the largest surface area:volume ratio tends to have equal amount of drug in its separate pools, whereas the differences in amount of drug between the pools increases with decrease in surface area:volume ratio.

Figure 8.12 shows that CPt-loaded devices tend to hold the similar amount of drug in their Pools B. The amount of drug in Pool A is also observed to increase with increase in lactide:glycolide acids ratio.

In order to compare the competence of the *in vitro* cisplatin release profile to the real drug dosage used in chemotherapy treatment, the drug release profiles were reproduced as the amount of cisplatin released in buffer as a function of measured time. Example is shown in Figure 8.13 using the drug release profiles of PLGA solid fibres and microspheres of the smallest size fractions (53-38 μm). For clarity, error bars are omitted. The intravenous (IV)

cisplatin regimen previously discussed in Section 2.2.1 suggested a drug dosage of 170 mg cisplatin/cycle.

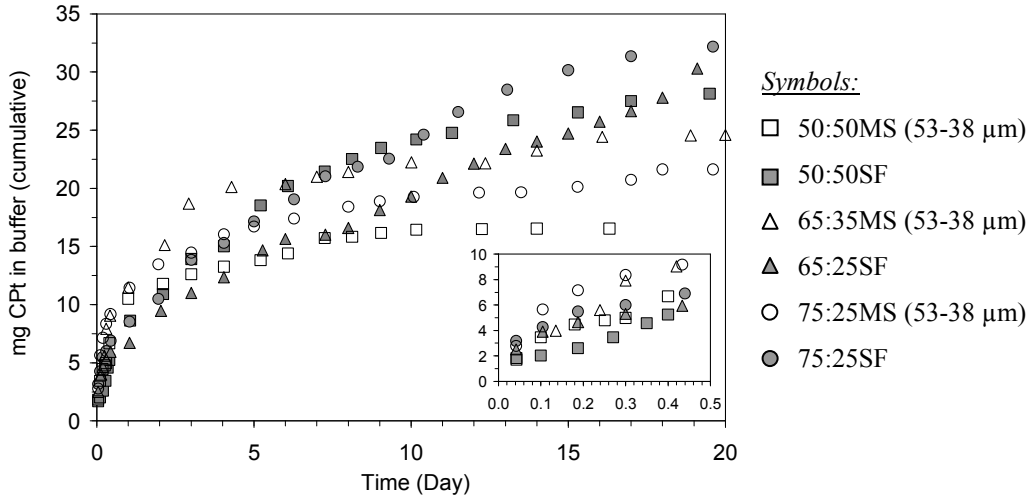

Figure 8.13: Cumulative drug release from 50:50, 65:35, 75:25 PLGA solid fibres and microspheres of the smallest size fraction (53-38 μm). Inset: Drug release during the first half day.

Table 8.7: Final cumulative (%) drug release on Day-20 of PLGA solid fibres and microspheres of the smallest size fraction (53-38 μm).

PLGA	% Cumulative Release at Day-20		Estimate amount of sample required to deliver a 170 mg CPt (g)	
	MS (53-38μm)	SF	MS (53-38 μm)	SF
50:50	99.58 ± 7.45	98.33 ± 6.03	2.2	1.2
65:35	95.69 ± 6.54	93.04 ± 5.29	1.4	1.1
75:25	87.81 ± 5.29	78.48 ± 5.28	1.2	0.9

Table 8.7 tabulates the percentages of cumulative release from PLGA samples at Day 20. Microsphere and solid fibres made of 50:50 PLGA reached to complete drug release faster than those made of 65:35 and 75:25 PLGA. In the case of 50:50SF, complete drug release is observed just before twenty days whereas complete drug release from 50:50MS is observed after approximately ten days. CPt-loaded 65:35 and 75:35 PLGA clearly exhibit a prolonged drug release characteristic for up to three weeks. In the case of 50:50 PLGA devices, they are more suitable for a two weeks treatment schedule. These products offer the options of two or three weeks CPt delivery while they can also serve as sequential treatment or follow-up chemotherapy treatment. The chemotherapy treatment cycle is usually three weeks as time allowance is required for the patients to recover from tissue damage caused by previous chemotherapy treatment.

The initial rapid release is advantageous because a higher dose is useful to penetrate the tumour cells. This causes higher cancerous cell death rate at the surface of the tumour and induces apoptosis. Subsequent effect would be the creation of passages to drugs to penetrate into the tumour. CPt-loaded microsphere can also be injected into the IP cavity at desired time should their initial "burst effect" is required. Larger amount of microspheres would not be a problem because IP delivery usually involves up to two litres of saline solution to be transfused into the peritoneal cavity (Gilby, 2008). The submicron devices are designed for the purpose of increasing the exposure of the cancer cells to the drug. The distribution of larger amount of microspheres in the IP cavity is likely to increase the local therapeutic effect of the cytotoxic drug.

The amount of 1 g of solid fibre is most likely to constitute > 50 fibres of 8 cm in length. This amount provides a practical amount of material for fabrication of a fibre-patch. Preliminary experiments have shown the viability of producing a fibre patch. The rational of developing a CPt-loaded fibre patch is to attach the product to the peritoneum cavity after debulking in order to kill residual cancerous materials (Gilby, 2008). The flexibility of these polymeric fibres can easily adapt to the curvature the of the peritoneum cavity.

8.4 Conclusion

1. Cisplatin was successfully encapsulated into PLGA microspheres and solid fibres. Drug loadings tend to be higher in 75:25 PLGA devices compared to 50:50 PLGA. This is because of the higher lactic acid ratio and the higher viscosity of 75:25 PLGA. Lactic acid is less amorphous than glycolide acid and therefore offers a lower freedom for medium transport. Thus, drug diffusion is lower and drug leakage is minimised during the solidification process.

2. Solid fibre tend to have higher drug loadings compared to microsphere because the former system has lower surface area which reduces the diffusion area for drug leakage. The formation of skin layer during the phase inversion is also thought to have beneficial effect against drug loss.

3. Overall the drug releases from PLGA solid fibres was slower than from PLGA microspheres. The main reason is because the solid fibres offer much lower surface area:volume ratio for drug diffusion. Likewise, their hydrolytic degradation rates are

also lower compared to microspheres. The skin layer of solid fibre is also thought to offer high mass transfer resistance thereby reducing the drug release rate.

4. In the approach to characterise CPt release profiles, a biphasic release pattern is used. Drug release during the first day is described as Phase 1 and is associated with a "burst release". This burst release is attributed to the release of CPt located at the surface of the microspheres or solid fibres. This condition caused by the tendency of drug leakage during the production process. Upon solidification, the drug is entrapped in the peripheral layer of the microspheres or solid fibres. Hydration in microspheres or solid fibres then permits the release of drugs located in this layer.

5. The drug release in Phase 1 can be characterised using the Higuchi-diffusional model for both PLGA microspheres and solid fibres. The drug release is proportional to the square root of time. Reasons contributing to this initial diffusional drug release are described in (4) above. Furthermore, the swelling susceptibility of the developed PLGA microsphere also contributes to an initial rapid release.

6. The burst effect during Phase 1 release is more prominent in CPt-50:50MS compared to 65:35MS and 75:25MS. Findings in Section 7.1 showed that PLGA microspheres underwent hydration and led to swelling. Swelling leads to pore expansion and shifts the system to rubbery state. These conditions permitted higher degree of medium transport and drug diffusion is higher. Hence, drug release is faster. The pores in 50:50MS were found to be more susceptible to swelling compared to 65:35MS and 75:25MS. This tendency of 50:50MS can lead to faster medium diffusion and transport. As a result, more rapid drug diffusion into the buffer is observed. In contrast, 75:25MS restricted pore swelling and therefore burst release is not as rapid as in 50:50MS.

7. The deviations of Phase 2 drug release profiles from empirical models; Higuchi model ($Q_t = k_H.t^{0.5}$), first order kinetic ($\ln Q_t = \ln Q_o + k_F.t$) and zero order kinetic ($Q_t = Q_o + k_z.t$) are mainly attributable to: (1) the influence of PLGA degradation, (2) inhomogeneities in drug distribution and (3) the evolutionary swelling and shrinking of the polymeric devices. The empirical models expressed in Equations 8.1 to 8.3 did not account for all these factors.

8. Equation 8.13; i.e. $Q_1 = \left[Q_2(\infty).(1-e^{-k_1 t})\right] + \left[Q_3(\infty).(1-e^{-k_2 t})\right]$ was found to better fit CPt release profiles without partitioning the release profiles. This model suggests that there are a fraction of drug in the device will be readily release and thereafter the release of the remaining drug. Those readily release drug are likely to be located at or near the surface of the device whereas the remaining would be entrapped deeper in the device.

9. Results show that the copolymer ratio of PLGA is more prominent in influencing the drug release rate regardless of the sizes of the microspheres. Comparing the overall drug release profiles of CPt-50:50MS, CPt-65:35MS and CPt-75:25MS, CPt-50:50MS released its CPt content the fastest. This trend is attributable to the fast degradation rate of 50:50 PLGA and its highest affinity for medium transport.

10. Other factors influencing the drug release rates are proposed below:
    i. The different availability of the entrapped different regions in the microsphere. The amorphous structure of PLGA hinders a homogeneous drug distribution which promoted spatial heterogeneous distribution of the entrapped drug.
    ii. The bulk and autocatalytic degradations occurring in microsphere changes the morphology and structure of the device. As a result, both interior porosity and tortuosity are altered. This consequently changes the diffusion passage of drug.
    iii. Similar to microsphere, the distribution of CPt in solid fibre may not be homogeneous. Given the length of solid fibre, the amount of CPt entrapped in across the fibre will be less homogenous. Similarly for the heterogeneous degradation across the solid fibre due to bulk and autocatalytic degradations.
    iv. The presence of inhomogeneities in batch-to-batch samples.

11. Results of *in vitro* CPt release show that CPt-50:50SF can provide a prolong drug release for more than two weeks. Devices made of 65:35 and 75:25 PLGA have higher drug loadings and degradation resistances than 50:50 PLGA devices. Therefore they are more competent to deliver an IV or IP dose for a period three weeks or longer.

CHAPTER 9: *IN VITRO* LIDOCAINE RELEASE PROFILES

9.1 Lidocaine-Loaded PLGA Microspheres and Hollow Fibres

Lidocaine (LID) was selected as the model drug in this work for the application of pain relief. This is because of the abdominal pain issues associated with intraperitoneal route of administration. The objectives of this chapter were two-fold; firstly, to study the effects of both drug and polymer concentrations on drug loading. Secondly, to compare the *in vitro* drug releases from microspheres and hollow fibres. For ease, LID-loaded 50:50 PLGA microsphere will be abbreviated as LID-50:50MS and LID-loaded 50:50 PLGA hollow fibre as LID-50:50HF henceforth. Similarly for devices made of 65:35 and 75:25 PLGA.

9.2 Production of LID-Loaded PLGA Microspheres and Hollow Fibres

LID-loaded 50:50, 65:35 and 75:25 PLGA microspheres were produced using the method described in Section 4.1.3. Briefly, 10 g of polymer/drug solution was homogenised in 100 ml PVA solution (0.5 % w/w). Then the nascent microspheres were transferred to magnetic stirring before they were harvested. Only the concentration of the polymer and the ratio of drug-to-polymer were varied. Table 9.1 shows the experimental conditions and variables.

Table 9.1: Production conditions for LID-loaded 50:50, 65:35 and 75:25 PLGA microspheres.

PLGA (% w/w)	LID-to-PLGA Ratio	Homogenisations Speed & Time
8	1:1	6500 rpm, 15 min
	1:2	
	1:3	
10	1:1	6500 rpm, 15 min
	1:2	
	1:3	
15	1:1	6500 rpm, 15 min
	1:2	
	1:3	
20	1:1	6500 rpm, 15 min
	1:2	
	1:3	

LID-loaded PLGA hollow fibres were produced using the method described in Section 4.2.3. A drug-to-polymer ratio of 1:1 was used with LID powder premixed to the polymer solution prior to spinning. Typically, a 50 g of polymer/drug solution was used to spin a batch of

hollow fibre using 20 % (w/w) 50:50, 65:35 and 75:25 PLGA. For lumen-filling experiment, lidocaine-hydrochloride solution (20 mg/ml) was injected into the lumen of the LID-loaded hollow fibres using a syringe with a 19G needle. Each fibre was estimated to accommodate approximately 30 µl of drug solution. With a free flow of solution through its lumen, one end of the fibre was sealed with Epoxy® resin and left to dry at room condition overnight. The other end of the fibre was sealed in a similar way.

The similar procedure was carried out to fill the lumen of LID-loaded hollow fibres with LID-loaded microspheres. In this case, the lumen was filled with approximately 30 µl of buffer solution containing LID-loaded microspheres. The latter suspension was freshly prepared prior to each experiment by immersing 0.2 g of microspheres in 1 ml of PBS. Table 9.2 tabulates the abbreviations representing the hollow fibres with different lumen fillings.

Table 9.2: Abbreviations for PLGA hollow fibres with lumen filled with drug-solution or microsphere.

Abbreviation	Sample Condition	
	Hollow Fibre	Lumen Content
LID-50:50HF	LID-loaded 50:50 PLGA hollow fibre	Blank
LID-50:50HFso	LID-loaded 50:50 PLGA hollow fibre	Filled with LID-hydrochloride solution
LID-50:50HFms	LID-loaded 50:50 PLGA hollow fibre	Filled with LID-50:50MS
LID-65:35HF	LID-loaded 65:35 PLGA hollow fibre	Blank
LID-65:35HFso	LID-loaded 65:35 PLGA hollow fibre	Filled with LID- hydrochloride solution
LID-65:35HFms	LID-loaded 65:35 PLGA hollow fibre	Filled with LID-65:35MS
LID-75:25HF	LID-loaded 75:25 PLGA hollow fibre	Blank
LID-75:25HFso	LID-loaded 75:25 PLGA hollow fibre	Filled with LID- hydrochloride solution
LID-75:25HFms	LID-loaded 75:25 PLGA hollow fibre	Filled with LID-75:25MS

Five preweighed samples were prepared from each PLGA microsphere and hollow fibre for *in vitro* drug release analyses. LID concentration and drug loading were determined using methods described in Sections 4.3.1 and 4.4 respectively. *In vitro* drug release analysis was carried out by incubating the sample in a shaking water bath maintained at 37^{o}C. More details of incubation condition can be found in Section 4.5.

9.3 Results and Discussion

The effects of the drug-to-polymer ratio and polymer concentration on drug loading are shown in Figure 9.1. Figure 9.1A shows that the drug loading are higher towards higher

concentration of 50:50 PLGA. Section 5.1.1 showed that a higher polymer concentration tended to produce larger microsphere. This leads to an increase in diameter and a decrease in the overall surface area, which reduces the possibility drug loss by diffusion towards the aqueous phase during the production process (Görner *et al*., 1999 and Polakovič *et al*., 1999). The same reason is applied for the higher drug loadings with increased 65:35 and 75:25 PLGA concentrations.

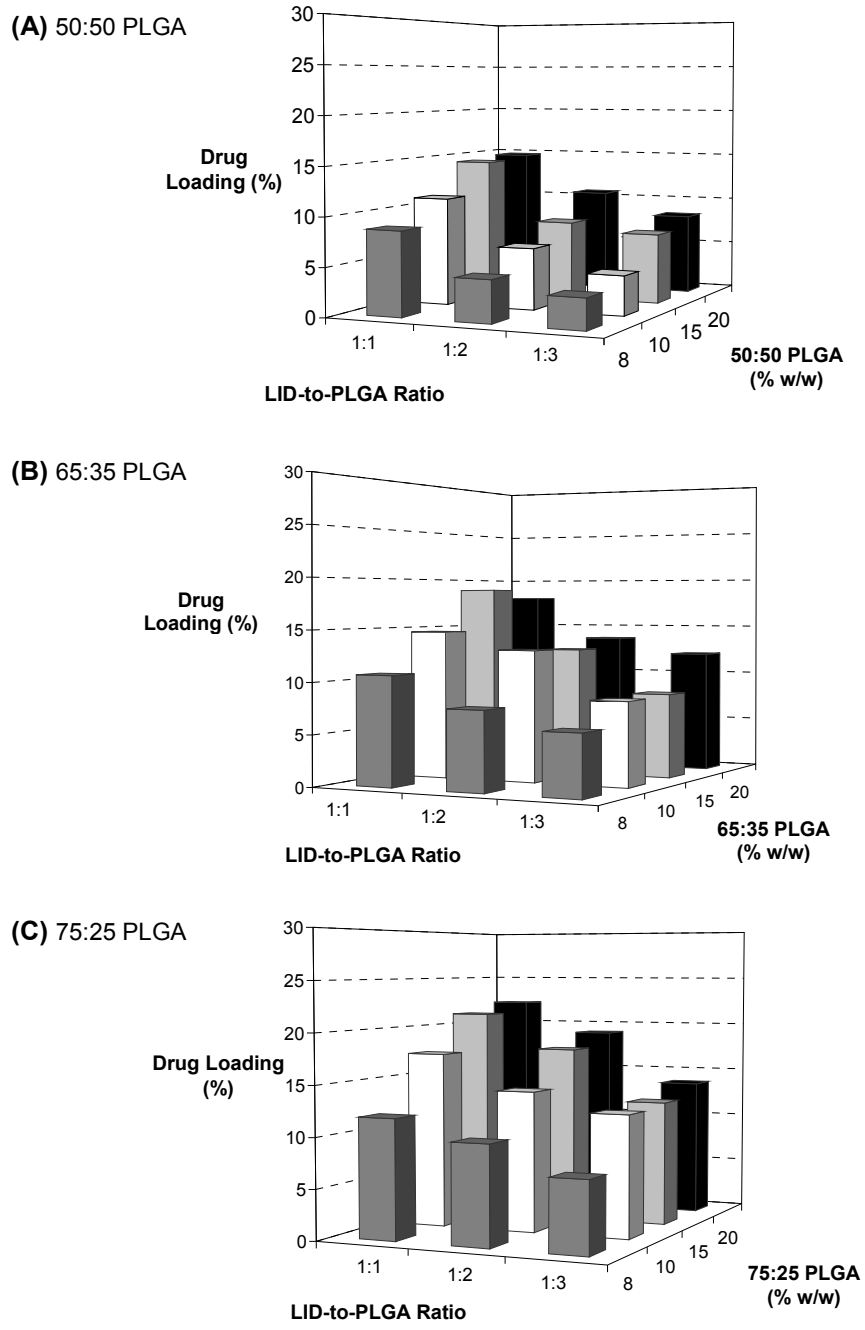

Figure 9.1: The effects of polymer concentration and LID-to-PLGA ratio on drug loading for (A) 50:50, (B) 65:35 and (C) 75:25 PLGA.

Figure 9.1 indicates that the drug loadings in LID-65:35MS and LID-75:25MS tend to be higher than in LID-50:50MS. This trend is attributed to the higher viscosities of both 65:35 and 75:25 PLGA compared to 50:50 PLGA. The amount of drug encapsulated in polymeric device depends on the degree of the partition of the drug in the aqueous phase during the production process. Hydrophilic drug such as lidocaine with high partition degree will tend to diffuse into the aqueous phase while its concentration in the polymeric droplets decreases. This drug loss can be minimised by having a more viscous polymer solution, such as 75:25 PLGA, which offers higher resistance for medium diffusion and promotes a faster rate of solidification (Matsumoto *et al*., 2005). The as-reported viscosity presented in Table 5.1 shows that PLGA with higher lactic acid ratio tends to have higher viscosity and it has been confirmed by previous a researcher (Shearer, 2007).

Figure 9.1 also indicates that higher LID-to-PLGA ratio tends to yield higher drug loading. This is generally due to the presence of more drug in the system that improves the frequency of drug entrapment. However, at a 1:1 LID-to-PLGA ratio, there exists a critical point where further increase in polymer concentration will not further increase the drug loading (Ghaderi *et al*., 1996). This is due to the increased viscosity in the system (Yan *et al*., 1994). At a constant homogenisation speed, the shear force is no longer sufficient to emulsify the organic phase. This deficiency can lead to the formation of microspheres with non-uniform morphology. Evidence can be found in Section 5.1 where various homogenisation effects were investigated.

Sandrap and Moës (1993) showed that improved drug loading was associated with microspheres system with constant sizes and narrow size distribution. The deficiency in achieving a stable emulsion in an increased viscosity system may have also led to deficiency in drug loading even when 1:1 drug-to-polymer ratio is used. For PLGA microsphere system, Yan *et al*. (1994) showed that there was no obvious relationship between drug loading and PLGA concentration once the polymer concentration was ≥ 15%.

For material and cost effectiveness, a polymer concentration of 15 % (w/w) and a 1:1 drug-to-polymer ratio were employed for *in vitro* drug release studies. The cumulative release of LID from 50:50 PLGA devices is shown in Figure 9.2. The drug release of 50:50 PLGA devices exhibit biphasic profiles which can be termed as Phase 1 and Phase 2, as previously described in Chapter Eight. Phase 1 release is associated with a burst release and other factors that can affect burst release are such as the dimensions within the microparticles; the polymer matrix density and the particle porosity.

Burst release can be defined as the quantity of drug that escapes from microparticles prior to the onset of polymer erosion-mediated drug release (Allison, 2008b). Burst release may be an inherent property of diffusion-controlled drug delivery devices and this will be shown later by fitting the Higuchi model to LID release profiles. Hydrophilic lidocaine has a tendency to diffuse towards the aqueous phase during production (Perez *et al*., 2000). This leads to an increased drug concentration near the surface of the device due to convective solvent flow. Upon hydration, these drugs are easily released into the solution. The termination of burst release may be explained by structural relaxation due to increased particle density and surface pore closure (Allison, 2008a).

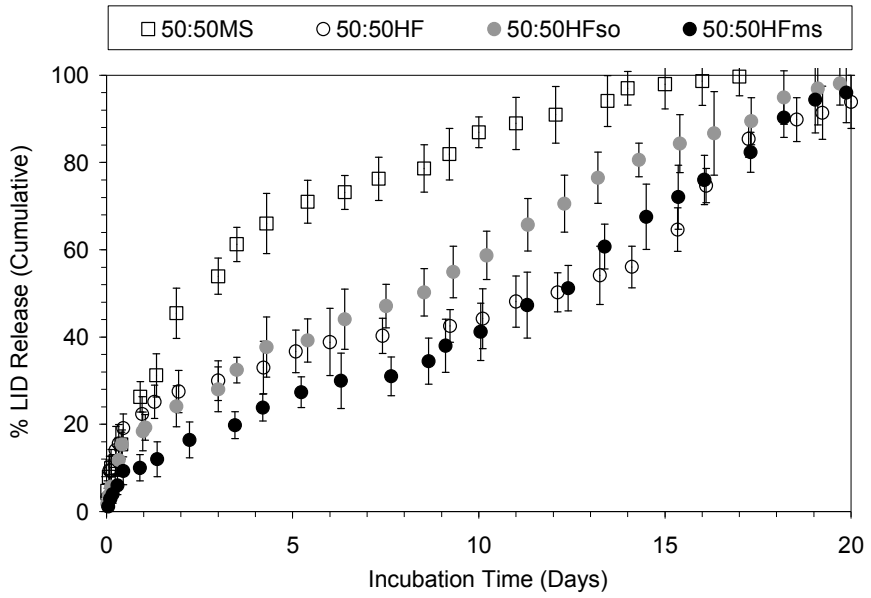

Figure 9.2: The percentage (%) LID cumulative release from LID-50:50MS (□), LID-50:50HF (○), LID-50:50HFso (●) and LID-50:50HFms (●). [*LID-50:50HFso = lidocaine-loaded 50:50 PLGA hollow fibre with its lumen filled with lidocaine hydrochloride solution; LID-50:50HFms = lidocaine-loaded 50:50 PLGA hollow fibre with its lumen filled with lidocaine-loaded 50:50 PLGA microsphere*.]

From Section 6.2 (Figure 6.11), degradation was visible for 50:50MS after ten days and polymeric disruption was evident after twenty days. This situation may be accounted for the drug release from LID-50:50MS after two weeks. The degradation and swelling effects are thought to have changed the morphology of 50:50MS by increasing its porosity forming more passages for drug diffusion. Hence, drug release rate is increased and complete drug release is achieved after two weeks. This result suggests that 50:50MS can offer a LID release of less than three weeks.

For 50:50HF, degradation effect led to micropores formation on the fibre surface after ten days in buffer (Section 6.4, Figure 6.20). As degradation progresses, disintegration of the 50:50HF structure increases and this decreases the diffusion resistance of 50:50HF. These conditions are thought to account for the drug release from LID-50:50HF during the first ten days. After approximately two weeks, from the disintegration of its polymeric structure and when the onset of mass loss was observed (Section 6.4, Figure 6.23), the degrading 50:50HF release its remaining drug into the buffer. The LID-50:50HF exhibits a higher drug release rate during the first four days compared to LID-50:50HFms and LID-50:50HFso. This may due to the higher medium influx rate through its unsealed lumen. The open-ends LID-50:50HF permit buffer penetration into the structure and subsequently promotes drugs diffusion and release.

For LID-50:50HFso, its drug release rate is higher than LID-50:50HF. This is attributed to addition of LID solution in its lumen which enhances the drug diffusion across the fibre wall. The drug solution may have also promoted hydrolytic degradation in the fibre lumen. Degradation on 50:50HF led to the pore formation on the lumen surface after ten days in buffer. In this case, these pores would promote drug solution transport into the fibre wall. Consequently, this drug solution would enhance the diffusion of LID entrapped in the fibre and leads to the release of LID.

For LID-50:50HFms, its drug release during the first week is the lowest compared to other samples. This may be due to the retardant barrier formed by the dense structures within the fibre wall, which limit the drug release. Discussions in Sections 3.5 and 6.5 suggested that the unique structures in the fibre wall offer better control of drug release due to their higher mass transfer resistances. Meanwhile, with their sealed-fibre ends, the degradation products from the microsphere may be trapped within the lumen.

The accumulation of the acidic products in the fibre lumen may have caused autocatalytic reaction thereby increasing the hydrolytic degradation in the lumen. This condition can consequently promote heterogeneous degradation across the hollow fibre. Thus, disruption of the amorphous regions might be greater in the case of LID-50:50HFms, and produces a faster drug release compared to LID-50:50MS and -HF. On the other hand, the drug release from LID-50:50HFms is slower than LID-50:50HFso because in the latter, medium diffusion across the fibre wall is enhanced by the additional drug solution.

Overall, the drug release from LID-50:50MS completes drug release faster compared to LID-50:50HF samples. Comparing the forms of hollow fibre and microsphere, hollow fibre is a cylindrical device whereas the microspheres present as multiple submicron particles. Table 9.3 shows the comparisons of estimate surface area:volume ratios of microspheres and hollow fibres. Sample calculations are shown in Appendix VI.I. Because of their much higher surface area:volume ratios, microspheres show the tendency to exhibit faster drug release compared to hollow fibre.

Table 9.3: Estimate surface area:volume ratios of 20 % (w/w) PLGA hollow fibres, and 15 % (w/w) PLGA microspheres based on their median sizes.

PLGA Device	Diameter (10^{-6} m)	Number of sample	Surface Area of one sample (10^{-5} cm^2)	Total Volume of one sample (10^{-9} cm^3)	Total Surface Area:Volume Ratio
50:50MS	26	1.41×10^7	2.12	9.20	23.08
65:35MS	45	2.72×10^6	6.36	47.72	13.33
75:25MS	53	1.67×10^6	8.83	77.96	11.32
50:50HF	690	10	16.84	2.99	5.80
65:35HF	750	10	18.10	3.53	5.33
75:25HF	850	10	19.10	4.54	4.71

An example of ten days degraded LID-65:35HF is shown in Figure 9.3 in order to correlate drug release to structural changes due to degradation in PLGA hollow fibres. It was found that the hydrolytic degradation on PLGA hollow fibres will alter the integrity of the fibre wall structure such as increased porosity. This increment is likely offer higher freedom of medium transport therefore increases drug release rate.

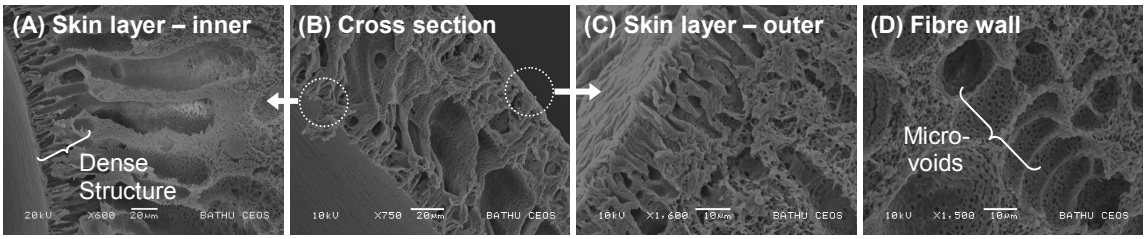

Figure 9.3: The ten days degraded 65:35HF with increased porosity in fibre wall structure. (A) Skin layer near lumen. (B) Cross section of fibre wall. (C) Skin layer near outer surface. (D) Fibre wall.

The nature of asymmetric hollow fibre derives from its different skin layers and fibre wall. Both the skin layers at the lumen (Figure 9.3A) and outer surface (Figure 9.3C) have finger-like cavities adjacent to them. Macrovoids constitute the core layer between these skin layers in the fibre wall (Figure 9.3D). The microvoids offer higher freedom for drug transport as oppose to the denser structures near the skin layers. The latter offers higher resistance to drug

diffusion and decreases drug release. In this regard, the hollow fibre acts as a retardant barrier against rapid drug release. The above phenomenon is attributable to one of the reasons why the drug release from hollow fibre is slower than microsphere.

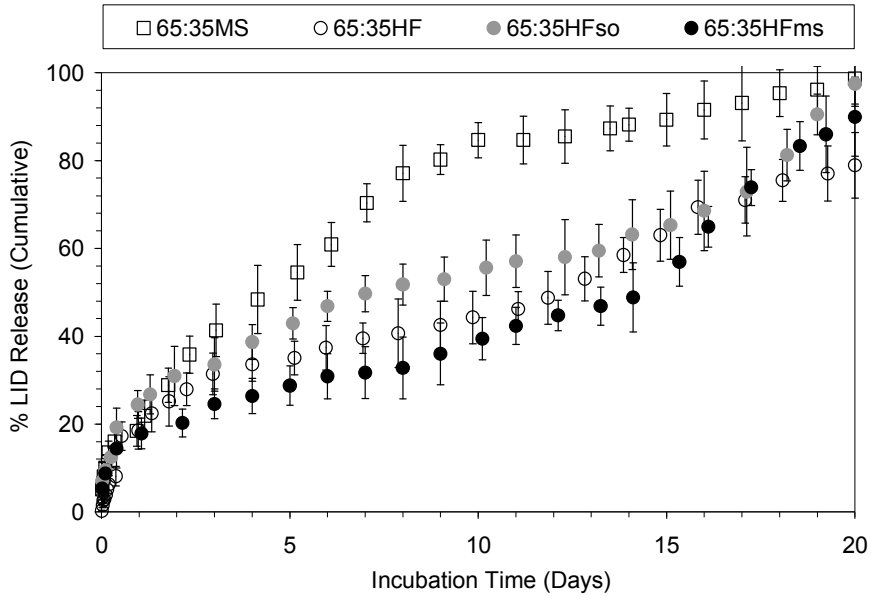

Figure 9.4: The percentage (%) LID cumulative release from LID-65:35MS (□), LID-65:35HF (○), LID-65:35HFso (●) and LID-65:35HFms (●). [*LID-65:35HFso = lidocaine-loaded 65:35 PLGA hollow fibre with its lumen filled with lidocaine hydrochloride solution; LID-65:35HFms = lidocaine-loaded 65:35 PLGA hollow fibre with its lumen filled with lidocaine-loaded 65:35 PLGA microsphere.*]

Figure 9.4 shows the cumulative release of LID from 65:35 PLGA samples. As expected, the higher surface area available for drug diffusion offered by 65:35MS would result in the fastest drug release compared to the other samples. After the initial rapid release, buffer influx provides a medium for drug diffusion and coupled with drug located at the surface of the microspheres, LID is released into the buffer during the first two weeks. After that, drug release is probably from the drug entrapped deeper in the structure. While 65:35MS experiencing swelling effect, the drug slowly diffused towards the surface of the microsphere. These two phenomena and coupled with a better degradation resistance, a slow drug release towards the end of the twenty days period is observed.

The Phase 1 release of LID-65:35HF is attributable to a rapid release of drugs located at or near the surface of the fibre, thereafter followed by drug release from those entrapped in the fibre structure. The entrapment of these drugs and the time required for buffer influx, may have delayed the drug release while these drugs diffused from the inner structure to the surface. The skin layers of the hollow fibre also increase the residence time of drug diffusion.

These conditions could be accounted for the slower drug release throughout the twenty days period. SEM images in Section 6.4 (Figure 6.21) indicated that surface micropores of the degrading 65:35HF were not as prominent as those observed on 50:50HF. The delay in surface micropores formation is attributed to the degradation resistance of 65:35 PLGA. As a result, the drug release is slower. After approximately fifteen days, buffer influx through lumen surface and degradation eventually disrupted the structure of 65:35HF, resulting in a faster drug release towards the end of twenty days.

The initial rapid drug release from LID-65:35HFso is thought to cause by enhanced drug diffusion through the fibre wall promoted by the drug solution in its lumen. The drug solution diffuses into the fibre through the lumen surface and provides additional medium for drug release. This condition provides a near zero order release from Day 5 onwards.

For LID-65:35HFms, there is an increase in drug release after approximately ten days. This may have caused by an autocatalytic degradation inside 65:35HF. Due to the sealed ends of LID-65:35HFms, the accumulated of degradation products from the microsphere in the fibre lumen may have promoted heterogeneous degradation across the fibre. This may have consequently disrupted the fibre interior structure and given rise to more diffusion passages. When prominent effect sets it, together with the increased medium transport, a faster drug release is observed after ten days.

The cumulative release of LID from 75:25 PLGA samples is shown Figure 9.5. For LID-75:25MS, its drug release rate tends to parallel to that of LID-75:25HFso during the first four days. The drug release rate of LID-75:25HF is also observed to be similar to that of LID-75:25HFms during the first week. Previous SEM images showed that 75:25MS (Section 6.2, Figure 6.11) and 75:25HF (Section 6.4, Figure 6.22) experienced minimal degradation effect after twenty days in buffer. The slow drug releases observed in Figure 9.5 during the first two weeks are attributable to the high degradation resistance of 75:25 PLGA. With its least amorphous property that limits the freedom of drug transport within the device, drug release rates are reduced.

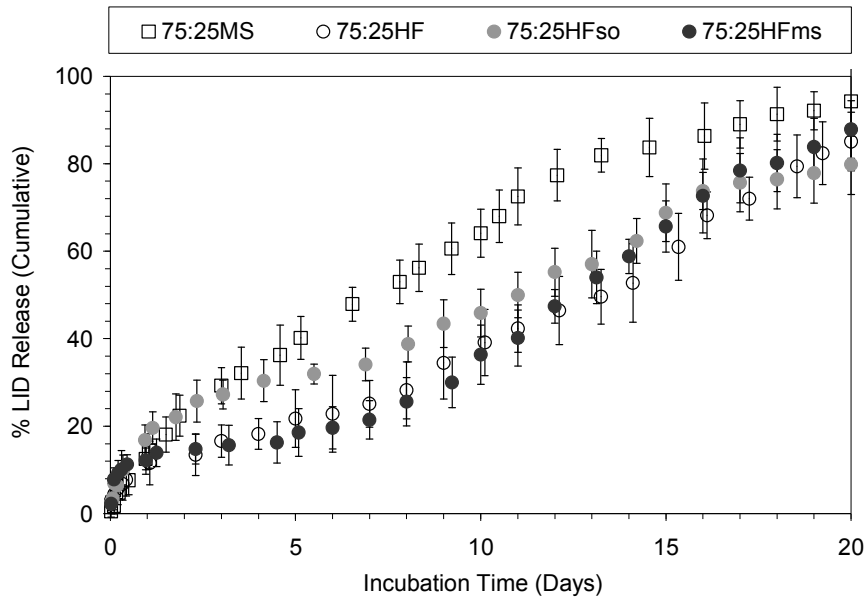

Figure 9.5: The percentage (%) LID cumulative release from LID-75:25MS (□), LID-75:25HF (○), LID-75:25HFso (●) and LID-75:25HFms (●). [*LID-75:25HFso = lidocaine-loaded 75:25 PLGA hollow fibre with its lumen filled with lidocaine hydrochloride solution; LID-75:25HFms = lidocaine-loaded 75:25 PLGA hollow fibre with its lumen filled with lidocaine-loaded 75:25 PLGA microsphere.*]

After Phase 1 drug release, medium influx enables the entrapped drug to diffuse to the surface of 75:25HF. This effect is reflected on its increased drug release after approximately a week. Meanwhile, the open-ends of LID-75:25HF permit buffer penetration and as a result, drug release continued due to more medium to transport the drug in the fibre.

The higher drug release from LID-75:25HFso compared to LID-75:25-HF and -HFms, is likely to cause by the presence of drug solution in its lumen which promotes faster drug diffusion across the fibre wall. The drug release from LID-75:25HF, LID-75:25HFso and LID-75:25HFms tend to coincide after approximately eighteen days. This may due to the structural collapse in 75:25HF which was seen earlier in Figure 6.22 (Section 6.4). As a result, the reduction in diffusion passage produces a retardant effect on drug release. The increased crystallinity by the remaining lactide acid as glycolide acid is removed from the chain also reduces the amorphous regions in the fibre. Hence, drug release becomes slower.

When PLGA undergoes random polymer chain scission, its average molecular weight decreases (Mohr *et al*., 1999). This reduces the length of the polymer chain which in turns reduces the entanglement of the chain. Consequently, the mobility of the molecules is increased and this flexibility permits more amorphous regions for diffusion. Hence, drug diffusion within the device is increased and an increase in subsequent drug release can be

observed. These phenomena help to explain the tendencies of LID-50:50-MS and -HF to exhibit faster drug release because of their faster degradation rate. The swelling susceptibility of 50:50 PLGA that shifts the polymeric devices into rubbery states also permitted higher drug diffusion. The opposite observations are assumed for 75:25 PLGA samples.

The penetration of residual PVA from the production process can introduce plasticising effect on the mobility of PLGA chain. However, Bouissou *et al*., (2006) reported that the total amount of PVA remaining on/in the microspheres only increases water uptake at high relative humidities and residual PVA seemed to only weakly influence the molecular mobility or free volume of PLGA particles.

Similar approach applied in Chapter Eight in terms of model fittings were applied for LID release profiles. The three models expressed in Equation 8.1 to 8.3; Higuchi Model ($Q_t = k_H.t^{0.5}$), first order kinetic ($\ln Q_t = \ln Q_i + k_F.t$) and zero order kinetic ($Q_t = Q_i + k_z.t$) were fundamentally used to fit to Phase 1 and Phase 2 drug release profiles. Phase 1 represents the drug release during the first day and thereafter, Phase 2. The Higuchi model shows good fit to the Phase 1 LID release and examples are shown in Figure 9.6. Full set of result can be found in Appendix VII.D and VII.E.

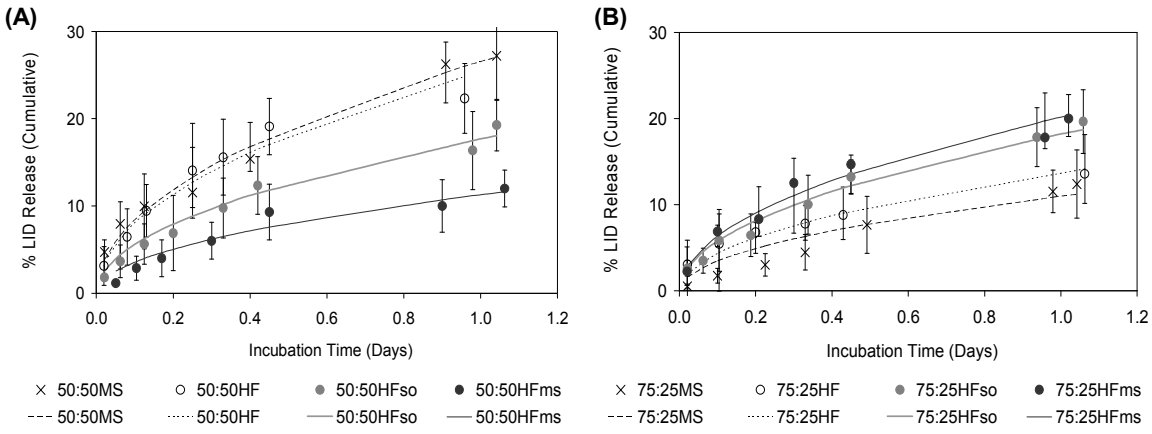

Figure 9.6: The fittings of Higuchi Model ($Q_t = k_H.t^{0.5}$) to drug releases from (A) 50:50 and (B) 75:25 PLGA microsphere and hollow fibre samples during Phase 1. Symbols (×, ○,● ,●) represent experimental data and lines (- - - , ····· , ——— , ——) represent Higuchi model.

Similar to previous findings in Chapter Eight, Equations 8.1 to 8.3 were unable to provide good fit to LID release profiles. Hence, the mono- and biexponential model Equations 8.11 and 8.13; i.e. $Q_1 = Q_o(\infty).(1-e^{-k_o t})$ and $Q_1 = [Q_2(\infty).(1-e^{-k_2 t})] + [Q_3(\infty).(1-e^{-k_3 t})]$ respectively were also used to fit to LID release profiles. Examples of results are shown in Figure 9.7.

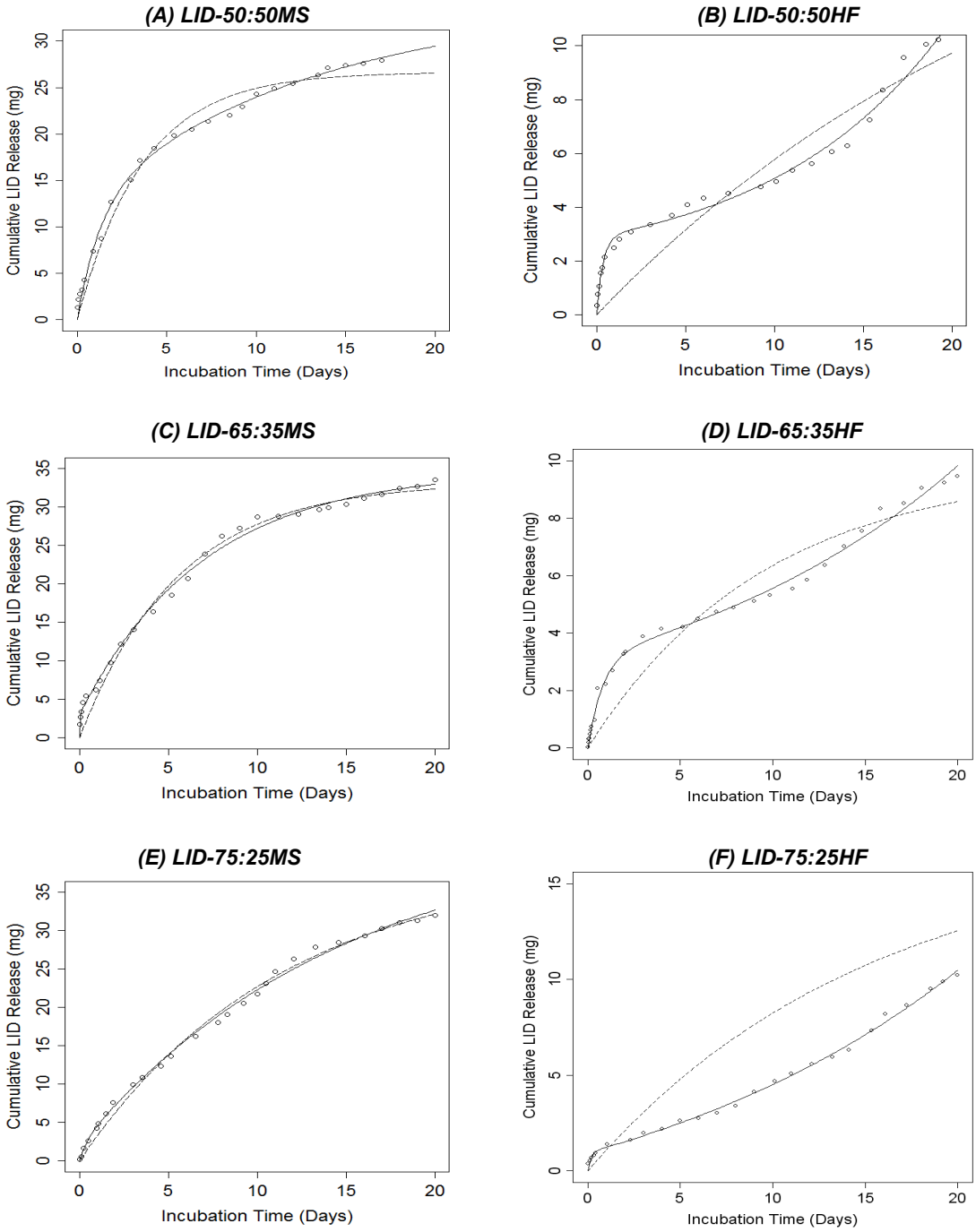

Figure 9.7: Results of model Equations 8.11 and 8.13 fittings to LID release profiles of (A) LID-50:50MS, (B) LID-50:50HF, (C) LID-65:35MS, (D) LID-65:35HF, (E) LID-75:25MS (F) LID-75:25HF. Solid lines represent Equation 8.13 and dashed lines represent Equation 8.11.

A summary of AIC and degrees of freedom generated based on fittings of Equations 8.11 and 8.13 are shown in Table 9.4. Equation 8.13 was found to better fit the LID release profiles based on the lower values of AIC and degrees of freedom. This suggests that the biexponential model is more suitable to describe LID release from the developed PLGA

microspheres and hollow fibres. This model is based on two pools present in the depot; one pool represents a fraction of drug which is readily released and another pool represents the remaining drug entrapped deeper in the depot.

Table 9.4: Summary of goodness of fit of model Equations 8.11 and 8.13 to LID release profiles.

LID-Loaded Device	Bi-exponential - Equation 8.13 Mono-exponential - Equation 8.11	AIC	Degrees of Freedom
LID-50:50MS	Bi-exponential	58.1083	20
	Mono-exponential	86.0025	22
LID-50:50HF	Bi-exponential	21.4055	22
	Mono-exponential	85.0514	24
LID-50:50HFso	Bi-exponential	4.3099	23
	Mono-exponential	60.1035	25
LID-50:50HFms	Bi-exponential	8.0958	20
	Mono-exponential	39.1433	22
LID-65:35MS	Bi-exponential	68.3661	23
	Mono-exponential	102.0084	25
LID-65:35HF	Bi-exponential	9.0574	23
	Mono-exponential	68.0395	25
LID-65:35HFso	Bi-exponential	50.7528	21
	Mono-exponential	95.8173	23
LID-65:35HFms	Bi-exponential	24.9815	19
	Mono-exponential	94.2173	23
LID-75:25MS	Bi-exponential	57.4923	23
	Mono-exponential	73.7451	25
LID-75:25HF	Bi-exponential	56.6755	21
	Mono-exponential	66.1725	24
LID-75:25HFso	Bi-exponential	28.1547	22
	Mono-exponential	76.4795	24
LID75:25HFms	Bi-exponential	45.1416	22
	Mono-exponential	77.4150	24

The parameters of the biexponential model Equation 8.13; i.e. $Q_2(\infty)$ (mg) and $Q_3(\infty)$ (mg), the amount of drugs remaining in two separate pools which will be released after a long time, k_1 (day^{-1}) and k_2 (day^{-1}), the drug release rate constants of the two pools are plotted in Figure 9.8. The complete set of results can be found in Appendix VII.A and VII.B.

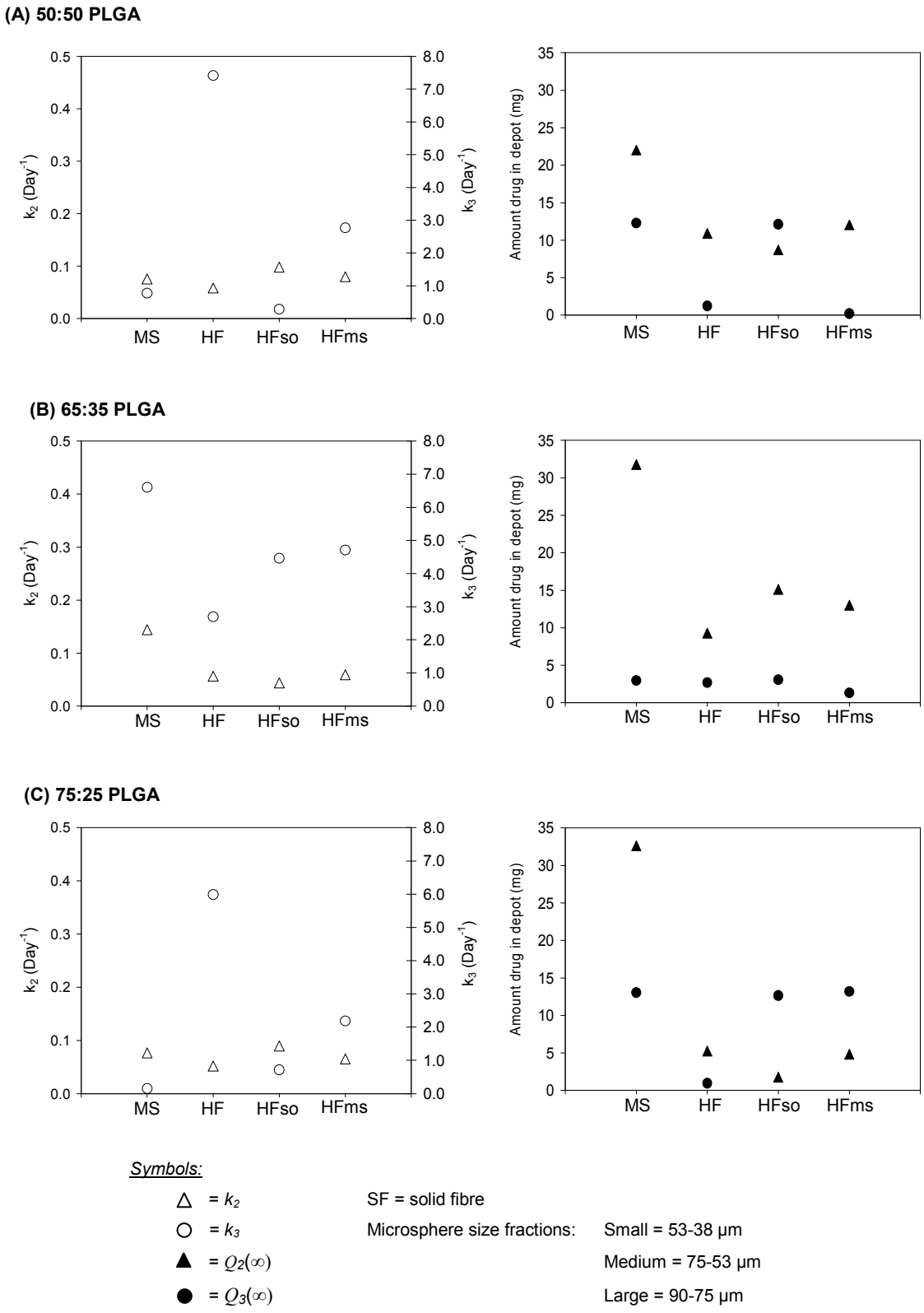

Figure 9.8: Estimated parameters of biexponential model Equation 8.13. k_2 and k_3 are the rate constants associated to Pools A and B respectively. $Q_2(\infty)$ and $Q_3(\infty)$ are the amount of drug in Pools A and B which will be released after a long time respectively. [*HFso = hollow fibre with lumen filled with lidocaine hydrochloride solution; HFms = hollow fibre with lumen filled with lidocaine-loaded microsphere.]*

The biexponential Equation 8.13 with two pools is thought to be not appropriate to predict the systems of hollow fibres with additional loading in their lumens. This is because of the altered physics of the systems where the combinations of hollow fibre with drug-solution or drug-microsphere essentially form a new system comprises two depots and four pools. This helps to explain the random trends in results shown in Figure 9.8 for the samples of HFms and HFso.

Figure 9.8 indicates that "Pool A" of all the PLGA samples have similar rates of drug release where k_1 values were of similar magnitudes; i.e. ≤ 0.1 day^{-1} while k_2 values tend to be more random. LID-50:50MS, -65:35MS and -75:25MS also tend to have higher amount of drugs in both their Pools A and B compared to LID-50:50HF, -65:35HF and -75:25HF. This may be attributed to the higher drug loadings in microspheres.

In the cases of drug release profiles of devices made of 65:35 PLGA (Figure 9.4) and 75:25 PLGA (Figure 9.5), these systems tend to require more than twenty drugs for complete drug release. The conditions may have contributed to the inappropriateness of biexponential Equation 8.13 to be applied on these profiles.

For the developed LID-loaded hollow fibres (blank lumens), the estimate parameters indicate that LID-50:50HF, -65:35HF and -75:25HF have higher amount of drug in their fast releasing Pool A than in Pool B. For LID-50:50HF, -65:35HF and -75:25HF, preliminary fittings using a first order kinetic model, results indicate that the second phase (i.e. Phase 2) is highly first-ordered. Examples of plot can be found in Appendix VII.E. Based on these observations, it is suggested that partitioning the drug release profiles to Phase 1 and Phase 2, would ease the prediction of LID releases from hollow fibre samples. Phase 1 can be characterised using a Higuchi Model while Phase 2, a first order kinetics model would be a better fit for the drug release profiles.

Results above indicate that the semi-mechanistic Equation 8.13 can be improved further. The presences of additional drug loadings in the lumens were anticipated to further cause deviation from the model. Siepmann *et al*. (1998) has reported consideration in geometry and dimension of drug release devices in their drug release modelling. As discussed earlier, the degradation within these lumen-filled fibres would be different from lumen-blank fibres. The effect of degradation in PLGA depots has been considered Göpferich and Langer (1995) and

Göpferich (1997) where factors such as pH, polymer composition, water uptake by polymer, surface and bulk degradation are important in drug release modelling.

Ehtezazi and Washington (2000), and Messaritake *et al*. (2005) proposed percolation theory which relates drug release to morphology and transports property of the drug-loaded microspheres. This approach takes into account of the pore network tortuosity. Drug release from PLGA microspheres during later stages when permanent degradation effect had set it, the erosion-mediated release can produced non-Fickian release and percolation theory should be incorporated to describe the drug release kinetic. Other approaches in drug modelling can include simultaneous consideration of polymer degradation and drug diffusion (Charlier *et al*., 2000), triphasic model that includes burst release, degradative drug release and diffusional release (Lao *et al*., 2008).

Findings from Section 6.1.3 indicated the heterogeneity in spatial distribution of entrapped agent in 75:25MS. This further suggests that the drug release will not be purely a diffusive process. Drugs that are thermodynamically compatible with the encapsulating polymer tend to be uniformly dissolved in the polymer matrix, while incompatible drugs are dispersed as a separate phase within the microparticle (Allison, 2008a). Drug releases from dissolved and dispersed systems are treated by distinct mathematical models (Arifin *et al*., 2006).

Discussion is presented below to explore the possible LID release from PLGA hollow fibres. For hollow fibre, buffer penetration through its lumen increases the contact areas between fibres and buffer. This leads to an enhance hydration effect and medium transport will be greater producing greater freedom for drug diffusion in the fibre matrix. Assuming that initially the fibre matrix is not completely saturated with the buffer, times may be required for buffer influx and later, outflow of drug. This in turn will create a lag phase where the rate of drug release is slow. An important factor which can increase the outflow of drug is the formation of micropores on the fibre surface which depends on the polymer degradation rate.

The main external component, the medium or water plays active roles such as excipient for drug and species to cause hydrolysis on the polymer (Schmitt *et al*., 1994). During buffer immersion, buffer influx provides a medium for drug transport within the device. Studies in Chapters Six and Seven suggested that drug can travel between cavities through interconnecting channels in microsphere. This transport is likely to be random and drug will be displaced over time. Consequently, drug redistribution within the depot will and drug

distribution is usually accounted for the release rate of entrapped drug (Matsumoto *et al*., 2005). Polakovič *et al*. (1999) had suggested that the diffusional distance between the initial and final drug locations inside the microspheres can affect drug release rate.

In the case of hollow fibres with lumens filled with drug-solution or –microspheres, these conditions raised the complexness in the prediction of drug release. Assuming a perfect sealing with no leakage on the ends of these fibres, the effect of buffer penetration through their lumens is removed. The presence of drug solution in the fibre lumen is thought to enhance the drug diffusion across the fibre wall and therefore leads to a faster drug release. In the case of lumen filled-microspheres, the degradation of products from the microsphere was anticipated to cause interior autocatalytic degradation in the lumen. Comparing hollow fibre to microspheres, larger sample tends to undergo bimodal degradation (Grizzi *et al*., 1995). Dunne *et al*. (2000) showed that the molecular weight of larger particles decreased faster than smaller particles. They attributed the trend to autocatalytic degradation.

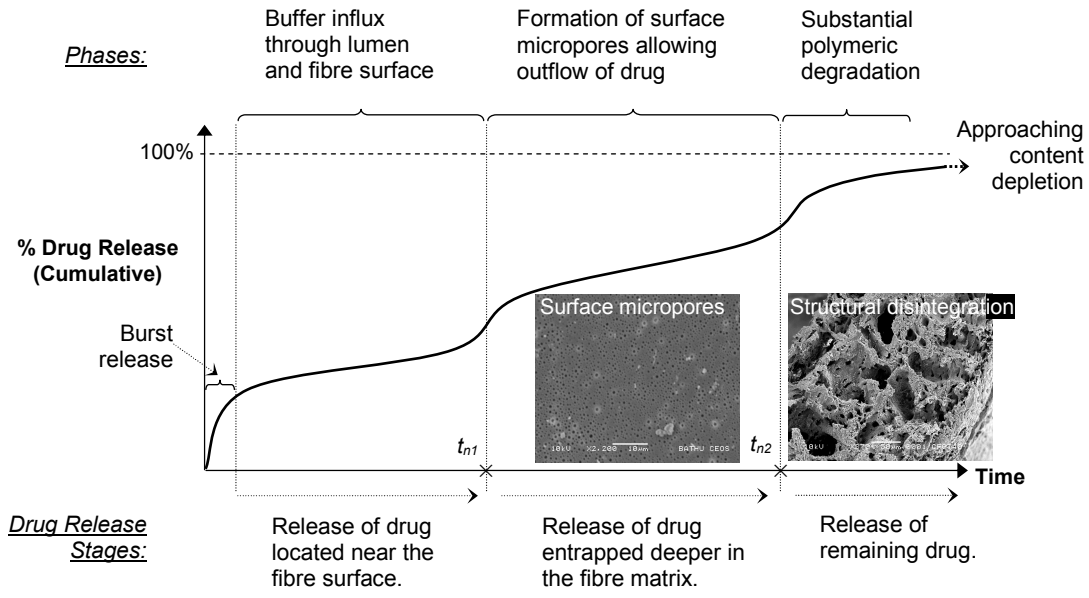

Figure 9.9: Hypothetical drug release profile of hollow fibres.

A hypothetical profile of drug release from hollow fibre is illustrated in Figure 9.9. The degradation susceptibility of the polymer may alter the onset or the duration of different drug release stages. Owing to the tendency of the hydrophilic lidocaine to diffuse into the aqueous phase during the solidification process, the drug could be located in the peripheral of the device. During the Phase 1 release, drug release is from the drugs located near or at the fibre surface. Meanwhile, the buffer influx takes place through both the outer and lumen surfaces. The degradation effect increases the drug diffusion and drug release rate increases at 't_{n1}'.

Following this release, drug release continues from the drug entrapped deeper in the fibre matrix. The formation of surface microspores sets in and degradation continues. At stage 't_{n2}', morphological changes are prominent and the device eventually loses its integrity, i.e. collapse and the remaining drug are released.

Figure 9.9 is an approach with partitioning between drug release stages but the presence of overlapping and random mechanisms such as, structural swelling/shrinking or restriction exerted by certain structures can be anticipated. These mechanisms would change the interior tortuosity and consequently affect drug diffusion within the matrix. Attempts to model LID release from the developed PLGA devices show the inadequacy of simple empirical model to account for the mass transport mechanisms and chemical processes that occur in these disparate systems. Further modelling work should consider the rate-controlling mechanisms such as diffusion-, swelling- and erosion-controlled drug release as reviewed by Kanjickal and Lopina (2004).

By comparing the cumulative drug release of the PLGA devices, complete drug release is observed on LID-50:50MS after fifteen days and twenty days for LID-50:50HF samples. LID-65:35 PLGA samples can probably provide sustain release of just after three weeks, and most likely few days longer for the case of 75:25 PLGA samples. Table 9.5 shows the total amount of LID encapsulated in the PLGA samples produced in this study.

Table 9.5: Estimated total drug content in the PLGA microspheres and hollow fibres samples used in *in vitro* drug releases analyses. Data represent average ± standard deviation (n = 5). *HFso = hollow fibre with lumen filled with drug solution; HFms = hollow fibre with lumen filled with drug-loaded microsphere.*

PLGA	Estimated Total Drug content in a 0.2 g sample (mg)			
	MS	HF	HFso	HFms
50:50	27.24 ± 5.72 (DL = 12.40 ± 2.87 %)	11.12 ± 3.21 (DL = 5.60 ± 2.54 %)	14.60 ± 2.84	13.17 ± 3.64
65:35	34.04 ± 4.69 (DL = 18.69 ± 4.77 %)	12.22 ± 2.87 (DL = 6.73 ± 2.17 %)	15.11 ± 3.26	14.64 ± 3.50
75:25	38.92 ± 3.77 (DL = 20.40 ± 3.67 %)	18.34 ± 2.87 (DL = 8.76 ± 2.45 %)	21.94 ± 4.64	20.28 ± 4.32

Figures in brackets represent drug loading (DL) of microsphere and hollow fibre calculated using method described in Section 4.4.

Devices made of 50:50 PLGA tend to have the lowest drug loadings and coupled with its fast degradation nature, complete drug release is reached within the measured period. The higher

lactide acid ratio in the copolymer shows higher drug loading. Both higher drug loading and degradation resistance in 75:25 PLGA may have lead to a longer drug release compared to 50:50 PLGA. The drug loadings of microspheres and hollow fibres made of the same PLGA were significantly different (*t*-test, $p < 0.05$). Comparing drug loadings among PLGA microspheres, only LID-50:50MS and LID-75:25MS show significant difference in drug loadings. Likewise, for the drug loadings between LID-50:50HF and LID-75:25HF (ANOVA-single factor).

Local anaesthetic such as lidocaine are usually given to patient at a dose of 10-20 ml of 2 % drug solution (20 g/l) prior to intraperitoneal surgery (Willemse and de Vries, 2003, and Ye *et al*., 2004). This equals a dose of 100-200 mg of anaesthetic drug. Example of cumulative lidocaine release (mg) from 50:50 PLGA samples is shown in Figure 9.10. The plot shows that a 0.2 g sample of LID-50:50MS could deliver up to 25 mg of lidocaine over a period of three weeks.

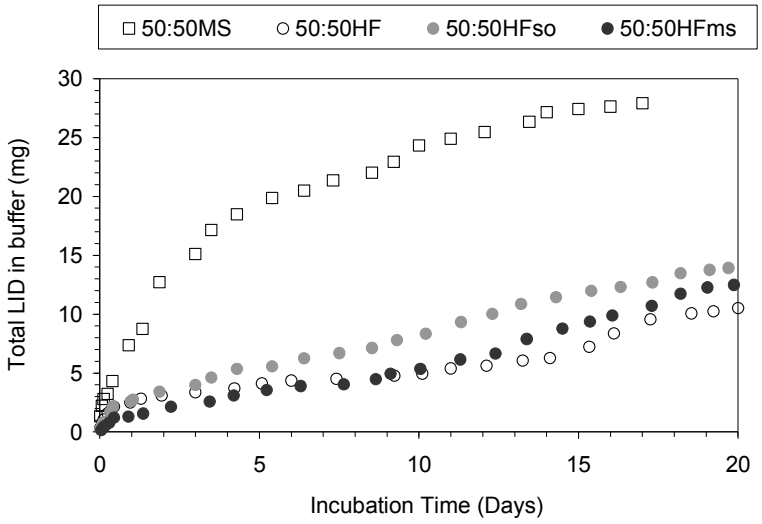

Figure 9.10: Plot showing the cumulative release of LID in 10 ml of PBS.

In order to achieve an anaesthetic dose of 20 ml 2% drug solution, approximately 3.5 g of LID-50:50MS is required. This amount of microsphere may be an advantage where they could spread over a larger area in the peritoneum for better local anaesthetic effect. The dose of local anaesthetic could vary depending on the physical health condition of the patient. LID-microspheres could be given in conjunction with IV local anaesthetic or the prolong drug release from LID-microsphere/hollow fibre can be applied for minor surgery with persisted surgical pain. The additional drugs in the lumen of hollow fibres enhanced the drug release and their lower dose is also suitable for minor surgery.

The rational of developing LID-hollow fibre is the additional drug loading in its lumen. It has been shown that the drug release from HFms or HFso were higher than hollow fibre alone. The higher drug loading offered by 65:35 and 75:25 PLGA can deliver higher dose of lidocaine. Figures 9.2, 9.4 and 9.5 show that each PLGA exhibit prolong lidocaine release of at least two weeks and higher lactide:glycolide acid ratio tends to exhibited longer drug release period. The combination of microsphere and hollow fibre made of different PLGA can potentially diversify the duration of drug release.

9.4 Conclusion

1. LID was encapsulated into PLGA microspheres and hollow fibres produced using the single emulsion and wet-spinning methods respectively. The estimated drug loadings for PLGA microspheres ranged from 10-20% whereas for hollow fibres, it was 5-8%. The drug loading of hollow fibres can be increased by the addition of drug-loaded microsphere or drug solution into the lumen.

2. Preliminary model fittings using Equations 8.1 to 8.3 to Phase 1 drug release suggest that LID-loaded PLGA devices can exhibit diffusional-controlled drug release based on the Higuchi model. Reasons are due to the tendency of hydrophilic lidocaine to diffuse to the aqueous phase during the solidification process. Thus, drug tended to accumulated at the peripheral layer of the device. Hydration effect on the device then permits the rapid release of the drug located in this layer. Other factors are such as those previously concluded in Section 8.4, no. (3) and (4).

3. The Phase 2 release could not be fully characterised using the Higuchi , first and zero order kinetics models. The main reasons are the systems used herein are degrading and the degradation process affects the internal structures of both microspheres and hollow fibres. This effect alters the internal porosity of the polymeric devices while changing the freedom of drug diffusion within the matrix and out into the buffer. Other factors are such as those previously concluded in Section 8.4, no. (10).

4. For the hollow fibres with sealed ends, the local autocatalytic effect is expected to be greater than opened-end hollow fibres due to lesser passages for degradation products transport. The accumulation of the degradation products from microspheres in the

fibre lumens is likely to enhance autocatalytic effect. On the other hand, the lumen impregnation with drug solution is thought to enhance drug diffusion within and out from the fibre matrix.

5. The combination of microspheres and hollow fibres have complicated the prediction of drug release profiles but from a therapeutic point's of view, the combination of the duo can offer higher drug dosage. Hollow fibre can offer a "retardant" barrier against burst release exhibited by microspheres.

6. Devices made of 50:50 PLGA tended to show a faster release rate reaching to content depletion due to its fast degradation property, which is in contrast to the high degradation resistance of 75:25 PLGA.

7. The three compartmental model expressed in Equation 8.13 was found to better fit the LID release profiles of the developed PLGA microspheres. This condition suggests the presence of two fractions of drug in the device, a fraction of this drug is readily release while the remaining entrapped drug will be subsequently released into the solution. For PLGA hollow fibres, their Phase 2 drug releases highly resemble first order release kinetic.

8. The hypothetical model of different drug release phases illustrated in Figure 9.9 is preliminary used to describe the release of drug from hollow fibre. This system differs from microsphere system based on the larger matrix and the lumen of the hollow fibre that offers a channel for medium transport.

CHAPTER 10: CONCLUSIONS AND FURTHER WORK

10.1 Overall Conclusions

The aim of this thesis was to develop drug-loaded PLGA devices which are suitable to be used for IP treatment of advanced ovarian cancer. PLGA was selected as the model polymer because of its proven history, versatility and approval by the FDA. An effective cytotoxic drug used to treat ovarian cancer, cisplatin (CPt), was selected as the model chemotherapy drug. Lidocaine (LID) was also used as a model drug for the reason of IP treatment-associated pain issue. Different copolymer ratios of 50:50, 65:35 and 75:25 PLGA were used to produce drugs-loaded PLGA microspheres, novel hollow and solid fibres. This selection of copolymers enabled the studies and comparisons of their drug loadings, degradation and drug release profiles.

This thesis has made several contributions to the field of controlled-drug delivery particularly for the IP treatment of advanced ovarian cancer by: (1) developing CPt-loaded PLGA microspheres and solid fibres, and (2) LID-loaded PLGA microspheres and hollow fibres. The development of these systems required multidisciplinary approach. One of the major novelties of this thesis is combining the concepts of biodegradable-controlled drug delivery system with membrane technology (hollow fibre), along with detailed characterisation work to understand the behaviours of the developed systems. This novelty also enabled the evaluations of *in vitro* drug release profiles of the developed microspheres, hollow and solid fibres to be presented in a single thesis for the first time.

Drug-loaded microspheres systems were successfully produced through investigations into the effects of both PLGA and PVA concentrations, homogenisations speed and time. A standard production condition was established as: 100 ml of 0.5 % (w/w) PVA, homogenisations time and speed of 15 minutes and 6500 rpm respectively to process 10 g of polymer/drug solution. The drug loadings of CPt-loaded PLGA microspheres vary with different size fractions and copolymer ratios. Maximum drug loading for microsphere was approximately 10% and 15% for solid fibre. CPt-loaded microspheres exhibited different release rates and this condition show the flexibility of the developed systems to be used for a two weeks (CPt-50:50MS) or three weeks (CPt-75:25MS) chemotherapy delivery.

To the best knowledge of the author, limited literature concerning the development of CPt-loaded PLGA solid fibre has been reported. New system taking the form of CPt-loaded

PLGA solid fibres was successfully produced and this work showed that this system can offer higher drug loading than microspheres. PLGA solid fibres were found to degrade slower in comparison to PLGA microspheres, benefited from their small surface area:volume ratios, and skin layers which is associated with high mass transfer resistance. The latter fulfilled the rationale of using phase inversion membrane to provide better control of drug release. Results showed that CPt-65:35SF and CPt-75:25SF can potentially offer a chemotherapy delivery of longer than three weeks.

The *in vitro* release of CPt from microspheres and solid fibres demonstrated good competence in mimicking an IP or IV dose for chemotherapy regimen. For example, approximately 2 g of CPt-50:50MS with the smallest size fraction (53-38 μm) and 1 g of CPt-50:50SF will be required to deliver a CPt dose of 170 mg. For ovarian cancer treatment, chemotherapy is used to treat residual cancerous materials after primary surgery. For this reason, the CPt-loaded solid fibre could ultimately fabricate into a drug delivery patch and can be attached to the IP cavity to kill residual cancerous cells. The flexibility of the fibre could also provide good adaptation to the curvature of the peritoneal cavity.

The CPt release profiles are fundamentally characterised as a biphasic release. Phase 1 release is the drug release during the first day and thereafter, Phase 2. Phase 1 is associated with a “burst” release and drug release in this phase was found to closely resemble a Higuchi diffusional-controlled release for both PLGA solid fibres and microspheres. Simple empirical models were found inadequate to describe the overall CPt release profiles. A biexponential equation was found to better fit the CPt release profiles. This model suggests that there are two fractions of drug present in the device. A fraction of this drug is located near or at the surface which are readily release into the buffer. The remaining drug fraction is thought to be entrapped deeper in the device and will be subsequently released into the solution.

Similar to the case of CPt-loaded PLGA solid fibre, limited literature concerning the development of LID-loaded hollow fibre system has been reported. LID-loaded hollow fibres were successfully developed in this work and their behaviours were evaluated in terms of their degradation and drug release profiles. The phase inversion technique was studied closely and applied to spin both hollow and solid fibres. A standard spinning condition was established as: air gap of 10 cm, starting bore liquid flowrate of 2.5 ± 0.5 ml/min, starting polymer solution extrusion rate of 2.0 ± 0.5 ml/min and 7 ± 2 rpm as the starting speed for the collection motor. Additional drug loadings were highly feasible in this case where drug

solution and drug-loaded microsphere were post-filled into the lumen of the hollow fibres. For future application, these combinations could offer co-delivery of therapeutic agents.

The Phase 1 LID release was also found to follow a Higuchi-diffusional release model for both microspheres and solid fibres. A biexponential model was also used to fit to the LID release profiles. Results indicated that an assumption of a system consists of a depot with two pools is suitable to describe the drug release kinetics. However, Phase 2 LID release profiles also indicate a first order release kinetic. The presence of additional drug loadings in the fibre lumen is though to alter the mass transport property of the system. Therefore, the biexponential model could no longer adequately characterise the drug release profiles.

Studies of the diffusion of imbibe water showed that polymeric PLGA microspheres underwent pore swelling and shrinking. 50:50MS was found most susceptible to pore swelling possibly due to the higher amorphous region in its polymer matrix. In the case of 75:25MS, copolymer with higher lactide acid ratio has higher crystallinity therefore restricted pore swelling. Pore swelling and immersion in buffer may shift the system from a glassy state to a rubbery state. Medium diffusion is thought to be faster in the latter state. The findings in PFG-NMR experiments help to explain the initial faster drug release in PLGA devices. However, burst release may also associate to structural relaxation due to a condition where the glassy devices are attempting to reach thermodynamic equilibrium.

A bulk degradation pathway is used to describe the degradation characteristics of the developed PLGA systems. Results showed agreement to the trends reported in the literature whereby copolymer PLGA with higher lactide:glycolide acids ratio shows better resistance against hydrolytic degradation. Studies following the degradation of PLGA hollow and solid fibres also highly suggested the presence of autocatalytic degradation. This is attributable to the accumulation of acidic degradation products. Devices of larger structure are also thought to be more susceptible to biomodal or heterogeneous degradation.

10.2 Suggestion for Further Work

1. Chapters Five and Six study the morphologies of the developed PLGA devices and their degradations. The chemistry of polymer often involves the studies of glass transition temperature and crystallinity of the polymer. PLA (semi-crystalline) and PLGA (amorphous) polymers rapidly undergo chain alterations or structural relaxation

due to plasticiser effect from absorbed moistures or water ions, or the thermodynamically unstable nature of the polymer chain.

In order to fully comprehend the degradation profiles of the developed PLGA depots, differential scanning calorimetry (DSC) can be used to follow the time-dependent physical and morphological changes within the hydrated or dried microparticles. This can help to determine the effect of the absorbed water, and to detect the penetration of buffer ions into the particle bulk. The main affect of absorbed water is thought to contribute to the polymer chain mobility, which can alter the physical properties, such as T_g of the polymer. Information of this sort can then be correlated to the morphological changes within the particles. In general, the polymer below its T_g behaves as a glassy material and gradually shifts to rubbery state as the temperature approaches and exceeds the T_g.

X-ray diffraction (XRD) or small-angle x-ray scattering (SAXS) techniques are commonly used to study the crystallinity of a polymer. The latter technique is used to study polymer with smaller matrixes. The data generated from these techniques are often presented as the scattered intensity as a function of wave-number. Using Bragg's Law, the interplanar distance between the polymer matrixes can be determined. This information can then be translated to give the crystallinity profile of the polymer. Hence, the evolution of crystallinity or amorphous regions of the degrading PLGA depots can be studied in details.

2. Characterisation of PLGA microspheres:

Atomic force microscopy (AFM) can resolve the issue of heat sensitivity of PLGA encountered in SEM imaging. Preliminarily analysis using AFM generated useful information showing the porous nature of the surface of 75:25MS (Figure 10.1).

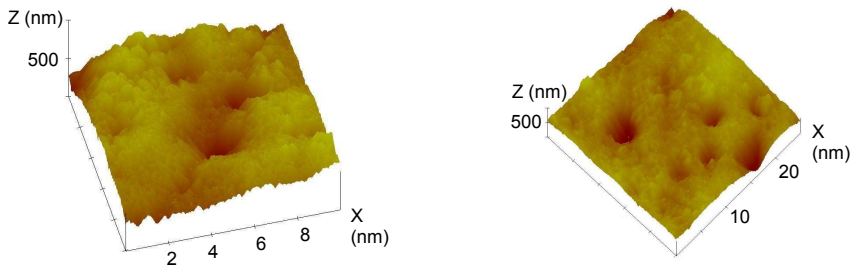

Figure 10.1: AFM images showing the surface conditions of PLGA microspheres.

Result shows that single-emulsion 75:25MS has surface pores of nano-scale. This is indicated by the indentation and denser colour density observed in the AFM images shown in Figure 10.1. This result can further agree with the freezing of interior pores by the ingress of ice through surface pores suggested in Chapter Seven. For future work, AFM imaging should be applied for better characterisation of the morphology of PLGA microspheres or correlate with NMR studies in pore structural information.

3. Drug-loaded Microsphere System:

Burst effect is common in microparticulate system and future effort should be given to circumvent this rapid release. A direct solution is to prewash or prerelease the drug-loaded microspheres. However, this would not be economical. It has been shown by Tamura *et al*. (200l) and Matsumoto *et al*. (2005) that double-layered microspheres could reduce the burst release. Additional layers or coatings serve the purpose of introducing higher diffusion resistance at the surface to attenuate rapid drug release.

Confocal laser scanning microscopy has generated useful information regarding the distribution of the entrapped component. This method can be calibrated to relate the intensity of the fluorescence to the concentration of the entrapped component. Analysis of this sort can provide information of local drug population in the microspheres, and can be further related to drug release characteristic.

4. Drug-loaded Hollow Fibre System:

A circular spinneret was used in this work and there are spinnerets which produce hexagonal or pentagonal shaped hollow fibres. These new systems will require new approach and the increased dimension of these non-circular hollow fibres can offer greater surface area for drug diffusion. Hence, they have the potential to revolutionise the current circular hollow fibres in relation to drug release kinetic. Double or triple layered hollow fibres can also be produced using specially designed spinnerets. An example of double-layered hollow fibre is shown in Figure 10.2A. These extra layers not only could help to reduce both the burst release and drug release rate, but co-encapsulation of other drugs can also be formulated into these layers.

There are alternative methods to incorporate drug into hollow fibres. The macrovoids in the core matrix are suitable to contain drug solution. Drug solution can be post-loaded into the hollow fibre matrix by applying a vacuum at one end (open) of the fibre,

with its other end sealed. The sealed end is then immersed in the desired drug solution. Through a vacuum effect, the drug solution will be drawn into the fibre matrix. Preliminary experiment has shown the viability of this approach and the apparatus setup is shown in Figure 10.2B.

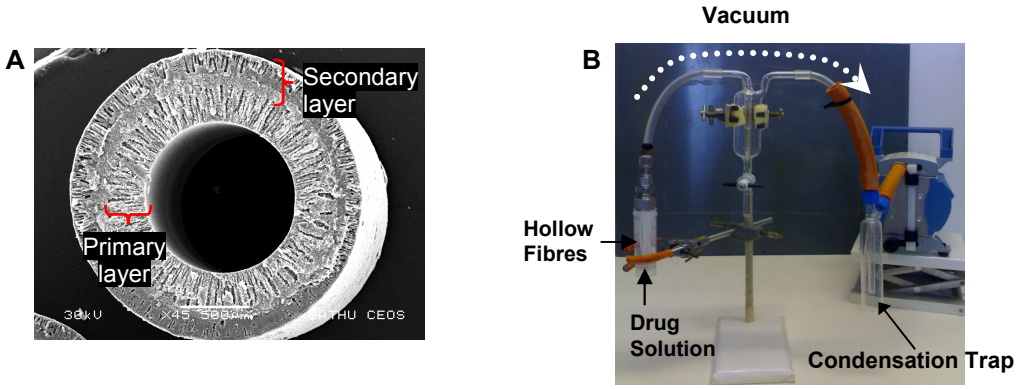

Figure 10.2: (A) Cross section of a double layered polyethersulfone hollow fibre. (B) A vacuum system for the loading of drug solution into hollow fibres.

CHAPTER 11: REFERENCES

Akaike H. A. (1974) A new look at the statistical model identification. *IEEE Transactions on Automatic Control*. 19 (6); 716-23

Akhtar S. and Agrawal S. (1997) *In vitro* studies with antisense oligonucleotides. *Current Techniques*. 18;12-18

Aksnes D.W., Forland K., Kimtys L. (2001) Pore size distribution in mesoporous materials as studied by H-1 NMR. *Phys. Chem. Chem. Phys*. 3 (15); 3203–3207

Alberts D.S., Liu P.Y., Hannigan E.V., O'Toole R., Williams S.D., Young J.A. (1996) Intraperitoneal cisplatin plus intravenous cyclophosphamide versus intravenous cisplatin plus intravenous cyclophosphamide for stage III ovarian cancer. *New Engl J Medicine*. 335; 1950–1955

Ali S.A.M., Doherty P.J., Williams D.F. (1993) Mechanism of polymer degradation in implantable devices. 2. Poly(DL-lactic acid). *J Biomedical Materials Re*. 27; 1409-1418

Allen S.G., Stephenson P.C.L., Strange J.H. (1998) Internal surfaces of porous media studied by nuclear magnetic resonance cryoporometry. *J Chem Phys*. 108 (19); 8195–8198

Allison S. D. (2008a) Effect of Structural Relaxation on the Preparation and Drug Release Behavior of Poly(lactic-co-glycolic) acid Microparticle Drug Delivery Systems. *J Pharmaceutical Sciences*. 97 (6); 2022-2035

Allison S.D. (2008b) Analysis of initial burst in PLGA microparticles. *Expert Opinion Drug Delivery*. 5 (6); 615-628

Anderson J.M. (1994) *In vivo* Biocompatibility of Implantable Delivery Systems and Biomaterials. *Eur J Pharm Biopharm*. 40 (1); 1-8

Anderson, J.M., Shive M.S. (1997) Biodegradation and biocompatibility of PLA and PLGA microspheres. *Advanced Drug Delivery Reviews*. 28; 5–24

Arifin D.Y., Lee L.Y., Wang C.H. (2006) Mathematical modelling and simulation of drug release from microspheres: Implications to drug delivery systems. *Adv Drug Del Rev*. 58; 1274-1325

Armstrong D.K., Bundy B., Wenzel L.Huang Q., Baergen R. Lele S., Copeland L.J., Walker J.L., Burger R.A. (2006) Intraperitoneal Cisplatin and Paclitaxel in Ovarian Cancer. *New England J Medicine*. 354L; 34-43

Barth C., Goncalves M.C., Pires A.T.N., Roeder J. and Wolf B.A. (2000) Asymmetric polysulfone and polyethersulfone membranes: effects of thermodynamics conditions during formation on their performance. *J Membrane Science*. 169; 287-299

Batycky R., Hanes J., Langer R., LANGER, Edwards, E.D. (1997) A Theoretical Model of Erosion and Macromolecular Drug Release from Biodegrading Microspheres. *J Pharmaceutical Sci*. 86 (12); 1464-1477

Beurroies I., Denoyel R., Llewellyn P., Rouquerol J. (2004) A comparison between melting-solidification and capillary condensation hysteresis in mesoporous materials: Application to the interpretation of thermoporometry data. *Thermochim Acta* 421 (1–2); 11–18

Birnbaum D. T. and Brannon-Peppas L. (2003) Molecular weight distribution changes during degradation and release of PLGA nanoparticles containing epirubicin HCL. *Biomater. Sci. Polym. Ed.* 14; 87–102

Bloom B.R. (1989) Vaccines for the Third World. *Nature*. 342 (6246); 115–120

Boisdron-celle M., Menei P.H., Benoit J.P. (1995) Preparation and Characterisation of 5Fu-loaded Microparticles as Biodegradable Anticancer Drug Carriers. *J Pharm Pharmacol*. 47; 108-114

Booth H.F. and Strange J.H. (1998) Organic nanocrystals: an NMR study of cyclohexane in porous silica. *Molecular Physics*. 93 (2); 263-269

Bouissou C., Potter U., Altroff H., Mardon H., van der Walle C. F. (2004) Controlled release of the fibronectin central binding domain from polymeric microspheres. *J Controlled Release.* 95; 557– 566

Bouissou C., Rouse J.J.J., Price R., van der Walle C.F. (2006) The Influence of Surfactant on PLGA Microsphere Glass Transition and Water Sorption: Remodeling the Surface Morphology to Attenuate the Burst Release. *Pharmaceutical Re*. 23 (6); 1295-1305

Bourne D.W. A. and Strauss S. (1995) Mathematical Modeling of Pharmacokinetic Data. Publisher: CRC Press.

Bristow R.E., Tomacruz R.S., Armstrong D.K., Trimble E.L., Montz F.J. (2002) Survival effect of maximal cytoreductive surgery for advanced ovarian carcinoma during the platinum era: a meta-analysis. *J Clin Oncol*. 20: 1248-59

Bristow R.E., del Garmen M.G., Pannu H. K., Cohade C., Zahurak M.L., Fishman E.K., Wahl R.L., Montz F.J. (2003) Clinically occult recurrent ovarian cancer: patient selection for secondary cytoreductive surgery using combined PET/CT. *Gynecologic Oncology*. 90 (3); 519-528

Brun M., Lallemand A., Quinson J.-F., Eyraud C. (1977) A new method for the simultaneous determination of the size and the shape of pores: The thermoporometry. *Thermochim. Acta* 21; 59–88

Bungay P. M., Lonsdale H.K., de Pinho M.N. (1986) Synthetic Membrane: Science, Engineering and Applications. D. Riedle Publishing Company, Netherlands

Buttet J., Car R., Mylse C.W. (1982) Size dependence of the conduction-electron-spin-resonance g shift in a small soldium particle: Orthogonalized standing-wave calculations. *Physical Review B*. 26 (5); 2414-2432

Callaghan P.T. and Jolley K.W. (1979) Diffusion of Water in the Endosperm Tissue of Wheat Grains as Studied by Pulsed Field Gradient Nuclear Magnetic Resonance. *J Biophys.* 28; 133-142

Callaghan P. T. (1991) Principles of Nuclear Magnetic Resonance Microscopy. Oxford University Press, Oxford.

Callaghan P.T., Le Gros M.A. and Pinder D.N. (1983) The measurements of diffusion using deuterium pulsed field gradient nuclear magnetic resonance. *J Phys Chem.* 79; 6372-6381

Cannistra S.A. (2004) Cancer of the ovary. *N Engl J Med*. 351; 2519-29.

Chellaiah S. and Viskanta (1989) On the supercooling during freezing of water saturated porous media. *Int Comm Heat Mass Transfer*. 16; 163-172

Chen W. and Lu D.R. (1999) Carboplatin-loaded PLGA microspheres for intracerebral injection: formulation and characterization. *J Microencapsulation*. 16 (5); 551-563

Christenson H.K. (2001) Confinement effects on freezing and melting. *J Phys: Condense Matter*. 13; R95–R133

Chung T.S. and Hu X. (1997) Effect of air gap distance on the morphology and thermal properties of polyethersulfone hollow fibres. *J Applied Polymer Sci*. 66; 1067-1077

Collins J.H.P., Gladden L.F, Hardy I.J., Mantle M.D. (2007) Characterizing the Evolution of Porosity during Controlled Drug Release. *Applied Magnetic Resonance.* 32; 185-204

Costa P. and Lobo J.M.S. (2001) Modeling and comparison of dissolution profiles. *European J Pharm Sci.* 13; 123–133

Coulson J.M. and Richardson J.F. (1999) Chemical engineering. Vol. 1, Fluid flow, heat transfer and mass transfer. 6th edition. Publisher: Oxford, Elsevier Butterwoth-Heinemen.

Crotts G. and Park T.G. (1995) Preparation of porous and nonporous biodegradable polymeric hollow microspheres. *J Controlled Release*. 35; 91-105

Cui F., Cun D., Tao A., Yang M., Shi K., Zhao M., Guan Y. (2005) Preparation and characterization of melittin-loaded poly (dl-lactic acid) or poly (dl-lactic-co-glycolic acid) microspheres made by the double emulsion method. *J Controlled Release*. 107; 310-319

de Jong S.D., Arias E.R., Rijkers D.T.S., van Nostrum C.F., Kettenes-van den Boschc J.J., Hennink W.E. (2001) New insights into the hydrolytic degradation of poly(lactic acid): participation of the alcohol terminus. *Polymer*. 42; 2795-2802

Dearnaley D.R., Judson I. and Root T. (2002) Handbook of Adult Cancer Chemotherapy Schedules. TMG Healthcare Communications Ltd., Oxford, UK.

Debenedetti P.G. (1996) Metastable Liquids: Concepts and Principles, Princeton University Press, Princeton, NJ

Dedrick R. L., Myers C.E., Bungay P.M., Devita V.T. (1978) Pharmacokinetic Rationale for Peritoneal Drug Administration in The Treatment of Ovarian Cancer. *Cancer Treatment Reports*. 62 (1); 1-9

Dedrick R.L. and Flessner M.F. (1997) Pharmacokinetic problems in peritoneal drug administration: tissue penetration and surface exposure. *J National Cancer Institute*. 89(7); 480-487

Denoyel R. and Pellenq R.J.M. (2002) Simple Phenomenological Models for Phase Transitions in a Confined Geometry. 1: Melting and Solidification in a Cylindrical Pore. *Langmuir*. 18; 2710-2716

Denoyel R., Beurroiesa I., Lefevre B. (2004) Thermodynamics of wetting: information brought by microcalorimetry. *J Petroleum Science and Engineering*. 45; 203– 212

Deshmukh S.P. and Li K. (1998) Effect of ethanol composition in water coagulation bath on morphology of PVDF hollow fibre membranes. *J Membrane Science*. 150; 75-85

Dong C.M., Guo Y.Z., Qiu K.Y., Gu Z.W., Feng X.D. (2005) *In vitro* degradation and controlled release behavior of d,l-PLGA50 and PCL-d,l-PLGA50 copolymer microspheres. *J Controlled Release*. 107; 53–64

Donovan H.S., Hartenbachb E.M., Methodc M.W. (2005) Patient–provider communication and perceived control for women experiencing multiple symptoms associated with ovarian cancer. *Gynecologic Oncology.*99; 404 – 411

Drioli E. and Nakagaki M. (1986) Membrane and Membrane Processes. Publisher: New York

Dunn R.L., Lewis D.H. and Goodson J.M. (1982) Monolithic fibers for controlled delivery of tetracycline, *Proc Int Symp Controlled Release Bioactive Materials.* 9; 157–163

Dunn R.L., English J.P., Stoner W.C., Potter A.G., Perkins B.H. (1987) Biodegradable fibers for the controlled release of tetracycline in treatment of peridontal disease. *Proc Int Symp Controlled Release Bioactive Materials* 14; 289–294

Dunne M., Corrigan O.I., Ramtoola Z. (2000) Influence of particle size and dissolution conditions on the degradation properties of polylactide-*co*-glycolide particles. *Biomaterials*. 21; 1659-1668

Duarte A.R.C., Costa M.S., Simplıcio A.L., Cardoso M.M., Duarte C.M.M. (2006) Preparation of controlled release microspheres using supercritical fluid technology for delivery of anti-inflammatory drugs. *Int J Pharm*. 308; 168–174

Eenink M.D.J., Feijen J., Oligslanger J., Albers J.H.M., Rieke J.C., Greidonus P.J. (1987) Biodegradable hollow fibers for the controlled release of hormones, *J Controlled Release.* 6; 225–237

Ehtezazi T. and Washington C. (2000) Controlled release of macromolecules from PLA microspheres: using porous structure topology. *J Controlled Release.* 68; 361–372

Ek R., Henriksson U., Nystrom C., Odberg L. (1994) Pore characterization in cellulose beads from diffusion studies using the spin echo NMR technique. *Powder Tech*. 81; 279-286

Ek R., Gren T., Henriksson U., Nyqvist H., Nystrom C., Odberg L. (1995a) Prediction of drug release by characterisation of the tortuosity in porous cellulose beads using a spin echo NMR technique. *International J Pharmaceutics.* 124; 9-18

Ek R., Lennholm H., Davidson R., Nystrom C. (1995b) Pore swelling in beads made of cellulose fibres and fibre fragments. *International J Pharmaceutics.* 122; 49-56

Ellis M.J. (2005) PhD Thesis: Development of a novel hollow fibre membrane for use as a tissue engineered bone graft scaffold. Dept. of Chemical Engineering, Uni. of Bath.

Ellis M.J., Chaudhuri J.B. (2007) Poly(lactic-co-glycolic acid) Hollow Fibre Membranes for use as a Tissue Engineering Scaffold. *Biotech and Bioeng*, 96 (1); 177-187

Eltabbakh G.H., Yadev P.R. Morgan A. (1999) Clinical Picture of Women with Early Stage Ovarian Cancer. *Gynecologic Oncology*. 75; 476–479

Faisant N., Siepmann J., Benoit J.P. (2002) PLGA-based microparticles: elucidation of mechanisms and a new, simple mathematical model quantifying drug release. *European J Pharm Sc*. 15; 355–366

Fan L.T. and Singh S.K. (1989) Diffusion-controlled release. In: L.T. Fan and S.K. Singh Editors, *Controlled Release: A Quantitative Treatment*. Publisher: Springer, Berlin

Freiberg S. and Zhu X.X. (2004) Review: Polymer microspheres for controlled drug release. *Int J Pharm* 282; 1–18

Freitas C, Muller R. (1998) Spray-drying of solid lipid nanoparticles. *Europ J Pharm Biopharm.* 46; 145–151.

Freitas S., Merkle H.P., Gander B. (2005) Microencapsulation by solvent extraction/evaporation: reviewing the state of the art of microsphere preparation process technology. *J Controlled Release*. 102; 313–332

Fujiyama J. Nakasea Y., Osakib K., Sakakura C., Yamagishi H., Hagiwara A. (2003) Cisplatin incorporated in microspheres: development and fundamental studies for its clinical application. *J Controlled Release*. 89; 397–408

Fukuda K., Kasauga T., Mizusaki T., Hira A., Eguchi K. (1989) Study of Self-Diffusion Process of Water Molecules in Porous Glass by Stimulated Spin Echo Method with Pulsed Field Gradients. *J Physical Society of Japan*. 58 (5); 1662-1666

Fung M.F.K., Provencher D., Rosen B., Hoskins P., Rambout L., Oliver T., Gotlieb W., Covens A. (2007) Intraperitoneal chemotherapy for patients with advanced ovarian cancer: A review of the evidence and standards for the delivery of care. *Gynecologic Oncology*. 105 (3); 747-756

Ghaderi R., Sturesson C, Carlfors J. (1996) Effect of preparative parameters on the characteristics of poly (D,L-lactide-co-glycolide) microspheres made by the double emulsion method. *Int J Pharm*. 141; 205 216

Gilby, E. (2008) Personal conversations. ed.gilby@ruh-bath.swest.nhs.uk

Glueckauf E. and Coates J. I. (1947) Theory of Chromatography. Part IV. The Influence of Incomplete Equilibrium on the Front Boundary of Chromatograms and on the Effectiveness of Separation. *J Chem Soc*. ;1315–1321

Görner T., Gref R., Michenot D., Sommer F., Tran M.N., Dellacherie E. (1999) Lidocaine-loaded biodegradable nanospheres. I. Optimization of the drug incorporation into the polymer matrix, *J. Control Release*. 57; 59–268

Göpferich A. and Langer R. (1995) Modelling monomer release from bioerodible polymers. *J Controlled Release*. 33; 55-69

Göpferich A. (1996) Mechanisms of polymer degradation and erosion. *Biomaterials*.17; 103-114

Grassi M. Colombo I., Lapasin R. (2000) Drug release from an ensemble of swellable crosslinked polymer particles. *J Controlled Release* 68; 97–113

Grizzi I., Garreau H., Li S. and Vert M. (1995) Size dependence hydrolytic degradation of devices based on poly(lactic acid). *Biomaterials.* 16; 305-311

Gunatillake, P.A. and Adhikari R. (2003) Biodegradable Synthetic Polymers for Tissue Engineering. *European Cells and Materials*. 5; 1-16

Gupta P.K., Hung C.T., Perrier D.G. (1986) Albumin microspheres. I. release characteristics of adriamycin. *Int J Pharmaceutical. Vol.* 33:137–146.

Gupte A. and Ciftci K. (2004) Formulation and characterisation of Paclitaxel, 5-Fu and Paclitaxel + 5-Fu microspheres. *Int J Pharmaceutics*. 276; 93-106

Hagiwara A., Takahashi T., Sawai K., Sakakura C., Tsujimoto H., Osaki K., Sakakibara T., Ohyama T., Ohgaki, Muranishi S., Ikada Y., Hyon S.H. (1993) Clinical trials with intraperitoneal cisplatin microspheres for malignant ascites-a pilot study. *Anti-cancer Drug Design.* 8; 463-470

Hansen E.W., Fonnum G., Weng E. (2005) Pore morphology of porous polymer particles probed by NMR relaxometry and NMR cryoporometry. *J Physical Chem B.* 109; 24295–24303

Hansen E.W., Schmidt R., Stocker M. (1996) Pore structure characterization of porous silica by ^{1}H NMR using water, benzene and cyclohexane as probe molecules. *J Physical Chem.* 100; 11396–11401

Hasirci, V., Lewandrowski, K., Gresser, J.D., Wise, D.L. (2001) Versatility of biodegradable biopolymers: degradability and an in vivo application. *J Biotech.* 86; 135–150

Hausberger A.G. and DeLuca P.P. (1995) Characterization of biodegradable poly(D,L-lactideco-glycolide) polymers and microspheres. *J Pharm & Biomed Analysis*. 13 (6); 747-760

Higby, D. J., Wallace, H. J., Albert, D. J. & Holland, J. F. (1974) Diaminodichloroplatinum: a phase I study showing responses in testicular and other tumors. *Cancer.* 33; 1219–1228

Higuchi T. (1961) Rate of release of medicaments from ointment bases containing drugs in suspension. *J Pharm Sci*. 50 (10); 874-875

Higuchi T. (1962) Analysis of data on the medicament release from ointments. *J Pharm Sci*. 51 (8); 802-804

Higuchi T. (1963) Mechanism of sustained-action medication. Theoretical analysis of rate of release of solid drugs dispersed in solid matrices. *J Pharm Sci*. 52 (12); 1145 – 1149

Hollewand M.P. and Gladden L. F. (1992) Modelling of Diffusion and Reaction in Porous Catalysts Using a Random Three-Dimensional Network Model. *Chemical Engineering Sci.* 47 (7); 1761-1770

Hollewand M.P. and Gladden L.F. (1993) Heterogeneities in structure and diffusion within porous catalyst support pellets observed by NMR imaging. *J Catalysis*. 144; 254–272

Hollewand M.P. and Gladden L. F. (1995) Transport Heterogeneity in Porous Pellets I – PGSE NMR Studies. *Chemical Engineering Sci* 50 (2); 309-326

Hofstra L.S., de Vries E.G., Mulder N.H. (2000) Intraperitoneal Chemotherapy in ovarian cancer. *Cancer Treatment Review*. 26; 133-143

Hopfenberg H.B. and Hsu K.C. (1978) Swelling controlled and constant rate delivery systems. *Polymer Eng. Sci.* 18; 1186-1191

Howell S.B., Pfeifle C.L., Wung W.E., Olshen R.A., Kucas W.E., Yon J.L., Green M. (1982) Intraperitoneal Cisplatin with Systemic Thiosulfate Protection. *Annals of Internal Medicine.* 97; 845-851

Hussain M., Beale G., Hughes M., Akhtar S. (2002) Co-delivery of an antisense oligonucleotide and 5-fluorouracil using sustained release poly (lactide-co-glycolide) microsphere formulations for potential combination therapy in cancer. *Int J Pharm.* 234 (1); 129-138

Hürlimann M.D., Helmer K.G., Latour L.L., Sotak C.H. (1994) Restricted Diffusion in Sedimentary Rocks. Determination of Surface Area-to-Volume Ratio and Surface Relaxivity. *J Magnetic Resonance* Series A. 111; 169-178

Ike, O., Shimizu, Y., Wada, R., Hyon, S.H., Ikada, Y (1992) Controlled cisplatin delivery system using poly(DL-lactic acid). *Biomaterials* 13, 230–234.

Illum L. (1987) Polymers in controlled drug delivery. Editors: Illum L. and Davis S.S. Publisher: Wright, Bristol

Illum L., Jorgensen H., Bisgaard H., Krogsgaard L. and Rossing N. (1987) Bioadhesive microspheres as a potential nasal drug delivery system. *Int J Pharm.* 39; 189-199

Isobe M., Yamazaki Y., Oida S., Ishihara K., Nakabayashi N., Amagasa T. (1996) Bone morphogenetic protein encapsulated with a biodegradable and biocompatible polymer. *J Biomedical Materials Research*. 32; 433-438

Itoi K., Tabata C.Y., Ike O., Shimizu Y., Kuwabara M., Kyo M., Hyon S.H., Ikada Y. (1996) *In vivo* suppressive effects of poly(glycolic/L-lactic acid) microspheres containing CDDP on murine tumor cells. *J Controlled Release.* 42; 175–184.

Jackson C.L., McKenna G.B. (1990) The melting behaviour of organic materials confined in porous solids. *J Chem Phys*. 93 (12); 9002-9011

Jackson J.K., Smith J., Letchford K., Babiuk K.A., Machan L., Signore P., Gunter W., Wang K., Burt H.M. (2004) Characteristion of perivascular poly(lactic-co-glycolic acid) films containing paclitaxel. *Int J Pharmaceutics*. 208; 97-109

Jalil R. and Nixon J.R. (1990a) Microencapsulation using poly(L-lactic Acid): Release properties of microcapsules containing phenobarbitone. *J Microencapsulation*. 7 (1); 53-66

Jalil R. and Nixon J.R. (1990b) Biodegradable poly(lactic acid) and poly(lactide-co-glycolide) microcapsules: problems associated with preparative techniques and release properties *J Microencapsulation*. 7 (3); 297-325

Jemal A., Murray T., Ward E., Samuels A., Tiwari R.C., Ghafoor A., Feuer E.J., Thun M.J. (2005) Cancer Statistic, 2005, *CA Cancer J Clin.* 55; 10-30

Janssen A.H., Talsma H., van Steenbergen M.J., de Jong K.P. (2004) Homogeneous nucleation of water in mesoporous zeolite cavities. *Langmuir.* 20; 41–45

Jeyanthi R., Thanoo B.C., Metha R.C., DeLuca P.P. (1996) Effect of solvent removal technique on the matrix characteristics of polylactide/glycolide microspheres for peptide delivery. *J Controlled Release.* 38; 235–244.

Johansen P., Men Y., Merkle H.P., Gander B. (2000) Review article: Revisiting PLA/PLGA microspheres: an analysis of their potential in parenteral vaccination. *European J Pharm Biopharm*. 50; 129-146

Kanjickal D.G. and Lopina S. T. (2004) Modeling of Drug Release from Polymeric Delivery Systems – A Review. *Crit Review™ in Therapeutic Drug Carrier Systems.* 21 (5); 345-386

Karger J., Lenzner J., Pfeifer H., Schwabe H., Heyer W., Janowski F., Wolf F., Zdanov S.P. (1983) NMR study of adsorbate self-diffusion in porous glasses. *J. Am. Ceram. Soc*. 66 (1); 69–72

Khokhlov A., Valiullin R., Kärger J., Steinbach F., Feldhoff A. (2007) Freezing and melting transitions of liquids in mesopores with ink-bottle geometry. *New J Physics.* 9; 272-279

Kirmani S., Braly, P.S., McCLay E.F., Saltzstein S.L., Plaxe S.C., Kim S., Cates ., Howell S,B, (1994) *Gynecologic Oncology,* vol. 54, 338-344

Kim T.H. and Park T.G. (2004) Critical effect of freezing/freeze-drying on sustained release of FITC-dextran encapsulated within PLGA microspheres. *International J Pharmaceutics*. 271; 207–214

Kiss E. and Vargha-Butler E.I. (1999) Novel method to characterize the hydrolytic decomposition of biopolymer surfaces. *Colloids & Surfaces B: Biointerfaces*. 15; 181-193

Koester L.S., Ortega G.G., Mayorga P., Bassani V.L. (2004) Mathematical evaluation of *in vitro* release profiles of hydroxypropylmethylcellulose matrix tablets containing carbamazepine associated to b-cyclodextrin. *European J Pharm Biopharm*. 58; 177–179

Kong J. and Li K. (2001) Preparation of PVDF Hollow Fibre Membrane via immersion precipitation. *J Applied Polymer Science.* 81

Landrum L.M., Gold M.A., Moore K.N., Myers T.K.M., McMeekin D.S., Walker J.L. (2008) Intraperitoneal chemotherapy for patients with advanced epithelial ovarian cancer: A review of complications and completion rates *Gynecologic Oncology* vol. 108, 342–347

Landry M.R. (2005) Thermoporometry by differential scanning calorimetry: experimental considerations and applications. *Thermochimica Acta*. 433; 27–50

Langer, R., Peppas, N. "Chemical and physical structure of polymers as carriers for controlled release of bioactive agents: a review", *J. Macromol. Sci.*; 23: 61-126, 1983.

Latour L.L., Mitra P.P., Kleinberg R.L., Sotak C.H. (1993) Time-dependent Diffusion Coefficient of Fluids in Porous Media as a Probe of Surface-to-volume ratio. *J. Magnetic Resonance.* Series A. 101; 342-346

Lao L.S., Venkatraman S.S., Peppas N.A. (2008) Modeling of drug release from biodegradable polymer blends. *European J Pharm Biopharm*. 70; 796–803

Le Corre, P., Rytting J.H., Gajan V., Chevanne F., Le Verge R. (1997) In vitro controlled release kinetics of local anaesthetics from poly (D, L-lactide) and poly(lactide-co-glycolide) microspheres. *J. Microencapsulation.* 14 (2); 243-255

Liggins R.T., Amours S.D., Demetrick J.S., Machan L.S., Burt H.M. (2000) Paclitaxel loaded poly(L-lactic acid) microspheres for the prevention of intraperitoneal carcinomatosis after a surgical repair and tumor cell spill. *Biomaterials*. 21; 1959-1969

Liu C., Desai K.C.H., Tang X., Chen X. (2006) Drug Release Kinetics of Spray-Dried Chitosan Microspheres. *Drying Technology*, 24; 769–776, 2006

Loo S.C.J, Ooi C.P., Wee S.H., Boey Y.C. (2005) Effect of isothermal annealing on the hydrolytic degradation rate of poly(lactide-co-glycolide) acids. *Biomaterials*. 26; 2827–2833

Machida Y., Onishi H., Kurita A., Hata H., Morikawa A., Machida, Y. (2000) Pharmacokinetics of prolonged-release CPT-11-loaded microspheres in rats. *J Control Release*. 66; 159-175

Mainardes R.M. and Evangelista R.C. (2005) PLGA nanoparticles containing praziquantel: effect of formulation variables on size distribution. *Int J Pharm.* 290; 137–144

Markman M. (1986) Intraperitoneal antineoplastic agents for tumors principally confined to the peritoneal cavity. *Cancer Treatment Reviews*. 13 (4); 219-242

Markman M., Reichman B., Hakes T., Rubin S., Jones W., Lewis J.L., Barakat R., Curtin J., Almadrones L., Hoskins W. (1992) Phase 2 trial of intraperitoneal carboplatin and etoposide as salvage treatment of advanced epithelial ovarian cancer. *Gynecologic Oncology*, 47 (3); 353-357

Markman M. (1996) Intraperitoneal Therapy of Ovarian Cancer. *The Oncologist*. 1; 18-21

Markman M., Bundy B.N., Alberts D.S., Fowler J.M., Clark-Pearson D.L., Carson L.F., Wadler S., Sickel J. (2001) Phase III Trial of Standard-Dose Intravenous Cisplatin Plus Paclitaxel Versus Moderately High-Dose Carboplatin Followed by Intravenous Paclitaxel and Intraperitoneal Cisplatin in Small-Volume Stage III Ovarian Carcinoma: An Intergroup Study of the Gynecologic Oncology Group, Southwestern Oncology Group, and Eastern Cooperative Oncology Group. *J Clinical Oncology.* 19 (4); 1001-1007

Markman M. (2004) Intraperitoneal Chemotherapy. *Diagnosis and Management of Ovarian ages.* 2nd Edition, pp. 505-*513*

Markman M. and Walker J.L. (2006) Intraperitoneal Chemotherapy of Ovarian Cancer: A Review, With a Focus on Practical Aspects of Treatment. *J Clinical Oncology.* 24 (6); 1-6

Massey B., Wen X., Rohr, L.R., Tresco P.A., Dahlstrom L., Park A.L. (2004) Resorption rate and biocompatibility characteristics of two polyester ventilation tubes in a guinea pig model. *Otolaryngology–Head and Neck Surgery*. 131 (6); 921-925

Matsumoto A., Matsukawa Y., Suzuki T., Yoshino H. (2005) Drug release characteristics of multi-reservoir type microspheres with poly(dL-lactide-co-glycolide) and poly(dL-lactide). *J Controlled Release.* 106; 172– 180

Matsumoto A., Matsukawa Y., Horikiri, Y. Suzuki T. (2006) Rupture and drug release characteristics of multi-reservoir type microspheres with poly(dl-lactide-*co*-glycolide) and poly(dl-lactide). *Int J Pharmaceutics*. 327; 110–116

Mayersohn M. and Gibaldi M. (1970) Mathematical methods in pharmacokinetics. I. Use of the Laplace transform for solving differential rate equations. *Amer J Pharm Ed*. 34; 608-614

McClay E.F. and Howell S.B. (1990) A review: Intraperitoneal cisplatin in the management of patients with ovarian cancer. *Gynecologic Oncology*. 36(1); 1-6

McGuire WP, Hoskins WJ, Brady MF, (1996) Cyclophosphamide and cisplatin compared with paclitaxel and cisplatin in patients with stage III and stage IV ovarian cancer. *N Engl J Med*, 334; 1-6.

McGuire D.E., Venu R.P., Brown R.D., Etzkorn K.P., Glaws W.R., Abu-Hammour A. (2000) Brush cytology for pancreatic carcinoma: an analysis of factors influencing results. *J. Pancreas.* 1(3); 108-110

McGuire W.P., Markman M. (2003) Primary ovarian cancer chemotherapy: current standards of care. *Br J Cancer.* 89 (3); S3-S8

McKinnell R.G. (1998) The Biological basis of cancer. Publisher: Cambridge University Press

Menei P., Venier M.C., Gamelin E., Saint-Andre J.P., Hayek G., Jadaud E., Fournier D., Mercier P., Guy G., Benoit J. P. (1999) Local and Sustained Delivery of 5-Fluorouracil from Biodegradable Microspheres for the Radiosensitization of Glioblastoma A Pilot Study. *Cancer.* 86 (2)

Messaritaki A., Black S.J., van der Walle C.F., RigbyS.P. (2005)NMR and confocal microscopy studies of the mechanisms of burst drug release from PLGA microspheres. *J Controlled Release*. 108; 271–281

Mehta R.C., Jeyanthi R., Calis S., Thanoo B.C., Burton K.W. Deluca P.P. (1994) Biodegradable microspheres as depot system for parenteral delivery of peptide drugs. *J Controlled Release*. 29; 375-384

Middleton J.C. and Tipton A.J. (1998) Synthetic biodegradable polymers as orthopedic devices", Biomaterials 21 (2000) 2335-2346

Mitchell J., Stark S.C., Strange J.H. (2005) Probing surface interactions by combining NMR cryoporometry and NMR relaxometry. *J. Phys. D: Appl. Phys*. 38; 1950–1958

Mitchell J., Webber J.B.W., Strange J.H. (2008) Nuclear magnetic resonance cryoporometry. *Physics Reports*. 461; 1–36

Mitra P.P., Latour L.L., Kleinberg R.L., Sotak C.H. (1995) Pulsed-Field-Gradient NMR Measurement of Restricted Diffusion and the Return-to-Origin Probability. *J Magnetic Resonance*. Series A, 114; 47-58

Mohr M., Wolff M., and Kissel T. (1999) Gamma irradiation for terminal sterilization of 17β-estradiol loaded poly-(D,L-lactide–co–glycolide) microparticles. *J Control. Release.* 61; 203–217

Morgan S.M., Tilley S., Perera S., Ellis M.J., Kanczlera J., Chaudhuric J.B. Oreffo R.O.C. (2007) Expansion of human bone marrow stromal cells on poly-(DL-lactide-co-glycolide) (PDLLGA) hollow fibres designed for use in skeletal tissue engineering. *Biomaterials*. 28; 5332–5343

Morishige K. and Nobuoka K. (1997) X-ray diffraction studies of freezing and melting of water confined in a mesoporous adsorbent (MCM-41). *J Chem Phys*. 107 (17); 6965-6969

Morishige K. and Kawano K. (1999) Freezing and melting of water in a single cylindrical pore: The pore-size dependence of freezing and melting behavior. *J Chem Phys*. 110 (10); 4867–4872

Mulder M. (2000) Basic Principle of Membrane Technology. Second Edition. Kluwer Academic Publisher, Netherland.

Mulye N.V. and S.J. Turco S.J. (1995) A simple model based on first order kinetics to explain release of highly water soluble drugs from porous dicalcium phosphate dihydrayte matrices. *Drug Development and Industrial Pharmacy*. 21 (8); 943-953

Niwa T., Takeuchi H., Hino T., Kunou N., Kawashima Y. (1993) Preparations of biodegradable nanospheres of watersoluble and insoluble drugs with DLlactide/glycolide copolymer by a novel spontaneous emulsification solvent diffusion method and the drug release behavior. *J. Control. Release.* 25; 89–98

Ogawa Y., Yamamoto M., Okada H., Yashiki T., Shimamoto T. (1988) A New Technique to Efficiently Entrap Leuprolide Acetate into Microcapsules of Polylactic Acid or Copoly(lactic/Glycolic) Acid. *Chem Pharm Bull*. 36 (3); 1095-1103.

Ogura Y. and Kimura H. (1995) Biodegradable polymer microspheres for targeted drug delivery to the retinal pigment epithelium. *Survey of Ophthalmology*. 39(1); S17-S24

Ozols R.F. (2003) Progress in ovarian cancer: an overview and perspective. *European J Cancer Supplements.* 1 (2); 43–55

Park T.G. (1995) Degradation of poly(lactic-co-glycolic acid) microspheres: effect of copolymer composition. *Biomaterials.* 16; 1123-1130

Perepechkin L.P. and Perepechkina N.P. (1999) Chemistry and Technology of chemical fibres for medical applications. A review. *Fibre Chemistry*. 31 (6); 411-421

Perez M.P., Zinutti M., Lamprecht A.L., Ubrich N., Astier A., Hoffman M., Bodmeierc R., Maincent P. (2000) The preparation and evaluation of poly(e-caprolactone) microparticles containing both a lipophilic and a hydrophilic drug. *J Controlled Release.* 65; 429–438

Perkins E.L., Lowe J.P., Edlerb K.J., Tanko N., Rigby S.P. (2008) Determination of the percolation properties and pore connectivity for mesoporous solids using NMR cryodiffusometry. *Chemical Engineering Sci.* 63; 1929 – 1940

Petrov O. and Furó I. (2006) Curvature-dependent metastability of the solid phase and the freezing-melting hysteresis in pores. *Physical Review E*. 73; 011608.1-7

Petrov O., Furó I., Schuleit M., Domanig R., Plunkett M., Daicic J. (2006) Pore size distributions of biodegradable polymer microparticles in aqueous environments measured by NMR. *Int J Pharmaceutics*. 309; 157–162

Petrov O.V., Vargas-Florencia D., Furo´ I. (2007) Surface Melting of Octamethylcyclotetrasiloxane Confined in Controlled Pore Glasses: Curvature Effects Observed by 1H NMR. *J Phys Chem. B*. 111; 1574-1581

Polakovic M., Gorner T., Gref R., Dellacherie E. (1999) Lidocaine loaded biodegradable nanospheres II. Modelling of drug release. *J Controlled Release.* 60; 169-177

Pitt C.G. and Schindler A. (1979) Sustained subdermal delivery of drugs using poly (ε-caprolactone) and its copolymers, U.S. Patent 4,148,871

Pitt C.G., Gratzl M.M., Jeffcoat A.R., Zweidinger R, Schindler A. (1979) Sustained drug delivery systems II: factors affecting release rates from poly (ε-caprolactone) and related biodegradable polyesters. *J Pharm Sci*, 68; 1534-1538

Qin J.J., Gu J., Chung T.S. (2001) Effect of wet and dry-jet wet spinning on the shear-induced orientation during the formation of ultrafiltration hollow fibre membranes. *J Membrane Sci*. 812 (1-2); 57

Rabik C.A. and Dolan M.E. (2007) Molecular mechanisms of resistance and toxicity associated with platinating agents. *Cancer Treatment Reviews*. 33; 9– 23

Rafati H., Coombes A.G.A., Adler J., Holland J., Davis S.S. (1997) Protein-loaded poly(DL-lactide-co-glycolide) microparticles for oral administration: formulation, structural and release characteristics. *J Controlled Release*. 43; 89–102

Rigby S.P., Cheah K.Y., Gladden L.F. (1996) NMR imaging studies of transport heterogeneity and anisotropic diffusion in porous alumina pellets. *Applied Catalysis A: General*. 144; 377-388

Rigby S.P., Van der Walle C.F., Raistrick J.H. (2004) Determining drug spatial distribution controlled delivery tablets using MFX imaging. *J Controlled Release*. 96; 97-110

Rixe O., Ortuzar W., Alvarez M., Parker R., Reed E., Paull K., Fojo T. (1996) Oxaliplatin, Tetraplatin, Cisplatin, and Carboplatin: Spectrum of Activity in Drug-Resistant Cell Lines and in the Cell Lines of the National Cancer Institute's Anticancer Drug Screen Panel. *Biochemical Pharmacology*. 52; 1855-1865, 1996.

Rosenberg B., Van Camp L. & Krigas T. (1965) Inhibition of cell division in *Escherichia coli* by electrolysis products from platinum electrode. *Nature.* 205, 698–700

Rosenberg B., Van Camp L., Trosko J. E. & Mansour V. H. (1969) Platinum compounds: a new class of potent antitumour agents. *Nature.* 222; 385-386

Rosenberg, B. (1985) Fundamental studies with cisplatin. *Cancer.* 55 (10); 2303–23l6.

Rothenberg M.L., Liu P.Y., Braly P.S., Wilczynski S.P., Hanningan E.V., Wadler S., Stuart G,, Jiang C., Markman M., Alberts D. (2003) Combined Intraperitoneal and Intravenous Chemotherapy for Women with Optimally Debulked Ovarian Cancer: Results from an Intergroup Phase II Trial. *J Clinical Oncology*. 21; 1313-1319

Ruan G., Feng S.S., Li Q.T. (2002) Effects of material hydrophobicity on physical properties of polymeric microspheres formed by double emulsion process. *J Controlled Release*. 84; 151-160

Sandstrap P., Fontaine J. and Moes A.J. (1999) Nifedipine-loaded PLGA microspheres: *in vitro/in vivo* comparison of drug release and polymer degradation. *S.T.P. Pharm.* 9; 443-446

Sansdrap P. and Moes A.J. (1993) Influence of manufacturing parameters on the size characteristics and the release profiles of nifedipine from poly(DL-lactide-co-glycolide) microspheres. *Int J Pharm*. 98; 157– 164

Sastre R.L., Blanco M.D., Teijón C., Olmo R., Teijón J.M., (2004) Preparation and characterisation of 5-flurouracil-loaded Poly(ε-Caprolactone) Microspheres for Drug Administration. *Drug Development Research*. 63; 41-53

Scherer G.W. (1998) Characterization of aerogels. *Adv. Colloid Interfac*. 77; 321–339

Schmitt E.A., Flanagan D.R., Linhardt R.J. (1994) Importance of Distinct Water Environments in the Hydrolysis of Poly (DL-lactide-co-glycolide). *Macromolecules.* 27; 743-148

Scholes P.D., Coombes A.G., Illum L., Davis S.S., Vert M., Davies M.C. (1993) The preparation of sub-200 nm poly (lactide-co-glycolide) microspheres for site-specific drug delivery. *J Controlled Release*. 25; 145-153

Shearer H. (2007) PhD Thesis: Hollow fibre bioreactors for bone tissue engineering. Dept. of Chemical Engineering, Uni. of Bath.

Siepmann J., Ainaoui A., Vergnaud J.M. Bodmeier R. (1998) Calculation of the Dimensions of Drug-Polymer Devices Based on Diffusion Parameters. *J Pharm Sci.* 87 (7); 827-832

Siepmann J., Faisant N., Akikib J., Richard J., Benoit J.P. (2004) Effect of the size of biodegradable microparticles on drug release: experiment and theory. *J Controlled Release.* 96; 123– 134

Sircar S. and Hufton J. R. (2000) Why does the Linear Driving Force Model for Adsorption Kinetics Work? *Adsorption.* 6; 137-147

Spenlehauer G., Veillard M., Benoit J.P. (1986) Formation and characterization of cisplatin loaded poly(D-Lactide) microspheres for chemo-embolization. *J Pharm Sci*. 75; 750–755.

Spenlehauer G., Vert M., Benoit J.P., Chabot F., Veillard M. (1988) Biodegradable cisplatin microspheres prepared by the solvent evaporation method: morphology and release characteristics. *J Controlled Release.* 7; 217–229.

Spenlehauer G., Vert, M. Benoit J.P., Boddaert A. (1989) *In vitro* and *in vivo* degradation of poly(DL-lactide-glycolide) type microspheres made by solvent evaporation method. *Biomaterials.* 10; 557- 563

Stejskal E.O. and Tanner J.E. (1965) Spin diffusion measurements: Spin echoes in the presence of a time dependent field gradient. *J Chem Phys*. 42; 288-292

Strange J.H., Rahman M., Smith E.G. (1993) Characterization of porous solids by NMR. *Physical Review Letters.* 71; 3589–3591

Strange J.H. (1994) Cryoporometry: A new NMR method for characterising porous media. *Nondestr Test Eval*. 11; 261-271

Strange J.H., Webber J.B.W., Schmidt S.D. (1996) Pore size distribution mapping. *Magnetic Resonance Imaging*. 14 (7); 803-805

Swainson I.P. and Schulson E.M. (2001) A neutron diffraction study of ice and water within a hardened cement paste during freeze–thaw. *Cement & Concrete Research*. 31; 1821–1830

Tai C.C. (2007) PhD Thesis: Novel adsorbent hollow fibres. Dept. of Chemical Engineering, Uni. of Bath

Tamura T., Imai J., Tanimoto M., Matsumoto A., Suzuki A., Horikiri Y., Suzuki T., Yoshino H. (2002) Relation between dissolution profiles and toxicity of cisplatin-loaded microspheres. *European J Pharm Biopharm*. 53; 241-247

Tan X., Tan S.P., Teo W.K., Li K. (2006) Polyvinylidene fluoride (PVDF) hollow fibre membranes for ammonia removal from water. *J Membrane Science*. 271; 59–68

Therin M., Christel P., Li S., Garreau H., Vert M. (1992) *In vivo* degradation of massive poly(alpha-hydroxy acids): validation of *in vitro* findings. *Biomaterials*. 13; 594–600

Thigpen T. (2004) The if and when of surgical debulking for ovarian carcinoma. *N Engl J Med*. 351; 2544-6

van Zutphen S. and Reedijk J. (2005) Review: Targeting platinum anti-tumour drugs: Overview of strategies employed to reduce systemic toxicity. *Coordination Chemistry Reviews*. 49; 2845–2853

Veith S.R., Hughes E., Vuataz G., Pratsinis S.E. (2004) Restricted diffusion in silica particles measured by pulsed field gradient NMR. *J Colloid and Interface Science*. 274; 216–228

Waeckerle-Men Y. and Groettrup M. (2005) PLGA microspheres for improved antigen delivery to dendriticcells as cellular vaccines. *Advanced Drug Delivery Reviews*. 57; 475– 482

Walter E., Dreher, D., Kok, M., Thiele, L., Kiama, S.G., Gehr, P., Merkle, H.P. (2001) Hydrophilic poly(DL-lactide-co-glycolide) microspheres for the delivery of DNA to human-derived macrophages and dendritic cells. *J Controlled Release*. 76, 149–168

Wang, S.H., Zhang, L.C., Lin, F., Sa, X.Y., Zuo, J.B., Shao, Q.X., Chen, G.S. and Zeng, S., (2005) Controlled release of levonorgestrel from biodegradable poly(d,l-lactide-co-glycolide) microspheres: *In vitro* and *in vivo* studies. *Int J Pharmaceutics*. 301(1); 217-225

Watts P.J., Davies M.C., Melia C.D (1990) Microencapsulation using emulsification/solvent evaporation: An overview of techniques and applications. *Cric. Rev. Carr.* 7; 235–259

Webber J.B.W., Strange J.H., Dore J.C. (2001) An evaluation of NMR cryoporometry, density measurement and neutron scattering methods of pore characterisation. *Magnetic Resonance Imaging*. 19; 395–399

Webber J. B. W., Dore J.C. (2008) Neutron Diffraction Cryoporometry—A measurement technique for studying mesoporous materials and the phases of contained liquids and their crystalline forms. *Nuclear Instruments and Methods in Physics Research A*. 586; 356–366

Wen X. and Tresco P.A. (2006) Fabrication and characterization of permeable degradable poly(DL-lactide-co-glycolide) (PLGA) hollow fiber phase inversion membranes for use as nerve tract guidance channels. *Biomaterials*. 27; 3800–3809

Willemse P.H.B. and de Vries E.G.E. (2003) Intraperitoneal chemotherapy for ovarian cancer: a question of feasibility*? Drug Resistance Updates*. 6; 165-167

Wiltshaw E, Kroner T. (1976) Phase II study of cis-dichlorodiammineplatinum(II) (NSC-119875) in advanced adenocarcinoma of the ovary. *Cancer Treat Rep.* 60: 55–60

Winet H., Hollinger J.O., Stevanovic M. (1995) Incorporation of polylactide-polyglycolide (PLG) in a cortical defect: neoangiogenesis and blood supply in a bone chamber. *J Orthop Res.* 13; 679-689.

Winet H. and Bao J.Y. (1997) Comparative bone healing near eroding polylactide–polyglycolide implants of differing crystallinity in rabbit tibial bone chambers. *J Biomaterials Sci Polymer Edition*. 8; 517–32.

Witt C., MaÈder K., Kissel T. (2000) The degradation, swelling and erosion properties of biodegradable implants prepared by extrusion or compression moulding of poly(lactide-co-glycolide) and ABA triblock copolymers. *Biomaterials.* 21; 931-938

Wolff G. (2005) Bruker Almonor Guidebook. www.bruker-biospin.com

Yan C., Resau J.H., Heweston J., West M., Rill W.L., Kende M. (1994) Characterization and morphological analysis of protein-loaded poly(lactide-co-glycolide) microparticles prepared by water-in-oil-in-water emulsion technique. *J Controlled Release*. 32; 231–241

Yang Y.Y., Chia H.H., Chung T.S. (2000) Effect of preparation temperature on the characteristics and release profiles of PLGA microspheres containing protein fabricated by double-emulsion solvent extraction / evaporation method. *J Controlled Release*. 69; 81–96

Yang Y.Y., Chung T.S., Ng N.P. (2001a) Morphology, drug distribution, and in vitro release of biodegradable polymeric microspheres containing protein fabricated by double-emulsion solvent extraction/evaporation method. *Biomaterials.* 22; 231-241

Yang S., Teo W.K., Li K. (2001b) Formation of annular hollow fibres for immobilization of yeast in annular passages. *J Membrane Science*. 184; 107–115

Ye M., Pan H.M., Wang H.Y., Lou F., Jin W., Zheng Y., Wu J.M. (2004) Catheterization-associated complications of intraperitoneal chemotherapy in advanced gastric cancer. *World J Gastroenterol*. 10(9); 1372-1374

Yen M.L., Yen B.L., Bai C.H., Lin R.S. (2001) Risk factors for ovarian cancer in Taiwan: a case-control study in a low-incidence population. *Gynecol Oncol*. 89; 318– 24

Yeo Y. and Park K. (2004) Characterization of Reservoir-Type Microcapsules Made By the Solvent Exchange Method. *AAPS Pharm Sci Tech.* 5 (4); 1-8 Article 52

Yoo H.S., Oh J.E., Lee K.H., Park. T.G. (1999) Biodegradable nanoparticles containing doxorubicin-PLGA conjugate for sustained release. *Pharmaceutical Res.* 16 (7); 1114–1118

Zambaux M.F., Bonneaux F., Gref R., Maincent P., Dellacherie E., Alonso M.J. (1998) Influence of experimental parameters on the characteristics of poly(lactic acid) nanoparticles prepared by a double emulsion method. *J Controlled Release.* 50; 31–40

Zhang Q. and Cussler E.L. (1985) Microporous hollow fibers for gas absorption. II. Mass transfer across the membrane. *J Membrane Sci.* 23; 333–345

Zilberman M. (2007) Novel composite fiber structures to provide drug/protein delivery for medical implants and tissue regeneration. *Acta Biomaterialia*. 3; 51–57

Zweers, M., Engbers, G., Grijpma, D., Feijen, J. (2004) In vitro degradation of nanoparticles prepared from polymers based on dl-lactide, glycolide and poly(ethylene oxide)", Journal of Controlled Release 100 347–356

Zylberberg B., Dormont D., Antoine J.M., Madelenat P., Ravina J.H. Uzan S., Salat-Baroux (1996) First line immunochemotherapy with cisplatin-based protocol by intraperitoneal and intravenous routes in ovarian cancer: technique and results of 82 cases. *European Journal of Obstetrics & Gynecology and Reproductive Biology*. 66; 57-64

www.cdc.gov/cancer/npcr/uscs/ Department of Health and Human Services. *United States Cancer Statistics*: 1999–2002 *Incidence and Mortality Web-based Report*. Atlanta, GA: Centers for Disease Control and Prevention and National Cancer Institute; 2005

www.iarc.fr WHO. International Agency for Research on Cancer; 2001

www.lakeshorebio.com/technical-polymer-information.html Lakeshore Biomaterials Inc., US

APPENDIX I

A. Sample Calculation for Drug Concentration Determination

Lidocaine concentration determination:

Absorbance measured at 266 nm using UV-spectrometer = 1.95

From calibration curve (Figure 4.5), y = 1.8829 x + 0.0811

Concentration of lidocaine in 10 ml PBS, x = 1.95 – 0.0811 / 1.8829 = 0.9925 mg/ml

Total lidocaine in 10 ml PBS = 0.9925 x 10 = 9.925 mg

Cisplatin concentration determination:

Absorbance measured at 265.9 nm using AAS = 0.45

From calibration curve (Figure 4.6), y = 0.6077 x + 0.0181

Concentration of cisplatin in 10 ml PBS, x = 0.45 – 0.0181 / 0.6077 = 0.7107 mg/ml

Total cisplatin in 10 ml PBS = 0.7107 x 10 = 7.107 mg

Drug loading determination:

0.2 g CPt-50:50MS acid-digested and redissolved in 10 ml 0.1M HCl, absorbance measured at 265.9 nm using AAS = 0.85, concentration of cisplatin = 1.3689 mg/ml

Total cisplatin in 10 ml 0.1M HCl = 13.689

$$\text{Drug loading (\%)} = \frac{\text{Total Drug Encapsulated (mg)}}{\text{Total Sample Used (mg)}} \times 100\% \qquad \text{(Equation 4.1)}$$

Drug loading = [13.689 / 200] x 100 % = 6.84 %

APPENDIX II

A. Sample Calculation for Gas Permeation Analysis

Membrane surface area, A (m^2):

$A=2.\pi.r.L$ π = Pi (3.142)

r = Hollow fibre radius (3.0×10^{-4} m)

L = Hollow fibre length (10×10^{-2} m)

$A = 2 * 3.142 * 3.0 \times 10^{-4} * 10 \times 10^{-2} = \underline{1.88 \times 10^{-4}\ m^2}$

Mean pressure across hollow fibre, P (Pa):

$P = (P_{in} + P_{out})/2$ P_{in} = Pressure inside fibre (2.0×10^5 Pa)

P_{out} = Pressure outside fibre / atmospheric (1.01×10^5 Pa)

$P = [(2 + 1) \times 10^5\ ] / 2 = \underline{1.5 \times 10^5\ Pa}$

Volumetric gas flow rate, Q (m^3/s):

$Q = V / t$ V = Volume of gas timed ($5 \times 10^{-5}\ m^3$)

t = Time taken (average 10 s)

$Q = 5 \times 10^{-5} / 10 = \underline{5 \times 10^{-6}\ m^3/s}$

Molar gas flow rate, N (mol/s):

$N = Q.P_{out} / R.T$ Q = Volumetric gas flow rate (m^3/s)

P_{out} = Pressure outside fibre / atmospheric (1.01×10^5 Pa)

R = Molar gas constant (8.31 J/mol.K)

T = Atmospheric temperature (298 K)

$N = (5 \times 10^{-6} * 1.01 \times 10^5) / (8.31 * 298) = \underline{2.02 \times 10^{-4}\ mol/s}$

Gas permeation flux, J ($mol/s.Pa.m^2$):

$J = N / A.P_{in}$ Molar gas flow rate, N (mol/s)

Membrane surface area, A (m^2)

P_{in} = Pressure inside fibre (Pa)

$J = 2.02 \times 10^{-4} / (1.88 \times 10^{-4} * 2.0 \times 10^5) = \underline{5.37 \times 10^{-6}\ mol/s.Pa.m^2}$

APPENDIX III

A. Cumulative release profiles of 5Fu from double emulsion PLGA microspheres (Section 5.1.2)

A number of PLGA microspheres loaded with fluorouracil (5Fu) were produced using double emulsion methods adapted from the literatures. Details of procedures, discussion and SEM images of the resultant microspheres were presented in Section 5.1.2. Figure 12.1 shows their corresponding 5Fu release (cumulative) measured over a period of one week. The concentration of 5Fu was measured using a uv-spectrometer with wavelength of 262 nm.

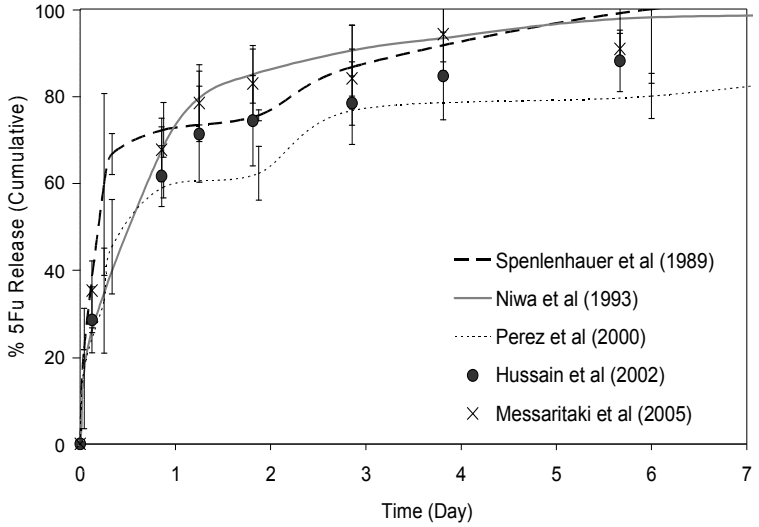

Figure 12.1: *In vitro* cumulative release of fluorouracil (5Fu) from microspheres produced in Section 5.1.2 using w/o/w emulsion methods.

APPENDIX IV

Modified Cryo-Fractioning Procedures for PLGA microspheres:

1. Sample preparation: Treat sample in liquid nitrogen and then freeze-dry overnight at -60^0C and 10^{-2} torr.
2. Mix an appropriate amount of Spurr Resin.
3. Place in capsules and allow the mixture to set (forming cylindrical blocks).
4. Trim one end of the hardened resin with razor blades until flat.
5. Mix an appropriate amount of araldite.
6. Using a cocktail stick, add a thin coat of araldite to the flat end of each block.
7. When araldite is still tacky, sprinkle on PLGA beads.
8. Leave block upright until Araldite® has solidified.
9. Blow off any excess beads with an air duster.
10. Place the samples on the resin blocks in suitable microtome chucks. Carefully ensure samples are as level as possible.
11. Cut down with razors the top of each block to give a central 1 mm x 1 mm square (retaining the original surface on the raised area).
12. Make a fresh glass knife for each sample.
13. Place a knife in the ultra microtome.
14. Place one of the chucks (with a sample) in the microtome.
15. Align each sample very carefully parallel with a sharp part of the knife.
16. Approach the knife to the sample using manual control.
17. If necessary, stop, realign sample to knife and approach again.
18. When close, use 3 mm/sec and 0.5 μm automated semi cuts until knife cuts the sample.
19. Stop and change microtome to 75 nm cuts and take two to five cuts.
20. Remove the block from its chuck.
21. Remove central cut area from block (the block can be reused).
22. Mount the cut area using aluminium dish and carbon double sided tape.
23. Gold coating for 4-5 minutes.
24. SEM imaging examination.

APPENDIX V

A. Results of water r.m.s displacement and pore diameter of PLGA Microspheres

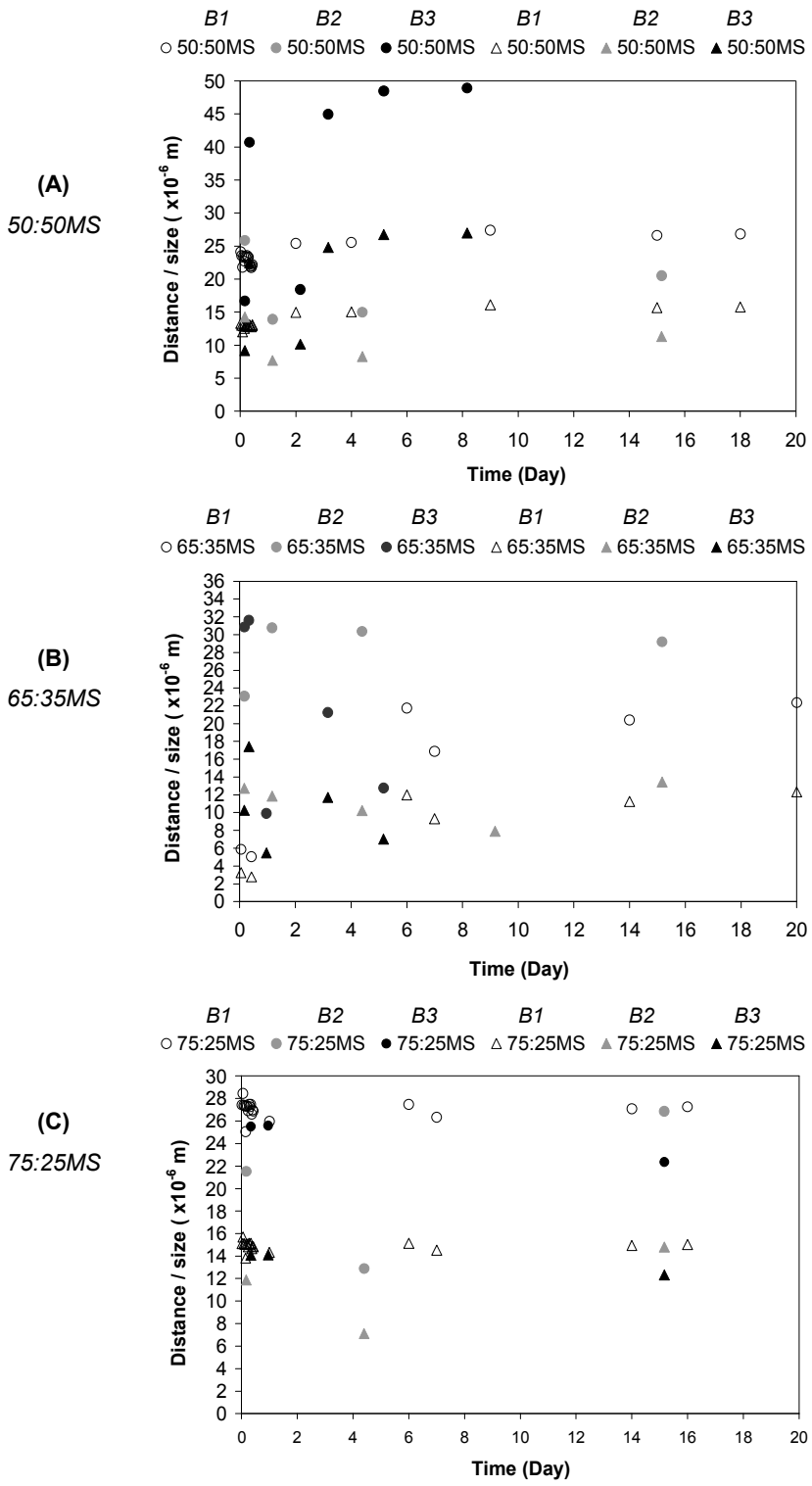

Figure 12.2: The r.m.s displacement and pore diameter of (A) 50:50MS, (B) 65:35MS and (C) 75:25MS from Batches 1, 2 and 3 (B1, B2 and B3). *Symbols: Circle = pore size diameter; Triangle = r.m.s displacement*

B. Results of tortuosity factor of PLGA Microspheres

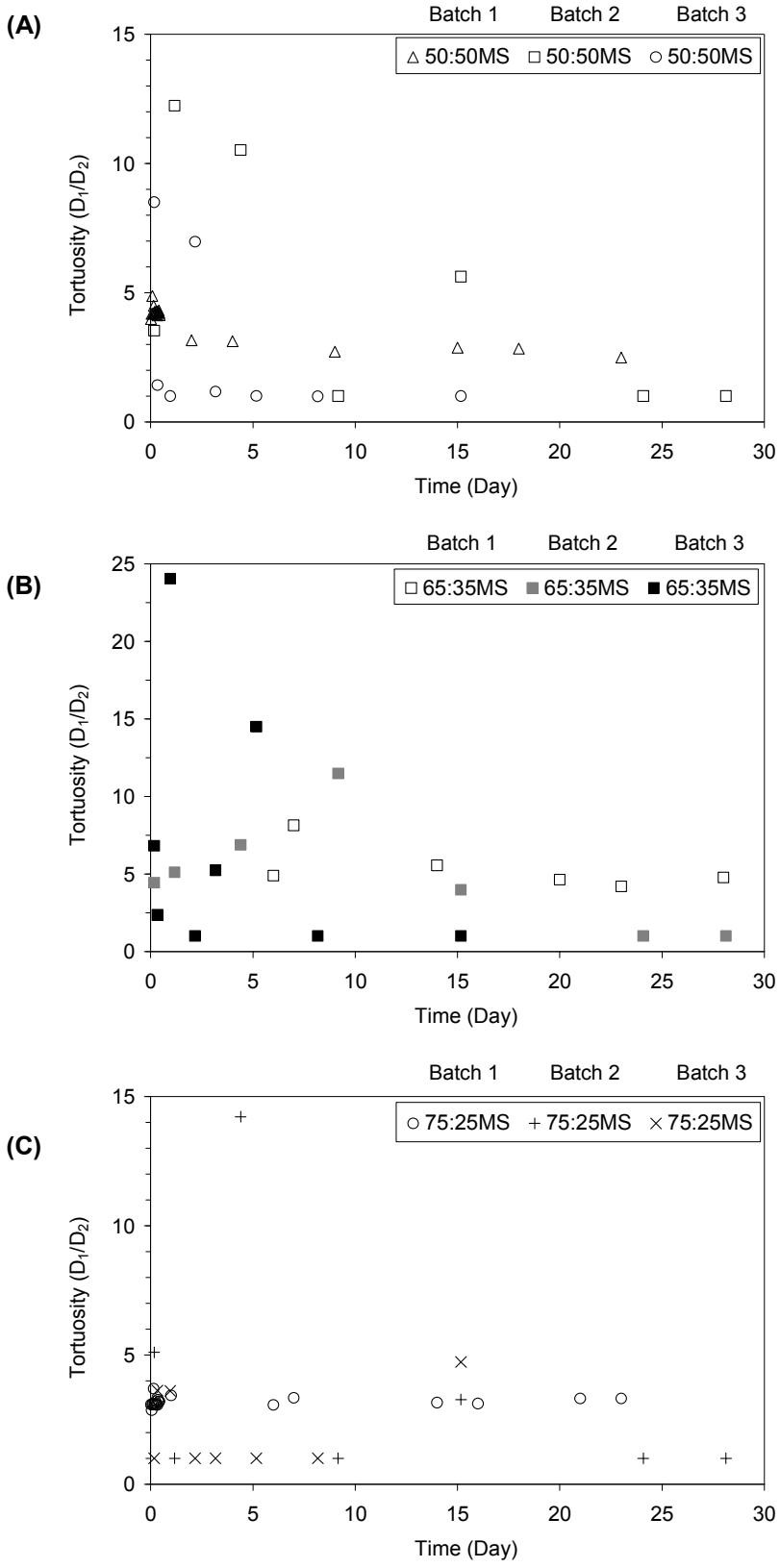

Figure 12.3: The results of tortuosity (D_1/D_2) calculated using the estimated diffusion coefficients of imbibed water (D_2) and free water (D_1) of (A) 50:50MS, (B) 65:35MS and (C) 75:25MS from Batches 1, 2 and 3.

C. Results of freezing cycles conducted on 50:50MS and 65:35MS

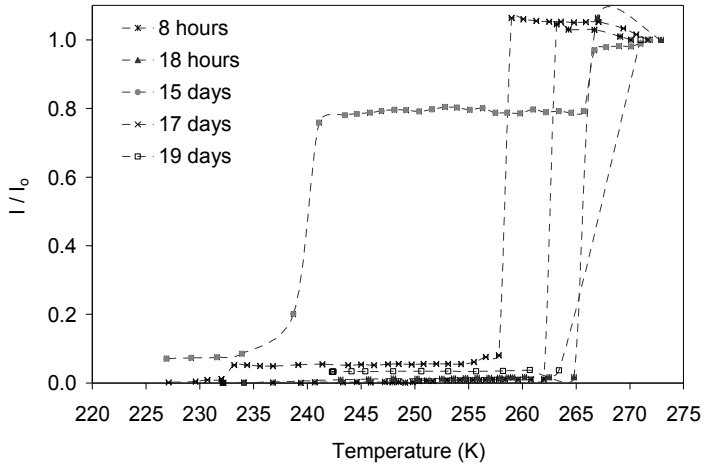

Figure 12.4: *IT* curves for the F-cycles of 50:50MS after immersion in water for 8 hours, 18 hours, 15, 17 and 19 days. Inset: A refocus on the lower scale of I/I_o.

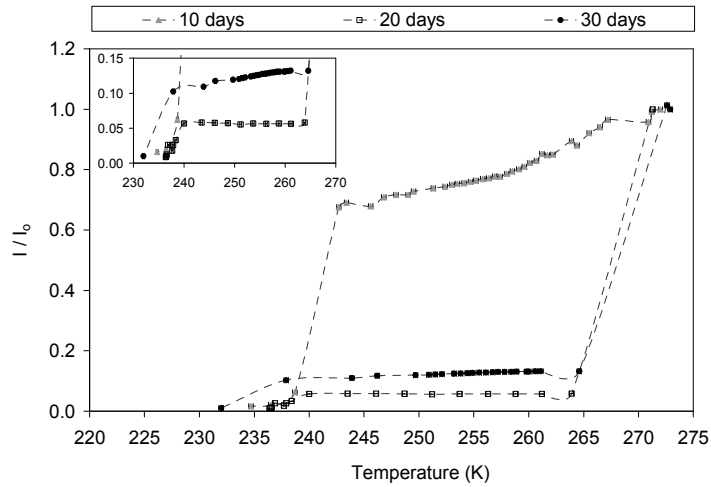

Figure 12.5: *IT* curves for the F-cycles of 65:35MS after immersion in water for 10, 20 and 30 days. Inset: A refocus on the lower scale of I/I_o.

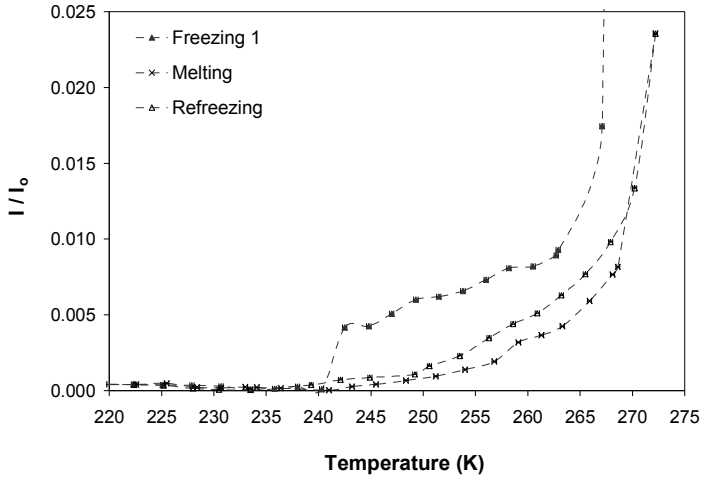

Figure 12.6: *IT* curves for F/M/F cycles of 75:25MS after 10 days immersion in water.

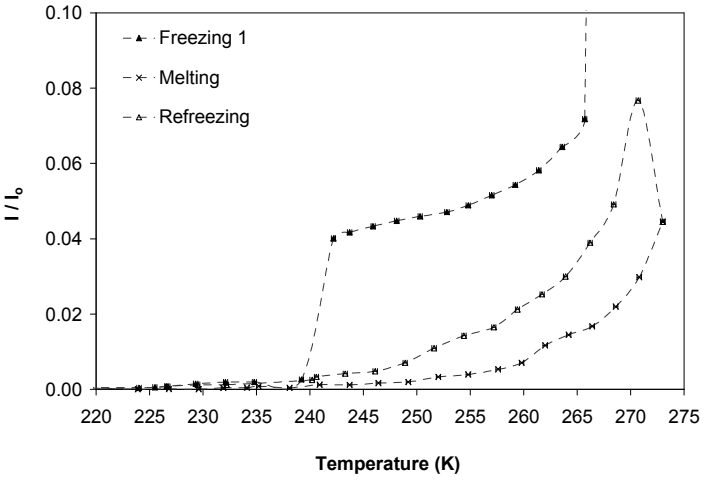

Figure 12.7: *IT* curves for F/M/F cycles of 75:25MS after 20 days immersion in water.

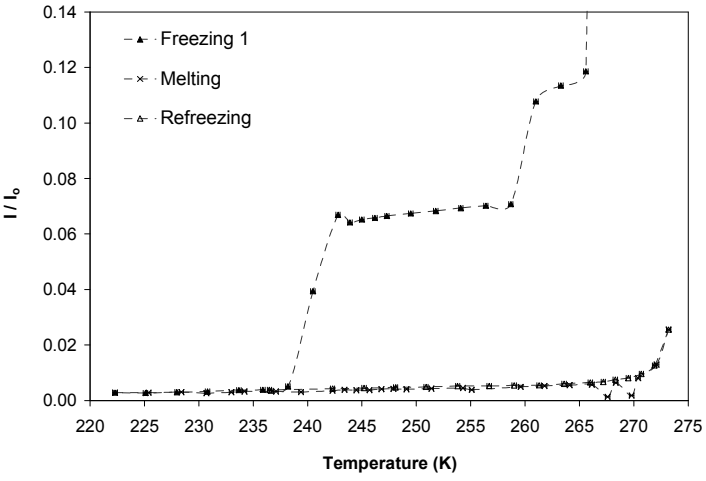

Figure 12.8: *IT* curves for F/M/F cycles of 75:25MS after 30 days immersion in water.

D. Results of pore size distributions of 50:50MS and 65:35MS

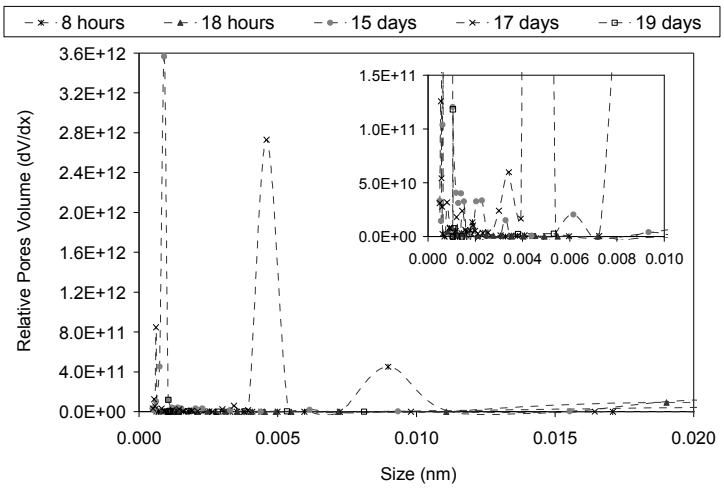

Figure 12.9: The measurement of *dV/dx* as a function of pore size distribution for 50:50MS immersed in water for 8 hours, 18 hours, 15, 17 and 19 days. Inset: Refocus on the lower scale of pore size distribution.

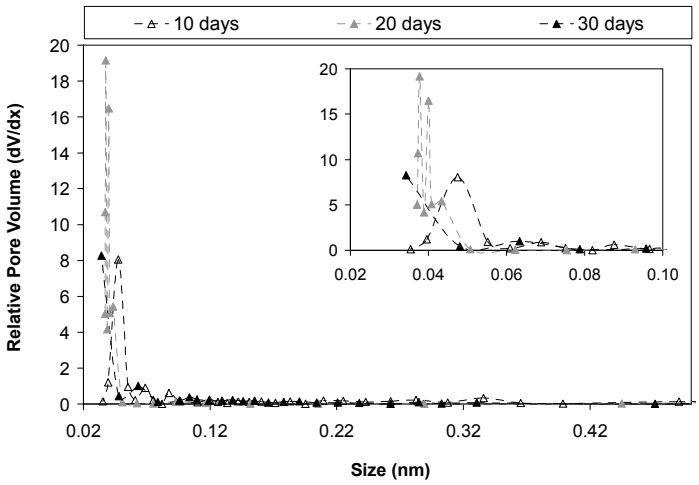

Figure 12.10: The measurement of *dV/dx* as a function of pore size distribution for 65:35MS immersed in water for 10, 20 and 30 days. Inset: Refocus on the lower scale of pore size distribution.

E. Samples calculation for r.m.s water displacement and pore size

D and D_o are the measured diffusion coefficient of imbibed water (e.g. 0.8 x 10^{-9} cm^2/s), Δ is the diffusion time (0.05s) and δ is the length of the gradient pulse (0.002s). From Equation 7.1;

Root mean square displacement of water, $\bar{r}^2$ $= 6 D_o \Delta$

$= 6 * 0.8 \times 10^{-9}\ cm^2/s * 0.05s$

$= 2.4 \times 10^{-10}\ cm^2$

$\bar{r}$ $= (1.55 \times 10^{-5}\ cm)^{0.5}$

$= 15.5\ \mu m$

From Equation 7.4; pore radius, $R = \sqrt{5D\left(\Delta - \frac{\delta}{3}\right)} = \sqrt{5 * 0.8 \times 10^{-9}\left(0.05 - \frac{0.002}{3}\right)}$ = 1.40 x 10^{-5} cm

Pore diameter = 2R = 2 * 1.40 x 10^{-5} cm = 2.80 x 10^{-5} cm = 28 μm

G. Hourly PFG-NMR measurements of Batch 1 50:50MS, 65:35MS and 75:25MS.

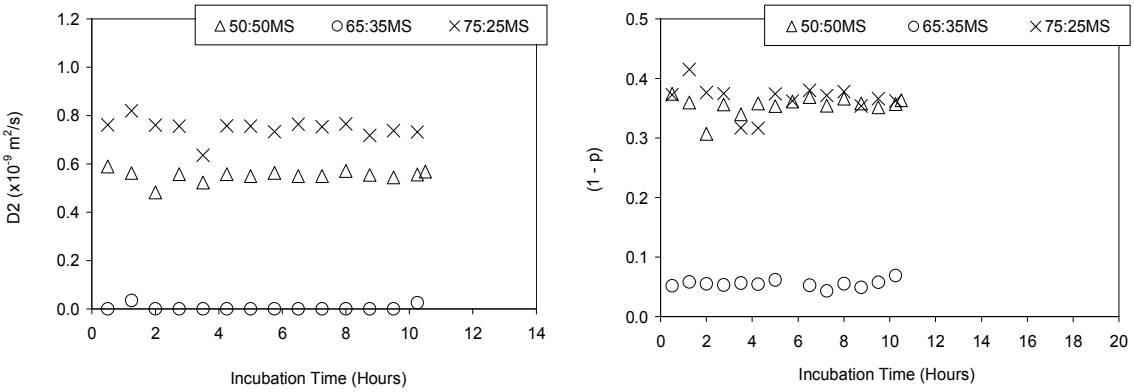

Figure 12.11: (A) The diffusion coefficient of imbibed water, D_2 of 50:50MS (△), 65:35MS (○) and 75:25MS (×). (B) The fraction of imbibed water (1 – p) in 50:50MS (△), 65:35MS (○) and 75:25MS (×).

APPENDIX VI

A. Summary of cumulative cisplatin release (%) from PLGA microspheres and solid fibres

Table 12.1: Different stages of cumulative CPt release rates estimated from 50:50SF and 50:50MS of different size fractions. Figures in brackets represent average release rate over the noted period.

Sample		Phase 1 Cumulative Release	Complete Cumulative Release	Rate of % Cumulative Release	
				Slowest	Fastest
50:50 MS	Size 53-38 μm	65 ± 4%	100 % Release Day 10	Day 6-10, 95% - 100% (1.25% / day)	Day 1-6, 65% - 95% (7% / day)
	Size 75-53 μm	36 ± 4%	94 % Release Day 20	Day 8-19, 91% - 93% (0.18% / day)	Day 1-8, 36% - 75% (7.9% / day)
	Size 90-75 μm	46 ± 3%	100 % Release Day 19	Day 8-20, 75% -99% (0.75% / day)	Day 1-8, 48% -95% (6.7% / day)
50:50SF		30 ± 4%	93 % Release Day 20	Day 10-19 87% - 94% (0.88% / day)	Day 1-7 33% - 75% (7% / day)

Table 12.2: Different stages of cumulative CPt release rates estimated from 65:35SF and 65:35MS of different size fractions. Figures in brackets represent average release rate over the noted period.

Sample		Phase 1 Cumulative Release	100% Cumulative Release	Rate of % Cumulative Release	
				Slowest	Fastest
65:35 MS	Size 53-38 μm	50 ± 4%	Day 19	Day 2-17, 76% - 75% (0.93% / day)	Day 1-2, 68% - 73% (5% / day)
	Size 75-53 μm	32 ± 2 %	Day 20	Day 6-12, 67% - 82% (2.5% / day)	Day 1-5, 40% - 68% (5% / day)
	Size 90-75 μm	26 ± 3 %	Day 20	Day 7-13, 73% -80% (1.17% / day)	Day 1-4, 48% -73% (8.3% / day)
65:35SF		24 ± 3 %	Day 19	Day 10-18 74% - 89% (1.88% / day)	Day 1-10 28% - 82% (6% / day)

Table 12.3: Different stages of cumulative CPt release rates estimated from 75:25SF and 75:25MS of different size fractions. Figures in brackets represent average release rate over the noted period.

Sample		Phase 1 Cumulative Release	% Cumulative Release on Day 20	Rate of % Cumulative Release	
				Slowest	Fastest
75:25 MS	Size 53-38 μm	58± 4%	~85%	Day 4-14, 72% - 80% (0.8% / day)	Day 1-3, 48% - 71% (11.5% / day)
	Size 75-53 μm	32 ± 4%	~100%	Day 9-19, 86% - 92% (0.6% / day)	Day 1-10, 32% - 85% (5.89% / day)
	Size 90-75 μm	21± 3%	~80%	Day 10-18, 71% -79% (1% / day)	Day 1-10, 21% -71% (5.56% / day)
75:25SF		16 ± 4%	~80%	Day 4-11 45% - 60% (2.14% / day)	Day 14-20 60% - 80% (3.33% / day)

B. Fittings of Higuchi Model to Phase 1 cisplatin release from 65:35-MS and -SF.

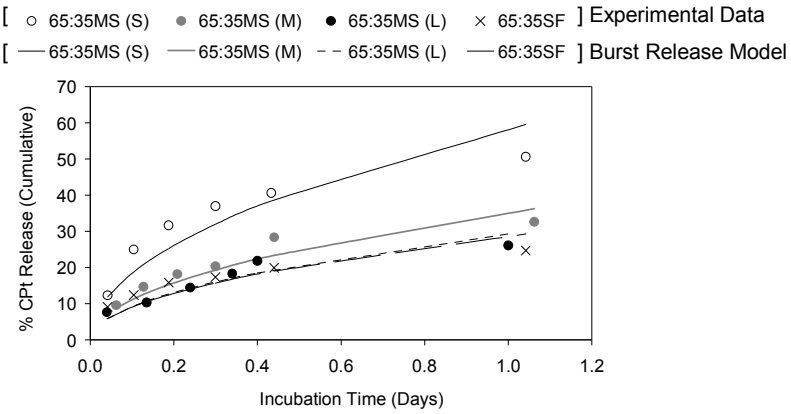

Figure 12.12: The fitting of Higuchi Model ($Q_t = k_H.t^{0.5}$) to *in vitro* Phase 1 cisplatin release from 65:35 PLGA microspheres and solid fibres.

C. Fittings of Higuchi, first and zero order kinetics models to Phase 2 cisplatin release.

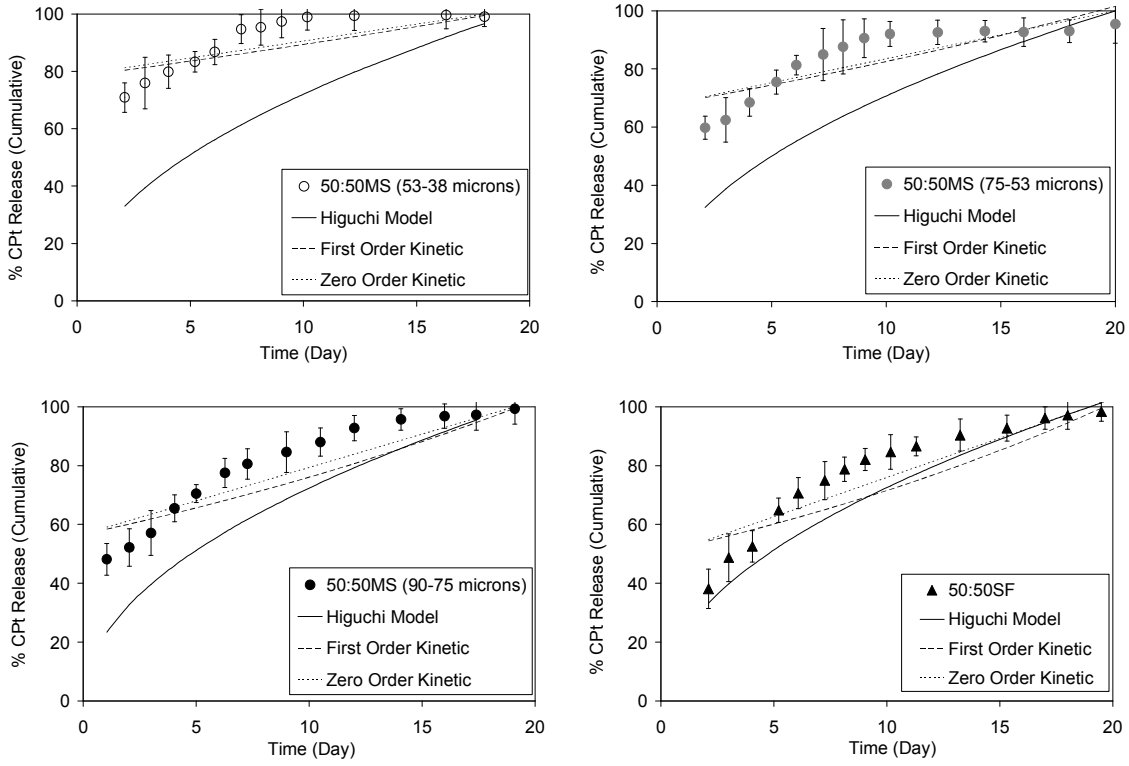

Figure 12.13: The fittings of Higuchi, first and zero order kinetics models to Phase 2 cisplatin release from 50:50MS and 50:50SF.

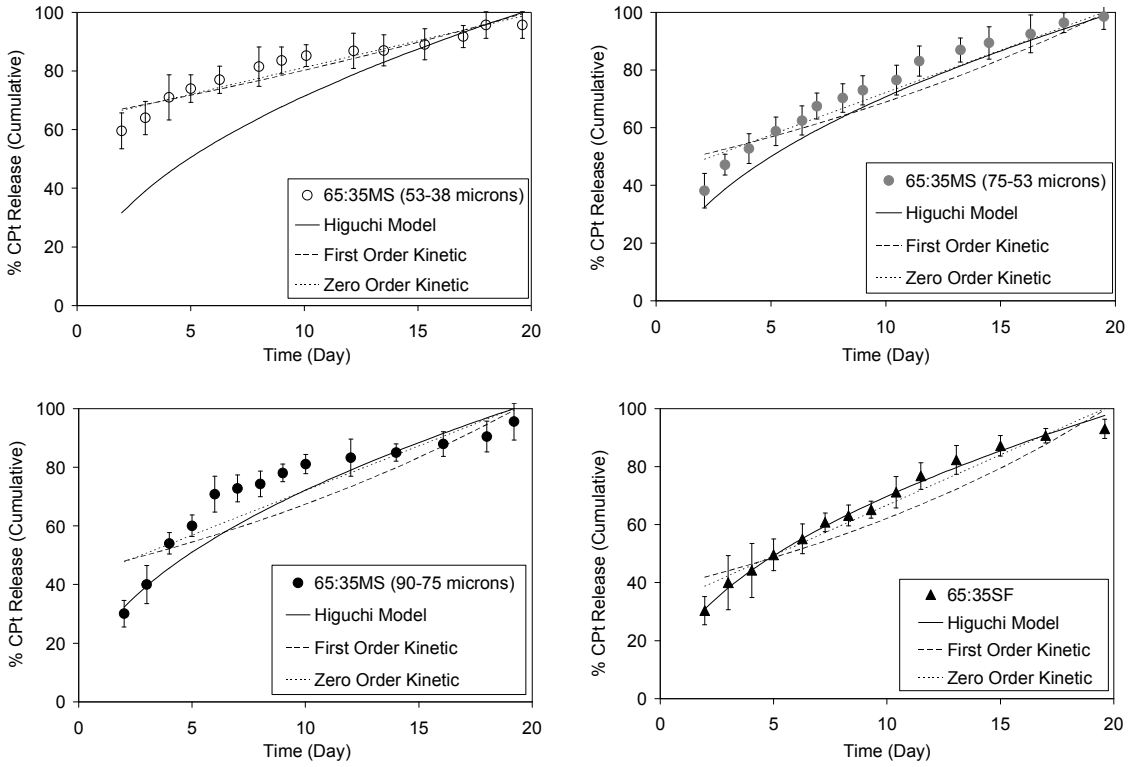

Figure 12.14: The fittings of Higuchi, first and zero order kinetics models to Phase 2 cisplatin release from 65:35MS and 65:35SF.

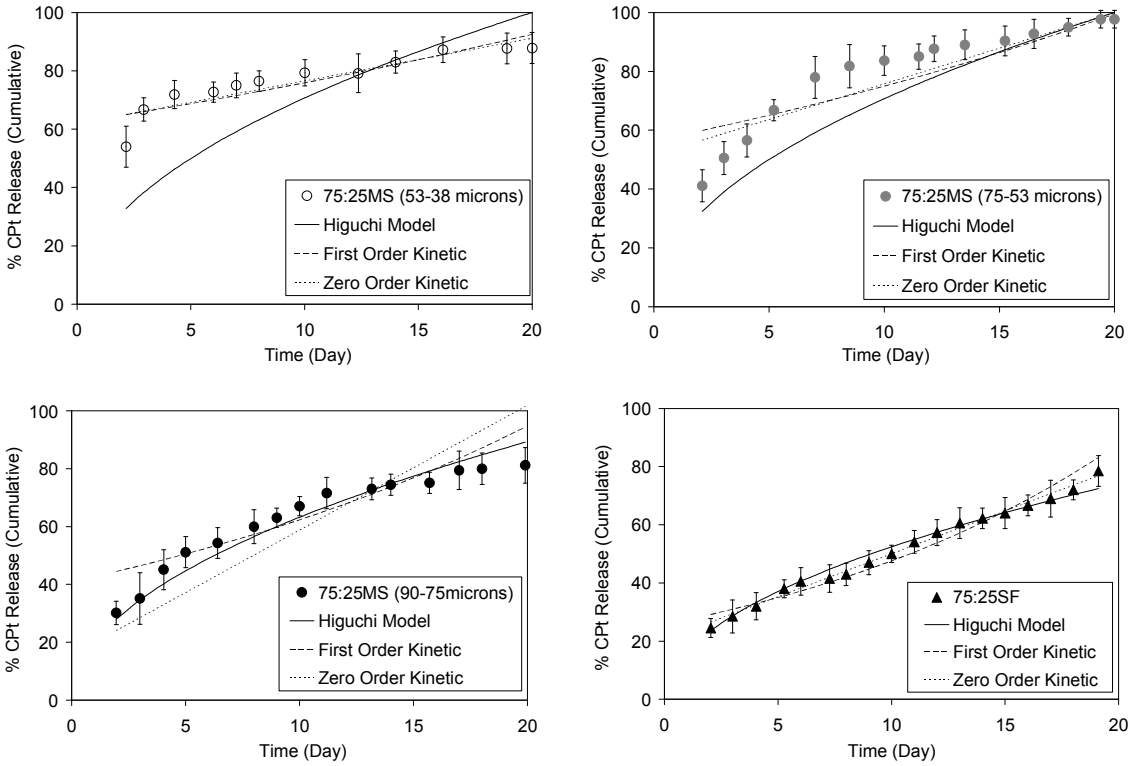

Figure 12.15: The fitting of Higuchi, first and zero order kinetics models to Phase 2 cisplatin release from 75:25MS and 75:25SF.

Table 12.4: Summary of the goodness of fit of Equations 8.1 to 8.3 to Phase 2 drug release from PLGA samples. The Higuchi constant, k_H was estimated for Phase 1 drug release. × denotes poor fitting; additional notes no. (i) to (vii), see text for discussion.

CPt-loaded PLGA Devices	Phase 1	Phase 2 – *Goodness of fit of models*			*Note*
	k_H	Higuchi Model	First Order Kinetic	Zero Order Kinetic	
5050MS (53-38 μm)	61.42	×	×	×	-
5050MS (75-53 μm)	51.85	×	×	×	-
5050MS (90-75 μm)	50.25	×	×	×	-
5050SF	27.52	*Possible fit*	×	×	(i)
6535MS (53-38 μm)	58.30	×	×	*Possible fit*	(ii)
6535MS (75-53 μm)	35.20	*Possible fit*	×	*Possible fit*	(iii)
6535MS (90-75 μm)	29.25	×	×	×	-
6535SF	28.67	*Good*	×	*Possible fit*	(iv)
7525MS (53-38 μm)	44.13	×	*Possible fit*	*Possible fit*	(v)
7525MS (75-53 μm)	30.33	×	×	×	-
7525MS (90-75 μm)	23.80	*Possible fit*	×	×	(vi)
7525SF	21.43	*Possible fit*	×	*Possible fit*	(vii)

For the Phase 2 drug release, 65:35 and 75:25 PLGA devices exhibited varied degree of similarities to the Higuchi, first and zero order kinetics models at different stages. The overall poor fitting of the three models in 50:50 PLGA devices may due to the fast degrading nature of 50:50 PLGA. The additional notes no. (i) to (viii) are discussed below:

(i) CPt-50:50SF exhibits partial similarity to the Higuchi model.

(ii) The zero order kinetic provides good fit to the drug release from CPt-65:35MS after day-five and thereafter.

(iii) The drug release profile of CPt-65:35MS with size fraction (75-53 μm) closely resembles the Higuchi model, and the zero order kinetic also fits well to the profile from day-four and thereafter.

(iv) The Higuchi model provides good fit to the drug release profile of CPt-65:35SF, and the zero order kinetic also fits well to the profile from day-four and thereafter.

(v) The first and zero order kinetics provide good fits to the drug release from CPt-75:25MS of size fraction (53-38 μm) after day-four and thereafter.

(vi) The Higuchi model provides good fit to the drug release profile of CPt-75:25MS of size fraction (90-75 μm) after day-one until the end of week-two.

(vii) The Higuchi model provides good fit to the profile of CPt-75:25SF. The profile also scatters closely to the zero order kinetic.

D. Derivation of three compartmental model, Equation 8.13

The pharmacokinetics of cisplatin release profiles can be derived from the rate equations using Laplace transformations (Mayersohn and Gibaldi, 1970). Converting a function into Laplace

space allows operations to be performed on the expressions more easily than in regular space. The Laplace transform (Equation 12.1) is widely used in science and engineering for solving integrals.

$$L\{f(t)\} = \int_0^\infty \exp(-s.t) f(t) dt \qquad (12.1)$$

Table 8.5: Common Laplace transformation of functions:

Function: f(t)	Laplace: f(s)
1	$\frac{1}{s}$
A	$\frac{A}{s}$
$A.e^{-at}$	$\frac{A}{(s+a)}$
$A/a.(1 - e^{-at})$	$\frac{A}{s(s+a)}$
$\frac{A}{(b-a)}(e^{-at} - e^{-bt})$	$\frac{A}{(s+a)(s+b)}$

Figure 12.16 (a reproduce of Figure 8.11) shows the scheme of drug release, where Q_2 and Q_3 are the amount of drug remained in two separate pools of the depot after the amount of drug, Q_1 has been released into solution. $Q_2(\infty)$ and $Q_3(\infty)$ are the amount of drug in the depot which will be released after a long time. k_2 and k_3 are the release rate constants of Pools A and B respectively.

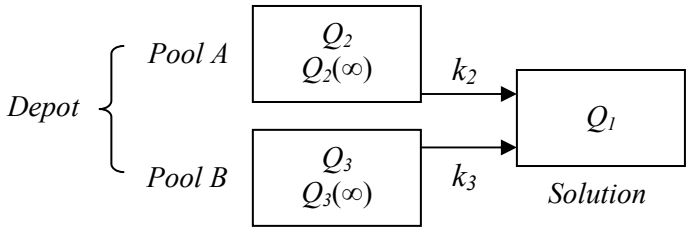

Figure 12.16: A three compartmental model showing the drug release from a two pools-releasing depot.

For the solution compartment: $$\frac{dQ_1}{dt} = k_2.Q_2 + k_2.Q_3 \qquad (12.2)$$

Q_2 decrease with: $$\frac{dQ_2}{dt} = -k_2.Q_2 \qquad (12.3)$$

Q_3 decrease with: $$\frac{dQ_3}{dt} = -k_3.Q_3 \qquad (12.4)$$

Transforming the differential Equations 12.2, 12.3 and 12.4 using Laplace transformation gives:

$$s.\overline{Q_1} - Q_1(0) = k_2.\overline{Q_2} + k_3.\overline{Q_3} \qquad (12.5)$$

$$s.\overline{Q_2} - Q_2(0) = -k_2.\overline{Q_2} \tag{12.6}$$

$$s.\overline{Q_3} - Q_3(0) = -k_3.\overline{Q_3} \tag{12.7}$$

$\overline{Q_2}$ and $\overline{Q_3}$ are Q_2 and Q_3 in Laplace space. With the initial conditions, $t = 0$; $Q_1(0) = 0$, $Q_2(0) = Q_2(\infty)$ and $Q_3(0) = Q_3(\infty)$. Rearranging Equations 12.6 and 12.7 give:

$$\overline{Q_2} = \frac{Q_2(\infty)}{s + k_2} \tag{12.8}$$

$$\overline{Q_3} = \frac{Q_3(\infty)}{s + k_3} \tag{12.9}$$

Substituting Equations 12.8 and 12.9 into Equation 12.5 gives:

$$\overline{Q_1}.s = k_2 \frac{Q_2(\infty)}{s + k_2} + k_3 \frac{Q_3(\infty)}{s + k_3} \quad \text{or,}$$

$$\overline{Q_1} = \frac{k_2.Q_2(\infty)(s + k_3) + k_3.Q_3(\infty)(s + k_2)}{s.(s + k_2)(s + k_3)} \tag{12.10}$$

The general partial fraction theorem states that the function P(s)/Q(s) can be expressed as a sum of partial fractions, where P(s) is a polynomial with a lower degree in s than another polynomial, Q(s). General partial fraction theorem can be used to solve first order rate equations. This method (Equation 12.11), described as the fingerprint method (Bourne and Strauss, 1995).

$$L^{-1}\left\{\frac{P(s)}{Q(s)}\right\} = \sum_{i=1}^{n} \frac{p(\lambda_i)}{Q_i(\lambda_i)} e^{\lambda_i t} \tag{12.11}$$

The inverse Laplace transformation of a quotient of two polynomials of the form *P(s)/Q(s)* can be expressed as the sum of the expression with each root substituted in turn. This is true provided that Q(s) has a higher degree in s and contains the factor $(s - \lambda_i)$ which is not repeated. P (λ_i) is the value of the numerator for each s term. Q_i (λ_i) is the value of the denominator when λ_i is substituted for s terms apart from the term containing λ_i which is excluded.

Equation 12.10 can be solved using the fingerprint method. The degree in s of the polynomial in the denominator of Equation 12.10 is higher than the polynomial in the numerator and there are no repeating terms so the fingerprint method may be applied. The roots are found by letting each factor of the denominator be zero so s = 0, $-k_2$ and $-k_3$. To transform this into an expression in real space each root is substituted for s in turn (excluding the polynomial term) and then multiplied by the exponential of the product of time and the root, $\exp(\lambda_i t)$. The sum of these three

values is the integrated function Q_1. By anti-Laplace transformation and solving Equation 12.10 for Q_1 will yield:

$$L^{-1}\{\overline{Q_1}\} = Q_1 = \left(\begin{array}{l} \dfrac{k_2.k_3[Q_2(\infty)+Q_3(\infty)]}{(k_2.k_3)} \\ + \dfrac{k_2.Q_2(\infty)(-k_2+k_3)}{-k_2(-k_2+k_3)}.e^{-k_2 t} \\ + \dfrac{k_3.Q_3(\infty)(-k_3+k_2)}{-k_3(-k_3+k_2)}.e^{-k_3 t} \end{array} \right)$$

$Q_1 = \left[Q_2(\infty).(1-e^{-k_2 t})\right] + \left[Q_3(\infty).(1-e^{-k_3 t})\right]$, as expressed in Equation 8.12

E. Fittings of two and three compartmental models to cisplatin release profiles.

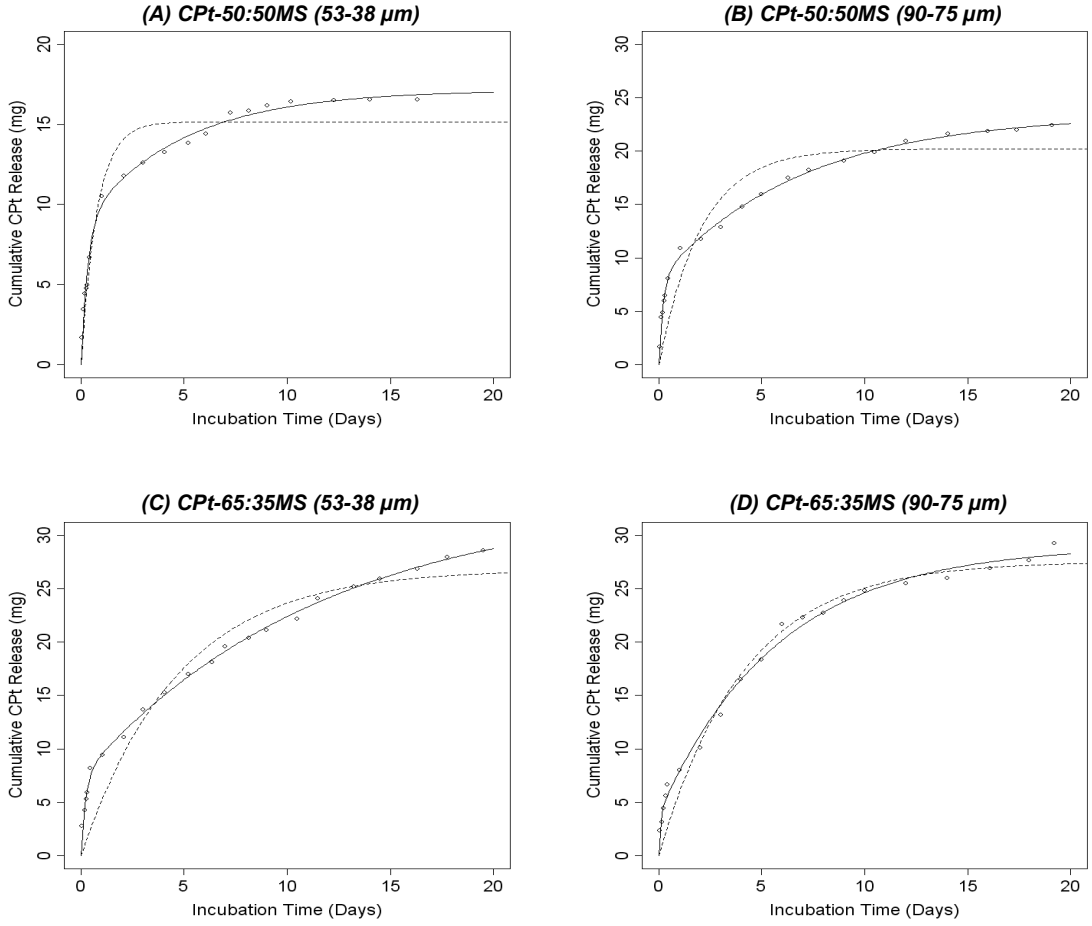

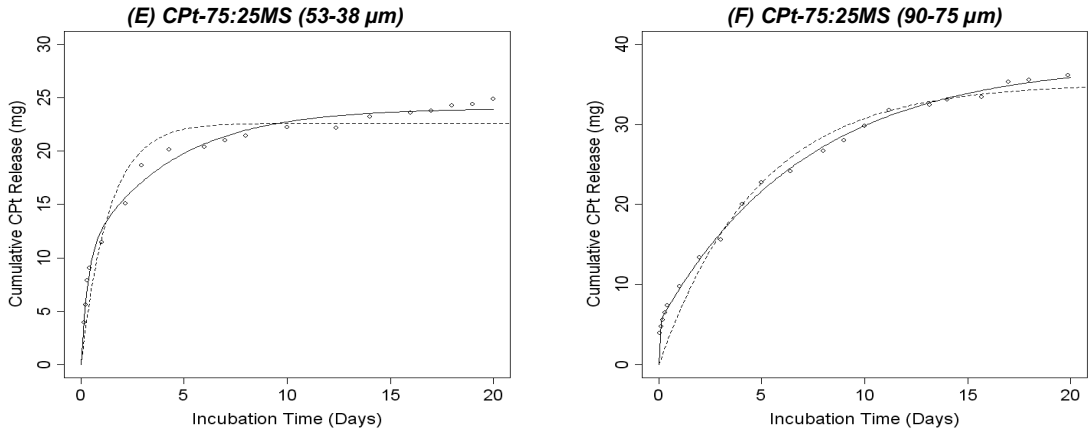

Figure 12.17: Fittings of a two compartmental model, Equation 8.11 (dashed lines) and a three compartmental model, Equation 8.13 (solid lines) to cisplatin release profiles of (A) CPt-50:50MS (53-38 µm), (B) CPt-50:50MS (90-75 µm), (C) CPt-65:35MS (53-38 µm), (D) CPt-65:35MS (90-75 µm), (E) CPt-75:25MS (53-38 µm) and (F) CPt-75:25MS (90-75 µm).

F. Statistics of model fittings using a two compartmental model (Equation 8.11) and a three compartmental model (Equation 8.13) to cisplatin release profiles.

CPt-50:50MS (53-38 µm)

$$Q_1 = \left[Q_2(\infty).(1-e^{-k_2 t})\right] + \left[Q_3(\infty).(1-e^{-k_3 t})\right]$$

Estimate	Std. Error	t value	Pr(>|t|)
$Q_2(\infty)$ 8.35005	0.72329	11.545	7.32e-09 ***
$Q_3(\infty)$ 8.79112	0.90312	9.734	7.11e-08 ***
k_1 0.20653	0.04765	4.334	0.00059 ***
k_2 3.07252	0.46977	6.541	9.35e-06 ***

Residual standard error: 0.4895 on 15 degrees of freedom
Number of iterations to convergence: 9
Achieved convergence tolerance: 1.707e-06
AIC: 32.28352

$$Q_1 = Q_0(\infty).(1-e^{-k_o t})$$

Estimate	Std. Error	t value	Pr(>|t|)
$Q_0(\infty)$ 15.1578	0.4103	36.944	< 2e-16 ***
k_o 1.2815	0.1881	6.814	3.02e-06 ***

Residual standard error: 1.359 on 17 degrees of freedom
Number of iterations to convergence: 15
Achieved convergence tolerance: 8.28e-06
AIC: 69.45698
*Significance codes: ***=0 ; **=0.001; *=0.01 ; .=0.5*

CPt-50:50MS (75-53 µm)

$$Q_1 = \left[Q_2(\infty).(1-e^{-k_2 t})\right] + \left[Q_3(\infty).(1-e^{-k_3 t})\right]$$

Estimate	Std. Error	t value	Pr(>|t|)
$Q_2(\infty)$ 16.52474	0.57272	28.853	7.00e-16 ***
$Q_3(\infty)$ 7.76413	0.61203	12.686	4.28e-10 ***
k_1 0.24569	0.01956	12.561	4.98e-10 ***

k_2	8.20045	1.47863	5.546	3.56e-05 ***

Residual standard error: 0.5491 on 17 degrees of freedom
Number of iterations to convergence: 9
Achieved convergence tolerance: 3.869e-06
AIC: 39.97783

$$Q_1 = Q_0(\infty).(1 - e^{-k_o t})$$

Estimate	Std. Error	t value	Pr(>|t|)
$Q_0(\infty)$ 22.3528	0.8036	27.814	< 2e-16 ***
k_o 0.6722	0.1328	5.062	6.93e-05 ***

Residual standard error: 2.577 on 19 degrees of freedom
Number of iterations to convergence: 15
Achieved convergence tolerance: 9.408e-06
AIC: 103.2542
*Significance codes: ***=0 ; **=0.001; *=0.01 ; .=0.5*

CPt-50:50MS (90-75 µm)

$$Q_1 = \left[Q_2(\infty).(1 - e^{-k_2 t})\right] + \left[Q_3(\infty).(1 - e^{-k_3 t})\right]$$

Estimate	Std. Error	t value	Pr(>|t|)
$Q_2(\infty)$ 15.39650	0.43822	35.134	< 2e-16 ***
$Q_3(\infty)$ 8.04881	0.47105	17.087	1.07e-11 ***
k_1 0.14412	0.01377	10.469	1.45e-08 ***
k_2 4.90482	0.60077	8.164	4.26e-07 ***

Residual standard error: 0.4154 on 16 degrees of freedom
Number of iterations to convergence: 8
Achieved convergence tolerance: 1.167e-06
AIC: 27.15193

$$Q_1 = Q_0(\infty).(1 - e^{-k_o t})$$

Estimate	Std. Error	t value	Pr(>|t|)
$Q_0(\infty)$ 20.21224	0.90969	2.219	1.55e-14 ***
k_o 0.48730	0.09921	4.912	0.000112 ***

Residual standard error: 2.541 on 18 degrees of freedom
Number of iterations to convergence: 16
Achieved convergence tolerance: 9.648e-06
AIC: 97.94559
*Significance codes: ***=0 ; **=0.001; *=0.01 ; .=0.5*

CPt-50:50SF

$$Q_1 = \left[Q_2(\infty).(1 - e^{-k_2 t})\right] + \left[Q_3(\infty).(1 - e^{-k_3 t})\right]$$

Estimate	Std. Error	t value	Pr(>|t|)	
$Q_2(\infty)$ 24.7724	0.5057	48.982	< 2e-16 ***	
$Q_3(\infty)$ 4.2862	0.5960	7.192	1.08e-06 ***	
k_1 0.1599	0.0096	16.605	2.32e-12 ***	
k_2 4.0296	1.0661	3.779	0.0014 **	
$Q_0(\infty)$ 27.4082	0.7202	38.05	< 2e-16 ***	
k_o 0.2274	0.0189	12.04	1.29e-10 ***	80.7240

Residual standard error: 0.4154 on 16 degrees of freedom
Number of iterations to convergence: 8
Achieved convergence tolerance: 1.167e-06
AIC: 27.15193

$$Q_1 = Q_0(\infty).(1 - e^{-k_o t})$$

Estimate	Std. Error	t value	Pr(>|t|)
$Q_0(\infty)$ 27.40817	0.72022	38.05	< 2e-16 ***

k_0	0.22739	0.01889	12.04	1.29e-10 ***

Residual standard error: 1.387 on 20 degrees of freedom
Number of iterations to convergence: 8
Achieved convergence tolerance: 2.792e-06
AIC: 80.72395
*Significance codes: ***=0 ; **=0.001; *=0.01 ; .=0.5*

CPt-65:35MS (53-38 µm)

$$Q_1 = \left[Q_2(\infty).(1-e^{-k_2 t})\right] + \left[Q_3(\infty).(1-e^{-k_3 t})\right]$$

Estimate	Std. Error	t value	Pr(>|t|)
$Q_2(\infty)$ 12.19541	0.43336	28.141	4.69e-15 ***
$Q_3(\infty)$ 9.01762	0.46339	19.460	1.46e-12 ***
k_1 0.19257	0.01928	9.990	2.79e-08 ***
k_2 7.81159	1.06592	7.329	1.70e-06 ***

Residual standard error: 0.4738 on 16 degrees of freedom
Number of iterations to convergence: 18
Achieved convergence tolerance: 5.379e-06
AIC: 32.41882

$$Q_1 = Q_0(\infty).(1-e^{-k_o t})$$

Estimate	Std. Error	t value	Pr(>|t|)
$Q_0(\infty)$ 18.6035	0.6641	28.012	2.69e-16 ***
k_o 1.3568	0.2965	4.577	0.000234 ***

Residual standard error: 2.396 on 18 degrees of freedom
Number of iterations to convergence: 23
Achieved convergence tolerance: 9.785e-06
AIC: 95.60209
*Significance codes: ***=0 ; **=0.001; *=0.01 ; .=0.5*

CPt-65:35MS (75-53 µm)

$$Q_1 = \left[Q_2(\infty).(1-e^{-k_2 t})\right] + \left[Q_3(\infty).(1-e^{-k_3 t})\right]$$

Estimate	Std. Error	t value	Pr(>|t|)
$Q_2(\infty)$ 26.05405	0.979779	26.592	2.72e-15 ***
$Q_3(\infty)$ 7.39633	0.468179	15.798	1.36e-11 ***
k_1 0.085761	0.008593	9.981	1.59e-08 ***
k_2 4.495799	0.653625	6.878	2.68e-06 ***

Residual standard error: 0.468 on 17 degrees of freedom
Number of iterations to convergence: 5
Achieved convergence tolerance: 8.527e-07
AIC: 33.26819

$$Q_1 = Q_0(\infty).(1-e^{-k_o t})$$

Estimate	Std. Error	t value	Pr(>|t|)
$Q_0(\infty)$ 26.8117	1.43159	18.729	1.05e-13 ***
k_o 0.21359	0.03464	6.167	6.32e-06 ***

Residual standard error: 2.563 on 19 degrees of freedom
Number of iterations to convergence: 10
Achieved convergence tolerance: 4.737e-06
AIC: 103.0168
*Significance codes: ***=0 ; **=0.001; *=0.01 ; .=0.5*

CPt-65:35MS (90-75 µm)

$$Q_1 = \left[Q_2(\infty).(1-e^{-k_2 t})\right] + \left[Q_3(\infty).(1-e^{-k_3 t})\right]$$

Estimate	Std. Error	t value	Pr(>|t|)
$Q_2(\infty)$ 25.13164	0.65202	38.544	< 2e-16 ***

$Q_3(\infty)$ 3.89737	0.54794	7.113	2.46e-06 ***
k_1 0.17419	0.01304	13.360	4.28e-10 ***
k_2 12.49721	7.10914	1.758	0.0979 .

Residual standard error: 0.7816 on 16 degrees of freedom
Number of iterations to convergence: 11
Achieved convergence tolerance: 7.323e-06
AIC: 52.43635

$$Q_1 = Q_0(\infty).(1 - e^{-k_o t})$$

Estimate	Std. Error	t value	Pr(>|t|)
$Q_0(\infty)$ 27.55376	0.96233	28.632	< 2e-16 ***
k_o 0.24053	0.02635	9.128	3.57e-08 ***

Residual standard error: 1.818 on 18 degrees of freedom
Number of iterations to convergence: 8
Achieved convergence tolerance: 2.204e-06
AIC: 84.56192

CPt-65:35SF

$$Q_1 = \left[Q_2(\infty).(1 - e^{-k_2 t})\right] + \left[Q_3(\infty).(1 - e^{-k_3 t})\right]$$

Estimate	Std. Error	t value	Pr(>|t|)
$Q_2(\infty)$ 33.90212	1.242404	27.288	7.60e-15 ***
$Q_3(\infty)$ 5.57445	0.315646	17.660	6.45e-12 ***
k_1 0.082115	0.006239	13.161	5.34e-10 ***
k_2 15.039469	3.467380	4.337	0.000509 ***

Residual standard error: 0.5228 on 16 degrees of freedom
Number of iterations to convergence: 12
Achieved convergence tolerance: 5.177e-06
AIC: 36.35148

$$Q_1 = Q_0(\infty).(1 - e^{-k_o t})$$

Estimate	Std. Error	t value	Pr(>|t|)
$Q_0(\infty)$ 32.23218	2.25083	14.320	2.79e-11 ***
k_o 0.15814	0.02675	5.911	1.35e-05 ***

Residual standard error: 2.621 on 18 degrees of freedom
Number of iterations to convergence: 8
Achieved convergence tolerance: 4.976e-06
AIC: 99.18538
*Significance codes: ***=0 ; **=0.001; *=0.01 ; .=0.5*

CPt-75:25 (53-38 μm)

$$Q_1 = \left[Q_2(\infty).(1 - e^{-k_2 t})\right] + \left[Q_3(\infty).(1 - e^{-k_3 t})\right]$$

Estimate	Std. Error	t value	Pr(>|t|)
$Q_2(\infty)$ 13.98408	1.41207	9.903	5.68e-08 ***
$Q_3(\infty)$ 10.04156	1.55952	6.439	1.12e-05 ***
k_1 0.23892	0.04307	5.547	5.59e-05 ***
k_2 3.19795	0.77464	4.128	0.000894 ***

Residual standard error: 0.8156 on 15 degrees of freedom
Number of iterations to convergence: 20
Achieved convergence tolerance: 5.022e-06
AIC: 51.6827

$$Q_1 = Q_0(\infty).(1 - e^{-k_o t})$$

Estimate	Std. Error	t value	Pr(>|t|)
$Q_0(\infty)$ 22.6096	0.5678	39.82	< 2e-16 ***
k_o 0.7371	0.1049	7.03	2.03e-06 ***

Residual standard error: 1.905 on 17 degrees of freedom
Number of iterations to convergence: 12
Achieved convergence tolerance: 9.495e-06
AIC: 82.2888
*Significance codes: ***=0 ; **=0.001; *=0.01 ; .=0.5*

CPt-75:25 (75-53 µm)

$$Q_1 = \left[Q_2(\infty).(1-e^{-k_2 t})\right] + \left[Q_3(\infty).(1-e^{-k_3 t})\right]$$

Estimate	Std. Error	t value	Pr(>|t|)
$Q_2(\infty)$ 25.0102	0.409857	61.022	< 2e-16 ***
$Q_3(\infty)$ 3.8942	0.404434	9.629	4.64e-08 ***
k_1 0.195255	0.009678	0.176	8.36e-13 ***
k_2 12.347591	4.226931	2.921	0.01 **

Residual standard error: 0.5112 on 16 degrees of freedom
Number of iterations to convergence: 16
Achieved convergence tolerance: 4.050e-06
AIC: 35.45113

$$Q_1 = Q_0(\infty).(1-e^{-k_o t})$$

Estimate	Std. Error	t value	Pr(>|t|)
$Q_0(\infty)$ 27.70841	0.73294	37.80	<2e-16 ***
k_o 0.26951	0.02653	10.16	7e-09 ***

Residual standard error: 1.666 on 18 degrees of freedom
Number of iterations to convergence: 9
Achieved convergence tolerance: 1.870e-06
AIC: 81.07726
*Significance codes: ***=0 ; **=0.001; *=0.01 ; .=0.5*

CPt-75:25(90-75 µm)

$$Q_1 = \left[Q_2(\infty).(1-e^{-k_2 t})\right] + \left[Q_3(\infty).(1-e^{-k_3 t})\right]$$

Estimate	Std. Error	t value	Pr(>|t|)
$Q_2(\infty)$ 32.6182	0.520628	62.652	< 2e-16 ***
$Q_3(\infty)$ 5.1879	0.321689	16.127	9.75e-12 ***
k_1 0.140962	0.006559	21.491	9.21e-14 ***
k_2 28.486878	9.210367	3.093	0.0066 **

Residual standard error: 0.586 on 17 degrees of freedom
Number of iterations to convergence: 15
Achieved convergence tolerance: 4.656e-06
AIC: 42.71155

$$Q_1 = Q_0(\infty).(1-e^{-k_o t})$$

Estimate	Std. Error	t value	Pr(>|t|)
$Q_0(\infty)$ 35.11144	1.33399	26.321	< 2e-16 ***
k_o 0.20826	0.02511	8.295	9.75e-08 ***

Residual standard error: 2.476 on 19 degrees of freedom
Number of iterations to convergence: 8
Achieved convergence tolerance: 2.994e-06
AIC: 101.5682
*Significance codes: ***=0 ; **=0.001; *=0.01 ; .=0.5*

CPt-75:25SF

$$Q_1 = \left[Q_2(\infty).(1-e^{-k_2 t})\right] + \left[Q_3(\infty).(1-e^{-k_3 t})\right]$$

Estimate	Std. Error	t value	Pr(>|t|)
$Q_2(\infty)$ 47.7667	7.448342	6.413	2.96e-06 ***
$Q_3(\infty)$ 5.6224	0.400147	14.051	7.98e-12 ***
k_1 0.035098	0.007781	4.511	0.000213 ***

k_2	9.929343	2.531226	3.923	0.000843 ***

Residual standard error: 0.6175 on 20 degrees of freedom
Number of iterations to convergence: 14
Achieved convergence tolerance: 9.686e-06
AIC: 50.59237

$$Q_1 = Q_0(\infty).(1 - e^{-k_o t})$$

Estimate	Std. Error	t value	Pr(>|t|)
$Q_0(\infty)$ 30.52106	2.61234	11.68	6.63e-11 ***
K_o 0.11638	0.02151	5.41	1.97e-05 ***

Residual standard error: 2.348 on 22 degrees of freedom
Number of iterations to convergence: 8
Achieved convergence tolerance: 2.629e-06
AIC: 112.9819
*Significance codes: ***=0 ; **=0.001; *=0.01 ; .=0.5*

G. Examples of residual error plots from fittings of model equation 8.13 to CPt release profiles.

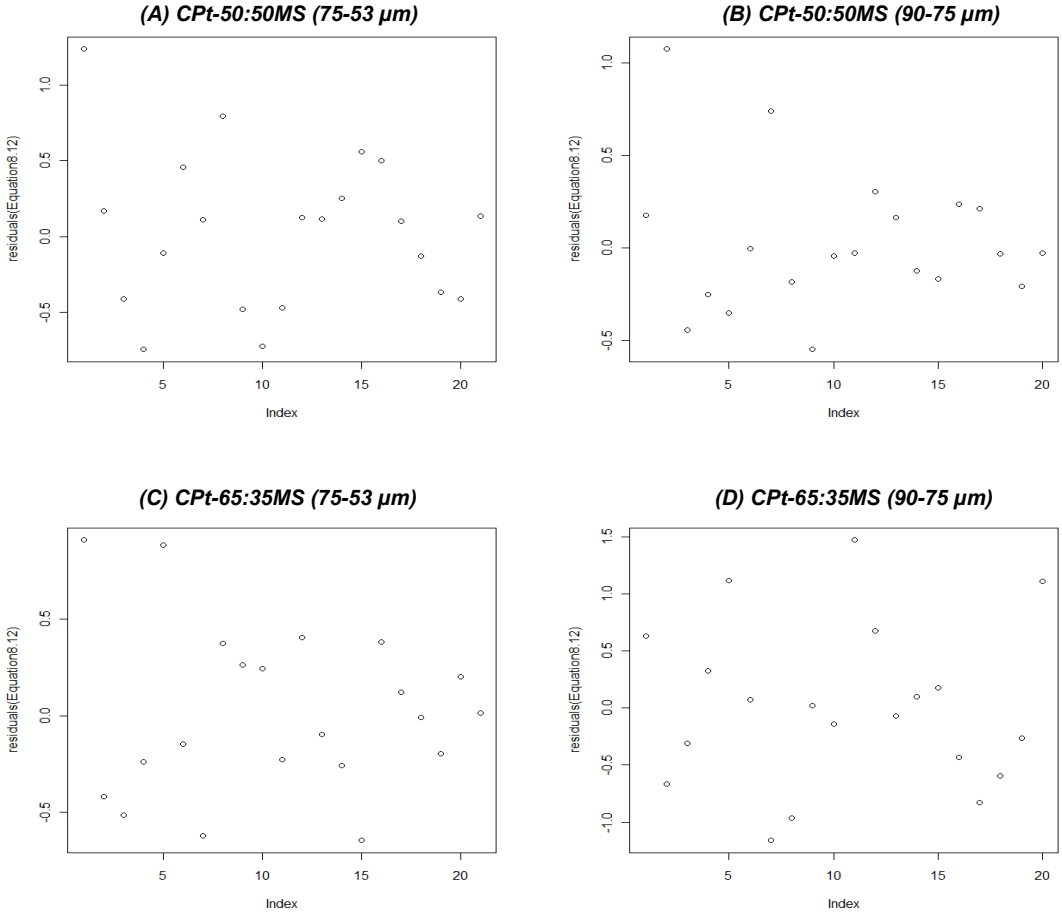

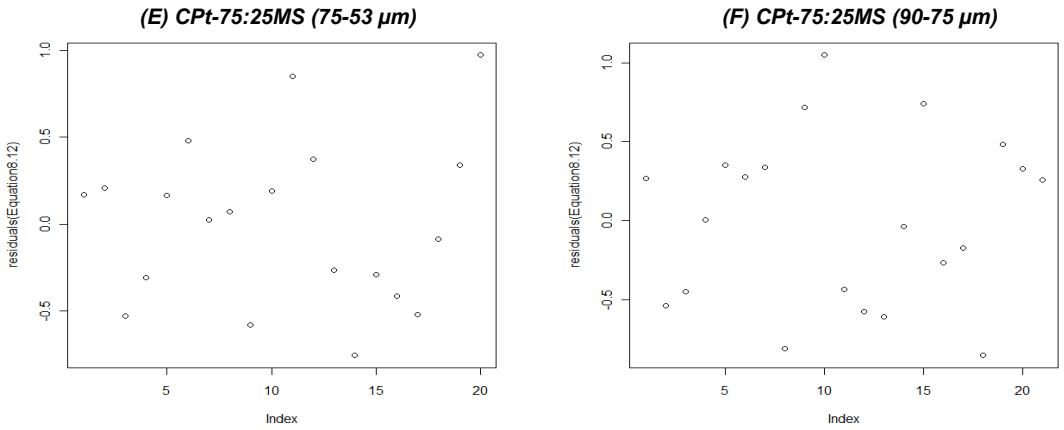

Figure 12.18: Examples of residual error plots from fittings of model Equation 8.13 to cisplatin release profiles of (A) CPt-50:50MS (75-53 µm), (B) CPt-50:50MS (90-75 µm), (C) CPt-65:35MS (75-53 µm), (D) CPt-65:35MS (90-75 µm), (E) CPt-75:25MS (75-53 µm) and (F) CPt-75:25MS (90-75 µm).

H. Akaike's Information Criterion (AIC)

Akaike's Information Criterion (AIC) (Akaike, 1974) allows comparison of mathematical models of data by trading off the number of parameters used against the residual error. AIC is calculated from statistical fitting parameters using Equation 12.12.

$$\mathrm{AIC} = 2p - 2.\ln(L) \qquad (12.12)$$

p is the number of parameters including the sum of squares, L is the likelihood function and 2 is the numeric penalty for each parameter. AIC values can be used to compare different models of a dataset. The model with the lowest AIC is preferred by this method. AIC can be used in conjunction with hypothesis testing methods such as analysis of variance/covariance during model comparison. The advantage of AIC is that unlike hypothesis testing there is no concern that the sequence of analysis will affect the results.

I. Samples calculation of surface area and volume of microspheres, hollow and solid fibres.

The density of a 200 mg sample was estimated by the displacement of water, with property of 15 % (w/w) 50:50MS; median size or D[v, 0.5] ≈ 26 µm, radius ≈ 13 µm.

Density = Mass / Volume
= 200 mg / 0.130 cm^3
= 0.154 mg/cm^3

Volume (one microsphere) = 4/3.π.(Radius of microspheres)^3
= 9.20 x 10^{-9} cm^3

Number of microspheres (sample) = Volume (sample) / Volume (one microsphere)
= 0.130 cm^3 / 9.2 x 10^{-9} cm^3 = 1.41 x 10^7

Surface area (one microsphere) = $4.\pi.(\text{Radius of microsphere})^2$
= 2.12×10^{-5} cm^2
Total Surface area (sample) = 2.12×10^{-5} $cm^2 * 1.41 \times 10^7$
= 299 cm^2 (radius of 13 μm)
= 92.86 cm^2 (radius of 42 μm, D[v, 0.9] ≈ 84 μm)

The density of a 200 mg sample was estimated by the displacement of water; with property of 20 % (w/w) 50:50SF; 8 cm in length, *OD* ≈ 670 μm and radius ≈ 335 μm.

Density (sample) = Mass / Volume
= 200 mg / 0.65 cm^3
= 307 mg/cm^3
Volume (one fibre) = $\pi.(\text{Radius of fibre})^2.\text{Length of fibre}$
= 2.83×10^{-2} cm^3
Surface area (one fibre) = $2.\pi.\text{Radius of fibre.Length} + 2.\pi.(\text{Radius of fibre})^2$
= 3.24 cm^2

Table 12.6: Estimate surface area:volume ratio of 15 % (w/w) PLGA microspheres in a 0.2 g sample.

PLGA	Size Fraction	Diameter (10^{-6} m)	Number of microspheres (10^7)	Surface area (10^{-5} cm^2)	Total Surface Area (cm^2)	Volume of one microsphere (10^{-9} cm^3)	Surface Area:Volume
50:50 MS	D [v, 0.1]	6	114.9303	0.1131	1300.00	0.1131	100.00
	D [v, 0.5]	26	1.4124	2.1240	300.00	9.2040	23.08
	D [v, 0.9]	84	0.0419	22.1700	92.86	310.3793	7.14
65:35 MS	D [v, 0.1]	8	48.4862	0.2011	975.00	0.2681	75.00
	D [v, 0.5]	45	0.2724	6.3626	173.33	47.7191	13.33
	D [v, 0.9]	90	0.0341	25.4502	86.67	381.7530	6.67
75:25 MS	D [v, 0.1]	4.7	239.1084	0.0694	1659.57	0.0544	127.66
	D [v, 0.5]	53	0.1667	8.8259	147.17	77.9619	11.32
	D [v, 0.9]	107	0.0203	35.9728	72.90	641.5142	5.61

Table 12.7: Estimate surface area:volume ratio of 20 % (w/w) PLGA hollow and solid fibres.

PLGA	Diameter (10^{-6} m)	Number of fibres	Surface area (10^{-5} cm^2)	Total Surface Area (cm^2)	Volume of one fibre (10^{-9} cm^3)	Surface Area:Volume
50:50SF	670	10	16.8432	168.43	2.8209	5.97
65:35SF	720	10	18.1002	181.00	3.2576	5.56
75:25SF	760	10	19.1057	191.06	3.6296	5.26
50:50HF	690	10	17.3460	173.46	2.9918	5.80
65:35HF	750	10	18.8544	188.54	3.5348	5.33
75:25HF	850	10	21.3683	213.68	4.5402	4.71
Lumen	210	10	5.2792	52.29	0.2771	19.05

APPENDIX VII

A. Fittings of two and three compartmental models to lidocaine release profiles.

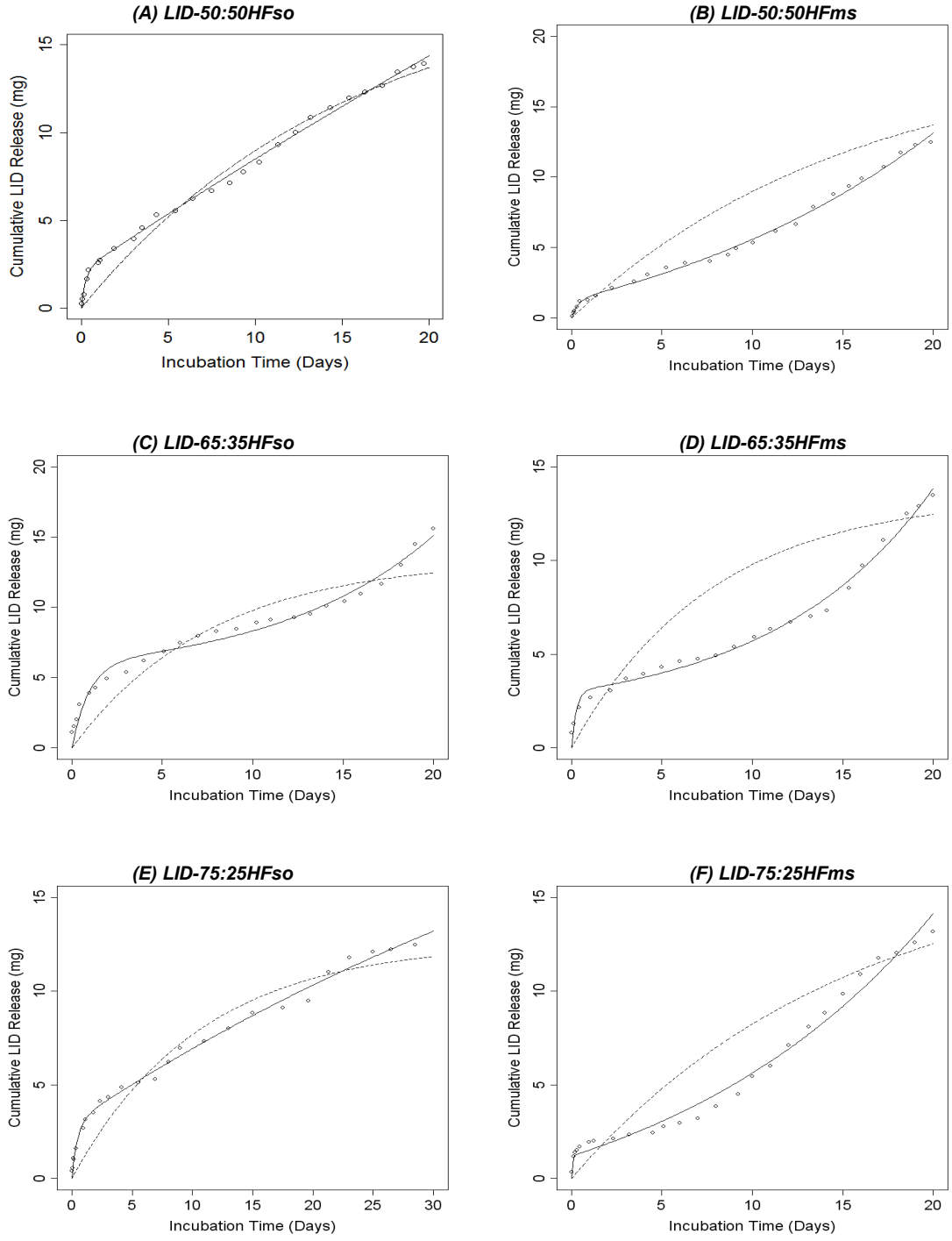

Figure 12.19: Fittings of a two compartmental model, Equation 8.11 (dashed lines) and a three compartmental model, Equation 8.13 (solid lines) to lidocaine release profiles of (A) LID-50:50HFso, (B) LID-50:50HFms, (C) LID-65:35HFso, (D) LID-65:35HFms, (E) LID-75:25HFso and (F) LID-75:25HFms.

B. Statistics of model fittings using a two compartmental model (Equation 8.11) and a three compartmental model (Equation 8.13) to lidocaine release profiles.

LID-50:50MS

$$Q_1 = \left[Q_2(\infty).(1-e^{-k_2 t})\right] + \left[Q_3(\infty).(1-e^{-k_3 t})\right]$$

Estimate	Std. Error	t value	Pr(>|t|)
$Q_2(\infty)$ 22.02026	3.17506	6.935	9.83e-07 ***
$Q_3(\infty)$ 12.29079	2.82720	4.347	0.000312 ***
k_2 0.07556	0.04218	1.791	0.088363 .
k_3 0.77467	0.19225	4.030	0.000656 ***

Residual standard error: 0.7222 on 20 degrees of freedom
Number of iterations to convergence: 8
Achieved convergence tolerance: 1.893e-06
AIC: 58.10834

$$Q_1 = Q_0(\infty).(1-e^{-k_0 t})$$

Estimate	Std. Error	t value	Pr(>|t
Q_0 26.66148	0.58721	45.40	< 2e-16 ***
k_o 0.27268	0.02062	13.22	6.03e-12 ***

Residual standard error: 1.338 on 22 degrees of freedom
Number of iterations to convergence: 9
Achieved convergence tolerance: 4.257e-06
AIC: 86.00245
*Significance codes: ***=0 ; **=0.001; *=0.05 ; .=0.1*

LID-50:50HF

$$Q_1 = \left[Q_2(\infty).(1-e^{-k_2 t})\right] + \left[Q_3(\infty).(1-e^{-k_3 t})\right]$$

Estimate	Std. Error	t value	Pr(>|t
$Q_2(\infty)$ 10.9094	0.1892	15.374	2.99e-13 ***
$Q_3(\infty)$ 1.2455	0.3818	3.262	0.00357 **
k_2 0.0756	0.5549	5.067	4.49e-05 ***
k_3 -7.4101	0.0132	-7.630	1.29e-07 ***

Residual standard error: 0.3276 on 22 degrees of freedom
Number of iterations to convergence: 13
Achieved convergence tolerance: 3.827e-06
AIC: 21.40553

$$Q_1 = Q_0(\infty).(1-e^{-k_0 t})$$

Estimate	Std. Error	t value	Pr(>|t
Q_0 18.33830	8.68559	2.111	0.0453 *
k_o 0.03782	0.02402	1.574	0.1285 .

Residual standard error: 1.174 on 24 degrees of freedom
Number of iterations to convergence: 11
Achieved convergence tolerance: 4.36e-06
AIC: 86.04993
*Significance codes: ***=0 ; **=0.001; *=0.05 ; .=0.1*

LID-50:50HFso

$$Q_1 = \left[Q_2(\infty).(1-e^{-k_2 t})\right] + \left[Q_3(\infty).(1-e^{-k_3 t})\right]$$

Estimate	Std. Error	t value	Pr(>|t|)
$Q_2(\infty)$ 8.707023	2.143706	1.567	0.130781
$Q_3(\infty)$ 12.120003	1.163884	12.936	4.87e-12 ***
k_2 0.098123	0.005647	1.439	0.163749
k_3 0.2874176	0.923485	4.195	0.000346 ***

Residual standard error: 0.2359 on 23 degrees of freedom
Number of iterations to convergence: 9
Achieved convergence tolerance: 3.356e-06
AIC: 4.309898

$$Q_1 = Q_0(\infty).(1 - e^{-k_0 t})$$

Estimate	Std. Error	t value	Pr(>|t
Q_0 18.94823	2.12056	8.935	2.95e-09 ***
k_o 0.06422	0.01156	5.557	8.88e-06 ***

Residual standard error: 0.7933 on 25 degrees of freedom
Number of iterations to convergence: 6
Achieved convergence tolerance: 3.661e-06
AIC: 60.1035
*Significance codes: ***=0 ; **=0.001; *=0.05 ; .=0.1*

LID-50:50HFms

$$Q_1 = \left[Q_2(\infty).(1 - e^{-k_2 t})\right] + \left[Q_3(\infty).(1 - e^{-k_3 t})\right]$$

Estimate	Std. Error	t value	Pr(>|t
$Q_2(\infty)$ 12.051739	2.763448	3.530	0.00210 **
$Q_3(\infty)$ 0.21886	0.021540	9.771	4.67e-09 ***
k_2 0.0799924	0.003278	3.028	0.00665 **
k_3 2.767558	0.811771	3.402	0.00283 **

Residual standard error: 0.1818 on 20 degrees of freedom
Number of iterations to convergence: 18
Achieved convergence tolerance: 4.391e-06
AIC: 8.095792

$$Q_1 = Q_0(\infty).(1 - e^{-k_0 t})$$

Estimate	Std. Error	t value	Pr(>|t
Q_0 19.092299	2.191163	8.713	1.39e-08 ***
k_o 0.034749	0.005872	5.918	5.91e-06 ***

Residual standard error: 0.5041 on 22 degrees of freedom
Number of iterations to convergence: 6
Achieved convergence tolerance: 3.177e-06
AIC: 39.14331
*Significance codes: ***=0 ; **=0.001; *=0.05 ; .=0.1*

LID-65:35MS

$$Q_1 = \left[Q_2(\infty).(1 - e^{-k_2 t})\right] + \left[Q_3(\infty).(1 - e^{-k_3 t})\right]$$

Estimate	Std. Error	t value	Pr(>|t|)
$Q_2(\infty)$ 31.783322	0.573098	55.459	< 2e-16 ***
$Q_3(\infty)$ 2.984791	0.408576	7.305	1.96e-07 ***
k_2 0.144029	0.008001	18.000	4.74e-15 ***
k_3 6.602064	25.005155	1.464	0.157

Residual standard error: 0.7727 on 23 degrees of freedom
Number of iterations to convergence: 18
Achieved convergence tolerance: 1.260e-06
AIC: 68.36618

$$Q_1 = Q_0(\infty).(1 - e^{-k_0 t})$$

Estimate	Std. Error	t value	Pr(>|t
Q_0 33.27496	0.79488	41.86	< 2e-16 ***
k_o 0.18006	0.01272	14.16	1.92e-13 ***

Residual standard error: 1.49 on 25 degrees of freedom
Number of iterations to convergence: 6

Achieved convergence tolerance: 8.995e-06
AIC: 102.0084

LID-65:35HF

$$Q_1 = \left[Q_2(\infty).(1-e^{-k_2 t})\right] + \left[Q_3(\infty).(1-e^{-k_3 t})\right]$$

Estimate	Std. Error	t value	Pr(>|t|)
$Q_2(\infty)$ 9.285845	1.177237	7.255	2.88e-07 ***
$Q_3(\infty)$ 2.696044	0.193290	-4.773	9.13e-05 ***
k_2 0.05629	0.0051826	2.564	0.0177 *
k_3 -2.60709	0.006985	-8.052	5.30e-08 ***

Residual standard error: 0.59873 on 23 degrees of freedom
Number of iterations to convergence: 31
Achieved convergence tolerance: 8.786e-06
AIC: 9.057404

$$Q_1 = Q_0(\infty).(1-e^{-k_0 t})$$

Estimate	Std. Error	t value	Pr(>|t
Q_0 18.94823	2.12056	8.935	2.95e-09 ***
k_o 0.06422	0.01156	5.557	8.88e-06 ***

Residual standard error: 0.7933 on 25 degrees of freedom
Number of iterations to convergence: 6
Achieved convergence tolerance: 3.661e-06
AIC: 68.03946
*Significance codes: ***=0 ; **=0.001; *=0.05 ; .=0.1*

LID-65:35HFso

$$Q_1 = \left[Q_2(\infty).(1-e^{-k_2 t})\right] + \left[Q_3(\infty).(1-e^{-k_3 t})\right]$$

Estimate	Std. Error	t value	Pr(>|t|)
$Q_2(\infty)$ 15.10920	3.49559	12.327	4.43e-11 ***
$Q_3(\infty)$ 13.07159	2.68636	-1.561	0.133409
k_2 0.04387	0.02167	4.817	9.25e-05 ***
k_3 4.46216	2.27811	-4.029	0.000606 ***

Residual standard error: 0.5965 on 21 degrees of freedom
Number of iterations to convergence: 34
Achieved convergence tolerance: 9.358e-06
AIC: 50.75284

$$Q_1 = Q_0(\infty).(1-e^{-k_0 t})$$

Estimate	Std. Error	t value	Pr(>|t
Q_0 13.46539	1.27793	10.537	2.82e-10 ***
k_o 0.12958	0.02953	4.388	0.000214 ***

Residual standard error: 1.521 on 23 degrees of freedom
Number of iterations to convergence: 9
Achieved convergence tolerance: 5.249e-06
AIC: 95.81732
*Significance codes: ***=0 ; **=0.001; *=0.05 ; .=0.1*

LID-65:35HFms

$$Q_1 = \left[Q_2(\infty).(1-e^{-k_2 t})\right] + \left[Q_3(\infty).(1-e^{-k_3 t})\right]$$

Estimate	Sd. Error	t value	Pr(>|t|)
$Q_2(\infty)$ 13.0230	0.2086	14.490	1.01e-11 ***
$Q_3(\infty)$ 1.3233	0.3407	3.885	0.000997 ***
k_2 0.07671	1.2393	3.147	0.005307 **
k_3 -0.15108	0.0114	-9.721	8.28e-09 ***

Residual standard error: 0.3687 on 19 degrees of freedom

Number of iterations to convergence: 16
Achieved convergence tolerance: 6.75e-06
AIC: 24.98150

$$Q_1 = Q_0(\infty).(1 - e^{-k_0 t})$$

Estimate	Std. Error	t value	Pr(>|t
Q_0 13.46539	1.27793	10.537	2.82e-10 ***
k_o 0.12958	0.02953	4.388	0.000214 ***

Residual standard error: 1.521 on 23 degrees of freedom
Number of iterations to convergence: 9
Achieved convergence tolerance: 5.249e-06
AIC: 94.217332
*Significance codes: ***=0 ; **=0.001; *=0.05 ; .=0.1*

LID-75:25MS

$$Q_1 = \left[Q_2(\infty).(1 - e^{-k_2 t})\right] + \left[Q_3(\infty).(1 - e^{-k_3 t})\right]$$

Estimate	Std. Error	t value	Pr(>|t|)
$Q_2(\infty)$ 32.611974	1.886674	22.056	< 2e-16 ***
$Q_3(\infty)$ 13.050198	0.597512	3.431	0.00228 **
k_2 0.076667	0.006925	9.627	1.56e-09 ***
k_3 0.154683	0.880979	1.309	0.20334

Residual standard error: 0.6317 on 23 degrees of freedom
Number of iterations to convergence: 16
Achieved convergence tolerance: 7.98e-06
AIC: 57.49235

$$Q_1 = Q_0(\infty).(1 - e^{-k_0 t})$$

Estimate	Std. Error	t value	Pr(>|t
Q_0 38.922223	1.369952	28.41	< 2e-16 ***
k_o 0.087583	0.005659	15.48	2.58e-14 ***

Residual standard error: 0.8817 on 25 degrees of freedom
Number of iterations to convergence: 6
Achieved convergence tolerance: 3.897e-07
AIC: 73.74509
*Significance codes: ***=0 ; **=0.001; *=0.05 ; .=0.1*

LID-75:25HF

$$Q_1 = \left[Q_2(\infty).(1 - e^{-k_2 t})\right] + \left[Q_3(\infty).(1 - e^{-k_3 t})\right]$$

Estimate	Std. Error	t value	Pr(>|t|)
$Q_2(\infty)$ 5.250921	0.906609	-5.792	9.49e-06 ***
$Q_3(\infty)$ 0.954253	0.109974	8.677	2.19e-08 ***
k_2 0.051714	0.005512	-9.382	5.85e-09 ***
k_3 5.9882	2.403051	2.492	0.0211 *

Residual standard error: 0.1792 on 21 degrees of freedom
Number of iterations to convergence: 18
Achieved convergence tolerance: 9.621e-06
AIC: 56.67551

$$Q_1 = Q_0(\infty).(1 - e^{-k_0 t})$$

Estimate	Std. Error	t value	Pr(>|t
Q_0 7.13025	1.62075	4.536	8.05e-07 **
k_o 0.1065	0.03139	2.016	0.00219 ***

Residual standard error: 0.9767 on 24 degrees of freedom
Number of iterations to convergence: 9
Achieved convergence tolerance: 5.84e-06
AIC: 76.47952

*Significance codes: ***=0 ; **=0.001; *=0.05 ; .=0.1*

LID-75:25HFso

$$Q_1 = \left[Q_2(\infty).(1-e^{-k_2 t})\right] + \left[Q_3(\infty).(1-e^{-k_3 t})\right]$$

Estimate	Std. Error	t value	Pr(>|t|)
$Q_2(\infty)$ 1.784686	26.06097	1.207	0.24023
$Q_3(\infty)$ 12.65089	0.26338	10.065	1.07e-09 ***
k_2 -0.081471	0.01051	-1.400	0.17544
k_3 0.71748	0.82194	3.306	0.00321

Residual standard error: 0.373 on 22 degrees of freedom
Number of iterations to convergence: 19
Achieved convergence tolerance: 1.421e-06
AIC: 28.15474

$$Q_1 = Q_0(\infty).(1-e^{-k_0 t})$$

Estimate	Std. Error	t value	Pr(>|t|)
Q_0 15.15432	4.20675	3.236	3.5e-05 **
k_o 0.076565	0.01639	4.006	0.000519 ***

Residual standard error: 0.9767 on 24 degrees of freedom
Number of iterations to convergence: 9
Achieved convergence tolerance: 5.84e-06
AIC: 76.47952
*Significance codes: ***=0 ; **=0.001; *=0.05 ; .=0.1*

LID-75:25HFms

$$Q_1 = \left[Q_2(\infty).(1-e^{-k_2 t})\right] + \left[Q_3(\infty).(1-e^{-k_3 t})\right]$$

Estimate	Std. Error	t value	Pr(>|t|)
$Q_2(\infty)$ 4.82709	1.32170	3.652	0.00140 **
$Q_3(\infty)$ 13.19786	0.21355	5.609	1.22e-05 ***
k_2 -0.06511	0.01019	-6.390	1.98e-06 ***
k_3 2.18657	27.46614	0.808	0.42787

Residual standard error: 0.5171 on 22 degrees of freedom
Number of iterations to convergence: 29
Achieved convergence tolerance: 6.654e-06
AIC: 45.14155

$$Q_1 = Q_0(\infty).(1-e^{-k_0 t})$$

Estimate	Std. Error	t value	Pr(>|t
Q_0 17.13025	2.62075	6.536	9.25e-07 *
k_o 0.06565	0.01639	4.006	0.000519 ***

Residual standard error: 0.9767 on 24 degrees of freedom
Number of iterations to convergence: 9
Achieved convergence tolerance: 5.84e-06
AIC: 77.41502
*Significance codes: ***=0 ; **=0.001; *=0.05 ; .=0.1*

C. Examples of residual error plots from fittings of model equation 8.13 to LID release profiles.

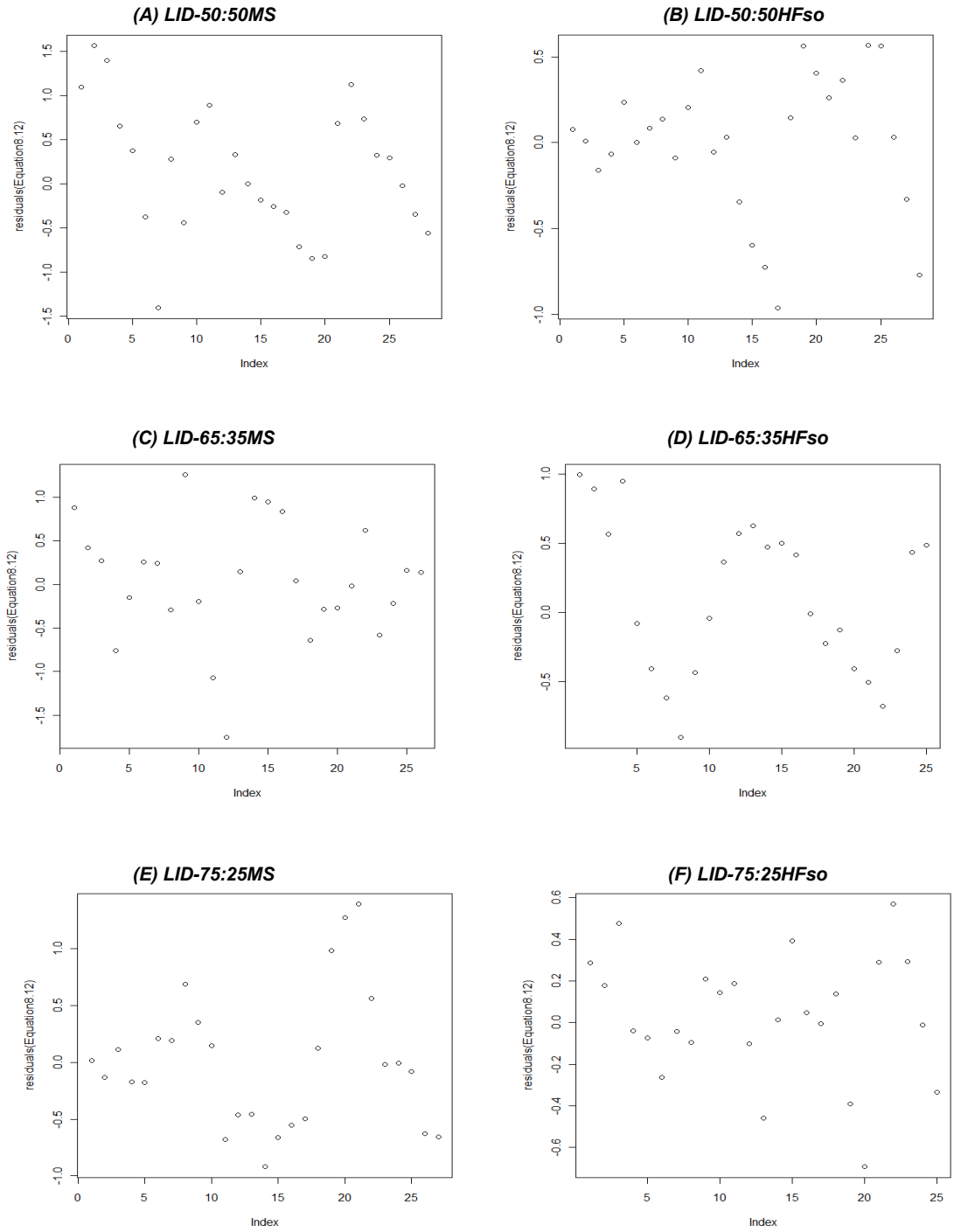

Figure 12.20: Examples of residual error plots from fittings of model Equation 8.13 to lidocaine release profiles of (A) LID-50:50MS, (B) LID-50:50HFso, (C) LID-65:35MS, (D) LID-65:35HFso, (E) LID-75:25MS and (F) LID-75:25HFso.

D. Fittings of Higuchi Model to Phase 1 lidocaine release from 65:35-MS and -SF.

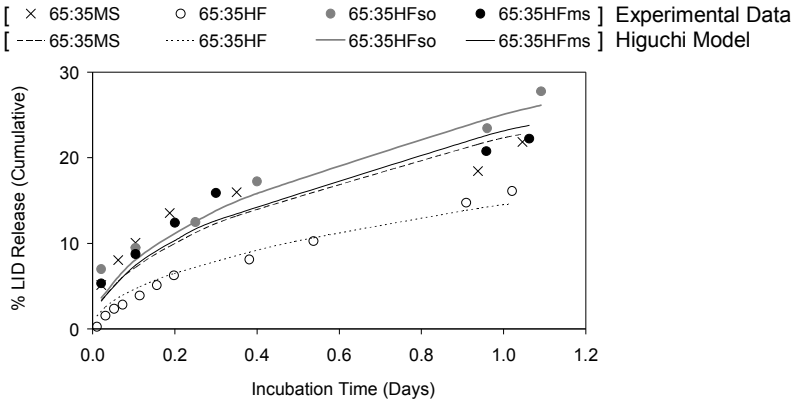

Figure 12.21: The fitting of Higuchi Model ($Q_t = k_H.t^{0.5}$) to *in vitro* Phase 1 lidocaine release from 65:35 PLGA microspheres and hollow fibres.

E. Fittings of Higuchi, first and zero order kinetics models to Phase 2 lidocaine release.

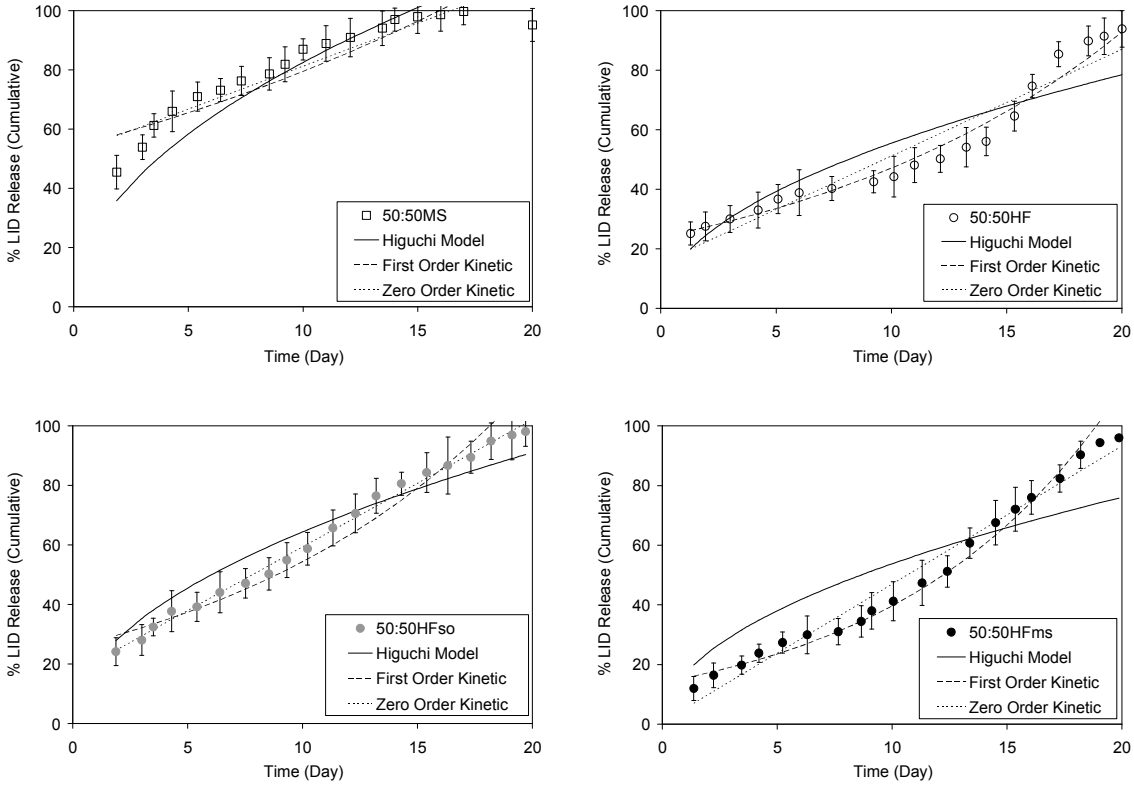

Figure 12.22: The fitting of Higuchi, first and zero order kinetics models in Phase 2 drug release from 50:50MS (□), 50:50HF (○), 50:50HFso (●) and 50:50HFms (●).

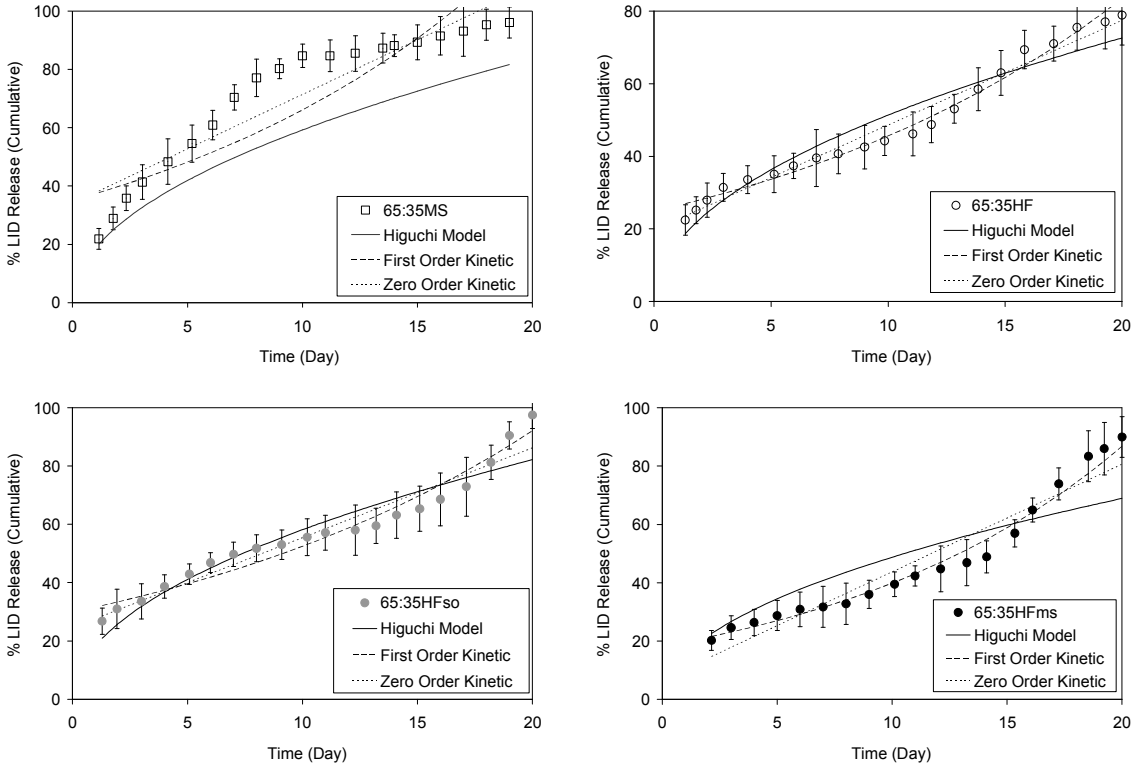

Figure 12.23: The fitting of Higuchi, first and zero order kinetics models in Phase 2 drug release from 65:35MS (□), 65:35HF (○), 65:35HFso (●) and 65:35HFms (●).

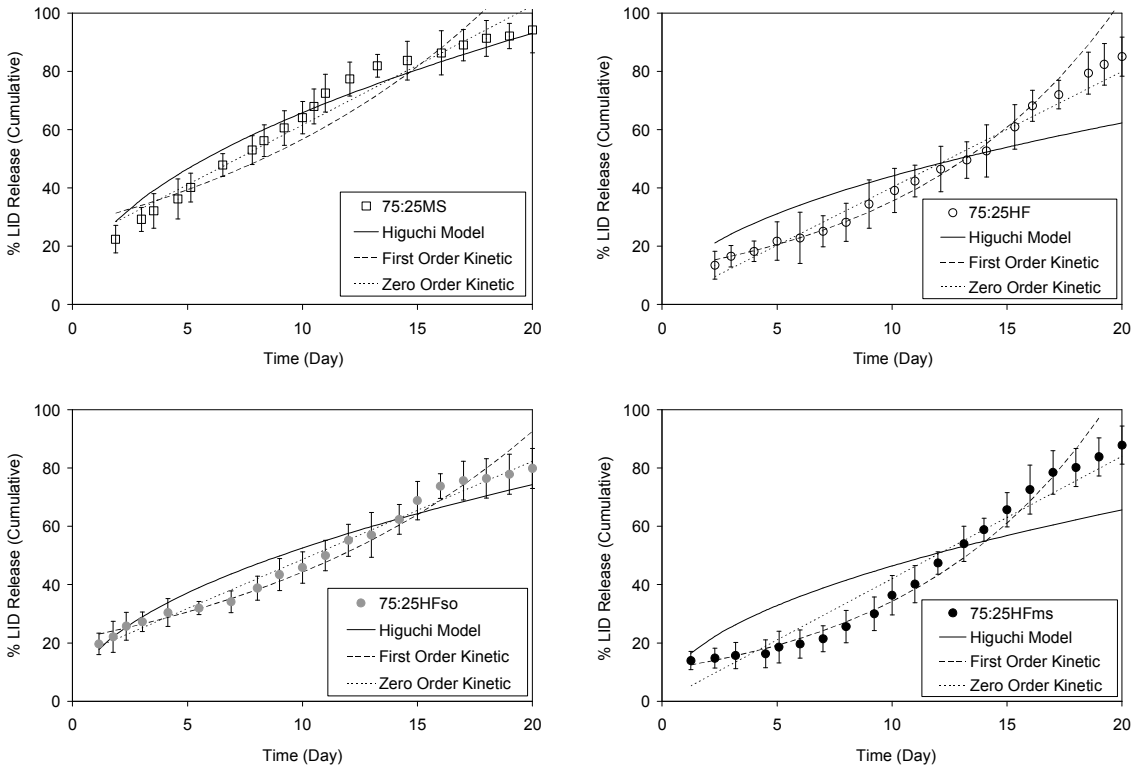

Figure 12.24: The fitting of Higuchi, first and zero order kinetics models in Phase 2 drug release from 75:25MS (□), 75:25HF (○), 75:25HFso (●) and 75:25HFms (●).

Table 12.8: Summary of the goodness of fit of Equations 8.1 to 8.3 to Phase 2 drug release from PLGA samples. The Higuchi constant, k_H was obtained from Phase 1 drug release. × denotes poor fitting; additional notes no. (i) to (vii) see text for discussion.

LID-loaded PLGA Devices	Phase 1	Phase 2 – *Goodness of fit of models*		
	Higuchi Model k_H (mg/s$^{0.5}$)	Higuchi Model	First Order Kinetic	Zero Order Kinetic
50:50MS	26.52	×	×	*Possible fit*
50:50HF	32.61	×	*Good*	×
50:50HFso	19.37	*Possible fit*	×	×
50:50HFms	11.27	×	×	*Good*
65:35MS	32.51	×	×	×
65:35HF	21.49	×	*Good*	×
65:35HFso	45.83	×	×	×
65:35HFms	17.76	*Possible fit*	×	*Possible fit*
75:25MS	11.68	×	*Possible fit*	×
75:25HF	11.22	×	*Good*	×
75:25HFso	17.92	*Possible fit*	×	*Possible fit*
75:25HFms	21.96	×	×	×

Comparing the Phase 1 release, the k_H's of 50:50MS and 65:35MS are larger than the k_H of 75:25MS. This is attributed to the least amorphous region in 75:25 PLGA which limits drug diffusion. 65:35HFso and 75:25HFso tend to have larger k_H than those of 65:35HF and 75:25HF, and this is due to the enhanced drug diffusion by the drug solution in their lumens.

75:25HFms has a larger k_H than 75:25HF/HFso and this is attributed to the presence of an osmotic gradient in the system caused by the burst effect from the microspheres in their lumens. This osmotic effect is not observed in 50:50HFms and 65:35HFms and the reasons are their more amorphous properties permitted easier drugs diffusion and release. The consistency in k_H of LID-75:25-MS and HF indicates the structural integrity of this copolymer ratio against rapid drug release.

For LID-65:35MS, its k_H is larger than the k_H of LID-65:35HF. This is attributed to the higher surface area:volume ratio of the microspheres. In the case of 50:50MS and 50:50HF, the latter has a larger k_H. In the production of LID-50:50HF, the spinning process involved massive aqueous volume and a hydrophilic lidocaine was used, with 50:50 PLGA having the most amorphous region, the drug tended to diffuse towards the aqueous phase and thus concentrated at the fibre surface layer. During buffer immersion, the channel through the lumen of 50:50HF permitted greater medium influx rate and increased drug transport. As a result, a more rapid initial release is observed.

APPENDIX VIII

A. Production of 75:25HF-Stent

20 % (w/w) 75:25 PLGA was used to produce hollow fibres (Section 4.2.3) and was manually woven into a "patch" (Figure 12.25A). A monofilament absorbable suture, PDS II from Ethicon (Johnson & Johnson Care), made of polydioxanone was used as the warp (lengthwise fibre). Briefly, a number of sutures were held vertically with equal space apart. Hollow fibres were then inserted horizontally across these sutures with alternate position. Each fibre was pushed gently close to the adjacent ones. The edges of the patch were then sealed with epoxy resin and left air-dried overnight for the resin to solidify. The patch was then incubated in 30 ml of PBS and maintained at 37 ^{o}C with a back-and-forth shaking of 100 rpm.

Figure 12.25: (A) A fibre-patch fabricated using 20% (w/w) 75:25HF and absorbable suture from Ethicon. (C) After 5 hours of incubation, fibres started to bend and separate between fibres.

Figure 12.26: After 30 days incubation. The breakages continued until a big number of fibres had displaced, departed from their original parallel structure due to the failure of the suture material to provide a structure to hold these fibres in place as themselves, had also underwent displacement.

At the end of the incubation after thirty days, the patch was observed to be distorted in comparison to its original flat and horizontal form (Figure 12.26). Fibres were degraded and disintegrated into short lengths while the sealing at the patch's ends were displaced. Due to the fact only the site ends were sealed with adhesive and not between parallel fibres, the fibres were able to move freely caused the fibre-patch to deform. One of the important findings is that these fibres should be securely held in place in parallel to each others. Collagen could be a candidate to "glue" these fibres together as it has been safely applied in medial purposes.